Depositional record of historic lahars in the Whangaehu Gorge, Mt. Ruapehu

A thesis
submitted in partial fulfilment
of the requirements for the degree
of
Master of Science in Earth and Ocean Science
at
The University of Waikato

by
ALISON HOLLOMON GRAETTINGER

THE UNIVERSITY OF
WAIKATO
Te Whare Wānanga o Waikato

2008

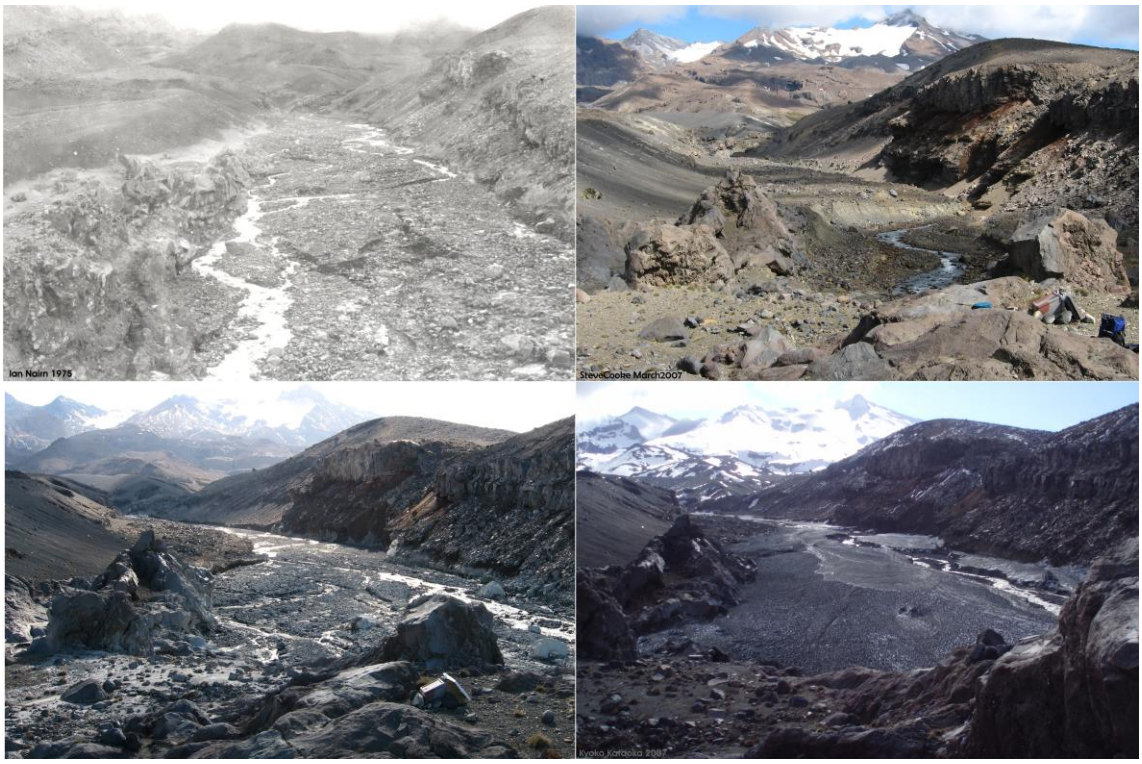

Frontispiece: Historic photographs of progressive historic lahar terrace development at the Round the Mountain Track, Whangaehu Gorge, Mt. Ruapehu. Upper left: Terrace development following the 1975 valley wide eruption-generated lahar. Photo: Ian Nairn. Upper right: Erosion and terrace development following the 1995/96 eruption sequence. Photo: Steve Cooke. Lower left: Aggradation resulting from the March 2007 Crater Lake outburst lahar (Photo: Steve Cooke). Lower right: Initial frozen deposits of the September 25, 2007 snow slurry lahar. Photo: Kyoko Kataoka. Photos taken from the GNS equipment site 7 km from Crater Lake.

Abstract

Mt. Ruapehu is one of the most lahar prone volcanoes in the world, having both a crater lake and six small glaciers upon its 2797 m summit. The major outlet for the crater lake, the Whangaehu Gorge, has hosted over 46 historic lahars. However, the low preservation of debris flow deposits, as a result of frequent remobilisation on steep slopes, allows for the detailed description of only 9 lahar events over the last 150 years. Field investigation, historic aerial photos, two airborne LiDAR surveys and direct measurements have been utilised to describe the sedimentology, geomorphology and distribution of historic lahar deposits in the first 11 km of the Whangaehu Gorge. Inundation maps have been created for 1945, 1953, 1975, September 1995, October 1995, March 2007 and September 2007. Grain size distribution, componentry and geomorphology of the 1861, 1975, September 1995, October 1995, 1999 and 2007 lahar deposits have been compared.

The lahar deposits are massive, very poorly sorted, silty gravels that form a series of unconsolidated terraces. The limited sediment sources in the steep sided Whangaehu Gorge, including minor historic eruption products, results in significant recycling of lahar deposits. However, the deposits can be differentiated by proportions of lithological components and in some cases anthropogenic debris. The abundance of hydrothermally altered material reflects the role of Crater Lake in lahar formation, although, some of these materials (gypsum, sulphur and snow) are only temporary.

Non-cohesive debris flows and occasional snow slurry lahars have been formed by a range of triggering mechanisms associated with and independent of eruptions. Lahars have been formed in the Whangaehu Valley as the result of ejected crater lake water and associated snow melt (1975, September 1995 and September 2007), as well as the progressive displacement of lake water as a result of lava dome growth (1945) and uplift of the lake floor (1968). Inter-eruption lahars occur as a result of Crater Lake outburst floods (1861, 1953 and March 2007) and remobilisation by precipitation and the collapse of tephra laden snow (October 1995 and 1999).

The comparison of historic lahars also reflects the range of lahar magnitudes experienced historically on Ruapehu. The most recent Crater Lake outburst of March 2007, with a peak discharge of 1700-2500 m^3/s is the second largest recorded lahar, behind only the eruption-generated lahar of April 1975 with a peak discharge of 5000-7500 m^3/s.

Lahar mitigation can subsequently be based on lahar generation and incorporation of the vast amounts of data collected before and after the 2007 outburst flood. Recent remobilisation and phreatic activity suggest the significant under-representation of small volume events like rain-generated and snow slurry lahars in the geologic record.

Acknowledgments

This project would not have been possible without the assistance and encouragement of my supervisors Dr. Roger Briggs (Doc) and Dr. Vern Manville. Although he did not get to play with the lahars, I am indebted to Dr. Richard Smith for developing the project and funding. My time in the field and understanding of Ruapehu and its lahars were improved by the opportunity to work with Dr. Katherine Hodgson, Dr. Kyoko Kataoka, Dr. Sarah Fagents and Dr. Bruce Houghton.

2006 and 2007 LiDAR data were collected and provided by GNS Science and Massey University. Vertical aerial photos were borrowed from the GNS Science collection. Field sieving data were collected by and used with permission from the University of Hawaii.

This research was enabled by the clever financial support of the University of Waikato, the Geological Society of New Zealand and GNS Science. Additional support in the form of accommodation, food and transportation from the Department of Conservation, Stanley's and Pete Masters, Massey University, University of Hawaii, the Batmobile and my adopted Kiwi families. I should also thank my family for supporting and encouraging me, even across an ocean.

I received ample technical support from Steve Cooke (self-proclaimed Dopey), Dolan Hewit, Chris McKinnon, Stephanie Nyman, Jacinta Pareenze, Renat Radosinsky, Annette Rodgers, Dr. Ganqing Xu, Antonia Bat Lema Trevino and the Tiburons for LAHAR! All of my enthusiastic field assistants: Louise Fisk (Bashful), Kate Jackson (Happy), Janine Krippner (Snow White in training), Rachel Pickett (Sleepy), Michael Bolton Tayler (Sneezey) and Janelle Hurrell (Grumpy).

Any historical study is dependant on photographs, and I am indebted to a long list of photographers who have made many of my comparisons possible. GNS images are credited to Katie Hodgson, Lloyd Homer, Kyoko Kataoka, Vern Manville and Ian Nairn (Paul Otway and Thor Thordason). Additional images were provided by Steve Cooke, Kate Jackson, and Michael Bolton Tayler (Janine Krippner, Rachel Pickett, Roger Briggs, Steve Hood and Vicki Moon).

The field season was occasionally limited by foul weather and safety concerns, however, few geological events have been so well timed to allow pre-and post-event field work for two volcanic events within the limited schedule of a MSc thesis, and for this I must thank Mt. Ruapehu.

Table of Contents

List of Figures

List of Tables

Appendix Contents

Chapter 1 Introduction

Mt. Ruapehu is a unique natural laboratory, being one of the most lahar prone volcanoes in the world, and yet having one of the lowest associated risks. All the historic lahars in the Whangaehu Valley have been channel confined, and the threat associated with these events is limited to bridges and roadways. A lahar in 1953 resulted in the largest railway disaster in New Zealand history, killing 151 people; the memory of this event has prompted the continued assessment and mitigation of lahar hazards at Ruapehu. Lahar mitigation along the Whangaehu Valley has developed so that the March 18, 2007 Crater Lake release lahar was a relatively minor event in comparison, requiring only an estimated NZ$111,000 in clean up ("Ruapehu Bulletin" 27 March 2007) and no casualties or injuries. On the north and west side of Ruapehu two popular ski fields, Whakapapa and Turoa, are located adjacent to eruption-generated lahar paths and have their own extensive warning systems in place.

Mt. Ruapehu is the southernmost andesitic cone in the Taupo Volcanic Zone, located in the central North Island. Ruapehu hosts a $9x10^6$ m^3 crater lake and six small glaciers. The Whangaehu River serves as the natural outlet for Crater Lake situated at 2529 m a.s.l. More than 46 lahars have been documented since 1861 in the Whangaehu River (Cronin et al. 1997c). The steep sided gorge opens up onto the Whangaehu Fan in the Rangipo Desert on the eastern side of Ruapehu. The river becomes confined and turns sharply to the south before running a meandering course to the Tasman Sea. Deposits within the gorge, first 11 km from Crater Lake, occur as temporary terraces that are readily redistributed by frequent lahar activity.

A tephra dam was formed during the 1995/96 eruption sequence causing Crater Lake to fill above its bedrock rim. In anticipation of the impending Crater Lake outburst lahar, caused by this temporary increase of lake volume, GNS Science, Massey University and the University of Waikato undertook the detailed description of the pre-event conditions of the Whangaehu Valley. As part of this characterisation, the sedimentology, morphology and distribution of the historic lahar deposits within the Whangaehu Gorge have been described in this thesis to reconstruct the depositional record of historic lahar activity on eastern Ruapehu.

A LiDAR (light detection and ranging) survey was collected to create a digital elevation model of the flow path, with a matching set of high resolution orthophotos. The sedimentology and geomorphology of the March 18, 2007 lahar were investigated immediately following the event. A post-event LiDAR survey was obtained in April 2007. A small lahar generated during a phreatic eruption on September 25, 2007 overtopped a significant portion of the March deposits within the Whangaehu Gorge. The resulting deposits were studied immediately following emplacement and progressively during melting of the snow component.

1.1 Objectives: Depositional record of historic lahars

The aim of this study is to compare historic lahar deposits in the upper Whangaehu Gorge through direct study of the available sediments, aerial photographs and digital elevation models. The history of the valley was constructed through the following objectives:

- Terrace distribution of historic lahar deposits in the Whangaehu Gorge
- Comparison of historic lahar fan inundation areas using aerial photo record
- Sedimentological description of historic deposits near source
- Description of historic lahar terrace geomorphology
- Comparison of lahar triggering mechanisms affecting the Whangaehu Valley
- Calibration of Manning's n for historic lahars in the Whangaehu Gorge
- Comparison of historic lahar magnitude in the Whangaehu Gorge

The purpose of this research is to provide constraints for Ruapehu predictive and reconstructive lahar modelling, as well as to serve as an example of a steep, confined lahar path. The success of the March 18, 2007 lahar management can be used as an example of how to study, document and mitigate anticipated lahar events.

The historic deposits within the Whangaehu Gorge are a result of a wide range of lahar triggering mechanisms, but this variability has been subject to oversimplification. The steep angle and impermeable nature of the gorge makes near-source lahar behaviour distinct from flow behaviour downstream. Initial lahar evolution is highly dependent on flow path, which controls flow momentum as a product of potential energy, friction, and flow bulking, controlled by channel

gradient, geometry, permeability and sediment budget. Lahar potential in the Whangaehu Valley cannot be fully understood without analysing the initial evolution within the first 11 km of the flow path in the gorge, in addition to the greater length of the meandering river.

1.2 Lahar fluid mechanics

Sediment gravity flows occur in a variety of environments, requiring only a driving mechanism (gravity), available sediment (loose or easily erodable), water and a triggering mechanism. Volcanic terrains with steep slopes and an abundance of unconsolidated sediment, have ideal conditions for a wide range of concentrated sediment flows.

The term lahar is used to describe the transportation of a mixture of debris and water, other than normal stream flow, with a volcanic origin down a gradient (Smith and Fritz 1989). This term encompasses a continuum of sediment concentrations and resulting flow rheologies. However, it does not provide information on the behaviour of the flow, rather it is used when more specific terms are inappropriate (Lavigne and Thouret 2000; Donoghue and Neall 2001).

Rheological classifications are embedded with implications of fluid mechanics, support mechanisms, concentrations, particle interactions, stopping mechanisms, viscosity, competence and capacity. While these classifications are associated with trends in travel distance, velocity, composition and volume, they are not associated with specific values. Additional terms can be added to the rheologic classification for descriptive purposes. Terms such as coherency reflect the proportion of clays within the flow and also have behavioural implications.

Lahars can exhibit multiple flow rheologies during run out. Flow behaviour is controlled by the interaction of sediment and water in an open system. Depending on the triggering mechanism (initial energy) and flow path (energy dissipation) these components can be added or removed and cause flow rheological transformations. Lahar sediment concentrations can be described as a continuum from clear water to dry granular flows. The sediment budget, water availability and nature of the flow path dictate flow velocity, functional volume, flow thickness and run out time (Bathurst et al. 1997; Ferrucci et al. 2005; Crosta et al. 2006). Natural mixtures contain variable grain size distributions and particle characteristics, which also impart controls on flow behaviour.

Flow behaviour over this continuum includes ideal liquids (Newtonian fluids) and plastics (non-Newtonian Bingham plastics; Fig. 1.1). As sediment concentration increases, fluids develop shear strength or yield strength, which must be exceeded in order to deform, thereby being classified as plastics (Pierson and Scott 1985; Pierson and Costa 1987). This shear strength is the result of interaction between suspended particles and the transportational medium, the development of cohesion and the electrostatic bonding of fine grained particles (Pierson and Scott 1985; Pierson and Costa 1987; Iverson 1997). Clay and silt frequently remain in suspension for the duration of a lahar, and can be considered an intrinsic part of the fluid. The presence of suspended sediment increases the fluid density which increases shear strength. This development of yield strength hinders the ability of larger particles to fall out of suspension, decreasing fall velocity (Pierson and Scott 1985), as the solid and fluid phase of the flow loose their ability to behave independently. The fluid begins to support sediment weight by a reduction of normal stress causing the flow to fluidise (Pierson and Costa 1987).

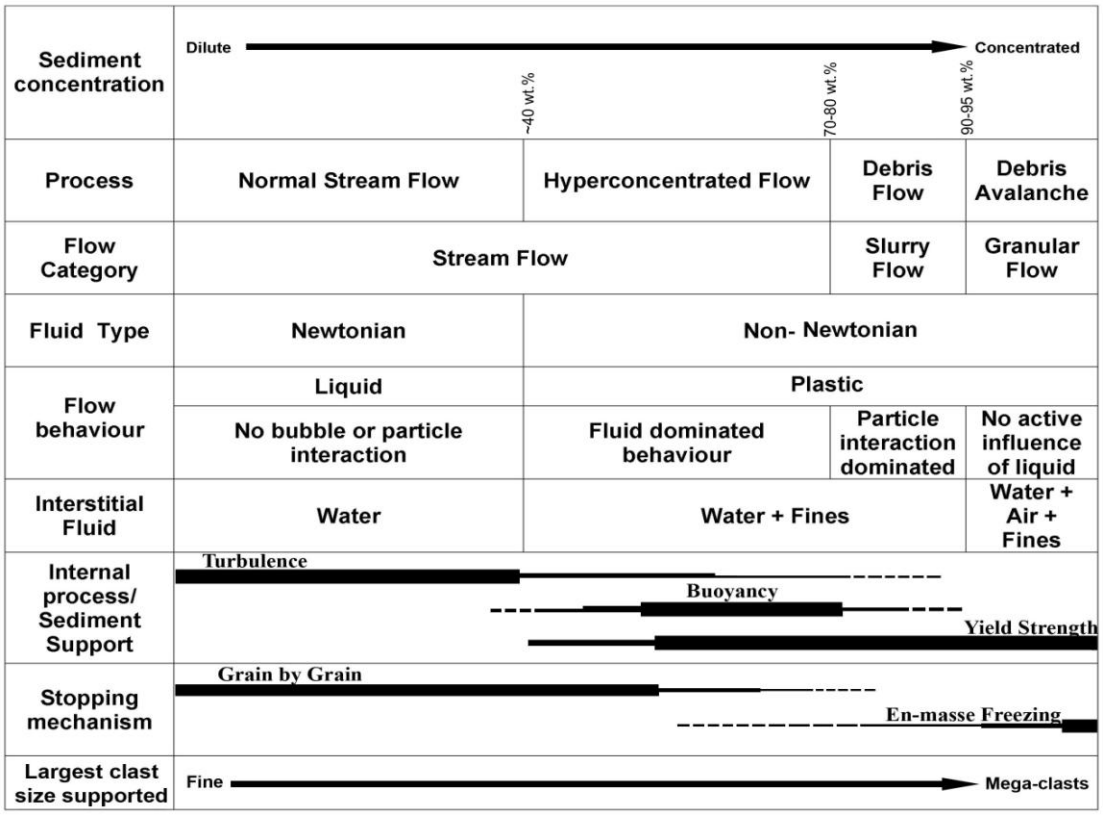

Fig. 1.1 Summary of sediment flow rheology classifications (adapted from Pierson and Costa 1987; Smith and Lowe 1991).

Yield strength increases at a constant rate until liquefaction behaviour, or slurry flow, begins. This fairly concentrated mass is dominated by particle interactions, but the interstitial fluid still contributes to flow motion (Smith and Lowe 1991). When particle interactions become dominantly frictional (continuous grain contact) and the interstitial fluid becomes passive, granular flow dominates (Pierson and Costa 1987). Flow resistance is derived internally from grain interactions, and externally through friction (Iverson and Vallance 2001).

These rheological transitions have been lumped into classifications: normal stream flow to hyperconcentrated flow (development of yield strength), debris flow (slurry flow) and debris avalanches (granular flow). Hyperconcentrated flow is generally defined as a flow with sediment concentrations between 40-80% by weight (Smith and Lowe 1991; Vallance and Scott 1997; Manville and White 2003; Fagents and Balgoa 2005) or 20-60% by volume (Vallance and Scott 1997; Cronin et al. 2000; Lavigne and Suwa 2004). Debris flow concentrations range from 70-90% sediment by weight or >60% sediment by volume (Smith and Lowe 1991; Vallance and Scott 1997; Fagents and Baloga 2005; Glade 2006). The inception of granular flow, associated with debris avalanches, is associated with concentrations of 90-95% sediment by weight (Capra et al. 2002).

Sediment gravity flows are highly unstable processes transitioning between flow types rapidly (Pierson 1997; Iverson and Vallance 2001). This instability is exacerbated by convoluted flow paths and the tendency of flows to develop temporary natural dams because of increased friction at flow fronts (Iverson and Vallance 2001; Lavigne and Thouret 2002; Macías et al. 2004). Flow behaviour is highly sensitive to changes in water content. A variation of 2-4% by weight of water can result in a significant change in velocity which may affect the ability of the mixture to flow or transport larger clasts (Pierson and Scott 1985; Manville et al. 1998). Lahars transform more than their non-volcanic counterparts due to the highly complex geomorphologic conditions in which they form, like the Whangaehu Gorge and low clay content (Smith and Lowe 1991).

Yield strength not only controls the ability of a flow to deform, but dictates the ability of a flow to transport particles, or competence (Fig. 1.2; Iverson 1997; Manville and White 2003). When the clay content is greater than 3% of the matrix, the flow is cohesive (Capra et al. 2002). This relationship can

also be expressed as a ratio of clay to the total sand, silt and clay volumes, with cohesive flows having a value around 0.05 (Cronin et al. 1997c; Vallance and Scott 1997).

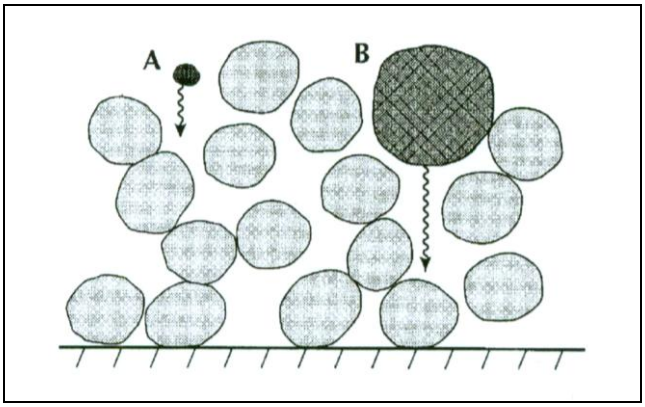

Fig. 1.2 Schematic of particle support in a concentrated lahar flow. Particle **A** represents small particles kept in suspension by viscous forces, increasing fluid density. Particle **B** is held in suspension by interaction with other grains in the flow (after Iverson 1997).

1.2.1 Flow Classifications

Dilute Stream Flow- Hyperconcentrated Flow

Hyperconcentrated flow (hcf) is turbulent, like normal stream flow, but displays some properties of more laminar flow where buoyancy and grain interactions contribute to flow strength (Pierson and Costa 1987; Smith and Lowe 1991). As a result hyperconcentrated flow is discussed as an intermediate stage between dense debris flow and dilute stream flow, with concentrations greater than 40% by weight, approximately 530,000 mg/L (Dinehart 1997). The velocity, discharge and transport capacity of flows with increased concentration are significantly higher than normal streamflow (Lavigne and Thouret 2002). Active hyperconcentrated flows are distinguishable as having a noticeable increased sediment concentration that still moves as a fluid (Cronin et al. 2000). The resulting deposits are distinguishable by high levees with low relative sediment accumulation reflecting the high water content (Hodgson and Manville 1999; Glade 2006). Typical deposits display coarse sandy clast-supported (Pierson and Scott 1985; Lecointre et al. 1998) textures with poor sorting that is distinctly poorer than normal fluvial deposits. Vertical stratification is common, with lenses of extreme density clasts (pumice, or lithics), including rafted clasts along the surface (Pierson and Scott 1985; Hodgson and Manville 1999). Hyperconcentrated flows can either form from the bulking of normal stream flow or the dilution of a more concentrated flow. Hyperconcentrated flows have been described as preceding, following, or being a lateral facies of debris flows (Lirer

et al. 2001; Capra et al. 2004). Hyperconcentrated flows have been observed in association with historic eruptions of Ruapehu, leaving deposits on the Whangaehu Fan and downstream (Cronin et al. 1997c).

Debris Flow

Slurry flow reflects a marked increase in yield strength and is usually associated with concentrations around 80% by weight. An active debris flow (df) is distinguishable from more dilute flows as the concentration is visible and the flow is transported in a series of pulses (Pierson 1995; Cronin et al. 2000; Lavigne and Thouret 2002). The result is plastic steep lobate flows with lateral levees and gravel sized particles in suspension. In some cases the flow may develop into rigid plugs, if yield strength is not exceeded, where sliding, instead of deformation, dominates motion (Pierson and Costa 1987). As yield stress increases, sediment laden flows have a tendency to create natural dams in confined and convoluted flow paths, the periodic release of material from transient lakes and ponds increase the occurrence of pulses within a single flow event (Lavigne and Thouret 2002). Debris flow deposits are unsorted, unstructured and matrix-supported, muddy sand and gravel deposits (Pierson and Scott 1985; Lecointre et al. 1998). Rafted or floating clasts, most commonly low density pumice and scoria, are common on the surface of debris flow deposits (Pierson 1997; Hodgson and Manville 1999). Debris flows can be independent events or derived from other mass movements such as landslides, rock falls, debris avalanches and bulked hyperconcentrated flows. Historic lahars observed in the Whangaehu Valley have been classified as debris flows for the first 16 to 40 km of flow (Cronin et al. 1997b; Cronin et al. 1997c).

Debris Avalanche

As water is not a contributing factor to the rheology of debris avalanches (containing only 5% by weight water), flow mobility is created through the sheer magnitude of the failure event. However, without water to allow some differentiation a debris avalanche deposit has far less variability with distance than its more fluid counterparts (Capra et al. 2002). The result is a rapid gravity driven granular flow capable of moving large blocky clasts (Bret et al. 2003). Debris avalanches are the result of collapse from high cliffs or volcanic flanks

(Capra et al. 2002; Bret et al. 2003). Volcanic-generated debris avalanches tend to be more voluminous and have longer run out distances than their alpine equivalents. This is in part due to the increased clay content derived from the hydrothermally altered collapsing flank (Iverson 1997). Debris avalanche deposits are generally distinguished as hummocky, unsorted, matrix supported diamictons (Palmer and Neall 1989; Capra et al. 2002) that contain discrete clasts and semi-competent blocks of source material (Palmer and Neall 1989; Palmer et al. 1991).

Debris avalanches commonly incorporate water during transport and can generate or evolve into debris flows (Sousa and Voight 1991). Although there are great similarities between debris avalanche and debris flow deposits, the scale and hummocky topography of debris avalanches make them distinct (Smith and Lowe 1991; Palmer et al. 1991; Capra et al. 2002; Bret et al. 2003). Debris avalanche deposits are described as bimodal, displaying two levels of matrix: megaclasts (>1.0 m) are dispersed in a range of boulder and cobble sized clasts, which occurs in a fine grained matrix. The grain size range exhibited in these deposits is diagnostically large, being only slightly smaller than glacial till (Scott et al. 2001).

Although there are no historic records of debris avalanches at Ruapehu, deposits of the Onetapu Formation (2.0 ka) in the eastern ring plain and Mangaio Formation (4.6 ka) and Murimotu Formation (9.5 ka) to the northwest, reflect a number of large scale sector collapses in the volcano's history (Palmer and Neall 1989; Hodgson 1993; Hodgson et al. 2007).

1.2.2 Flow evolution

Flow transformations

Lahar sediment concentrations are the combination of an initial mobilised sediment mass and additional material entrained from the flow path. Initial sediment concentrations are the direct result of the triggering mechanism, and final concentrations are the result of flow evolution (bulking, dilution, deposition). Unconsolidated pyroclastic material is readily incorporated to inter- and syn-eruptive flows, but high concentration flows are capable of entraining clasts derived from competent rock (Stock and Dietrich 2003). The intensity of

triggering mechanisms required to mobilise a given volume of loose material is significantly smaller than for consolidated materials (Pareschi et al. 2002).

Bulking is the process where available (loose or easily eroded) sediment along the flow path is entrained by the passing flow, increasing concentration and density, and thus mobility of a flow (Pierson 1995). Bulking can continue throughout the run out of a lahar, as long as the flow is erosive (Pierson 2002). Particle entrainment is determined by size, shape, density, size distribution, pivoting angle, and relative protrusion of clasts into the flow (Pierson and Costa 1987). The magnitude of the flow controls the rate at which the flow bulks (Manville 2004), and large debris flows have been documented as increasing by a factor of 4 while smaller debris flows have been observed to increase 15 to 20 times in volume (Pierson 1995). The erosive power of a flow, and thus bulking, is determined by the gradient and morphology of the flow path which control the shear stress applied to the bed and banks by the overriding fluid (Pierson 1995; Scott et al. 2001; Manville et al. 2005). The evolution from clear water flood to debris flow can occur over slopes as low as 2º but is more likely to occur at slopes greater than 8º (Pierson 2002).

The dilution of a concentrated flow can occur through the incorporation of water, or the progressive settling of coarser particles during deposition (Pierson and Scott 1985; Fairchild 1987; Cronin et al. 1995; Hodgson and Manville 1999; Lavigne and Thouret 2002). The volume of water incorporated into a lahar and the rate of delivery (instantaneous vs. delayed) controls the proportions of sediment and water and thus flow rheology. Sources of water include rain, permanent or temporary lakes, snow, ice, or hydrothermal fluids. Water incorporated during flow, or dilution, is controlled by the sediment concentration (density), sorting (flow permeability) and mixing mechanisms (turbulence). The proportion of water to sediment determines whether water plays an active or passive role in flow mechanics and deposition (Pierson 1997).

When turbulence is dampened the sediment-laden flow and less dense stream flow would remain independent flows (Cronin et al. 1999; Manville et al. 2000b; Manville and White 2003). Cohesive flows are less likely to dilute as they are less permeable, effectively retarding the inclusion of external water (Pierson 1995). Mixing of the dense sediment laden flow and normal stream flow is dependent on the behaviour of the flow front and can create a wedge of clear flood

water pushed along in front of the concentrated flow (Cronin et al. 1999; Manville et al. 2000b).

Flow Path: Morphology

The geometry of the flow path is important to the duration and distance of flow transport (Pareschi et al. 2002). Slope changes can increase or decrease the kinetic energy of a flow and create friction along the ground surface and flow margins (Sousa and Voight 1991; Fagents and Baloga 2005; Ferrucci et al. 2005). This basal interaction also serves as a source of sediment supply, where erodible material can be incorporated into the flow (Sousa and Voight 1991).

The confinement of a flow by channel or valley walls contributes both to energy loss through friction along flow margins and energy conservation by reducing lateral spreading. Flow confinement results in increased flow thickness, which contributes to flow mobility and velocity, outweighing frictional losses (Sousa and Voight 1991). An unconstrained flow can have distal variations in sediment water concentrations and develop differences in rheology or lead to vertical segregation (Cronin et al. 1999; Cronin et al. 2000). These impacts however, decrease as flow magnitude increases. Small scale roughness factors are submerged and overshadowed as flow thickness increases (Chow 1959; Manville et al. 2002).

As long as the flow travels over a slope above a critical gradient motion will continue as gravitational forces outweigh internal and external frictional deceleration (Bathurst et al. 1997). This critical value is still a matter of debate; however, there is consensus that slopes over 25º result in 100% of material transportation down slope (Ferrucci et al. 2005). Physical models of debris flows have suggested that flow will continue to slopes of 10º, but that flow failure can still be initiated on slopes as low as 3-5º (Bathurst et al. 1997). This critical value does not represent the slope o which a mobile flow will cease or that flow failure cannot occur, rather it is a guide that suggests when gravitational mobilisation no longer dominates the behaviour of loose debris.

Deposition occurs when flow capacity decreases either through changes in gradient, increased sediment budget, decreased velocity and decrease in flow thickness (widening channel) (Pierson 1995; Pierson 1998; Cronin et al. 1999; Cronin et al. 2000). This occurs at the very base of the flow (which may behave

independently of upper mobile portions of the flow) or at the tail end of a flow (Pierson 1995). This results in sediment accumulation in channels (highest concentrations) (Pierson and Scott 1987), as overbank deposits and on alluvial fans with shallow slopes (2º; Pierson 1995). However, sedimentation in channels and on the alluvial fan are subject to subsequent flows and preservation is limited (Cronin et al. 2000). Idealised en masse freezing of a deposit, as is associated with plastic and granular flow (Pierson and Costa 1987; Smith and Lowe 1991), should reflect the flow as it was in motion. However, it has been observed that deposition of hyperconcentrated flows and debris flows are more complex augmented by the progressive accumulation of sediment by flow pulses (Cronin et al. 2000; Lavigne and Thouret 2002; Manville and White 2003).

The water trapped within the deposit imparts post-depositional characteristics, produced by the compaction and dewatering of the deposits. The most significant result of this process is a decrease in deposit thickness, accompanied by the removal of suspended fines in escaping water (Iverson 1997).

1.2.3 Types of triggering mechanism

The mechanisms for remobilising volcanic deposits are numerous and range from large scale processes like the collapse of a volcanic edifice, to precipitation events. During an eruption lahars can evolve from pyroclastic density currents, the melting of snow and ice, phreatic and phreatomagmatic ejection of crater lake water, acoustic tremors, and the displacement of lake water by a growing lava dome (Mastin and Witter. 2000). Lahars are also formed when accumulations of unconsolidated debris or unstable portions of the volcano are remobilised by precipitation events, the collapse of tephra laden snow, wall or dam failure in semi-permanent and permanent lakes, earthquakes and landslides. The scale and magnitude of these events is related to the amount of material available (both water and sediment) and the rate of triggering. A slow progressive flood will have far less impact than sudden lake release (Pierson 1998).

Sediment gravity flows produced by watery floods, like crater lake outburst or snow melt floods, tend to produce debris flows. Flank collapse and phreatomagmatic and phreatic eruption-triggered flows have been associated with hyperconcentrated stream flows (Lecointre et al. 2004). Avalanches, landslides,

sector collapse, are essentially all mass failures that, with the incorporation of water, can transform into mobile sediment-laden flows.

Precipitation and snow/ice melt can contribute to flows that have been triggered by another event or can trigger discrete lahar events.

Eruption-triggered generation

Volcanoes that have perennial crater lakes, glaciers, or snow packs have increased hazard potential as there are significant volumes of water stored on the top of dynamic slopes (Pierson et al. 1990; Cronin et al. 1996a; Waythomas et al. 1996; Manville et al. 2000a). Water can be ejected from the crater lake by phreatic and phreatomagmatic eruptions through the lake (Nairn et al. 1979), the melting of snow and ice (Lowe et al. 1986; Pierson et al. 1990; Pierson 1997) and the displacement of lake water by the growth of a lava dome or deformation caused by rising magma (Mastin and Witter. 2000). The locations of lahar initiation will be impacted by accumulations of fresh tephra and the direction of water release. This can result in the simultaneous formation of lahars in multiple catchments on a volcano (Cronin et al. 1997c). Lahars that form from the melting of snow and ice or travel over snow fields and glaciers can incorporate quantities of snow and ice with significant transport distances up to 50 km (Pierson et al. 1990; Cronin et al. 1996b; Manville et al. 2000a). The lahar size and run out are weakly correlated to eruption size, as flow volume and mobility are controlled by the sediment and water budget and geometry of the flow path (Mastin and Witter. 2000).

Remobilisation-generation

Rain-generated lahars are most frequently associated with tropical regions, where monsoonal rains and cyclones easily remobilise recent and ancient pyroclastic and volcaniclastic deposits (Mt. Semeru; Lavigne and Suwa 2004). However, as the events of October 1995 and 1999 in the Whangaehu displayed, this hazard has been overlooked in more temperate environments (Ronaldo et al. 1996; Manville et al. 1997; Hodgson and Manville 1999; Lirer et al. 2001; Lavigne and Thouret 2002). The collapse of tephra laden snow was the most common trigger for remobilisation lahars during the 1995/96 eruption sequence.

Flood events efficiently mobilise loosely consolidated or free material through rapid saturation and erosion. Saturation increases the weight of sediment and pore pressure eventually overcomes friction (Pareschi et al. 2002; Glade 2006). Permeability is a major control of sediment erodibility and the ease of remobilisation (Fig. 1.3). Low permeability hinders infiltration, creating surface runoff. The channel bed is eroded by the surface shear stress that creates scour and lift. Moderate permeability results in saturation. Unconsolidated sediments are remobilised by pore water pressure overcoming the pressure of overlying sediments through saturation. In most cases total saturation is not required for the material to mobilise (Ferrucci et al. 2005; Manville et al. 2005). A saturated sediment mass, for example a previous lahar deposit, is easily mobilised requiring only 10% water content (Capra et al. 2004).

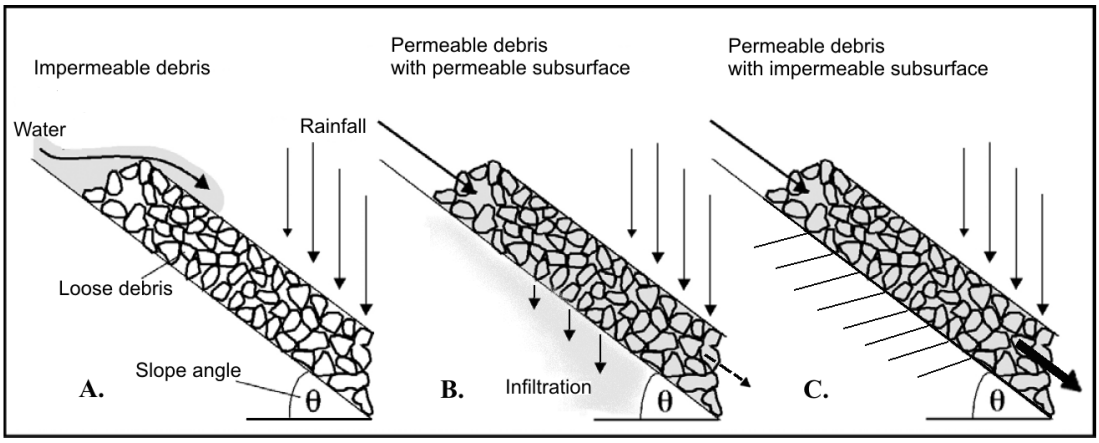

Fig. 1.3. Remobilisation of unconsolidated sediment on steep slopes as a result of saturation, resulting from permeability contrasts. **A.** Impermeable debris cause surface runoff of flood or rainwater. Erosion occurs from scour and lift of the overriding flow. **B.** Permeable debris with a permeable subsurface result in saturation only with rapid release of large volumes of water. **C.** Permeable debris over an impermeable subsurface effectively saturates and destabilises sediment, easily mobilising with slight increases in moisture content (adapted from Ferruci et al. 2005).

Outburst Flood

The sudden release of lake water is the most efficient mechanism for creating a high peak discharge lahar (Smith and Lowe 1991; Cronin et al. 1997b; Ferrucci et al. 2005). The volume of volcanic lakes varies substantially, but can reach the size of the 1.8 ka Lake Taupo, New Zealand ($6.0 \times 10^{10} m^3$)(Manville et al. 1999; Manville and White 2003) and modern Crater Lake, USA ($1.9 \times 10^{10} m^3$;

Waythomas et al. 1996). Historic lake outburst floods have occurred globally at Mt. St. Helens (Pierson 1997), Mt. Spurr, USA (Waythomas 2001), Mt. Pinatubo, Philippines (Ronaldo et al. 1996), and Mt. Ruapehu (O'Shea 1954; Manville et al. 2007). Massive ancient paleo-floods from volcanically dammed lakes have been described from Lake Taupo (Manville et al. 1999; Segschneider et al. 2002a,b; Manville and White 2003; Manville and Wilson 2004; Manville et al. 2007), Lake Tarawera, New Zealand (White et al. 1997), Aniakchak, USA (Waythomas et al. 1996) El Chichón, Mexico (Macías et al. 2004) and Laacher See, Germany (Park and Schmincke 1997).

The most common mechanisms for dam breach are piping and seepage, overtopping followed by erosion, and defects in the dam. Breaches tend to extend only through the material blocking the spillway (Walder and O'Connor 1997) creating a triangular or trapezoidal outlet (Scott et al. 2001).

Overtopping occurs as water spills over the crest of the dam and erodes a channel along the downstream face of the dam. The head of the breach channel retreats upstream as the escaping water continues to erode assisted by mass failures and bank collapse within the dam (Walder and O'Connor 1997).

Piping is the result of water percolating through the dam at high hydraulic gradients to carry away sediment. This creates pipes through the dam, first appearing as seeps at the downstream face of the dam. The pipes erode headward, enlarging and forming a channel on the downstream face of the dam. Ultimately a breach forms when the overlying material collapses into the eroded cavity. As most natural volcanic lake dams have reasonable permeability, piping may occur concurrently with overtopping (Walder and O'Connor 1997).

The rate of water release, a product of the rate and size of breach formation, is critical to the behaviour of the lahar. For lakes with sufficiently large volumes, for a given depth, the breach formation can be considered almost instantaneous (e.g. Lake Taupo; Manville et al. 1999; Manville and White 2003). In such events breaching is completed before significant drawdown of lake water occurs. For smaller lakes the drawdown that occurs during the erosion of the lake breach is far more significant relative to the total volume, and peak discharge is therefore a factor of the rate of breach formation (Walder and O'Connor 1997; Manville et al. 1999).

However, in the absence of a permanent lake, outburst type floods can still form as the result of transient lake outflow. The self-damming nature of lahars (Park and Schmincke 1997; Waythomas 2001), eruption of fresh pyroclastic deposits and glacial moraines (Walder and O'Conner 1997) can create temporary reservoirs for water and sediment-laden flows, which can then be released in a rapid more dangerous flow or series of flows (Cronin et al. 1997b).

Historic lahars on Mt. Ruapehu, occurring mainly in the Whangaehu River, have been produced by a wide range of trigger mechanisms. The most recent mitigation strategies for Mt. Ruapehu lahar hazards are based on the occurrence of a dam collapse, similar to the 1953 event known as the Tangiwai disaster, where an intra-eruption lahar destroyed a railway bridge moments before the arrival of a passenger train (Pierson 2002). These efforts were recently tested in the March 18, 2007 Crater Lake outburst lahar and were quite successful.

Chapter 2 History of the Whangaehu Valley

Mt. Ruapehu, the tallest volcano in New Zealand (2,797 m), is a typical andesitic composite cone that was constructed in 4 major episodes over a period of 250,000 years (Hackett and Houghton 1989). Historic activity at Ruapehu has consisted of very frequent, relatively small phreatomagmatic and magmatic eruptions, with larger episodes occurring in 1895, 1945 and 1995-96. The active vent is located in the south crater, which hosts the acidic crater lake and hydrothermal system. The 100 km^3 cone only represents a portion of the volcanic record (Fig. 2.1); a more complete history is preserved in the equivalent volume radial ring plain, composed of laharic debris and distal pyroclastic material. Geological studies have been conducted on the southeast (Palmer et al. 1993; Donoghue and Neall 2001), northeast (Cronin et al. 1996a, 1997a), northwest (Palmer 1991) and western (Palmer and Neall 1989; Lecointre et al. 1998) portions of the ring plain. These studies created depositional histories for the ring plains through tephra layers, paleosols and erosional surfaces that are interbedded with loess, laharic and normal fluvial deposits. The deposits of the last two thousand years reflect the presence of a crater lake over the active vent, resulting in phreatomagmatic eruptions and lahar production (Lecointre et al. 1998). There are sediments from a wide range of flow types, from channel constrained hyperconcentrated flows (Cronin et al. 1997b) to large scale debris avalanches (Palmer and Neall 1989) with no uniform pattern of distribution or frequency (Lecointre et al. 1998).

2.1 Setting

The Whangaehu Valley runs from the southern edge of Crater Lake and serves as the natural drainage of the lake (Fig 2.2). The river then runs east down the flank of the volcano in a deeply entrenched gorge. This upper portion of the gorge bifurcates and converges several times, including the overflow channel of the chute 11 km from the lake. The river spreads out onto the Rangipo Desert creating the gently sloping Whangaehu Fan (6 km long by 4.5 km wide; Palmer et al. 1993; Manville 2004). The braiding channels of the fan are once again constrained by a northeast trending horst created by the Rangipo Fault (17.4 km

from Crater Lake) (Villamor and Berryman 2006). The river turns sharply southward for several kilometres before beginning a meandering path entrenched in uplifted Miocene-Pleistocene marine sediments of the Wanganui Basin to the south and west before entering the Tasman Sea. The course of the river runs under the Tangiwai Railway Bridge 39 km from Crater Lake. The Whangaehu River flows for 203 km before reaching the Tasman Sea (Hodgson 1993).

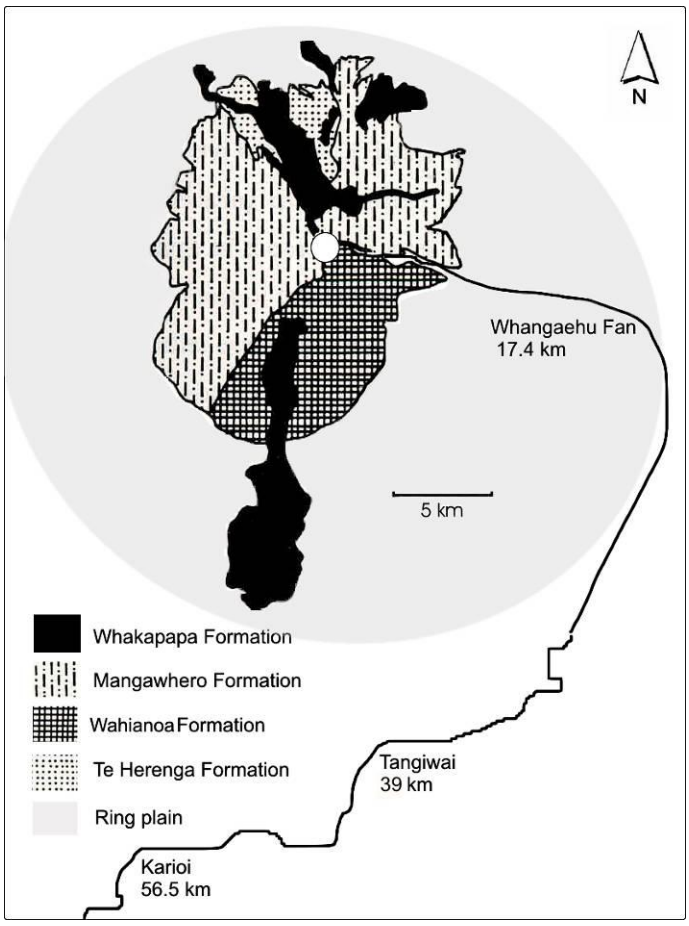

Fig. 2.1 Constructional history of Mt. Ruapehu, spanning 250,000 years. The volcanic edifice only represents one third of the volcano's volume including the volcaniclastic ring plain (adapted from Hodgson 1993).

The flow path of the Whangaehu River can be divided into three major sections: (1) the gorge (crater to apex of the Whangaehu Fan 0-11km), (2) the Whangaehu Fan (ring plain 11-18 km), and (3) the meandering river incised into Tertiary basement (18-203 km). The focus of this study was the first 11 km of the flow path, the location of initial flow evolution (Fig. 2.3).

Within the gorge the highly complex flow path transitions rapidly from confined to unconfined channel configurations with rapid changes in slope. The first 11 km of the valley is characterised by repeated bifurcations, sharp bends, waterfalls, and multiple transitions occurring over short distances (c. 500 m)

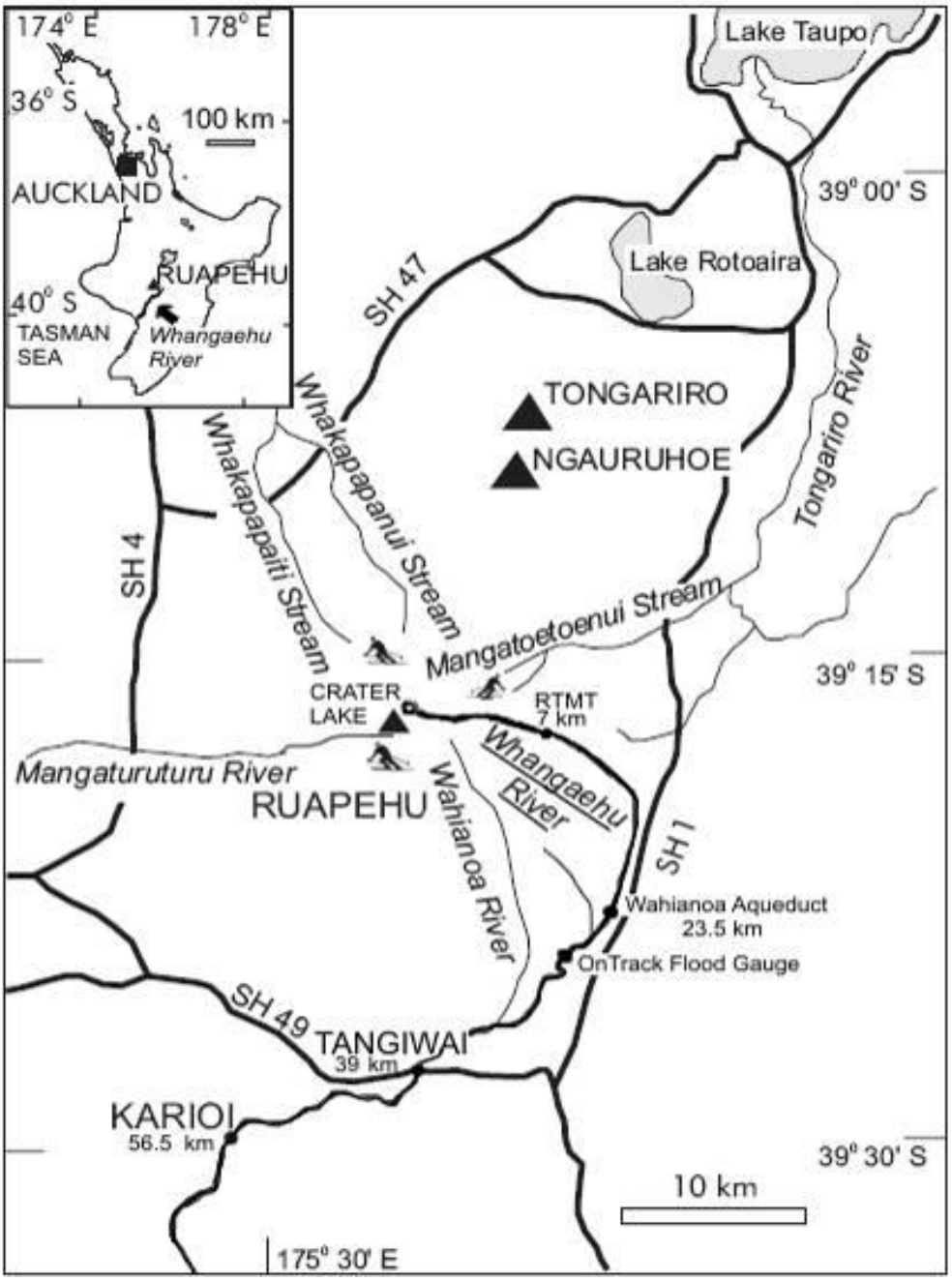

Fig. 2.2 Location map of Mt. Ruapehu and the Whangaehu River in the North Island of New Zealand (adapted from Manville et al. 2000a).

between steep confined bedrock gorges to broader but still defined valleys floored with colluvium and lahar deposits (Fig. 2.4).

Because of the steep and highly channelised nature of the upper valley, the volume of lahar deposits preserved within the gorge is relatively small. The depositional record within the gorge is short as the deposits are located immediately in the flow path causing reworking by almost all lahar events. The events of 2007 are an example of the continuous processes of sediment remobilisation within the Whangaehu Valley.

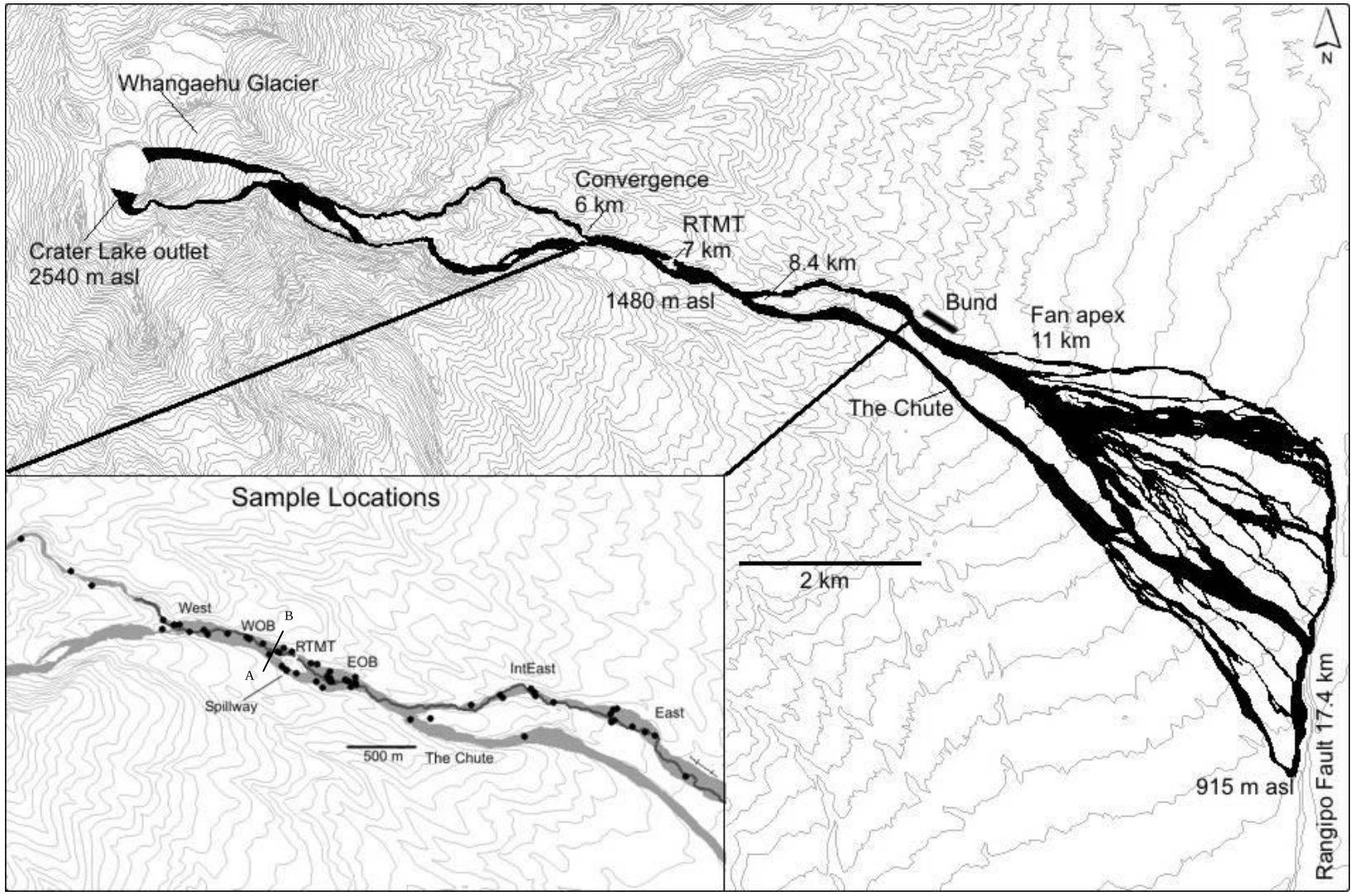

Fig. 2.3 Lahar paths of the Whangaehu Valley. Inset of sample area including sample locations (1975 lahar inundation). Cross-section A-B in figure 2.5. Sample Localities: WOB= west of bridge, RTMT= Round the Mountain track, EOB= east of bridge, IntEast= Intermediate east.

Fig. 2.4 Flow path complexities of the Whangaehu Gorge. **A.** View upstream, first bifurcation of the valley 2.5 km from Crater Lake. **B.** View west overlooking the 'Spillway' at Round the Mountain Track, 7.0 km from source. **C.** Looking east towards the Whangaehu Fan. The 'Chute,' 8.0 km from source, is the southern highly erosional overflow channel that rejoins the main channel at the toe of the Whangaehu Fan. Photos: Lloyd Homer.

As the valley winds away from Crater Lake (2530 m a.s.l.) there are four main points at which large lahars bifurcate by overtopping topographic divides into sub-parallel channels. The first major split occurs upstream of the Tukino ski field, approximately 2.5 km from source. At this point, eruption-triggered lahars generated by Crater Lake water explosively ejected over the eastern rim of the crater basin flow down the steep Whangaehu Glacier and jump across the main Whangaehu Gorge into a more southern gorge. Large lahars flowing down the main Whangaehu Gorge, in which the overflow from Crater Lake runs, along with snowmelt and precipitation runoff, also bifurcate at this point across a topographic

divide into the southern gorge. Another topographic divide c. 1 km further downstream from this primary one is also overtopped by large lahars in the main gorge to reach the southern channel. The main, northern, and the southern gorge unite c. 6.0 km downstream from Crater Lake at a site referred to herein as the convergence. The second location of interest is west of the Round the Mountain Track (RTMT) where a small overflow channel has formed behind a low point in the outcropping bedrock (7.5 km, 1480 m a.s.l.). The resulting island has been used as an equipment repository and monitoring station for GNS. The last major bifurcation occurs 8.4 km from source at the 'Chute'. Here, the Whangaehu Gorge splits to either side of a large, post-glacial, lava flow that travelled c. 11 km down the gorge. The upstream portion of the lava flow is smoothed and polished by thousands of years of lahar activity, while the distal portion retains a coarse rubbly carapace. Large lahars in the Whangaehu River overtop a topographic divide to enter the chute, where they travel in a relatively straight line across the southern side of the Whangaehu Fan, rejoining the main channel at the toe. The main route of laharic activity lies in the northern channel (Scorpion Gully). The variation in distribution of lahar deposits between the north and south valleys is significant.

Lahars of the Whangaehu River are routed into the valley by two major pathways. The natural drainage of Crater Lake occurs as seepage and overflow at the lowest point in the crater rim at the southern edge of the basin. During eruptions, water is ejected from the crater in all directions. Water pushed out onto the Whangaehu Glacier, northeast of the crater, is routed back into the Whangaehu Valley. Catchments on the south (Wahianoa), west (Mangaturuturu) and north (Whakapapa River and Mangatoetoenui) also host lahars, but with lesser frequency (Fig.2.2). The catchments on the northern and western side of Ruapehu remain channelised for the length of the river and the deposits are valley confined, unlike the Whangaehu where the deposits have accumulated to produce the Whangaehu Fan (Donoghue and Neall 2001).

2.2 Whangaehu Stratigraphy

The entrenchment of the Whangaehu River, despite its normal small discharge, suggests that this drainage has been established as long as Crater Lake has existed on the summit. The gorge is the product of post-glacial erosion of the

volcanic flank with incision occurring dominantly by lahar activity (Hackett and Houghton 1989; Stock and Dietrich 2006). Historic eruptions have not dramatically altered the morphology of the crater and the Whangaehu Valley has remained the normal drainage for the lake. Within the Whangaehu Fan, and downstream, there are thick deposits of the ≤2 ka Onetapu Formation (estimated volume of $10^8 m^3$; Donoghue and Neall 2001; Lecointre et al. 2004). These pre-historic deposits have been correlated to minor upstream exposures uncovered only in the gorge walls and modern channel bed (Palmer et al. 1993; Donoghue and Neall 2001; Lecointre et al. 2004).

The gorge is carved into >60 ka andesite lava flows of the Wahianoa Formation (Fig. 2.1; Hackett and Houghton 1989) and Mangaio Formation debris avalanche deposits (4600 yr BP; Donoghue and Neall 2001), upon which are situated terraces of unconsolidated historic lahar diamictons. The confined and steep nature of the upper Whangaehu Gorge results in highly erosive flow behaviour with interspersed pockets of pooling and eddies that appear behind obstructions (boulders and bedrock outcrops) along the flow margins. Segments dominated by erosion have fairly clean bedrock channel beds with scattered and thin deposits of only the most recent lahar events. In the regions of ponding or pooling up stream of constrictions in the flow path, the terrace sequences are more complete.

Volcaniclastic deposits from Ruapehu in the last 2000 years are recorded in the Onetapu Formation, with contemporaneous tephra accumulations of the Tufa Trig Formation (Tf). These deposits include all accumulations on Ruapehu's ring plain stratigraphically above the 1.8 ka Taupo Pumice. Lahar deposits within the gorge are a series of diamicton terraces that are progressively removed by continued lahar activity. As of January 2007 exposed terraces of 1861, 1975, 1995 and 1999 covered the valley floor (Fig. 2.5). Deposits from 1995 can be divided into eruption-generated, 1995E, and remobilisation generated 1995R units. Deposits of interim events have been buried and/or removed from the gorge and downstream. On the Whangaehu Fan and further downstream to Karioi (56.5 km), deposits from the 1861, 1953, 1975 and 1995/96 episodes have been described as minor units in the Onetapu Formation (Table 2.1; Hodgson 1993; Cronin et al. 1997b; Lecointre et al. 2004; Hodgson et al. 2007). The deposits referred to as 1861 are not well constrained, having limited exposure in the

Historic lahar terrace distribution in the Whangaehu Gorge, February 2006

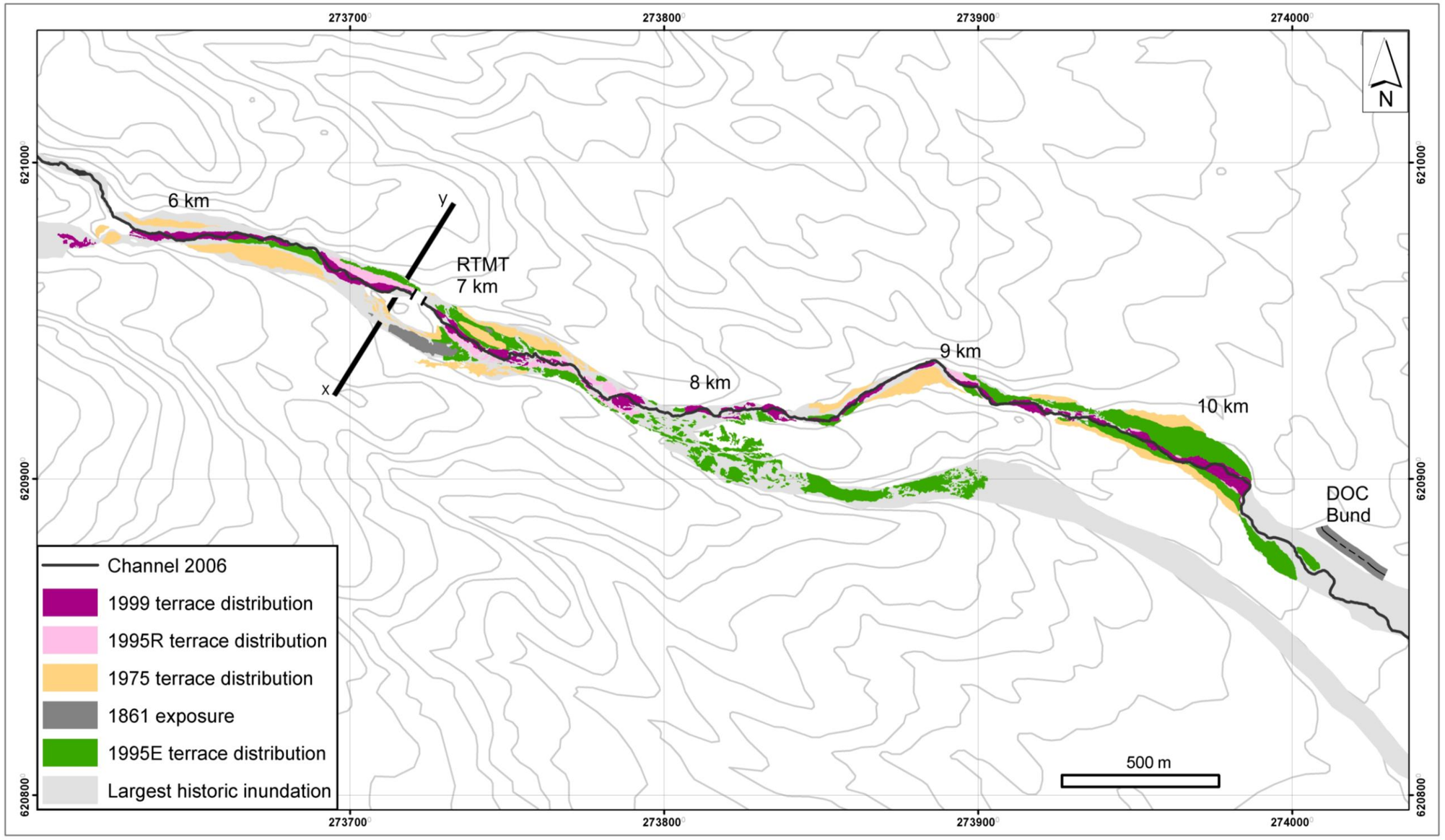

Fig. 2.5 Distribution of historic lahar terraces in the Whangaehu Gorge in Febrary 2006. The distribution is the result of erosion and depostion from large volume eruption-generated lahars in 1975 and 1995 with remobilisation from 1995 to 2007. X-Y section line for Fig. 4.3 a.

gorge and a radiocarbon date of 1750-1950 A.D. (Hodgson et al. 2007). The identification is based solely on the interpreted scale of observations by Taylor (1861) and descriptions of deposits downstream by Donoghue et al. (1997) and Hodgson et al. (2007).

Table 2.1 Onetapu Formation units identified in the Whangaehu Fan compared with historic deposits in the Whangaehu Gorge.

Events	Cronin et al. (1997b)	Donoghue and Neall (2001)	Hodgson et al. (2007)	This study
1861	On-m	Ong	One-3	1861
1953	On-n		One-4	Not in study area
1975	On-o		One-5	1975
1995/96			One-6	1995E[1] and 1995R[3]
1999				1999
2007				2007L[2] 2007E[1]

[1] E denotes eruption generation
[2] L denotes lake outburst
[3] R denotes remobilisation

In 2007 two lahar producing events significantly altered the deposits within the Whangaehu Gorge. An outburst flood from Crater Lake occurred on March 18, 2007 and eroded historic deposits, reducing their terrace volumes and locally aggrading the stream bed by 12 m, is referred to as 2007L. A phreatic eruption on September 25, 2007 produced two small snow slurry lahars after ejecting lake water onto the Whakapapa and Whangaehu Glaciers. Initial deposits in the Whangaehu Valley, referred to as 2007E, were up to 2 m thick, but only 20 cm of deposit remained after melting.

2.3 Crater Lake

There is evidence that a lake, similar to the current Crater Lake, had been established on Ruapehu sometime after the emplacement of the 1.8 ka Taupo Pumice (Donoghue et al. 1997). The volcaniclastic record for Crater Lake reflects two major periods of accumulation separated by a period of quiescence and followed by a period of moderate activity. The cumulative volcaniclastic deposits are described as the Onetapu Formation (Lecointre et al. 1998). The last 350 years represent a decrease in volcaniclastic aggradation and younger deposits are constrained to existing channel systems eroded into previous deposits (Lecointre

et al. 2004). The presence of lake sediment in the earliest dated Onetapu Formation deposits constrains the age of the lake to at least 1500 C^{14} (Hodgson et al. 2007).

The Tufa Trig Formation of tephras exposed in the eastern ring-plain has also been used to date the lake. The beginning of the Tf is marked by a distinct change in eruptive style, reflecting a dramatic increase in water:magma interactions at Ruapehu. It has been suggested that this change is a direct result of the inception of an ancestral Crater Lake (Donoghue et al. 1997). The ages of these tephras and the increased frequency and distribution of lahars suggest the establishment of a semi-permanent lake in the current southern crater location by 1.8 ka (Hodgson 1993; Donoghue et al. 1997).

2.3.1 Changes at the Crater

The geometry of Crater Lake and its outlet to the Whangaehu River, have experienced changes with each historic eruption. In a general sense, the changes to the crater that impact lahar initiation and evolution are the lake volume and obstruction of the outlet (by glacial ice or tephra). The volume of water stored on the mountain is a function of both the depth and shape of the lake basin, which can vary with eruptive activity, and the level of water within the basin. Changes in the hydrothermal system located at the bottom of the lake influence the chemistry of the water and alter lake sediments, the crater walls and volcanic ejecta in and around the lake.

Table 2.2 Historic changes in Crater Lake depth.

	Depth [1] /Volume [2]	Source
1945	300 m steep sided vent	O'Shea 1954
1953	$9x10^6$ m^3	Manville 2004
1970	56- 70 m deep	Nairn et al. 1979
	$7x10^6$ m^3	Dibble 1972
1976	Exceeded 90 m	Nairn et al. 1979
1989	180 m deep	Hackett and Houghton 1989
	$1x10^7$ m^3	
1995	134 m deep	Christenson and Wood 1993
	$9x10^6m^3$	

[1] minimum measurements
[2] estimates

Observations and sporadic depth surveys of Crater Lake reflect large variations in the depth of the lake basin and the volume of water stored therein (Table 2.2). For example, the 1995-96 eruptions increased the volume of the lake basin by c. 40% through collapse and erosion of the vent walls. This is in addition to the semi-permanent snow pack and six diminished glaciers. In many cases, the morphology of the lake surface does not reflect dramatic changes to the geometry of the vent that serves as the lake basin. For example, between 1970 and 1976 the lake depth increased by a minimum of 20 metres in depth with no dramatic changes in the surface of the lake as recorded in aerial photos.

As the geometry and water level within Crater Lake varies, so too does exposure of materials deposited at the crater. Clasts of baked Crater Lake sediments are frequent components in Whangaehu lahars. Sediments accumulating in the lake have been exposed in 1945, 1953, 1995 and 2007. The sediment was examined briefly in 1945 and 1953 (section 2.4).

The geometry of the lake outlet is also highly variable. The rate at which water is released in the event of a breakout flood or displacement of lake water through eruption and wave generation, is dependent on the geometry of this outlet. The history of the southern outlet has been recorded in aerial photographs and observations at the crater and are summarised in Table 2.3.

Table 2.3 Conditions of the Crater Lake outlet on the southern edge of the lake.

Record	Status of Crater Lake	Status of outlet
1926	Frozen	Ice[2]
1945	Empty	Ice and tephra dam[1]
1948	Filling	Small ice tunnel[1]
	Breakout flood	New ice tunnel and collapse of
1953	7.9 m drop in lake level	tephra dam[1]
1969	3 m drop in lake level	Rock rim, minor tephra/snow[3]
1975	8 m drop in lake level	Snow and ice [4]
1982	Refilling	Reduced ice, minor overflow[5]
1995	Empty	Tephra dam (5 m) [6]
1996	Re-established	Tephra dam (6.5 m) [6]
4 October 2006	1.3 m increase in lake level	Not overflowing
	Breakout flood	40 metre wide outlet on rock
2007L	6 m drop in lake level	rim
2007E	3 m drop in lake level	Rock rim outlet

[1] O'Shea 1954
[2] Gregg 1960
[3] Healy et al. 1978
[4] Nairn et al. 1979
[5] Beetham 1982
[6] Pierson 2002

As recently as 1953 the Crater Basin Glacier was c. 120 m thick over the outlet area, but the thickness had decreased by 50% by 1982, exposing the outlet channel across a series of water falls formed by stepped lava flows (Beetham 1982). The 1995-96 eruptions seriously impacted the remnant Crater Basin Glacier, completely exposing the outlet area through disruption and enhanced melting as a result of burial by ash. Historically, Crater Lake has only frozen over twice, most recently in 1926 (Gregg 1960), and typically the temperature cycles between c. 20 and 40 degrees centigrade on a biannual basis. Consequently, overflow is generally warm enough to melt an overflow tunnel through any ice on the crater rim. Throughout the last 150 years the presence of ice and tephra has led to increased lake levels.

2.4 Lahar History of the Whangaehu Valley

Historic records of Ruapehu's volcanic activity begin in the 1880's, but the lahar history is patchy and based on scattered observations. The most consistent observation point for Whangaehu events has been Tangiwai, after the construction of both a railway bridge in 1909 and SH49 road bridge over the Whangaehu River 39 km downstream of the crater Volume estimates from these events are calibrated for single locations and simplify the nature of flow, but they are convenient for event size comparisons (Table 2.4).

1859

13 December, 1859 is associated with the first recorded observations of lahars from Ruapehu, described only as unusual floods in the Whangaehu Valley. Little is known about the events described, but the floods are not associated with a volcanic eruption. The event was significant because of the destruction of the newly constructed Whangaehu Bridge (O'Shea 1954).

1861

The next record, by Reverend Richard Taylor (1861), dramatically depicts a flood of trees, ice, snow and debris in the Whangaehu Valley in 1861. Taylor's descriptions of a concentrated mass of debris have been the basis of numerous

Table 2.4 Summary of deposit distribution and distinguishing characteristics.

Event	Extent	Current distribution	Estimated Volume(m^3) Hodgson 1993; Hodgson et al. 2007	Trigger
4.6 ka Mangaio Formation.	Valley wide	Channel bed and fan	$3.4x10^7$	Sector collapse/ eruption
1859	Unknown	No exposure	No estimates	Unknown (between eruptions)
1861	Valley wide	Remnant, channel bed	6×10^6	Possible lake outburst
1889/95	Unknown	No exposure	3×10^5 / $6.7x10^4$	Phreatomagmatic eruption
1903	Unknown	No exposure	$1x\ 10^5$	Phreatomagmatic eruption
1925	Unknown	No exposure	$1x10^6 m^3$/ 3.10^5	Unknown, possible lake outburst
1945	Constrained by larger terraces	No exposure	No estimates	Dome building eruption (progressive)
1953	Valley wide	No exposure	6.5×10^6	Lake outburst
1966	Unknown	No exposure	1.0×10^3	Phreatomagmatic eruption
1968	Highly constrained	No exposure	7.2×10^5	Eruption-generated (progressive)
1969	Highly constrained	No exposure	6.7×10^4	Phreatomagmatic eruption
1971	Unknown	No exposure	7.2×10^4	Phreatomagmatic eruption
1977	Unknown	No exposure	1.3×10^4	Phreatomagmatic eruption
1975	Valley wide	Moderate remnant terraces	1.8×10^6	Phreatomagmatic eruption
1988	Unknown	No exposure	1.3×10^4	Phreatic eruption
1995E	Constrained by larger terraces	Minor terraces	5.6×10^6 [1, 3]	Phreatomagmatic eruption
1995R	Constrained by larger terraces	Minimal marginal deposits	9.5×10^5 [2, 3]	Remobilisation
1999	Highly constrained	No exposure	1×10^4	Rain-generated
2007L	Constrained by larger terraces	Constrained, all branches	1.8×10^6 [4]	Lake outburst
2007E	Northern branch of gorge to 24 km	2007L northern branch	1.1×10^5/ 1.2×10^4 [4]	Phreatic eruption

[1] Total for September 25,1995 [2] Total for October 28, 1995 [3] Cronin et al. 1997c [4] Manville 2007 pers. comm. [5] This study

volume speculations. Estimates for the volume of this lahar have been placed around 6 x 10^6 m^3, supported by descriptions of the flood wave reaching the coast (Hodgson 1993; Cronin et al. 1997b). The trigger for this event is still unknown. The 1861 lahar is the largest observed lahar within the Whangaehu Valley, but there are no records of an eruption at this time. The quantity of ice and the sulphurous smell described by Taylor (1861) could suggest a lake outburst origin. But the magnitude of the event, as indicated by deposit distribution, appears far greater than documented lake outburst lahars in 1953 and 2007.

Both the 1859 and 1861 events occurred before direct observation of Crater Lake on the summit of Ruapehu. The first ascent to the crater was made in 1879 by Beetham and Maxwell (O'Shea 1954), changing both the means of observing and interpreting volcanic floods.

1889/95

During an eruption in August 1889, water was displaced from Crater Lake and the resulting lahar was observed at Tangiwai (39 km) and Wanganui (203 km) (O'Shea 1954). Based on a comparison of observed stage heights, Hodgson (1993) estimated the volume to be 1/6 the size of the 1953 Tangiwai lahar (on the order of 3x10^5 m^3; Cronin et al. 1997b).

Similar 'floods' were described associated with an extended magmatic eruption in 1895. These events were correlated with a 2-3 metre drop in lake level, with volume estimates at Tangiwai around 6.7 x 10^4 m^3 (Cronin et al. 1997b).

1925

Two events in 1925, January 23 and February 3 were observed downstream of Tangiwai, although no eruption was mentioned (Hodgson 1993). An 'unexplained drop in lake level' and enlargement of an ice cave at the head of the Whangaehu Valley suggests a crater outburst flood (O'Shea 1954). The two closely spaced events may reflect temporary damming within the Whangaehu Valley (Hodgson 1993). The volume estimates, on the order of 1x $10^6 m^3$ and 3x$10^5 m^3$ respectively, are comparable to events in 1889 (Hodgson 1993).

1945

The only major historic lava (andesite) producing eruption on Ruapehu (Reed 1945; Oliver 1945) occurred in the autumn and early winter of 1945. The growth and eventual collapse of two tholoids progressively emptied Crater Lake by July 22, 1945 (Fig. 2.6). Records of the event focus on dome growth and tephra accumulations from dome collapse (Johnston 1997), but a significant increase in discharge from 0.1 m^3/s to 1.5 m^3/s at the lake outlet was recorded (Oliver 1945). But as there were no observations downstream, there is a dispute over whether a lahar was associated with this period of lake emptying (Hodgson 1993; Lecointre et al. 1998). The loss of lake water can be partially attributed to the production of steam from contact with the emerging dome, with lake

Fig. 2.6 Dome growth between March and July 1945. Exposed Crater Lake mud separates the tholoid from the wall of the crater. All of the lake water had been displaced from the basin by July 1945 (Oliver 1945).

temperatures around 58˚C (Oliver 1945)**.** There are no deposits currently within the gorge or fan that have been correlated to this event, but aerial photographs taken in 1940 and spring 1945 show changes to the distribution of terraces within the gorge just above the fan apex (9 km from the crater lake) (See Chapter 4).

The significance of the 1945 events is twofold. Firstly, the explosive eruption from the collapse of the growing domes resulted in a drastic change in

crater morphology and depth, exposing a 300 m steep sided vent (Manville 2004) that would later be blocked and refilled.

Secondly, prior to the collapse of the domes, the emptied lake made it possible to observe and describe the Crater Lake sediment. The lake floor was described as coated in blue grey mud with conspicuous desiccation polygons that were rich in sulphur. Observations also describe a weakness of the crater wall above the head of the Whangaehu Valley (O'Shea 1954).

1953

The lahar of December 24, 1953 is well known and is the only confirmed lake break-out lahar prior to 2007. Hence, it was used as a model to prepare for the 2007 event. After the lake was emptied in 1945, the outlet of the lake was blocked in 1946 and the lake was re-established by 1948 (O'Shea 1954). Observations in 1950 and 1951 described the lake level as 'rising' and made no mention of an established ice tunnel as the lake level was still below the rock rim (O'Shea 1954). The failure of the tephra dam in December was not associated with any volcanic or seismic activity, and all of the water displaced from the lake flowed into the Whangaehu Gorge. The lake level dropped 7.9 m, generating an estimated peak outflow discharge of 350-400 m^3/s (Manville 2004). The escaping water created a new ice cave during overflow instead of enlarging the existing outlet (Fig. 2.7). Peak discharge in the gorge was estimated to have reached 2000 m^3/s (Manville 2004).

The majority of deposit observations were confined to the Tangiwai Bridge and surrounding areas. Investigations at the Crater Lake noted exposure of the 1945 lake floor at the margins of the lowered lake. Samples were collected, but no chemical or grain size analyses were conducted (O'Shea 1954). The initial distribution of sediment on the fan was quite widespread, but the porosity and permeability of the unconsolidated sands and gravels on the fan resulted in the diminished appearance of deposits on the fan by 1955 (O'Shea 1954). There was no grain size distribution sampling and no exposed deposits have been identified in the gorge during the course of this study.

The lahar of 1953 resulted in the greatest railway disaster in New Zealand history, and caused the greatest damage of all historic activity at Ruapehu. 151

people died when a passenger train reached the Tangiwai Rail Bridge that had been damaged by the lahar (O'Shea 1954).

Fig. 2.7 Crater Lake in December 1953. The arrow indicates the ice tunnel created by the outflow of the crater lake. The lake level dropped approximately 9 m on December 24 1953, the resulting lahar destroyed the Tangiwai Rail Bridge 42 km downstream (O'Shea 1954).

1968/69

1968 and 1969 were the climax of a prolonged period of minor phreatic eruptions that started in 1964 (Healy et al. 1978). Minor quantities of lake water were ejected onto the Whangaehu Glacier throughout this period. On April 24 1968 and June 22 1969, water was displaced from Crater Lake producing lahars in multiple catchments.

The Whangaehu lahar of 1968 is considered to have been the result, not of a single instantaneous triggering event, but the product of prolonged seismic activity over a period of several hours and uplift of the floor of Crater Lake due to rising magma. The lake level dropped a total of 3.5 m (Cronin et al. 1997b). This 'delayed' triggering (Vignaux and Weir 1990) reflects the varied nature of lahar formation and evolution experienced on Ruapehu. The effects of the flows were documented only in limited aerial photography (Fig. 2.8).

Vignaux and Weir (1990) addressed the unique behaviour of the event by modelling the lahar as seven discrete pulses released over time, and proposed that

with enough time, the waves would have coalesced to form a single wave front. This coalescence, however, would most likely occur downstream of Tangiwai (39 km from Crater Lake) (Vignaux and Weir 1990).

The June 22, 1969 eruption caused a 2-3 m drop in lake level. Because of the directed nature of the phreatic explosions that expelled lake water, the majority of this water was routed into the north-flowing Whakapapa River, but the Mangaturuturu and Whangaehu valleys also experienced small lahars (Paterson 1976; Healy et al. 1978; Hodgson 1993). The flow was measured at Karioi (56.5 km) with a volume of 6.7 x 10^4 m^3 that has been compared to estimates from 1895 (Hodgson 1993). There were no other direct observations of the event and no damage occurred. The only detailed sedimentary description was obtained at the Tokiahuru Confluence, downstream of Tangiwai Bridge (Hodgson et al. 2007).

There was no ash accumulation in the Whangaehu Valley associated with the 1969 eruption (Healy et al. 1978).

Fig. 2.8 Aerial view of the upper 5 km of the Whangaehu Gorge on May 2, 1968. One of many minor lahars produced during the eruption sequence cumulating in 1969. Most of the lahar travelled over the Whangaehu Glacier before being routed back into the valley (GNS photo archive).

1975

Minor phreatic activity occurred throughout 1971, but the next juvenile producing eruption and lahar producing sequence occurred in April 1975. Small volumes of water were ejected from the Crater Lake throughout the eruption

sequence (Nairn et al. 1979), but the largest volume of water was expelled from the lake on April 24. The eruption occurred again without witness upstream, because of the time of eruption (c. 3:59 a.m.) and low visibility caused by precipitation. Water was ejected in all directions from the crater causing lahars in eight catchments, the largest after the Whangaehu Valley were in the Whakapapa, and Mangaturuturu Rivers to the west and north (Paterson 1976; Nairn et al. 1979). The volume of water displaced from the lake, resulting in an 8 m drop in lake level, represented only 23% of the total lake volume (estimates from 1970, $7x10^6$ m^3; Dibble 1972). The eruption followed a warm summer, so the ice fields were described as "considerably reduced in size" prior to the eruption (Nairn et al. 1979). Current ice fields have receded farther because of melting by volcanic activity from April 27, 1975 to 1996 and warmer summers.

Due to the construction of the Wahianoa aqueduct (23 km from Crater Lake), part of the Tongariro Power Scheme, the Whangaehu River received a significant attention during the eruption. The precautions taken after the 1953 disaster were also under scrutiny (Paterson 1976; Cronin et al. 1997b). The footbridge for the RTMT was destroyed and minor damage occured at power scheme construction sites, but thankfully no construction workers were on the site when the lahar passed (Paterson 1976).

Peak stage observations were collected at Tangiwai (39 km) and Karioi (56.5 km) as usual, and estimates were made from super-elevation marks at 6.5 km within the gorge (Nairn et al. 1979). Initial estimates for flood volumes at Tangiwai of $1.6x10^6$ m^3 (Paterson 1976; Nairn et al. 1979) were the largest since 1895 (Cronin et al. 1997b). Initial calculations of instantaneous velocity and peak discharge (c. 5000 m^3/s) were made by Nairn et al. (1979), but detailed 1975 distribution and sedimentology suggest that these values underestimate the flow depth and require revaluation (see Chapter 6).

September 1995

Study of Ruapehu increased dramatically during the 1995/96 eruption. These observations became the basis of most of the current hazard plans for Ruapehu. Lahars were associated with the earliest eruptive activity in all major catchments (Fig. 2.9). The Whangaehu Valley received a range of lahars including snow slurry, high-sediment concentration and dilute flow (Cronin et al.

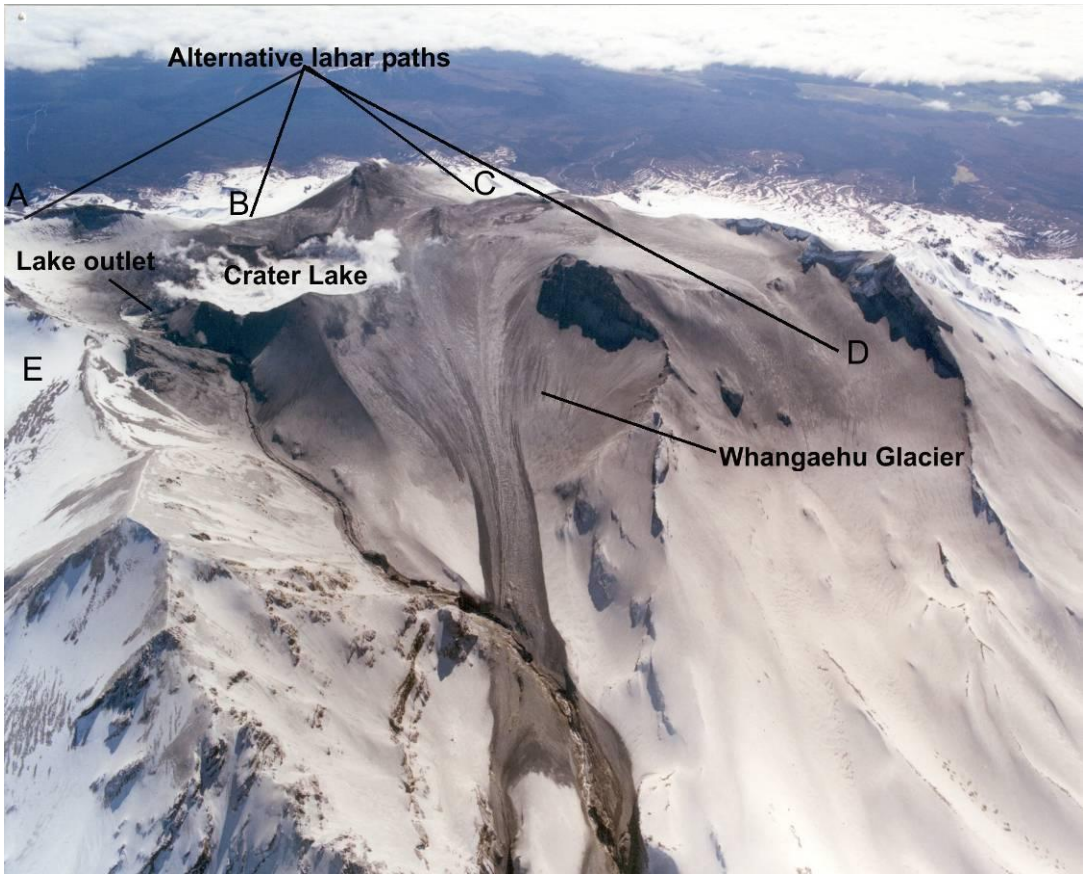

Fig. 2.9 Summit of Ruapehu on 23 September, 1995 with lahar deposits across the Whangaehu glacier. Alternative lahar paths, A-E are indicated. **A**. Mangaturuturu **B**. Whakapapaiti **C**. Whakapapanui **D**. Mangatoetoenui **E**. Wahianoa Rivers. During the 1995/96 sequence all major catchments experienced either eruption generated or remobilisation lahars. Photo: Lloyd Homer.

1997c). Initial events were dominated by snow, and deposited concentratedslurries of snow and debris up to 45 km from source (Cronin et al. 1996b). The largest laharic sequence (referred to as LH4 by Cronin et al. 1997c, deposits referred to as 1995E in this study) eroded and/or buried earlier deposits, and emplaced as the highest depositional terrace. The 1995E deposits were the result of seven different pulses travelling downstream on September 25 after the snow pack around the crater and flow path had already been melted or scoured by previous lahars. The cumulative volume of the multi-peaked LH4 lahar was $2.6x10^6m^3$ at Karioi (56.5 km) (Cronin et al. 1997c). The peaks were closely spaced, being recognisable only on instrumental hydrographs, cannot be distinguished in downstream deposits (Cronin et al. 1997c). The peak discharge gauged in the gorge was between 1400 and 1800 m^3/s (Cronin et al. 2000). The peak flow destroyed the footbridge on the RTMT 7 km from Crater Lake.

Observations were collected at multiple locations, as far upstream as the mid-fan (18 km) (Cronin et al. 2000). Below the fan, the 1995E lahar effectively removed the previous lahar deposits. The lahars progressively increased in volume following the commencement of eruption, causing sediment removal and re-deposition, with the largest lahar occurring on 25 September, 1995. Lahars continued in the Whangaehu and other main catchments until October 11/12 when the lake was finally emptied. Eruption-generated lahar activity resumed in early 1996 after the Crater Lake had begun refilling (Cronin et al. 1997c), with a single snow slurry lahar travelling c. 8 km down the Whangaehu Gorge.

October 1995 to April 1996

The earliest lahars of the September 1995 sequence were the direct result of water ejected from Crater Lake, but the increasing volume of loose unconsolidated debris became susceptible to rain- and snowmelt-triggered remobilisation. Not long after the draining of the Crater Lake in October 1995, spring warming and rainstorms remobilised the large quantities of loose eruptive material, including the September 1995E deposits. Most remobilisations were the result of melting and collapsing of accumulations of tephra covered snow (Manville et al. 1998; Hodgson and Manville 1999; Manville et al. 2000a). This process was accentuated by intense rainfall. The deposits from these events are referred to as 1995R, and are treated as a single prolonged depositional event throughout the spring and summer of 1995/96 (Manville et al. 2000a).

There are minimal records of individual remobilisation lahars during this time. These events were smaller in scale than the large eruption-generated lahars, and usually not distinguishable from normal stream flow 155 km from source (Cronin et al. 1997c). All drainages experienced remobilisation events, but catchments to the northeast and east, e.g. Mangatoetoenui and Whangaehu, had the greatest accumulations of juvenile material and the highest frequency of lahars. Lump volume estimates at 56.5 km from source were $1.2 \times 10^6 m^3$ for the Whangaehu alone (Cronin et al. 1997c). The heaviest accumulations of tephra resulted from the October 11-12 1995 lake-draining eruption in the catchments of the Wahianoa River and Mangatoetoenui Stream.

The largest single remobilisation event recorded in the Whangaehu Valley occurred on October 28, which had a volume of $9.5 \times 10^5 m^3$, and was the first lahar

of the series to make it all the way down the gorge (Cronin et al. 1997c). Most of the remobilisation events did not leave a seismic record (Manville et al. 2000). The October 28, 1995 event is associated with the highest terrace 1995R level within the gorge.

1999

In the fall of 1999 a small remobilisation lahar destroyed the RTMT bridge during a large precipitation event. There were no observations and minimal documentation of the lahar, however, this remobilisation event was part of the continued response of the Whangaehu River to the increased sediment load caused by the 1995/96 eruptions. All terraces younger than the immediate response to the 1995/96 eruption sequence are identified as 1999, as it was the largest lahar event between 1996 and 2007. The plank bridge design for the RTMT bridge was abandoned following the 1999 lahar for a cable swing bridge at a more elevated location over the river.

March 2007

The eruption of 1995/96 deposited roughly 7.6 m of unconsolidated tephra and ballistic fallout across the former outlet of the Crater Lake. A survey collected in 1997 indicates that the dam was initially 90 m long and 50 m wide at its base (Pierson 2002) (Fig. 2.10). Over the following 11 years, the lake refilled from a combination of precipitation and snow melt (75%) and fumarolic condensate (25%) from the hydrothermal system at the base of the lake. On 18 March 2007, the tephra dam was breached during a heavy rainstorm when the lake level was <115 cm below the top of the dam. 1.3 million m^3 of water was released with a peak discharge through the outlet of c. 530 m^3/s. The flood entrained clay to boulder-sized particles along the steep gorge of the upper Whangaehu Valley, to form a non-cohesive debris flow within 7 km from Crater Lake. The lahar reached the coast near Wanganui at approximately 3 a.m. the following morning as a sediment-laden flood <1 m rise in stage height.

A retrospective analysis of dam failure based on field observations, time-lapse images of collapse, in-situ geotechnical testing, and finite element modelling has been conducted by Massey et al. 2007 (in prep).

The collapse was well documented by a time-lapse camera positioned at

the Crater Lake on the morning of 18 March, 2007. Images reflect a progressive collapse that began with a series of sloughing failures at the erosion scarps starting around 9:56 a.m.[1]. The crest of the dam failed between 11:07 and 11:10 a.m.. Progressive flow over the smaller breach undermined the dam triggering a major collapse at 11:21 a.m. The breach was eroded until the lava rim was exposed by a 40 m wide breach by 11:32 a.m. (Fig. 2.11). The lake level dropped by a total of 6.3 m creating recessional terraces at the lake margin. The deposits are referred herein as 2007L.

Fig. 2.10 Seeps and erosion of the tephra dam face caused by piping by February 2007. White arrows indicate seeps #4 and #6 (left to right) that were the locations of initial failure. The black arrow indicates a GNS scientist and equipment station for scale (GNS photo archive).

Acoustic flow monitors (AFM) and broadband seismometers indicated a series of pulses with varying sediment load characteristics travelled through the gorge, bulking by a factor of 5. Downstream monitoring of stage height, velocity, water quality and sediment load was conducted by Massey University and Horizons Regional Council. No lives were lost and property damage was minimised, largely due to a comprehensive interagency response plan developed in the decade leading up to the lahar (Webby 1999; Gledhill and Scott 2001; Hancox et al. 2001; Pierson 2002). The only damage that resulted from this event was to the RTMT bridge, a toilet block at the Tangiwai Memorial, and a pump

[1] Times are recorded in New Zealand local time (GMT -12:00 hours)

Fig. 2.11 March 18, 2007 breach in the 1995/96 tephra dam on the southern edge of Crater Lake. The breach is 40 m at the base and resulted in a 6 m drop in lake level. Recessional terraces circumscribe the lake.

shed on the Tokiahoura Stream.

While not the direct result of an eruption, the destruction of the 1995/96 tephra dam was the final stage of the eruption sequence and primary sedimentary response. Under current conditions at Ruapehu the next lahar will be associated with renewed volcanic activity or a large seismic event.

September 2007

At 8:20 p.m. a "blue sky" eruption ejected water and mud from Crater Lake onto the summit plateau and surrounding glaciers. Snow slurry lahars were generated in the Whakapapa and Whangaehu Valleys. The deposits in the Whangaehu Valley are referred to as 2007E. For the first 10 km from the crater lake the Whangaehu Valley deposit overlapped the 2007L deposits smoothing out topography, with a maximum thickness of around 2 m. Evidence of snow was observed 23.5 km downstream. The 2007E lahar was predominantly (>70%) snow, which began to melt rapidly after emplacement. However, the initial deposit clearly reflected three discrete slurry pulses and a recessional water flood. The melting of the deposit was delayed by spring snow storms, but evidence of the event rapidly deteriorated with the melting of the deposit. By November the deposit volume had decreased by half, with an average of 20 cm of sediment mantling the 2007L deposits.

Chapter 3 Methodology

The depositional history for the historic lahars within the Whangaehu valley is based on field evidence, digital elevation models, aerial photographs and laboratory analysis of grain size and componentry. Additionally velocity and peak discharge estimates for historic lahars were based on a calibration of Manning's roughness coefficient n through the gorge (6 to 7 km from Crater Lake).

3.1 Mapping

In February 2006, in preparation for the anticipated Crater Lake outburst flood, a pre-event LiDAR survey was collected for the first 58 km of the Whangaehu River by GNS and Massey University as part of a collaborative project to document the geometry of the flow path and geomorphic changes resulting from the anticipated flow. On April 6, 2007 a post-event survey was carried out as a complement to the 2006 data set. LiDAR (light imaging and ranging) is a technique similar to sonar, where light is reflected off a surface and the travel time of the reflections is used to measure the topography of a surface. The surveys conducted on Ruapehu were processed to create pre- and post-event DEMs and 1 m contour maps of the flow path for comparison of the valley before and after deposition of the 2007L lahar. Positioning accuracy was obtained through calibration with a ground point elevation data set outside of the lahar path and manual editing of the data set. Additionally, high resolution (2006: 18 cm GSD; 2007: 20 cm GSD) orthophotographs were collected over the same area concurrently with the LiDAR data.

Historic photographs and the topographical information were used to support field observations and measurements of the geomorphology and terrace distribution within the gorge, and to extrapolate the terrace distribution to the upper gorge and fan. The DEMs were used to create comparative cross-sections of terrace development before and after the March 18, 2007 lahar near the RTMT (7 km from the Crater Lake).

3.1.1 Field Investigations

The field study area was divided into seven sections for grain size sampling, lithology, texture and geomorphologic descriptions (Fig. 2.3). These sections are based on major changes in the channel geometry, specifically bifurcations of the flow path (Table 3.1). The western-most section (WEST: 6.0 to 6.5 km from source) is located at a major convergence of the gorge just downstream from a series of small waterfalls. The section west of the RTMT bridge (WOB: 6.5 to 7.0 km) includes a minor divergence referred to as the

Table 3.1 Photo coverage of the Whangaehu River.

Dates	Type of photos	Coverage
1940	1:19000 vertical	Fan
1950	1:19000 vertical	Lower gorge, fan
1954/55	1:19000 vertical	Crater Lake, gorge, fan
1969	Aerial oblique	Crater Lake and upper gorge
1975, January	1:50000 vertical	Crater, gorge, fan
1975, April	Oblique aerials and oblique surface	Crater, gorge, fan, OnTrack warning gauge (25 km), Tangiwai (39 km)
1980	1:25000 vertical	Crater Lake, gorge, and fan
1995	Oblique aerials and oblique surface	Crater Lake, gorge, fan, Tangiwai
2000	1:50000 verticals	Crater Lake, gorge, and fan
2006	LiDAR, oblique, 1 km^2 orthophotographs 18 cm GSD	Flow path: Crater Lake to 58 km downstream
2007, April	LiDAR, oblique, 1 km^2 orthophotographs 20 cm GSD 1:6500	Flow path: Crater Lake to 58 km
2007, September	verticals 50 cm GSD	Crater Lake to 17 km

'spillway'. East of the bridge (EOB: 7.0 to 8.4 km) the valley broadens but is interrupted by minor lava outcrops until the 'Chute' divide, a large lava bluff that divides the channel into two branches. The northern branch meanders in a steep sided gorge (INT EAST: 8.4 to 9.0 km). Just before the apex of the Whangaehu Fan and the DOC bund, the northern valley of the branch begins to widen and lahar deposits accumulate at a major bend in the eastern-most section of the valley (EAST: 9 to 11 km). The chute branches off the main channel towards the south and runs from 8.4 km to the fan. Samples were only taken from the first kilometre of the chute.

Initial deposit distribution was established through field identification of lahar terraces and mapping (both prior to and following the 2007 lahars), vertical aerial photographs, oblique post-event photographs, and flow high-stands preserved by rafted debris. Diamictons from 1975, 1995, 1999 and 2007 were identified and described. Vertical photographs were used to map additional events from 1945, 1953 and incomplete segments from 1969. Deposits from 1861 were identified and described in the field; however, the exposure was too limited to reconstruct initial distribution. Identification of the 1861 deposit was based on stratigraphic position below younger deposits and descriptions of exposures in the Whangaehu Fan by Hodgson (1993).

The morphology of the deposits was described in four major periods corresponding to pre-existing and post-event conditions for two lahar events (2007L and 2007E). Morphology of the deposits was observed in January – February 2007 (pre-2007L), March – May 2007 (between 2007L and 2007E), September 2007 (post-2007E) and October- December 2007 (after melting of 2007E).

The deposits from September 2007 (2007E) posed a challenge to morphological and sedimentological description. The snow-dominated deposits degraded immediately following emplacement because snow transported within the flow was deposited at elevations well below the natural snow level at the time of the eruption (> 1600 m). Melting of the deposit was more rapid than pure snow because of the dark colour caused by presence of silt. The first four days following emplacement were sunny cloudless days causing the deposit to melt rapidly removing silt with the melt water, compacting and exaggerating surface morphologies. A snow storm the following week refroze the deposit on the upper reaches of the valley (> 1400 m) before secondary observations were conducted. The deposit was observed in October, November and December to document the melting process and compare the morphology after the snow fraction had completely melted with the flow path as observed in March through May of 2007.

Photographs of the upper flanks of Ruapehu and Crater Lake with exceptional documentation of the lake level in the crater, are archived in the GNS Science catalogue from as early as the 1920's. The vertical aerial photographic record of the eastern flank of Ruapehu does not begin until 1940. Historic orthophotos from 1940, 1950, 1954 (post-Tangiwai), 1975, 1980 (post April

1975), 2000, 2006, April 2007 and September 2007 supplemented by oblique photos from 1975, 1995 and 2007 were utilised in this study (Table 3.2).

Elevation data from two LiDAR surveys (February 2006 and April 2007) were used to constrain terrace heights and thus deposit thicknesses for the preserved units. The topography was also used to help map surface bedforms on the exposed terraces.

Table 3.2 Flow path constrained sampling sections and distance downstream.

Section	Geometry	Units sampled	Number of samples	km from Crater Lake
West	Convergence of two constrained waterfall dominated branches into a channel 112 m wide.	1975 1999 2007L	3 1 2	6 to 6.5
WOB	112 m wide, narrows to 30 m at RTMT. Includes minor (60 m by 400 m) spillway to the south just upstream of RTMT.	1861 1975 1995E 1995R 1999 2007L 2007E	2 3 2 1 1 2 15	6.5 to 7
EOB	Broader valley, up to 130 m, interrupted by lava outcrops.	1975 1995E 1995R 1999 2007L 2007E	7 5 3 1 2 2	7 to 8.4
Intermediate East	Pocket of deposits in a meander of a steep sided gorge. 15 m widens to 55 m.	1975 1995E 2007L	2 1 3	8.4 to 9
East	Widening of valley, to 150 m, and accumulation of deposits in a major bend upstream of the fan apex.	1975 1995E 1995R 1999 2007L	2 2 1 1 3	9 to 11
Chute	Steep-sided, straight gorge 140 m wide.	1975 1995E	1 2	8.4 to 11

Three lahar events (1975, September 1995, and 1999) destroyed foot bridges at the RTMT, damage also occurred at this site in 2007. Until March 2007 the debris from these bridges was scattered in the first kilometre past the RTMT bridge location. The debris from these bridges was distinctive, and the location of the wood debris was mapped to help with terrace and flow height

identifications. Only the 1975 debris is still in position following the 2007L and 2007E lahars.

Vegetation distribution was considered as a potential means of terrace identification, but investigation of plant diversity revealed that the degree of surface exposure controlled the occurrence of plant life on the terraces. Consequently, plant diversity would be controlled by morphology and the geometry of the gorge itself (e.g. overhangs, steep walls). The number of variables controlling plant growth is too high to confidently link plant distribution to individual deposits.

3.2 Sedimentology

3.2.1 Grain Size Analysis

Grain size analysis was accomplished through a combination of field and laboratory techniques. The bulk of samples were taken from the near surface matrix of exposed diamictons. Up to three 1.5 kg samples (weight of <16 mm fraction) were collected for units exposed in each 500 m to 1 km section from 1861, 1975, 1995E, 1995R, 1999 and 2007L lahar deposits. The distribution and number of these samples within each segment varied due to accessibility and presence of terraces within a given region (Appendix A.1.1). Matrix was defined as material below 16 mm and samples were typically taken 20 cm from the top of the deposit. All samples were put through a -4 phi sieve (16mm) in the field and coarser material was measured and weighed using a hanging scale (up to 64 mm)(Fig. 3.1). The samples were then wet sieved in the laboratory from 16 mm at half phi intervals to 0.125 mm.

The fraction below 0.125 mm was separated for analysis by Laser Sizer for particle size and XRD for clay mineralogy. Minor discrepancies occur between physical sieving and particle size analysis. Sieve data are obtained in weight percent and based on the smallest dimension of a particle. The Laser Sizer measures particle size assuming an idealised sphere and recorded in volume percent. The results can be compared by converting volume percent to weight percent, if the total weight of the fine fraction is known. Statistical analysis of grain size distribution results and grain size nomenclature were conducted according to the standard established by Folk (1980; Table 3.3).

Fig. 3.1 >-4 phi grains removed from a matrix samples. 1.5 kg samples (weight of <16 mm fraction) were collected of diamicton matrix, >16 mm clasts were separated, measured and discarded in the field. A -4 phi sieve was utilised to remove the coarser fraction.

Table 3.3 Grain size nomenclature abbreviations (Folk 1980).

Abbreviation	Meaning
M	mud[1]
S	sand
mS	muddy sand
gS	gravelly sand
gmS	gravelly muddy sand
mG	muddy gravel
sG	sandy gravel
msG	muddy sandy gravel

The use of () indicates minor quantities
[1] mud= silt +clay. Whangaehu sediments are clay depleted, having a lower limit of 0.016 mm (fine silt).

The larger grain size fraction was quantified in the field. After the 2007L lahar, field sieving was conducted by a team from the University of Hawaii for clasts from 16 mm to 512 mm using 800 to 1200 kg samples (only 1861, 1975, 1995E, and 2007L). A set of three sieves were constructed from garden trays for 16 mm, 32 mm and 50 mm fractions. Clasts over 64 mm were measured by hand and all fractions were weighed using a battery operated scale. The <16 mm fraction was collected and sieved in the laboratory and compared with initial matrix analyses.

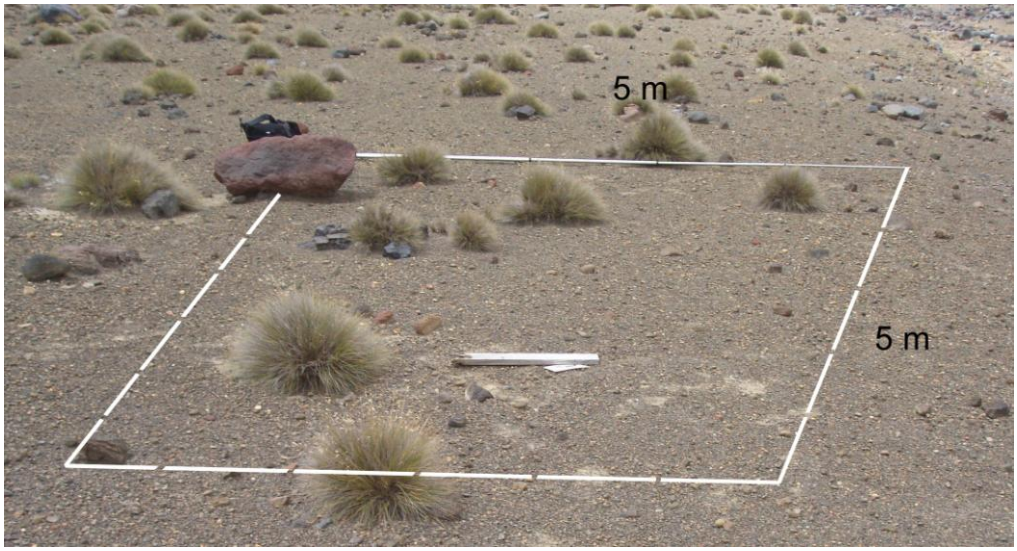

Fig. 3.2 Upper grain fractions of historic lahar deposits were measured in the field. **A.** A 25 m^2 grid for measuring outsized clasts (clasts greater than 6 cm in diameter) on historic lahar terrace surface (1975 deposit 7 km from Crater Lake). **B.** Maximum clast size measurement (3.46 m) in 1975 6.5 km from Crater Lake.

Maximum clast size point counts were conducted on terrace surfaces to establish the range of clasts in bedforms. These counts were conducted in 25 m^2 grids and included all grains > 7 cm as a limit of practical measurement (Fig. 3.2). Additional outsized clasts, entrained in the deposit or on the surface, were also measured to establish the competence of the flow. Maximum clast size observations include both clasts carried by the flow and those that are dragged, or stranded from previous deposits. Entrained clasts were identified as suspended in the deposit, but still incorporated into the matrix.

Clast density was measured for andesite lithics, scoria, Crater Lake sediment and hydrothermal alteration products. Samples were coated in parafilm and weighed using a Jolly Balance.

15 samples from the 2007E lahar were collected in 2 litre ice cream containers while the deposit was still frozen (Fig. 3.3). The samples were collected from three identified units along two transects perpendicular to flow direction. Using the known volume of the container and the mass of the sample the bulk density of the initial deposit was calculated. Additionally, the melt water was analysed for Cl^- and Mg^+ to determine the contribution of Crater Lake water relative to snow in the deposit.

Fig. 3.3 Frozen samples from 2007E lahar deposit in 2 L ice cream containers.

After the snow component had completely melted in October/November, 2 matrix samples of 2007E were collected in the same fashion as the pre-2007E deposits, for preliminary comparison of GSD.

3.2.2 Componentry

A generalised lithology was described in the field, and systematic matrix componentry was completed on the GSD samples from fine pebbles (8 mm) to medium sand (0.5 mm) for all units sampled. Comparisons of lithology were completed from both ends of the study area (7 to 9 km from Crater Lake) to identify any variation with downstream progression. Because of limited exposure only one sample from the 1861 deposit was described. Samples from 2007E were compared from one location (8 km from Crater Lake) because of the slow rate of

melting. Grain mounts were made for the +2 or (0.25 mm) fraction to help with mineralogical identification.

Clast petrography was studied for several interesting clast types and scoria varieties to aid with deposit identification and correlation with sediment sources.

X-ray diffraction (XRD) analysis of the <3 phi fraction of each unit was utilised to determine the presence of clay minerals. Clay mineral identification relied on previous mineralogical analysis by Nairn et al. (1979) and Cronin et al. (1997c). XRD analysis was also conducted on crystals of interest found in the matrix, clasts of lake sediment and the muddy portion of the 2007 mud coating.

3.3 Manning's n calibrations

Revised flow depth and flow path geometry derived from field investigations and the 2006 and 2007 LiDAR have potential for improving instantaneous velocity and peak discharge calculations. A calibration of Manning's n was based on the historic lahars in the Whangaehu Gorge. Between the convergence (6.0 km) and the RTMT Bridge (7.0 km) the gorge is steep sided and fairly straight with significant accumulations of historic lahar deposits. Flow path geometries and flow thickness estimates were derived from field investigations and the 2006 and 2007 DEM of the gorge. Historic aerial photographs were used to measure the peak flow stage from high water marks through the RTMT region for the 1975 and 1995E.

The peak discharge of the 1975, 1995E and 2007L lahars was calculated using a Manning's equation derived velocity estimate, where multiple values of Manning's roughness coefficient between 0.1 and 0.01 were used for comparison with previous discharge calculations. The Manning's equation is derived from the relationship between the slope, geometry and roughness of the flow path:

$$V = \frac{1}{n} \times S^{1/2} \times R^{2/3}$$

Manning's n is a unitless coefficient of roughness determined from empirical testing (Chow 1959). The slope (S) is measured in m/m and an average of 0.01 was used for the Whangaehu Gorge. The hydraulic radius (R) is derived from the cross-sectional area of the flow path, which can be treated as a trapezoid where:

$$A = \frac{(x + w)}{2} \times d$$

The flow depth (d), the width of the active channel (x), and the width of the deposit surface (w) were measured from the 2006 and 2007 DEMs. The relationship between the area (A) and the wetted perimeter (P) of the flow path is the hydraulic radius (R):

$$R = A / P$$

The instantaneous velocity derived from Manning's equation (above) can be used to calculate discharge for that same point, where:

$$Q_p = V \times d \times w$$

Q_p = discharge
V= velocity
d = stage height/ flow depth
w = width of the channel
or

$$Q_p = V \times A$$

V = velocity
A = cross-sectional area

The Whangaehu Gorge is well suited to Manning's equation estimates as discharge calculations are dependent on trial and error calibration based on detailed knowledge of the flow path (Pierson 1995), which were established by this study and the two LiDAR data sets.

3.4 Limitations

Field work was interrupted by the Crater Lake outburst flood lahar on March 18, 2007. The erosion caused by this event created excellent exposures of the internal structure of some of the larger historic terraces (e.g. 1975). However, the aggradation, up to 12 m in some locations, resulted in the burial of smaller terraces. A second phase of field work began following the September 25, 2007

phreatic eruption. Final observations of the valley occurred in December 2007 after the 2007E deposits had melted.

Field observations, sampling, and mapping were influenced by safety concerns both prior to and immediately following the 2007L and 2007E lahars. Certain steep walled gorges were deemed unsafe and were not included in the study area (upstream of the convergence <6.0 km from source and >9 km in the chute). Aggradation resulting from the 2007L lahar allowed access to certain terraces of 1975 and 1995E that were initially deemed unsafe, however, sampling and descriptions of the 1995R and 1999 lahar deposits were limited to pre-2007L observations as burial and erosion removed remaining exposures of the deposits.

Chapter 4 Distribution of historic lahar deposits in the Whangaehu Gorge and Fan

Lahar deposits are poorly preserved in steep terrains. In the Whangaehu Valley this is accentuated by the constrained geometry of the gorge and the frequency of lahar events within the valley. Initial deposit distribution can be described in terms of the surface area of a deposit and deposit thickness. The area inundated by a lahar directly correlates to the extent of deposition. The distribution of historic lahars in the Whangaehu Valley and Fan were constructed from field mapping and aerial photographs. Terrace thickness was measured directly in the field and supported by the 2006 DEM of the Whangaehu Valley (Fig. 4.1). Fluvial and laharic sedimentary accumulation were mapped for periods between 1940-1950, 1950-1954/55, 1975-1980, 1980-2000, 2006-2007 (Table 3.1) using the archival vertical aerial photographic record of eastern Ruapehu, and when possible remnant deposits from the gorge (Fig. 4.2 (separate) and Table 4.1).

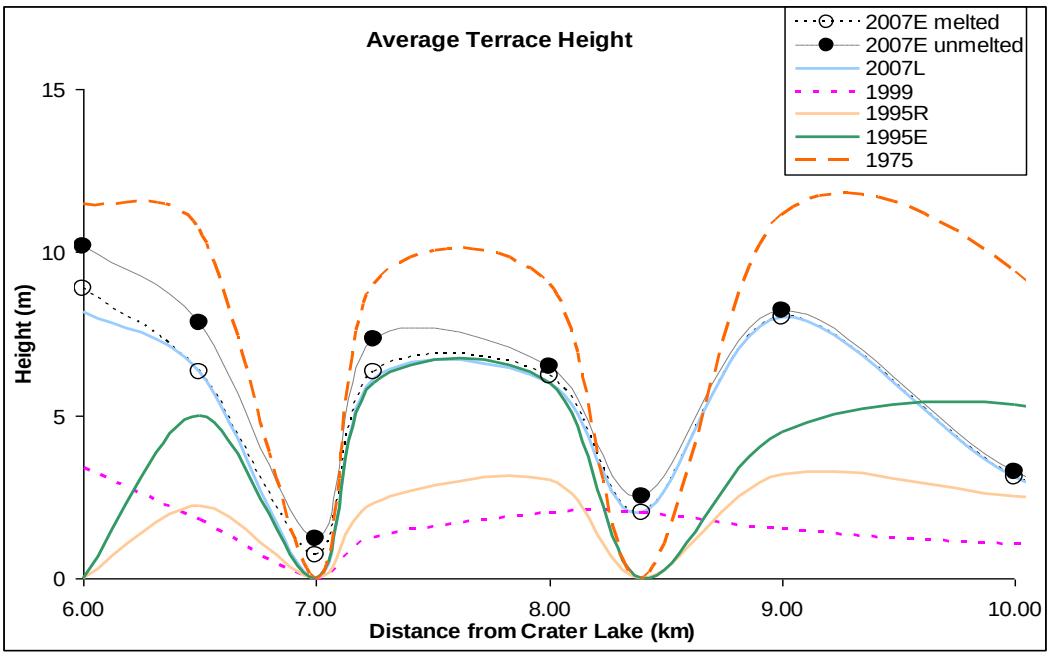

Fig. 4.1 Average historic lahar terrace heights with distance from Crater Lake. Terrace height changes significantly with the geometry of the flow path, as is evident at 7 and 8.4 km from Crater Lake which coincide with decreased valley width. The height of the active channel changed with the emplacement of the 2007L deposits. 2007E deposits were emplaced on top of the 2007L terrace. Unmetled 2007E deposit were ≤ 2 m thick. Melted deposits were ≤ 0.7 m thick.

The use of photographic records is limited by their coverage and the timing of the photographs relative to the events. The time lag between emplacement and available photos can result in various levels of deposit alteration, but most importantly, the contrast between a fresh deposit and the surrounding land surface decreases rapidly after emplacement. The greatest contrast is between the colour of fresh deposits versus older units, caused by saturation, muddy coatings and sulphur, and a decrease with exposure and precipitation following deposition. Dewatering and deposit collapse also result from the initial instability of lahar deposits. The volcaniclastic Whangaehu Fan is highly permeable and is a major source of fluid loss during flood events and lahars (Manville 2004). As a result, the fan is the location of most significant change following deposition. The 2007L and 2007E lahar deposits are well documented examples of the evolution of fresh deposits with time (see section 5.8).

Table 4.1 Historic lahar inundation areas as calculated from aerial photographs.

Event	Inundation Area
1945	$3.0x10^3m^2$
1954	$1.7x10^6m^2$
1975	$5.0x10^6m^2$
1995E	$4.0x10^6m^2$
1995R (deposit only)	$1.9x10^4m^2$
1999 (deposit only)	$5.1x10^4m^2$
2007L	$3.7x10^6m^2$
2007E	$1.1x10^6m^2$

Prior to March 18, 2007, five lahar deposits were identified in the Whangaehu Gorge corresponding to the 1861, 1975, 1995E, 1995R and 1999 events. These older lahar deposits in the gorge were incised and partially buried by the March 18 lahar, which left behind a new complex set of isolated terraces (Fig. 4.3 a-c; 4.4). The volumes of 1995 diamictons were significantly reduced and the 1999 deposits were completely removed by the 2007L lahar. Following each lahar the active channel returned locally to the level of underlying bedrock, which can be a rapid process in locations of high erosion. Within a month following the 2007L lahar the river channel had exposed bedrock over a substantial portion of the active channel bed. In September 2007 a snow slurry lahar buried the 2007L deposits with a thin deposit reaching up to 70 cm, 2007E (Fig. 4.5).

Historic lahar inundation areas

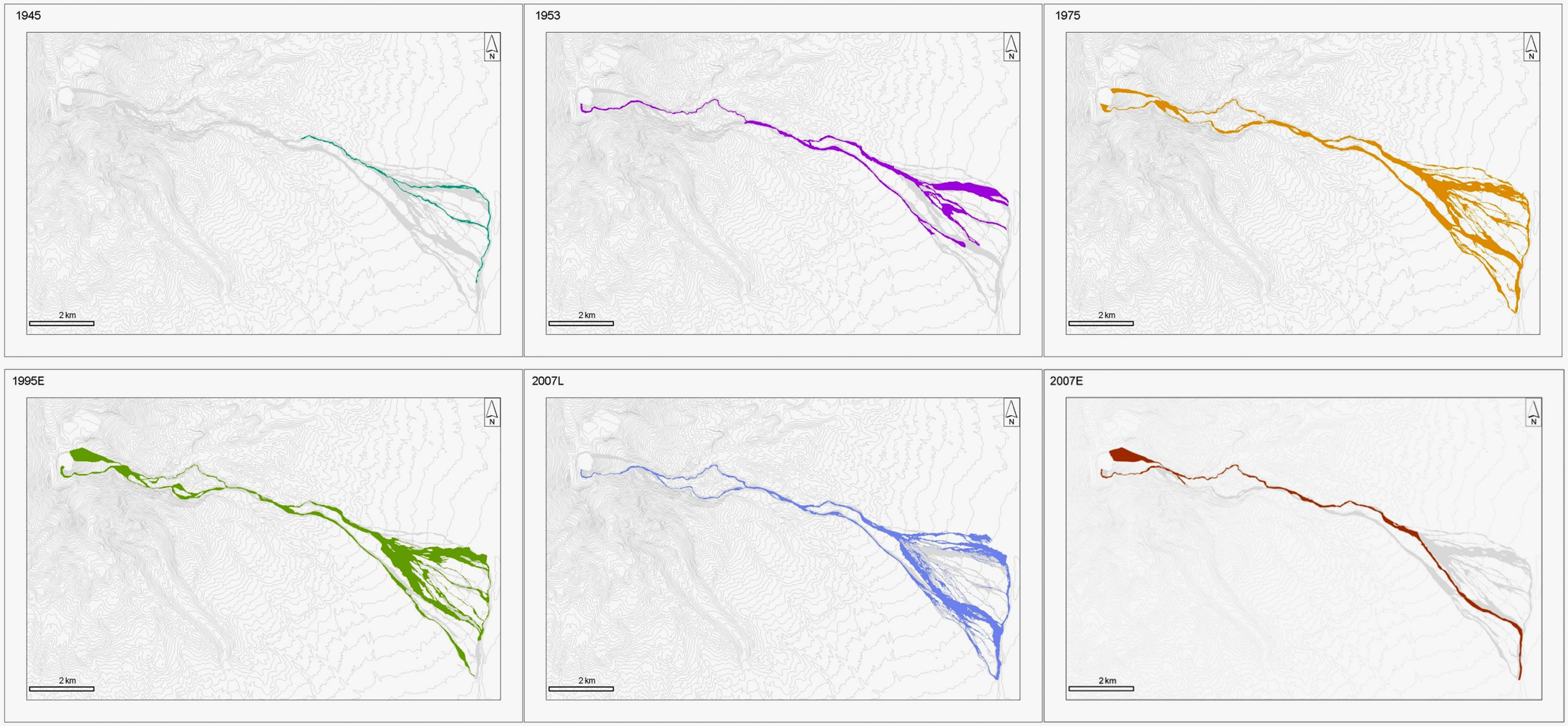

Fig. 4.2 Comparison of historic lahar inundation for the first 17.5 km of the Whangaehu Valley. Inundation area has been measured from historic aerial photos. 1945 inundation represents the area altered by the progressive displacement of lake water between 1940 and 1950. Photographic record does not extend closer than 9 km to Crater Lake. 1954 inundation area is an underestimate caused by the delay between emplacement and photograph. 1995 inundation for eruption-generated lahars only. The distribution of lahar deposits in the southern branch reflects high volume lahars and/or eruption-generation routing.

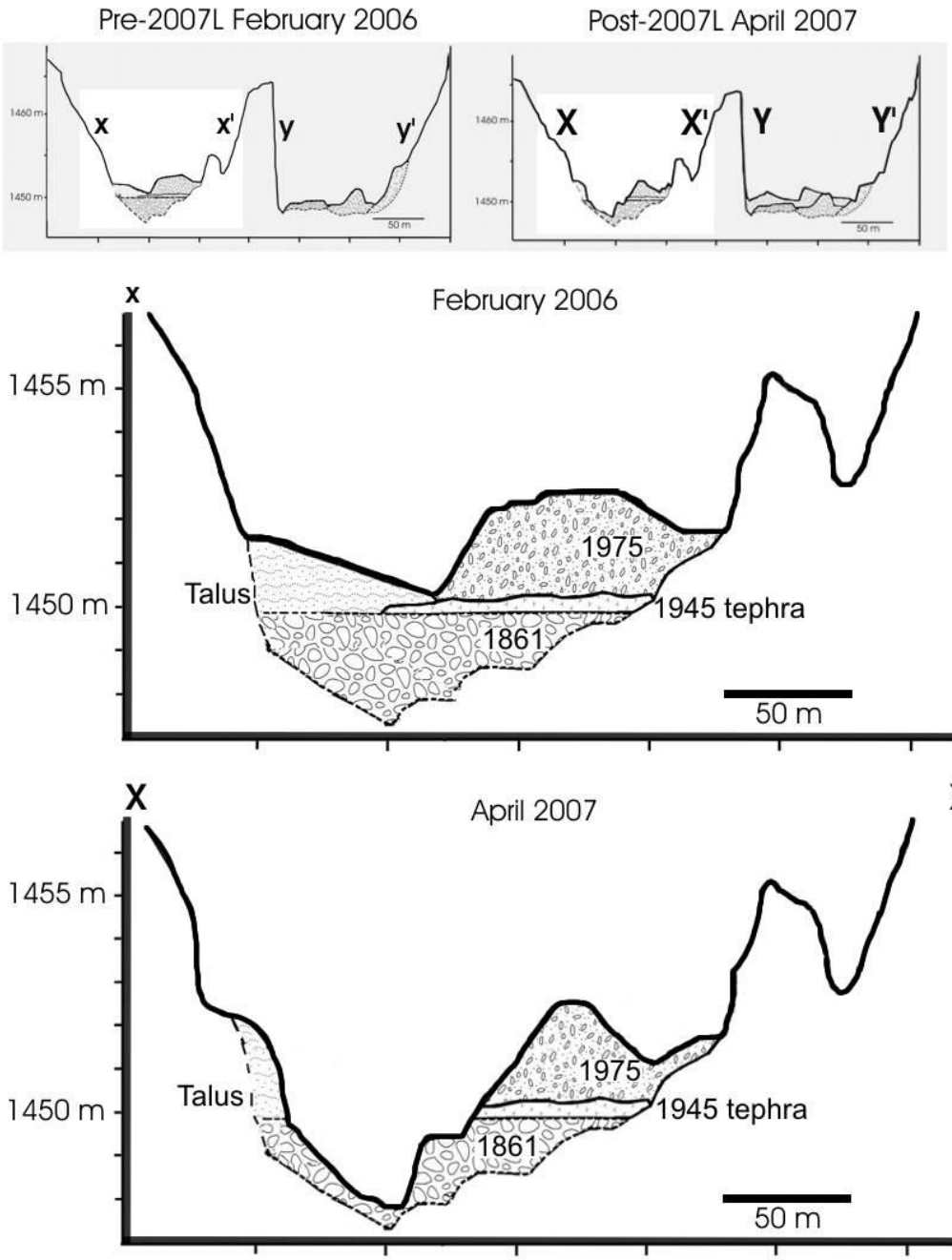

Fig 4.3a Comparison of terrace configuration before (x-x') (February 2006) and after (X-X')(April 2007) the 2007L outburst lahar. Cross-section through overflow channel (the spillway) (7 km from Crater Lake). Flow direction is out of the page. Profiles constructed from LiDAR based DEM. LiDAR courtesy of GNS and Massey University.

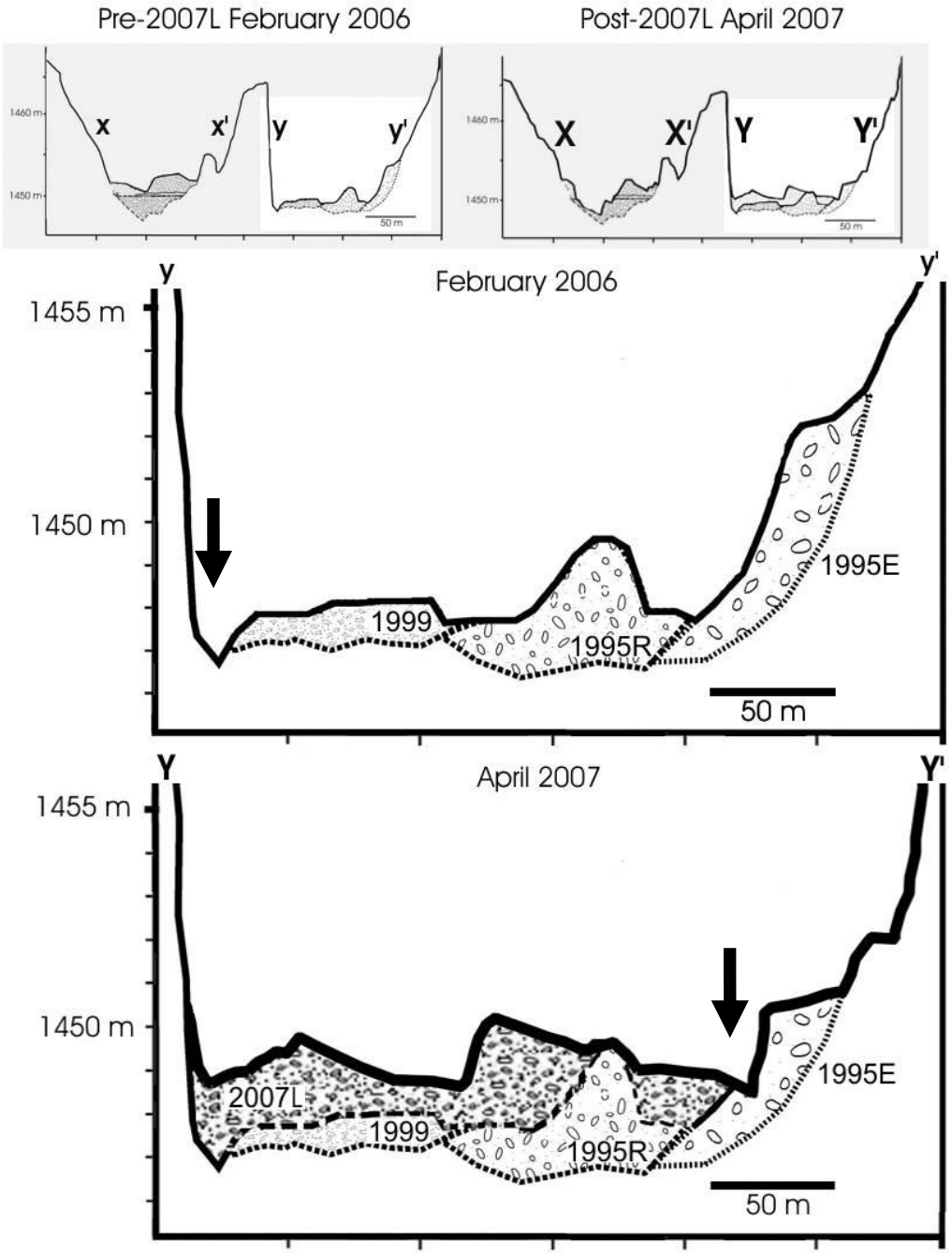

Fig. 4.3b Comparison of terrace configuration before (y-y') (February 2006) and after (Y-Y') (April 2007) the 2007L outburst lahar main northern channel of the Whangaehu Gorge near the RTMT (7 km from Crater Lake). Significant aggradation by the 2007L lahar buried deposits from 1999 and 1995R. The position of the active channel is indicated. By May 2007 incision by normal outflow exposed bedrock. Flow direction is out of the page. Profiles constructed from 2006 and 2007 LiDAR based DEM. LiDAR courtesy of GNS and Massey University.

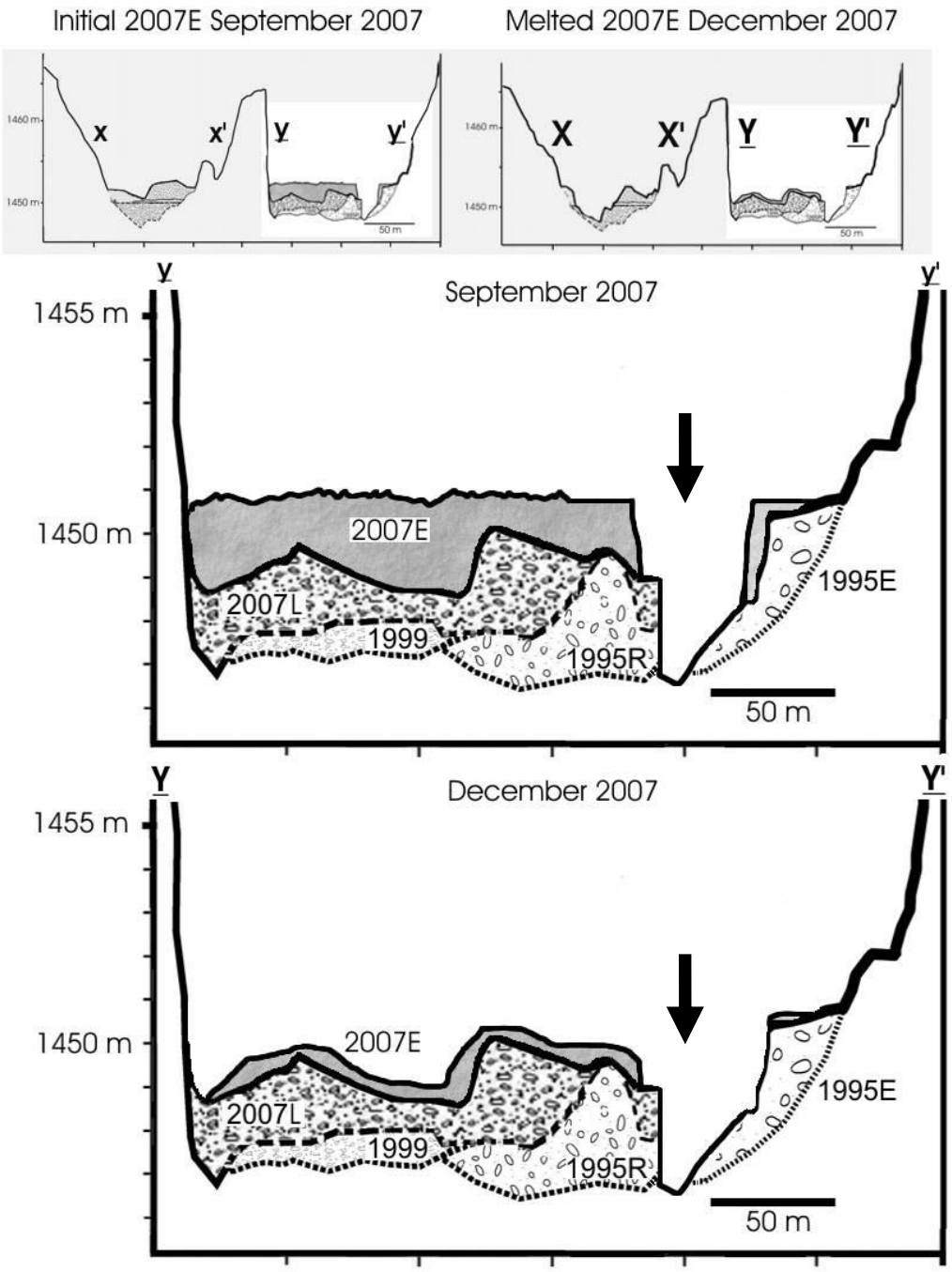

Fig. 4.3c Comparison of terrace configuration following the September 25, 2007 eruption generated snow slurry lahar before (y-y') and after (Y-Y')(December) melting. Bedrock exposure along active channel occurred prior to the emplacement of the 2007E deposits. The initial deposit displayed two types of surface texture, ropey and smooth (along eroded channel). Flow direction is out of the page. Profiles constructed from 2007 LiDAR based DEM and field measurements. LiDAR courtesy of GNS and Massey University.

Historic lahar terrace distribution in the Whangaehu Gorge, April 2007

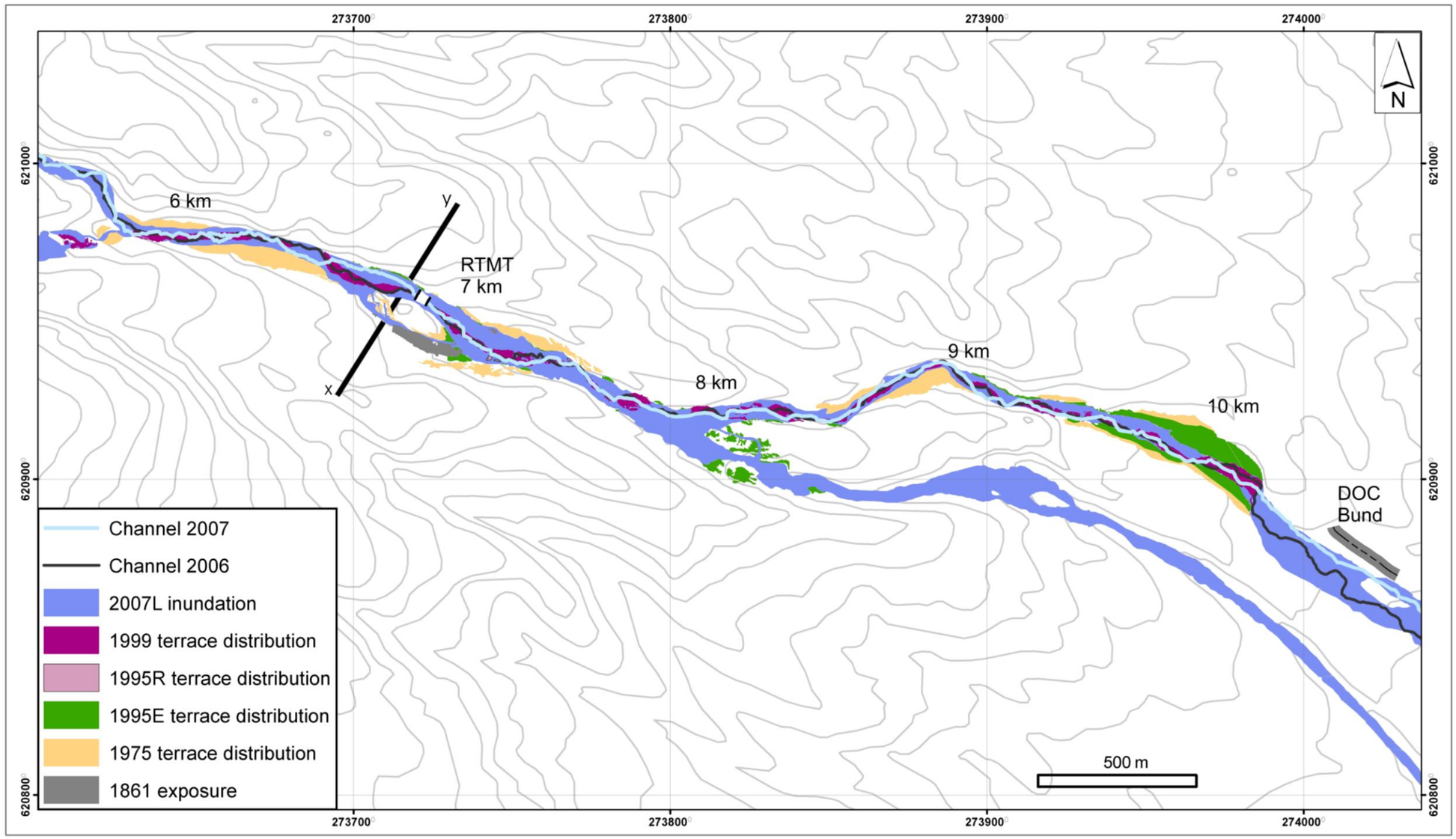

Fig. 4.4 Distribution of historic lahar terraces in the Whangaehu Gorge in April 2007. The 2007L deposits include high water marks that were still distinguishable one month after deposition. Significant erosion of the 1995E, 1995R, and 1999 terraces occurred. Erosion through the spillway increased the exposure of the 1861 diamicton. X-Y section line for Fig. 4.3 b.

Historic lahar terrace distribution in the Whangaehu Gorge, September 2007

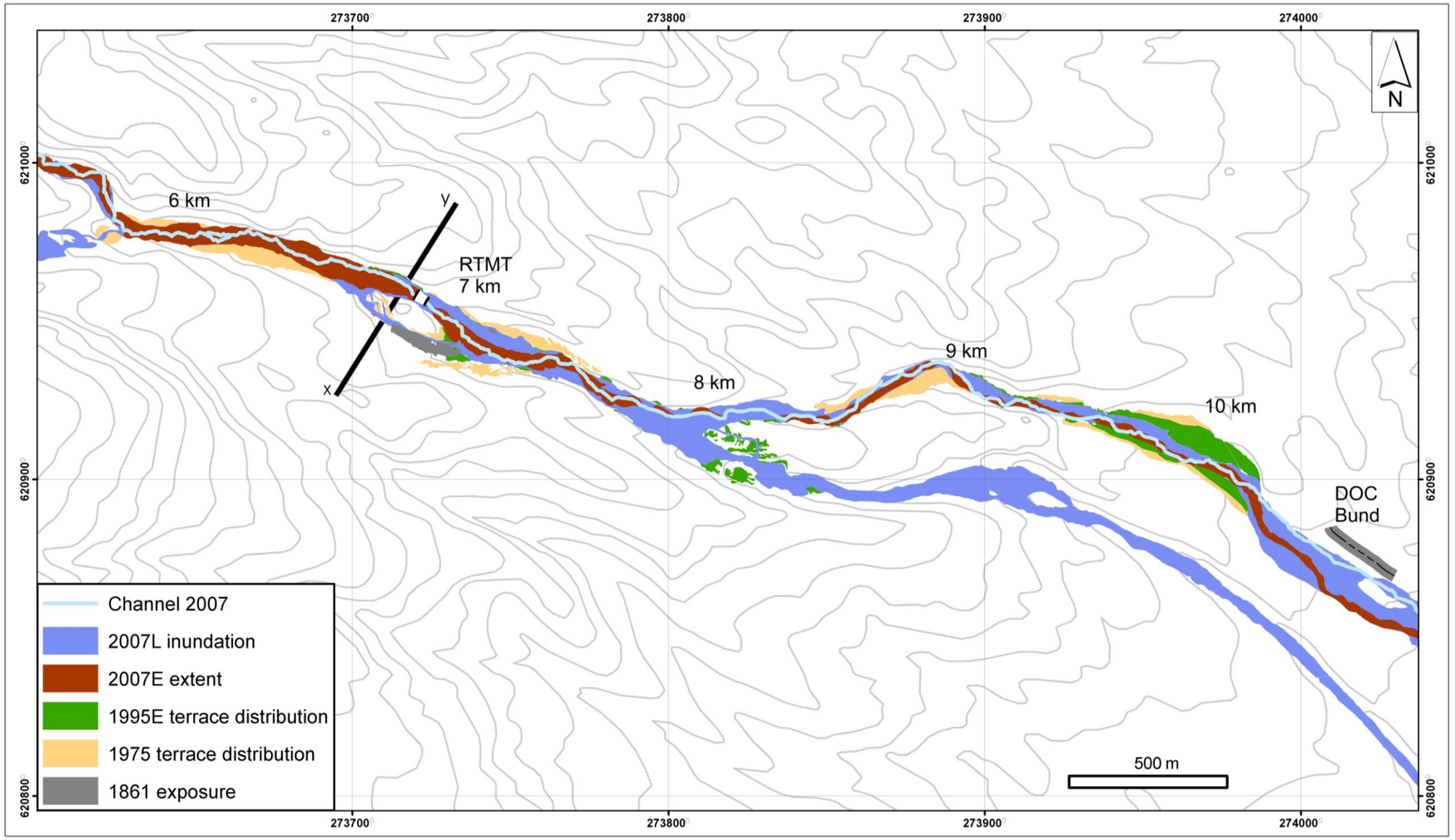

Fig. 4.5 Distribution of historic lahar terraces in the Whangaehu Gorge in September 2007. The 2007E deposits overtopped 2007L deposits, but were confined to the northern branch.

4.1 Lahar inundation area

Although there was no discrete lahar associated with the 1945 eruption, between 1940 and 1950 there were significant changes in terrace morphology in the lowest portions of the gorge (8 to 11 km) associated with displacement of Crater Lake water as a result of dome growth. The upstream impact during this time was not recorded as the photographs from this period begin 8 km from source. Just above the fan apex, 9 km from source, the channel shifted between 0.1 and 30 metres within the valley and a low terrace was developed by 1950 (Fig. 4.6). Significant transformation of terrace morphology occurred over an area of $3.0x10^3 m^2$.

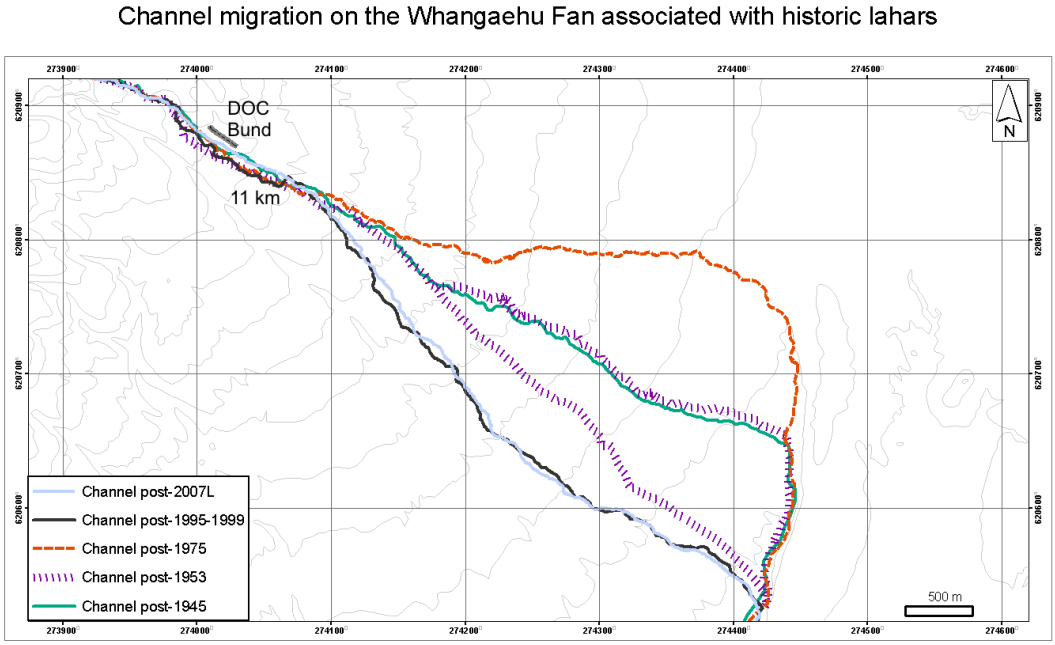

Fig. 4.6 Channel migration in the Whangaehu Valley associated with historic lahars. Channel positions are obtained from historic aerial photograph comparisons.

Between 1950 and 1954/55 the channel position again moved up to 30 metres but the alteration to terrace distribution was more striking, as a result of the 1953 Crater-Lake break-out Tangiwai lahar. A new terrace level was established in addition to a decrease in the size of existing terraces. The area inundated by the 1953 lahar was up to $1.7x10^6$ m^2, but the lahar only cut narrow channels through the central fan. While there is evidence for relocation of boulders in the chute, there are no significant accumulations of sediment.

The period between 1955 and 1975 was not associated with any major lahar events. Eruptions in 1966, 1968, 1969 and 1971 only resulted in the ejection of small volumes of Crater Lake water in the Whangaehu catchment. The events were observed and obliquely photographed in the Whangaehu Valley, but did not leave significant deposits within the gorge or on the fan. In this twenty year period, the channel shifted position in the gorge up to 20 metres laterally and the terraces decreased in size, but did not change in shape. Alterations to the fan were not significant enough to be observed in the photographs.

The deposits of the April 24, 1975 lahar in the Whangaehu Valley were recorded immediately in various oblique photo series. Vertical photographs were not obtained until 1980. These large scale photos, however, provide excellent detail of the large valley-wide terraces of the eruption generated event. Snow rafted on the surface of the deposits stand out on immediate post-event photos. Additionally, oblique photos of the upper gorge (6-7 km from source) recorded the high-water marks. The deposit's characteristic large scale bars and bedforms are visible in the vertical aerial photographs. On the Whangaehu Fan the main fan channel shifted 2 km to the north reactivating a pre-existing channel along the top of the fan. The total area of valley and fan that was inundated by the 1975 flow was the highest of the historic lahars, covering an area of $5x10^6m^2$. By 2007 the terraces emplaced by this flow had been decreased to an area of only $1.5x10^5m^2$ (Fig. 4.7). Within the gorge, syn-event landslides were incorporated into and deposited material on top of the 1975 lahar terraces. The slides triggered by undercutting and reactivation of older landslips were derived from the gorge walls and occurred at 6.5 km and 9 km from source. Although not documented, a large frequently activated landslip 500 m below the channel outlet may also have contributed to the 1975 lahar volume.

Between 1980 and 2000 the vertical photographic record is limited, but the 1995/96 eruption sequence and associated lahars are very well documented in ground and aerial oblique imagery. The variability of the valley during this period of heightened lahar activity was recorded, but not with enough detail to map short term variation in channel position and terrace distribution. A LiDAR survey and orthophotograph survey was collected in February of 2006 in preparation for the 2007 Crater Lake release lahar. The images from 2006 provide far better resolution (0.18 m GSD) than the images of 2000. Since no significant events

were recorded in the valley in the six years between photo series, the 2006 orthophotos are used in preference over the earlier images.

The emplacement of the 1995E terraces can be isolated in the 2000 and 2006 photos, but the 1995R and 1999 events are more difficult to differentiate. The 1995E lahar followed many of the same channels through the fan as the 1975 lahar, affecting a slightly smaller area of $4x10^6m^2$. However, the active channel moved to the southern fan after river stage returned to typical levels. Erosion by the 1995E lahar is evident in the decreased size of the 1975 terrace and 1975 syn-event landslides. The 1995E terraces were eroded and reduced in size by the remobilisation lahars (Fig. 4.8). The 1995R and 1999 deposits were subject to continued processing by normal fluvial action of the Whangaehu River as the distribution of 1995R and 1999 terraces, prior to the 2007L lahar, were confined to the active channel region (Fig. 4.9). Prior to March 18, 2007 the distribution of 1995R deposits had decreased to $1.9x10^4m^2$ and the 1999 deposits covered only $5.1x10^4m^2$.

A second LiDAR survey and orthophoto survey was obtained on 6 April 2007 to complement the pre-event data of 2006. Even 3 weeks after emplacement the high water marks of the 2007L lahar were still distinguishable along a large portion of the flow path. The deposits were emplaced in an erosionally widened channel through existing terraces, and caused repeated migrations of the active channel (Fig. 4.4). The final location of the active channel continued to change for at least the first three months after deposition. The 2007L lahar caused up to 12 m of aggradation in certain locations throughout the valley and 3 m of erosion in others. The erosion caused by the 2007L lahar significantly reduced the size of the marginal historic lahar terraces throughout the gorge, but did not completely scour the valley prior to deposition. Remnant terraces that have been eroded, but not completely removed occur sporadically throughout the valley and measure up to 15 m long by 10 m wide (see Chapter 5). Remnant terraces are mostly, but not always associated with boulders stranded just upstream of the preserved terrace. The area inundated by the 2007L lahar was similar to the 1995E lahar, measuring $3.7x10^6m^2$. The flow path was significantly different in the top 3 km of the gorge. On the Whangaehu Fan the flow was diverted to the edges, reactivating channels from 1975 and 1995 (Fig. 4.6). The post-event 2007L channel position did not shift drastically on the fan and only a few minor changes occurred in the gorge.

Comparison of 1975 lahar initial inundation and terrace distribution in 2006 and 2007

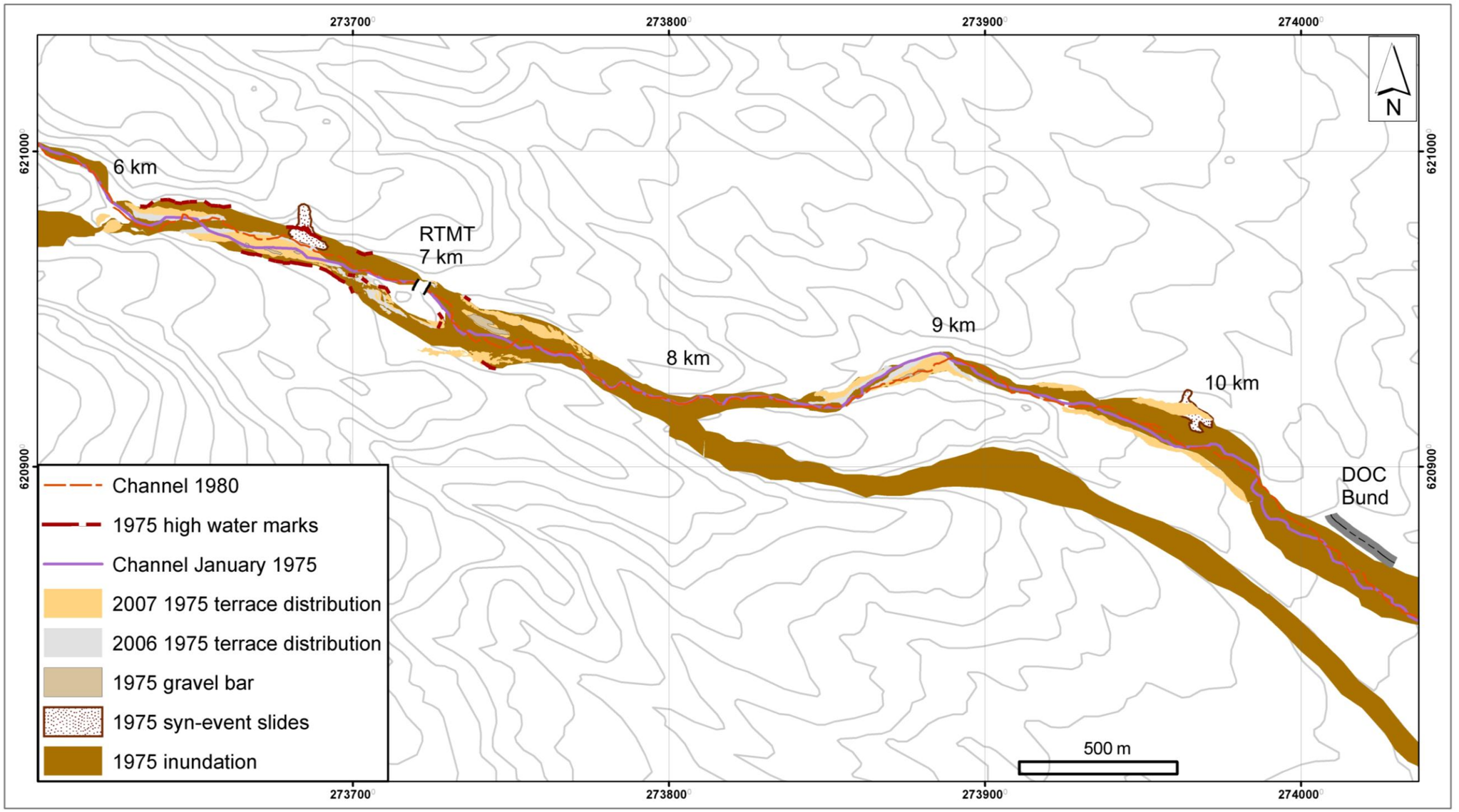

Fig. 4.7 Comparison of 1975 lahar inundation, 2006 and April 2007 terrace distribution. Pre- and post-1975 channels, high water marks and syn-event landslides are included. Minor erosion of the 1975 terraces occurred as a result of the March 18, 2007L lahar. No significant alteration occurred as a result of September 25, 2007E lahar.

Comparison of 1995E lahar initial inundation and terrace distribution in 2006 and 2007

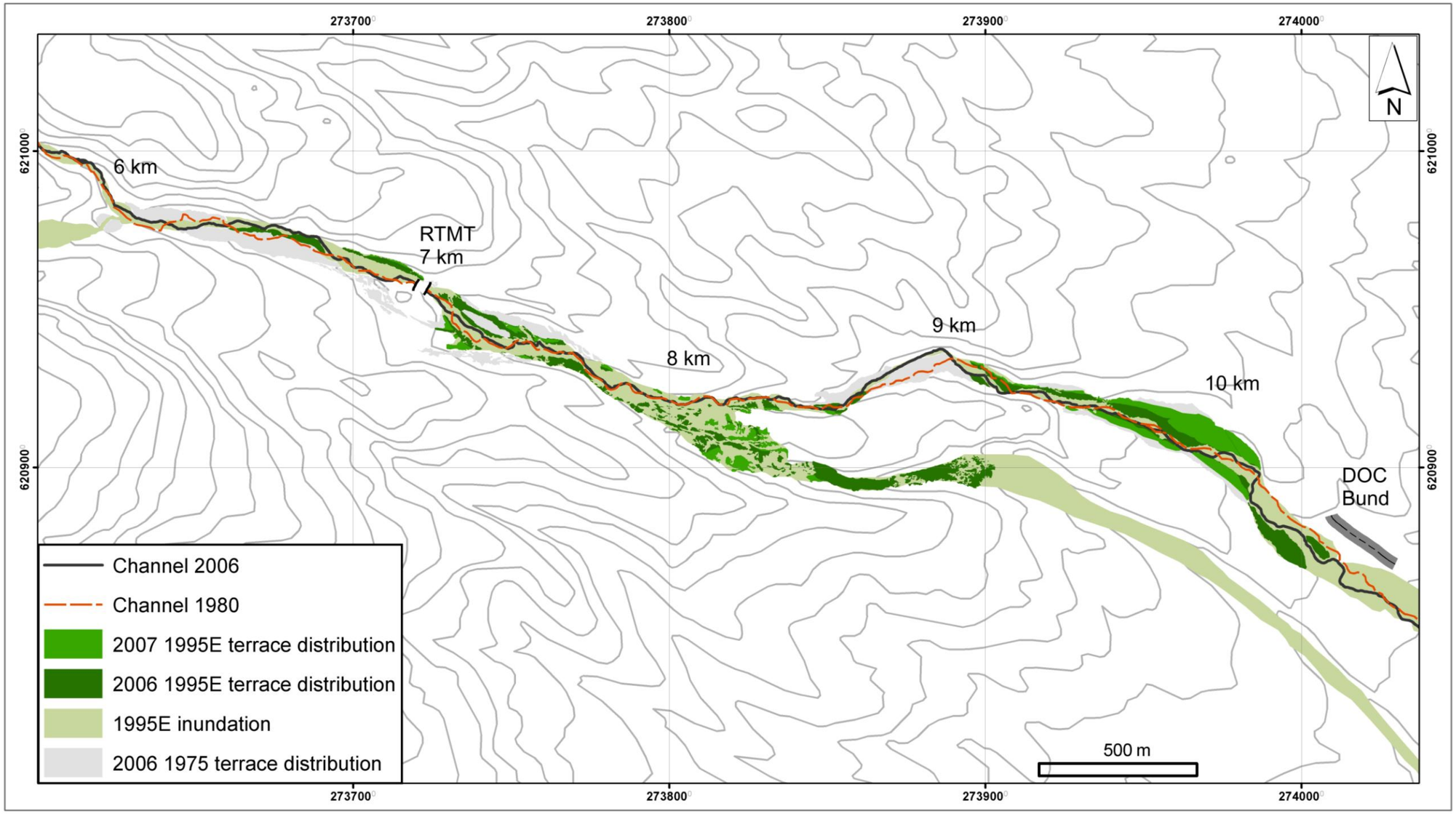

Fig. 4.8 Comparison of 1995E lahar inundation, 2006 and April 2007 terrace distribution. 1980 channel serves as a pre-event comparison to the post-event 2006 channel. Significant erosion of the 1995E terraces occurred as a result of the 2007L lahar. The 1995E terraces were overtopped by marginal deposits of the September 25, 2007 eruption-generated lahar, with no significant alteration.

Comparison of 1995R lahar initial inundation and terrace distribution in 2006 and 2007

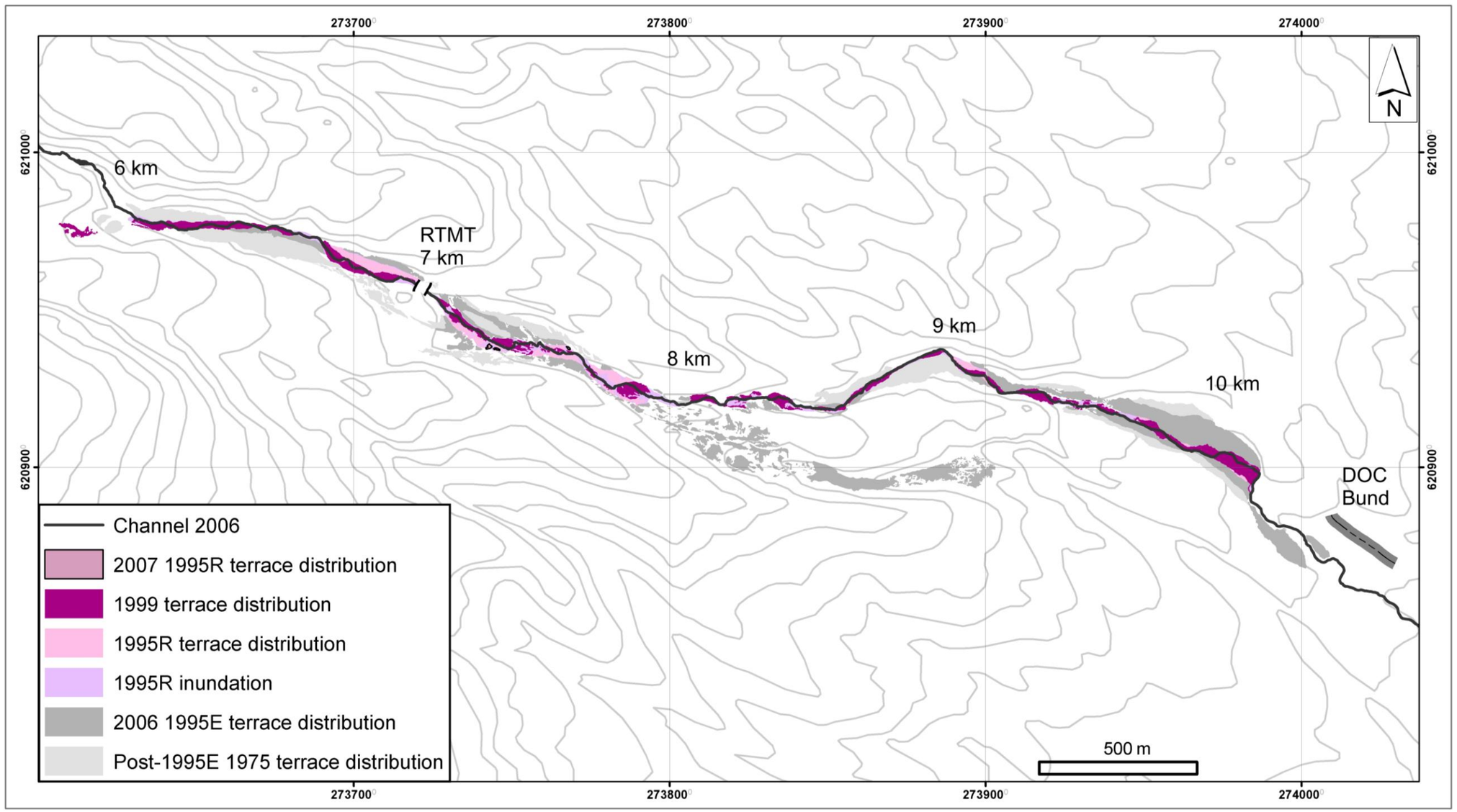

Fig. 4.9 Comparison of 1995R lahar inundation, 2006 and April 2007 terrace distribution. 1999 terrace distribution in 2006 is included. Changes in channel position in this period were not documented. Effective removal of the 1995R and 1999 terraces occurred as a result of the March 18, 2007L lahar.

A comparison of the 2006 and 2007 LiDAR revealed an inconsistency in the relocation of outsized clasts (over 200 cm) by the 2007L lahar. Anomalously large boulders (5 m in diameter) located near the active channel, outwardly part of the 1999 lahar deposits, were either buried or relocated by the 2007 flow. Aggradation 7 km from Crater Lake was between 50 to 500 cm above the height of these boulders. In marginal channel locations, where aggradation was less, outsized clasts between 3 and 6 m in diameter were eroded around, but not transported by the flow. At comparable distances downstream of these immobile remnant clasts, boulders of similar sizes were rafted on top of 2007L deposits after remobilisation. The transport distances for boulders of the order of 3 m in diameter exceeded 50 m downstream.

A snow slurry lahar on September 25, 2007 inundated the Whangaehu Gorge up to 2 m overtopping the 2007L deposits. The small volume lahar spread out on the Whangaehu Glacier and was routed onto the topographic divide at 2.5 km from Crater Lake, but did not travel significantly through the southern branch. Throughout the northern branch the 2007E flow remained confined to the pathway eroded by the 2007L lahar. Although the deposit melted rapidly, evidence of snow transported by the flow was observed up to 24 km from Crater Lake. After melting, the area inundated by the 2007E lahar was buried by a thin deposit reaching 20-70 cm in thickness. A broad active channel was eroded into the 2007E deposits revealing the gravelly surface of the 2007L deposit. In September 27, 2007 1.1×10^6 m^2 of deposit was measurable in the gorge. Melting throughout the months of October and November created isolated pockets of sediment that was subject to removal by rain, snow melt and fluvial processing as a result of the low position of the deposits relative to the active channel. By December the deposit had fully melted and only minor marginal exposure remained.

Chapter 5 Sedimentology of historic Whangaehu Gorge lahar deposits

The historic lahar deposits of the Whangaehu Valley were investigated over a five kilometre section of the gorge between 6 and 11 km from Crater Lake. Deposits from six lahar events were identified within this region and the sedimentology, geomorphology and distribution of each were described for each deposit. Grain size componentry analyses were conducted to document any variation with distance from source and between deposits.

5.1 1861

5.1.1 1861 Deposits

The distribution of bouldery diamictons is here identified as the deposit of the 1861 lahar limited to the region 7-8 km from Crater Lake where the Round the Mountain Track (RTMT) crosses the Whangaehu Valley. The 1861 lahar is the second recorded lahar at Ruapehu and is estimated to have been the largest in the historical sequence (Hodgson 1993). The surface of the deposit has been eroded and now serves as the marginal channel bed for younger deposits. Approximately two metres of vertical section of 1861 deposits are exposed over a 500 m^2 area in the region of the RTMT due to scour by the 2007L lahar. As a result no geomorphologic observations were possible, but the position of the deposits relative to the channel (17 m above bedrock channel) and internal structure of the diamicton reflects the larger relative size of the 1861 lahar. The 1861 lahar deposits are overlain by a tephra associated with the 1945 eruption, which is in turn buried by 1975 lahar deposits, supporting this identification.

Unlike younger deposits, the 1861 diamicton does not form terraces but is exposed as a clast-dominated, well-indurated gravel underlying more recent deposits. The nature of the contact between the 1861 deposits and all other units is erosional but presents a fairly uniform and flat surface. This contact is marked by the removal of fines and formation of a distinct clast-dominated surface (Fig. 5.1). The 1861 gravel is more indurated than younger deposits. Based on the prominence of bedrock outcrops throughout the valley the 1861 deposits are

estimated to be a minimum of 3 m thick. There is no evidence of any lahar deposits between the 1861 and 1975 and 1995E.

Erosion during the 2007L lahar increased the exposure of the 1861 gravel after the removal of a thin veneer deposit from the historic events (1995E and 1975). The resistant surface of the 1861 lahar deposit is exposed for 600 m on the south bank 7.5 km downstream of the Crater Lake, and for 400 m on the north bank underlying a 1975 gravel bar island, reflecting the initial valley-wide distribution of the 1861 lahar deposit.

Fig. 5.1 **A.** Exposure of 1861 lahar deposit in the spillway 7 km from Crater Lake with overlying 1945 ash and 1975 lahar deposits. **B. U**pper 1.6 m of the 1861 diamicton showing the clast-rich, fines-depleted surface (black arrow) exposed after the 2007L lahar on March 18, 2007, 7 km from Crater Lake.

The exposed portions of 1861 deposits reveal a very poorly sorted angular clast-dominated gravel (heavily coarse skewed), with boulders averaging 25.6 cm and very few outsized clasts that reach up to 154 cm (Fig. 5.2). The matrix is a sandy silt that comprises only about 13% of the mG (Table 3.2; Table 5.1). The lowest portions of the deposit are massive (total thickness unknown as the bottom contact is not exposed), but a crude normal grading develops in the upper metre as the matrix content increases slightly (Fig. 5.1).

Within the fan the 1861 diamicton is described as an angular to subangular andesitic gravel. As the thickest of the historic deposits, the 1861 gravel fluctuates from 0.25 to 1.2 m thick and is underlain by a 20 cm thick soil horizon (Hodgson et al. 2007).

Table 5.1 Comparison of historic Whangaehu Gorge lahar deposit grain size characteristics.

Unit	Sorting v.p.s.[1]	Max. clast size (cm)	weight % Matrix	Sediment nomenclature[3] (Folk 1980)
1861	2.95	154	13%[2]	mG
1975	2.54	450	37%[2]	msG
1995E	2.78	311	11%[2] (minimum, variable)	mG
1995R	2.85	258	30%	gmS
1999	2.45	108	40%	(g)mS
2007L	2.80	134	12- 50%[2] (variable)	sG to gS with variable mud
2007E	2.45	20	45% (snow) 55% (silt)	mS

[1] All values within one standard deviation
[2] Fagents 2007, unpublished data, courtesy of the University of Hawaii
[3] mud= silt >0.016mm in diameter

5.1.2 1861 Componentry

The lithology of the deposit is dominated by red and black scoria and lower abundances of andesitic lava. The red scoria is plagioclase-rich, and has a high density and low vesicularity; the black scoria is glassy (Fig. 5.3). The finer size fractions are dominated by andesitic glass. Some hydrothermally altered clasts and pyrite grains are present, but clasts of Crater Lake sediment are notably absent (Table 5.2).

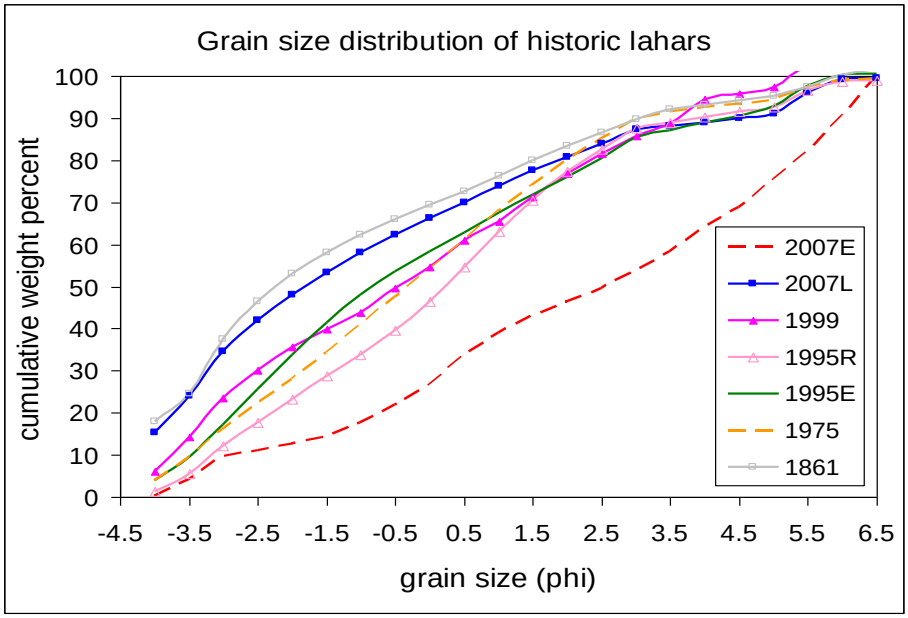

Fig. 5.2a Matrix (16 mm to 0.008mm) grain size distribution for historic diamictons preserved in the Whangaehu Gorge

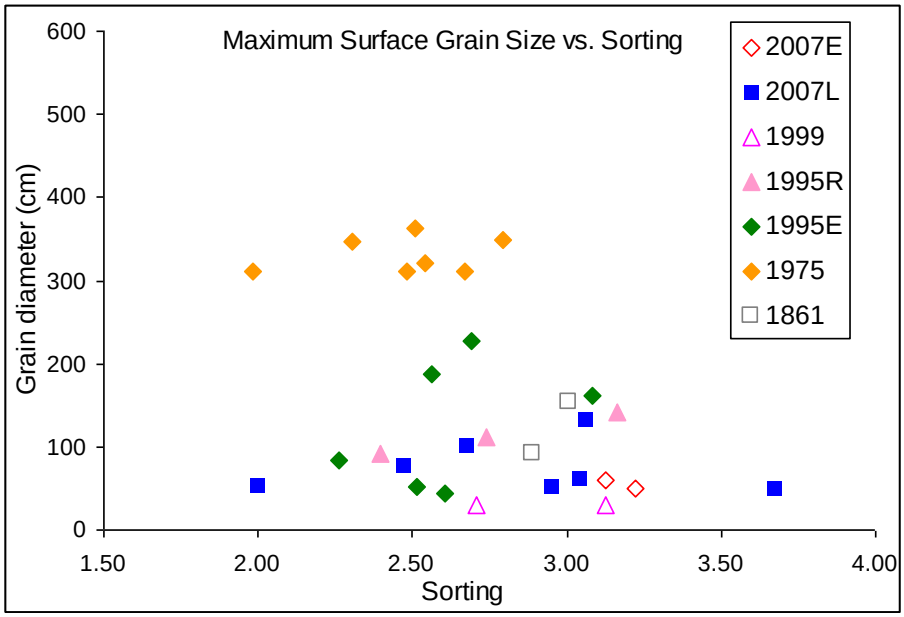

Fig. 5.2b Comparison of maximum grain size and matrix sorting for historic lahars in the Whangaehu Gorge. All deposits fall within the same range of very poorly sorted distributions.

5.2 1975 lahar

5.2.1 1975 Deposits

Deposits of the 1975 lahar are generally massive, matrix-supported, very poorly sorted diamictons with abundant outsized clasts up to 450 cm in diameter. Texturally the deposit varies greatly, displaying multiple lenses with indistinct contacts. These lenses vary in grain size and colouration between dark grey and dark brown and can be traced up to 10 metres downstream. Within these lenses occasional crude grading is present. Some units even display an openwork, fines-depleted, structure (Fig.5.4). The upper portions of the deposit are similar to stacked braided stream deposits, and are dominated by subangular clasts and slightly rounded scoria.

The msG is dominated by medium pebbles and medium silt, but has fluctuating sand content. Clasts over 16 mm compose less than half of the deposit by weight, resulting in a mildly coarse-skewed diamicton with outsized clasts up to 450 cm in diameter. The 1975 deposits have a low mean grain size but contain the largest outsized clasts of any lahar deposit within the gorge (Fig. 5.2a; Fig. 5.2b; Table 5.1).

Table 5.2 Generalised sedimentology of historic lahar deposits in the Upper Whangaehu Valley.

Unit	Support	Distinctive lithology	Clay	Imbrication	Clast Shape	Structure
1861	Clast	dominated by red scoria no crater lake sediment	Minor	No	Angular to subangular	Crude normal grading in lower unit
1975	Matrix	lake sediment black scoria	Minor	Semi-horizontal large clasts	Subrounded	Pulses with weak contacts; lenses of grain size concentrations lenses of weak normally graded sand
1995E	Both	lake sediment and hydrothermally altered clasts black scoria	Minor	Semi-horizontal large clasts	Subrounded	Massive
1995R	Both	altered black scoria	Minor	None	Subangular	Massive with alternating clast and matrix support
1999	Matrix	hydrothermally altered clasts	Minor	None	Subrounded	Massive
2007L	Both	lake sediment gypsum pyrite quartzite	Kaolinite	None yet observed	Subrounded to rounded	Braided stream, overlapping lenses of open work gravels, gravelly sands, and silty gravels.
2007E	Matrix	hydrothermally altered clasts sulphur gypsum pyrite		Horizontal preference of clasts	Subrounded	*Snow-rich*: two normally graded snow units with a veneer of silt. *Post-melting*: massive with snow melt structures

The best exposures of the internal structure of the 1975 deposit were revealed by bank erosion by the 2007L lahar. However, due to aggradation resulting from the same March 2007 event, only the top three metres of the deposit remain visible. Pre-2007L exposures indicated an increased concentration of cobbles and boulders with increasing depth, or crude normal grading. This lower gravelly base of the 1975 deposits can be differentiated from the 1861 by the upper contact of the gravel units. Pulse structures, common in unsteady non-uniform flow, have slight colour variations and grain size concentrations with laterally discontinuous contacts. The 1975 diamicton displays a gradational and inconsistent contact between the upper pulse-dominated and the lower gravel-dominated portions of the deposit, while the 1861 has a distinct fines-depleted clast-dominated contact. In the 1975 deposit, the appearance of pulses decreases with increasing gravel content towards the base of the deposit. Historic photos from 1995 indicate that the edges of the 1975 lahar terraces along the active channel were overtopped by thin edges of the 1995 eruption-generated lahars. However, sediments from these events cannot be differentiated from the bulk of the 1975 terraces.

In one section 7.5 km from source the 1975 deposit was exposed revealing an 80 cm-thick pebble-bearing coarse sand between two typical 1975 gravels (Fig. 5.4). The moderately sorted sand displays rounded pebble outsized clasts and definitive, but not strong, bedding with visible normal grading. The top of the pulse is marked by lenses of cobbles and pebbles.

The unit retains an even thickness before abutting a bedrock outcrop and does not reappear. The 1975 diamicton does not display consistent imbrication; however, outsized clasts are semi-horizontal (0-5 degrees) dipping upstream near parallel to stream direction, 7 km from Crater Lake.

The initial 1975 deposits were valley wide (10 to 165 metres wide), and erosion along the margins of the flow instigated syn-event landslides (at 6.8 and 8.5 km) that contributed to the flow volume and componentry. These slides are easily identified in aerial photographs and their scarps are still visible in the valley morphology (Fig. 4.5).

Within the fan the 1975 deposit is reported to reach 80 cm in thickness and are dominated by rounded to subrounded boulders of andesitic lava (Hodgson et al. 2007).

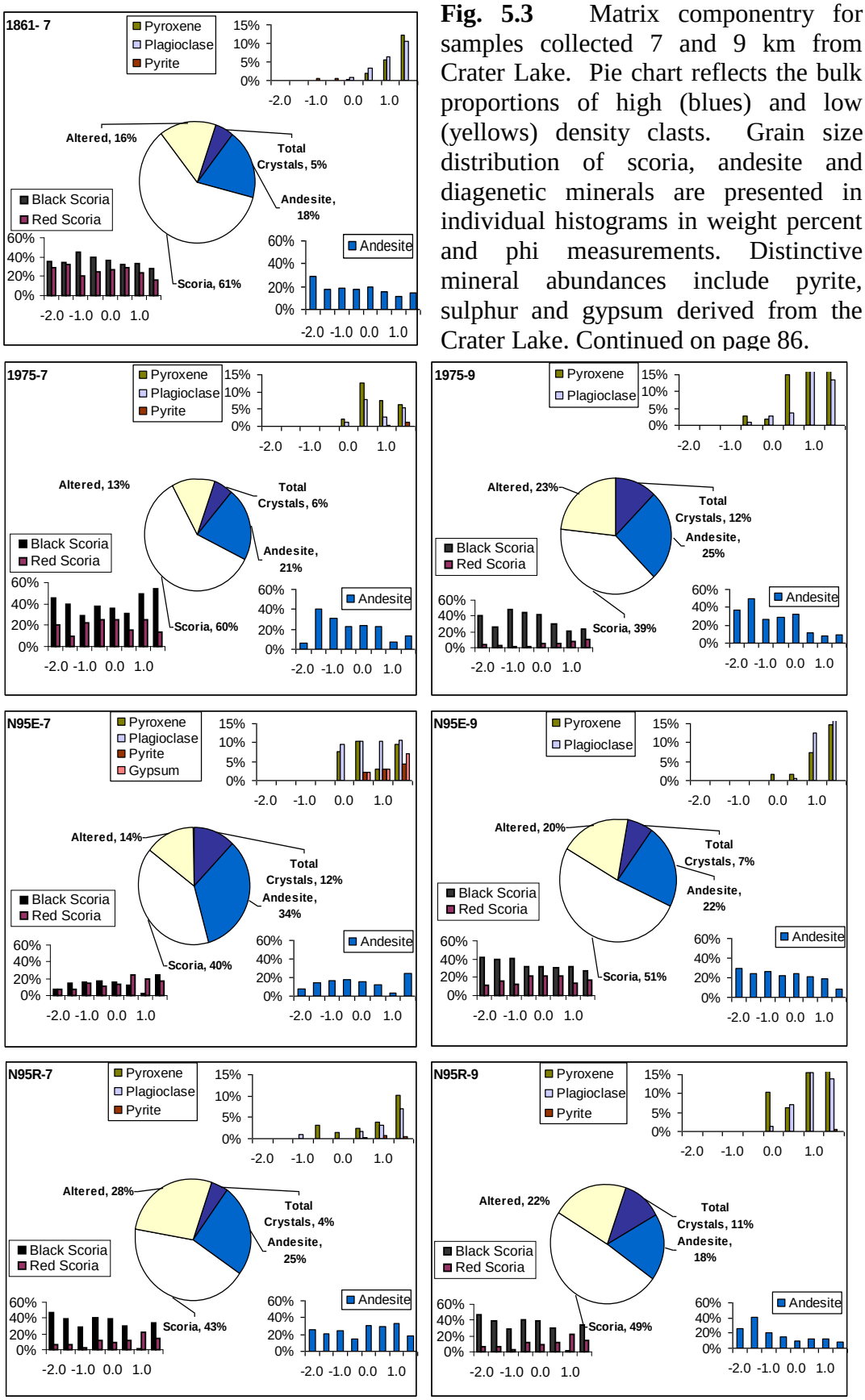

Fig. 5.3 Matrix componentry for samples collected 7 and 9 km from Crater Lake. Pie chart reflects the bulk proportions of high (blues) and low (yellows) density clasts. Grain size distribution of scoria, andesite and diagenetic minerals are presented in individual histograms in weight percent and phi measurements. Distinctive mineral abundances include pyrite, sulphur and gypsum derived from the Crater Lake. Continued on page 86.

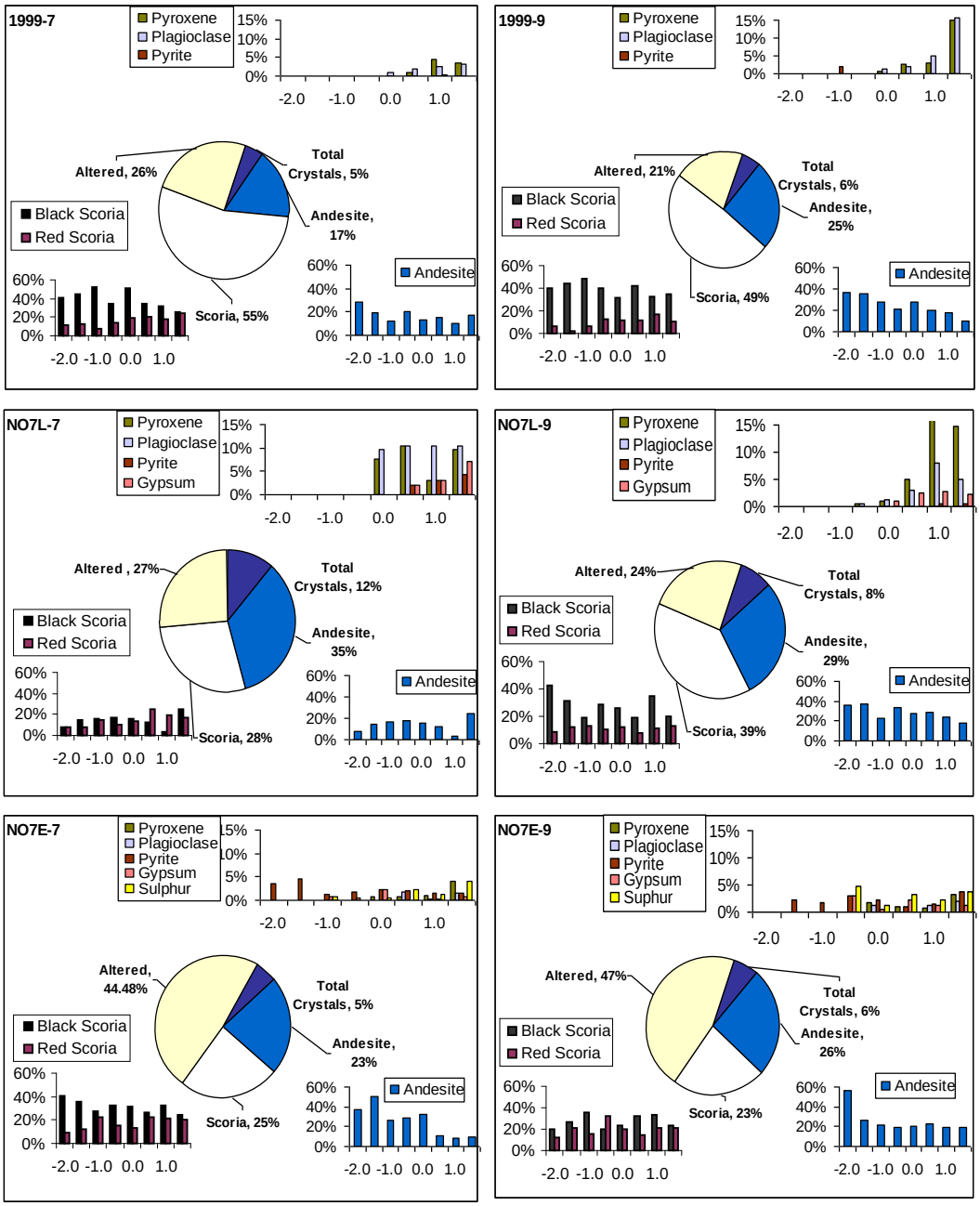

Fig. 5.3 cont.

5.2.2 1975 Componentry

The lithology of the 1975 deposit matrix is dominated by subrounded black andesitic scoria that rarely exceeds 128 mm. There is limited hydrothermally altered material, but broken round clasts of baked lake sediment are scattered on the surface (64 mm) and sand-sized grains are distributed throughout the matrix. Minor abundances (<2 % weight) of cubic pyrite grains occur in the fine sand fractions.

Outsized clasts are predominantly subrounded boulders of two types of andesitic lava. One type is dark grey plagioclase- and pyroxene-rich porphyritic lava which is variably weathered while the other type is a less common pyroxene andesite.

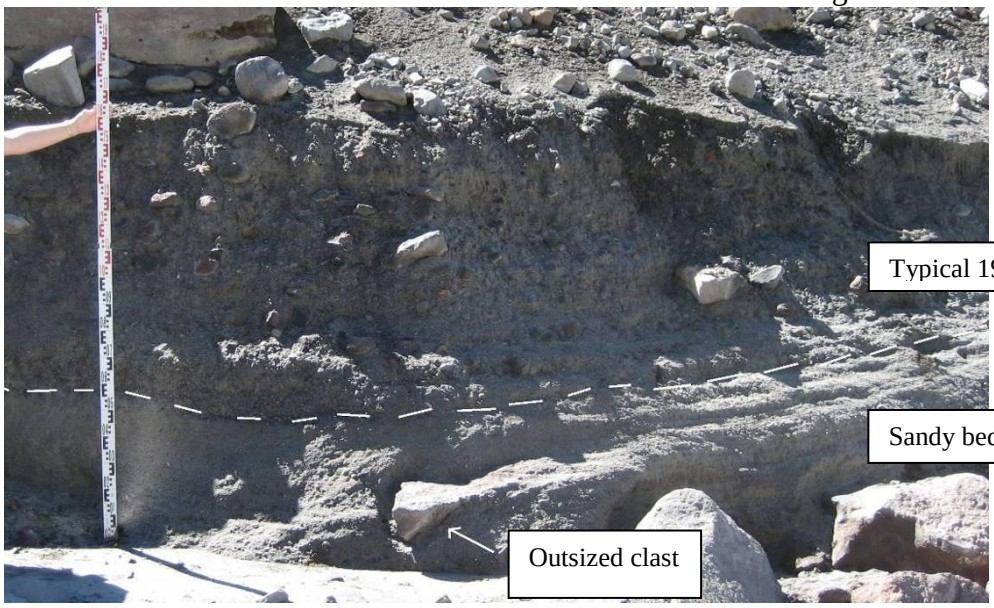

Fig. 5.4 **A.** Typical pulses and gravel concentrations in 1975 lahar deposits in a 4.6 m high section exposed by the erosion of the 2007L lahar. 9 km from Crater Lake. Flow direction from left to right. **B.** Marginal 1975 deposits internal structure that includes a lower sandy bedded unit, overlain by a gravelly sand. Outsized clast in lower unit indicated by arrow, 25 cm in diameter. Staff at 2 metres 7.5 km from Crater Lake. Flow direction from left to right.

5.2.3 1975 Morphology

The central 1975 terrace surface is distinctively covered with large scale braided streamlined bedforms averaging 10-15 m in width and 45 m in length. A large scale gravel bar (Fig. 5.5), composed of predominantly andesite blocks, is located directly east of the RTMT bridge and overlies the 1861 diamicton. This feature measures 30 m in width and 167 m in length with an average clast size of 48 cm, reaching a maximum of 311 cm in diameter. During 1995E and 2007L

lahars the gravel bar was eroded, leaving an isolated terrace remnant, with an armoured boulder surface. Oblique photos from 1995 and 2007 indicate that minor dilute flow reached the top of the terrace, but did not overtop or disturb the boulders. In general, the clast size in surface bedforms is larger than that of the average deposit grain size, but less than that of the outsized clasts suspended within the diamicton.

Fig. 5.5 Examples of 1975 terrace morphology. **A**. Braided terrace surface with streamlined bedforms highlighted by white arrows. Black arrow indicates flow direction. Terrace is 10 m high and 8 km from source. **B**. Large boulder cluster bedform 7 km from Crater Lake. The largest clast reaches a diameter of 360 cm. Staff at 3 m.

Streamlined boulder bedforms dominate terrace surfaces in the narrow sections of the channel. In particularly wide stretches of the channel, a smoothed lateral terrace dominates (up to 25 m wide). These flat-topped terraces are free of coarse grained bedforms, having a veneer of andesitic scoria and clasts up to 2 cm in diameter and outsized clasts of 30 to 60% scoria. Without the coarse-grained bedforms the morphology is subdued by a 6 cm thick ash layer predominantly from the 1995/96 eruptions.

5.3 1995E

5.3.1 1995E Sedimentology

The eruption-generated lahars of the main 1995 eruption sequence are the product of up to five discrete events. The largest terrace is attributed to the September 25 event (LH4; Cronin et al. 1997c). Remobilisation of juvenile

material produced low recessional terraces by reprocessing the initial lahar terrace and new juvenile material until the Crater Lake was ultimately emptied in October 1995. This package of deposits is referred to as 1995E.

The deposits are very poorly sorted subangular gravels with a silt matrix (Fig. 5.2; Table 5.1). The upper 1 m displays a braided structure similar to the 1975 deposits. The upper portion of the terrace is composed of openwork gravel lenses, muddy lenses, and matrix-supported gravels of variable clast sizes and colouration. The surface of the deposit is consistently covered by a pebbly veneer similar to the 1975 deposits.

Underlying the braided segments of the flow the deposit is dominated by a massive texture, where outsized clasts break up a variably matrix- and clast-supported diamicton. However, within this texture there remain significant variations in grain size and concentrations of clasts. This results in weakly defined lenses and pulse structures, which occasionally show crude normal grading (Fig. 5.6).

The deposit is dominated by fine pebbles in a medium silt. A sandy fraction appears sporadically, but is less pronounced than in the 1975 deposits. The sandy concentrations typically occur behind large bedrock obstructions.

Fig. 5.6 Internal structure of upper 1995E terrace with outsized clasts up to 311 cm (9 km from Crater Lake). Colour due to saturation and thin mud coating by 2007L lahar. Staff is 3 m high. Flow direction from left to right.

Within the Whangaehu Gorge the matrix of the 1995E has the highest silt content, up to 12%, of the historic lahars. According to observations made by Cronin et al. (1997c) the deposit becomes sand-dominated msG at the top of the fan, decreasing in gravel and mud content to a gmS downstream of the fan.

5.3.2 1995E Componentry

The dominant clast type within the 1995E deposit is andesitic lava and the bulk of outsized clasts reach up to 230 cm. 75% of the deposit's mass is above 16 mm, and outsized clasts of scoria and andesite occur with the greatest frequency of all the deposits in the Whangaehu Valley. Small boulder-sized bombs to pebble-sized lapilli of slightly altered, black, low density vesicular andesitic scoria are concentrated on the terrace surfaces.

Small pebble- to small boulder-sized blocks of fragile hydrothermally altered andesite and crater rim material also occur within the deposit. These clasts range in colour from white to a rusty red or bluish green. While the larger clasts are concentrated on the surface and have significantly disintegrated from exposure, more resilient sand-sized clasts are scattered throughout the deposit. Angular to subrounded fractured pebble-sized clasts of baked stratified Crater Lake siltstones are scattered over the surface of the terraces.

5.3.3 1995E Morphology

The distribution of the deposits of the 1995E lahar is controlled by the channel eroded through the larger 1975 terrace. The 1995E terraces were cut back by recessional flows, delayed eruption-generated flows, remobilised rain-generated flows, and in 1996 after the Crater Lake had been re-established, eruption-generated flows.

The terraces greatly resemble a smaller scale surface of the 1975 deposits. The surface is completely dominated by streamlined boulder bars and cluster bedforms, but there is a high occurrence of stratified fines in 'ponds' on the surface, up to 30 cm in thickness, similar to observations of the fresh 2007L deposit. The streamlined bedforms occur with less frequency than on the 1975 deposit surfaces, but with similar dimensions and grain size, averaging 16.5 cm, and up to 117 cm.

Additionally, portions of the flow protected by large boulders or protruding outcrops of lava, created small mounds of highly stratified fine-grained materials which accumulated throughout the sequence of eruption-generated lahars (September – October 1995) (Fig. 5.7).

5.4 1995R

5.4.1 1995R Deposits

The deposits of the October 1995 remobilised lahars were accumulated through a series of up to 16 events (Manville et al. 2000a). The largest of these events occurred on October 28 during a severe rain storm and had a peak discharge estimated at half the size of the largest eruption-triggered flow. Remobilisation continued intermittently until seasonal snow melted completely. The material incorporated into these deposits was a combination of tephra-laden seasonal and perennial snow, glacier ice, and previously deposited diamictons. The resulting terraces are collectively referred to as 1995R. In March 2007 the 1995R terraces were almost completely removed by the 2007L lahar. What little exposure of the 1995R remained in March 2007 was buried in September by the 2007E lahar.

Although not the product of a discrete water supply event, the rain-generated lahars (1995R) nevertheless deposited a distinct series of terraces in the eroded 1995E deposits. These terraces have been overprinted by rain-generated lahars in 1999. It is assumed that the highest terrace is minimally disturbed 1995R, and the lower deposits closer to the active channel are the result of further remobilisation in late 1995, 1996 and 1999.

The material mobilised during the 1995 eruption were thick accumulations of scoria, hydrothermally altered vent material and lake sediment on the upper slopes of Ruapehu as a result of sub-plinian and strombolian eruptive activity on October 12 and 14, 1995. The tephra was dominated by scoria bombs with a distinctive brown crust and a black, slightly more highly vesiculated interior. These deposits were readily remobilised by heavy rain, most notably on October 18 to generate multiple, rain-triggered lahars in a number of catchments (Manville et al. 2000a). The 1995R deposits predominantly composed of sand and silt,

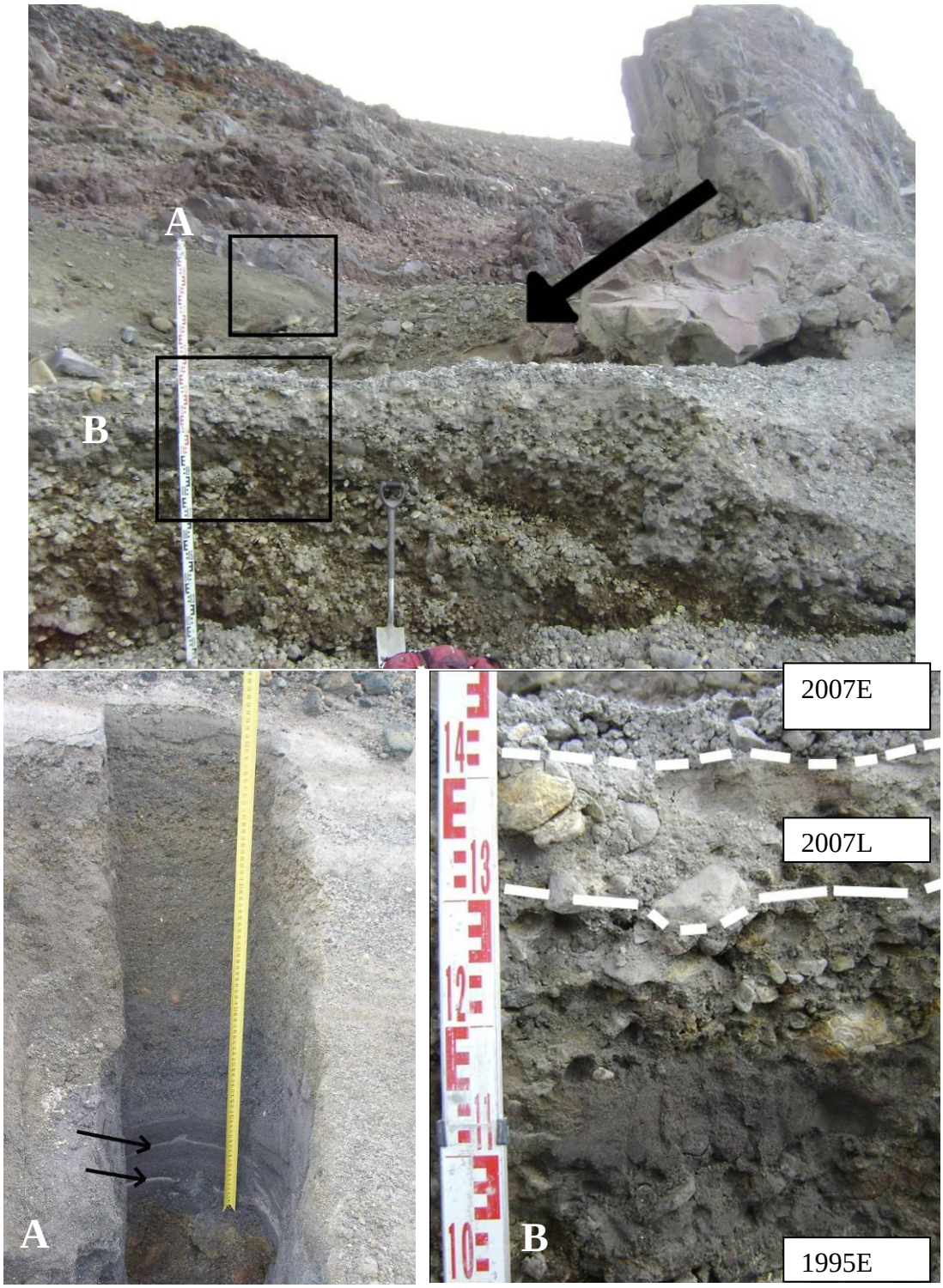

Fig. 5.7 1995E eddy deposits: stratified sands and silts, formed behind a bedrock obstruction of outcropping lava near the active channel. Black arrow indicates flow direction (obliquely out of image). Predominantly sand and silt with occasional outsized pebble clasts (7 km from source). Insets: **A**. The fluctuation in colour and grain size in the 84 cm section reflect the pulse-like nature of individual flows and number of lahar events produced during the early phases of the 1995 eruption sequence. Elutriated silt indicated by arrows. **B.** Sandy lenses occur in the 1995E behind obstructions, and accumulations of silt occurring along pulse contacts. Buried by thin deposits of 2007 lahars.

consequently have a distinctive orange-brown surface dominated by rafted low density hydrothermally altered clasts and scoria.

The limited distribution of the deposit restricted grain size analyses to a short segment of the flow path. The deposits are nearly bimodal, dominated by medium sand with fine pebbles and medium silt. Outsized cobble clasts are characteristically subrounded to rounded, with maximum clast sizes reaching diameters of 258 cm. Despite the smaller range in grain sizes, the 1995R deposits display the poorest sorting of the historic deposits (Fig. 5.2; Table 5.1). Many of the outsized clasts eroded out of the 1995E deposits and mobilised, but not carried by the 1995R lahar, are significantly larger than the thickness of the deposit itself (Fig. 4.1).

Although the deposits are thin and occur less than 4 metres above the active channel, they are massive in a general sense. The 1995R deposits display minor variation in grain size, sorting, and clast/matrix support similar to the pulses observed in the larger terraces. The deposits develop minor stratification and grading downstream in the Whangaehu fan 16 km from source (Cronin et al. 1997c).

5.4.2 1995R Componentry

The distinctive rafted scoria and hydrothermally altered clasts scattered on top of 1995R deposits, were observed during the active flow by Cronin et al. (1997c). The scoria clasts are highly rounded, while the white to rusty yellow hydrothermally derived blocks are surprisingly fragile and angular. Both types of rafted clast are predominantly small cobble to large pebble in size. Subangular andesitic lava blocks are sparser, and are of a more extreme grain size, up to 258 cm. The silt fractions are dominated by hypersthene crystals and andesitic glass.

5.4.3 1995R Morphology

Prior to March 2007, the 1995R deposits were preserved in very low terraces, averaging 0.5 m to 2 m above the active channel. These terraces are confined within the channel eroded into the 1995E and 1975 deposits, and directly on top of the exposed channel bedrock. The 1995R deposits are closer to the level of the active channel, and the terraces emplaced by the highest flow level are not significantly above the level of normal flood stage for the river. As a

consequence, the deposits are rapidly altered by all flood events, including small rain-generated lahars. Consequently, the terraces are not very distinct from younger deposits (1996 and 1999). Instead of the typical braided surface, the deposits have a stepped progression into younger deposits and finally the active channel (Fig. 5.8). Some braiding is still evident, but the bedforms are not discrete. Additionally, the 1995R deposits are frequently interrupted by protruding andesite bedrock outcrops.

Fig. 5.8 1995E, 1995R and 1999 terrace morphology highlighted in the right image with false colour overlay. The highest terrace in image is 1995E. The step-like terraces towards active channel are 1995R and 1999 (8 km from source).

5.5 1999

5.5.1 1999 Deposits

The sediments of the 1999 rain-generated lahars are difficult to distinguish from events that occurred after October 28 1995. In most cases the 1995-1999 deposits can be treated as a continuation of the sedimentary response to the 1995/96 eruption sequence. However, the destruction of the rebuilt RTMT bridge in 1999 reflects the largest remobilisation in the Whangaehu since the October 28 1995 event.

Any deposit referred to as 1999 is better described as accumulations following the emplacement of the 1995R terraces and prior to the 2007L lahar, of normal fluvial processes with intermittent remobilisation lahars, and one small scale eruption-generated event in June 1996 (run out of 8 km) following the reformation of Crater Lake (1% of its pre-eruption volume; DSIR 1989).

The deposits are silty sands with a high occurrence (60%) of subrounded outsized clasts in a 40% matrix by weight. Some surficial pools of fines display

crude normal grading and an absence of outsized clasts. The poorly sorted deposit contains medium silt to clasts up to 108 cm in diameter (Fig. 5.5 and Table. 5.2).

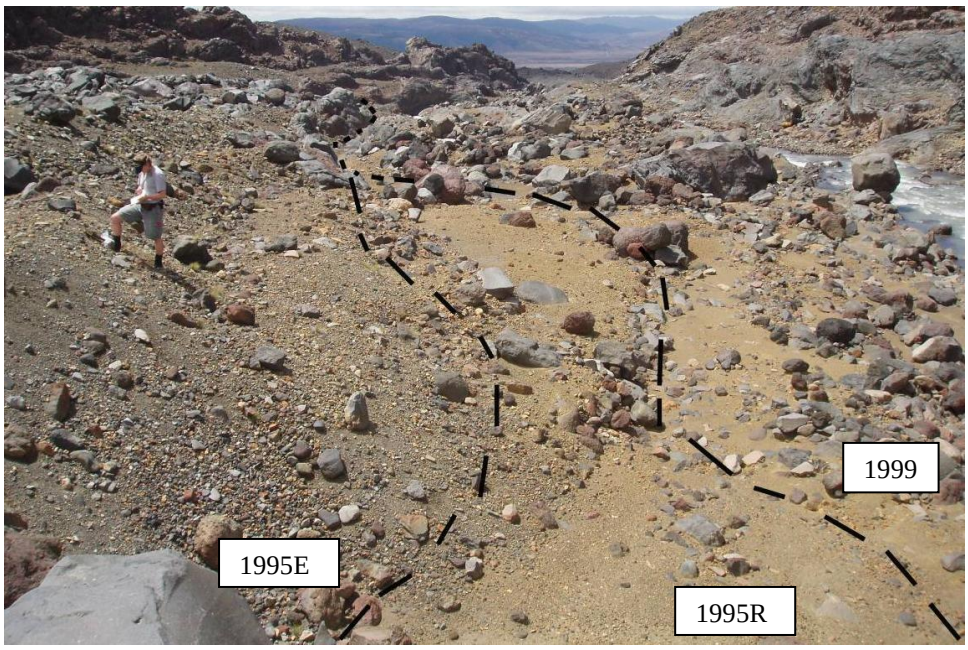

Fig. 5.9 1995E, 1995R and 1999 terrace morphology 7 km from source looking down valley. The highest terrace on the right hand side of the image is 1995E. The step-like terraces near the active channel are 1995R and 1999. Person for scale. Photo: K. Jackson.

5.5.2 1999 Componentry

The deposit is dominated by low density material, mainly scoria, but also includes fresh wood debris located 600 m from the bridge site (see section 5.7). The scoria displays various stages of weathering and includes accessory pyrite. The fine fractions are dominated by andesitic glass and occasional plagioclase and pyroxene. The andesitic lava content of 1999 is the lowest of all the historic deposits (Fig. 5.3).

5.5.3 1999 Morphology

Prior to erosion by the 2007L lahar deposits the 1999 deposits had a greater distribution than the 1995R diamictons, lining a majority of the active channel (Fig. 2.5). The stepped terraces ranged from 3 m to 30 cm thick and 30 to 60 cm below the 1995R terraces. Instead of terrace morphology the deposits sloped gently into the active channel, as a result of continual reworking by normal stream flow (Fig. 5.9). The 1995R and 1999 deposits are of similar colouration,

with the 1999 deposits occasionally displaying a more vivid orange-brown, to rust colour.

Unlike the larger terraces the 1999 lahar deposits did not display streamlined bedforms, although concentrations of cobbles were controlled by large outsized clasts and bedrock outcrops.

5.6 2007L

5.6.1 2007L Sedimentology

The deposits of the March 18, 2007 lahar resemble earlier Whangaehu lahar deposits; however, morphological complexity is much more apparent in the fresh deposits. The new sediments were deposited in an erosionally widened channel cut into the 1995 and 1975 terraces and as a veneer (up to 30 cm thick) on top of marginal and isolated remnant terraces (Fig. 4.3). Within the first few months following the event, the majority of the deposit in the study area was within half a metre of the active stream, and subject to continued reworking. Occasional intermediate terrace 'islands' occur throughout the valley and measure up to 2 metres above the surrounding deposit.

A mud coating up to 1 cm thick was found both on valley walls and terraces, within the channel. The coating is a sandy mud with occasional dispersed pebbles. Splash marks, super-elevation marks, etc. were composed of the same material (Fig. 5.10).

Exposures of the internal structure of the 2007L deposit are limited due to the lack of incision within the first two months following deposition. Minor terraces display short vertical sections (70 cm) that were subject to reworking during the initial adjustment of the Whangaehu River to the changes in channel geometry and sediment load.

These sections reflect the complex braided morphology of the new deposit. The top fifty centimetres of the deposit is typical of a braided stream, being composed of alternating layers of different grain sizes and degrees of sorting. The rounded to subrounded clasts are predominantly cobble-sized with a medium silt dominated matrix (Table 5.1). A coarse sand fraction is sometimes present, occurring in only the broadest sections of the eroded channel (7-8 km) (Fig. 4.3). The clasts are moderately rounded throughout the deposit.

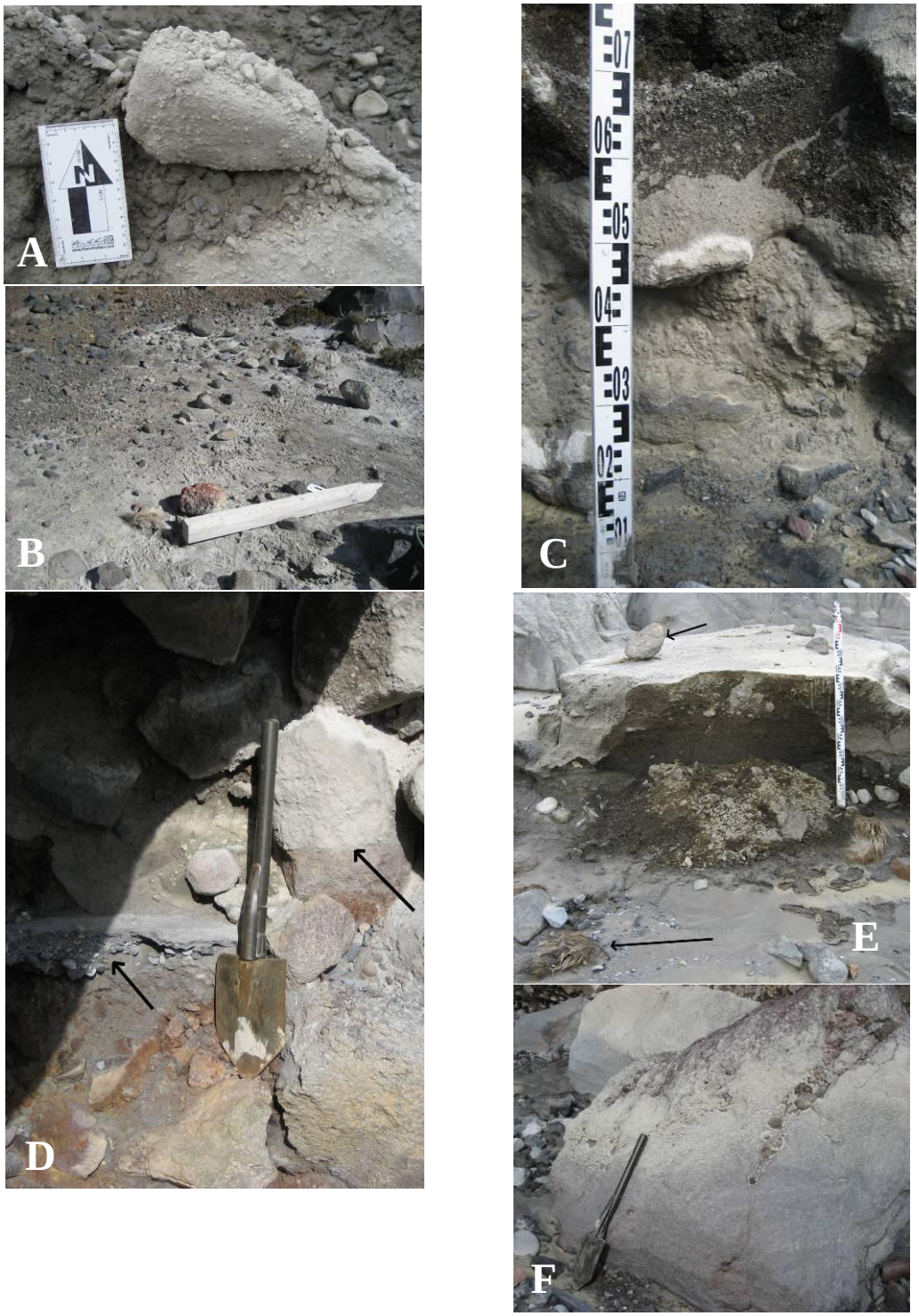

Fig. 5. 10 Range of fresh 2007L mud coatings as preserved in the first month after deposition. **A**. Example of mud coating up to 1 cm thick, composed of silt, medium sand, and small pebbles. **B**. High flow marks on 1975 terrace with stranded low density wood debris (beam 105 cm). **C**. Splash marks 60 cm above the highest 2007L terrace. **D**. Washed mud coating with a perched terrace remnant indicated by arrows, 10 cm below clean line. Spade at 62 cm. **E**. Remnant terrace of 1975 with a perched mud coated cobble and overridden plant highlighted by arrows. Staff at 1 m. **F.** Mud coating had been cleared off of first 50 cm above deposit surface.

While the mean grain size rarely exceeds the cobble size range, outsized clasts and channel bar and bedforms include boulders between 134 cm and 546 cm in diameter. The ratio of matrix to outsized clasts varies widely from 12 to 50%. This variation is not correlated with morphology or proximity to the channel.

The few vertical sections exposed (by 25.4.07) up to 40 cm of the deposit composed of multiple beds ranging from 3 cm to 8 cm in thickness and displaying both open-work and matrix-rich units (Table 5.2). Some cobbles up to 20 cm in diameter occur interrupting the braided segments.

5.6.2 2007L Componentry

The 2007L deposits have the most diverse componentry of all the Whangaehu diamictons, being made up of scoria from all previous eruptive units, andesitic lava, hydrothermally altered lake sediment and hydrothermally altered quartz.

Fresh, well-rounded to near spheroidal, black plagioclase-rich scoria clasts are very common but are limited to the cobble (2-7 cm) grain size. These scoria are sourced from upstream juvenile accumulations and eruption-generated deposits displaying less surface alteration (excepting the rounding) than other deposits.

Except for the 2007E deposits, the 2007L lahar deposits have the highest hydrothermally altered clast content. Unlike the hydrothermally altered materials of the 1975, 1995E, 1999 and 2007E, low density rounded cobble sized clasts of white to yellow, stratified Crater Lake mud were dominant.

Subangular and subrounded pebble to cobble sized clasts of hydrothermal quartz from the crater region were found in all grain fractions. These clasts are frequently coated in cubic pyrite crystals > 2 mm across. Recrystallised quartz

Table 5.3 Selected clast densities (g/cm^3).

Clast Type	1861	75	95E	95R	99	2007L	Average
Andesite lithic	2.43	2.38	2.40	2.33	2.48	2.45	2.41
Red scoria	1.69	2.15	2.09	1.85	1.60	1.47	1.81
Black scoria	2.09	1.58	1.64	1.84	1.93	1.91	1.83
Lake sediment		1.55	1.49			1.82	1.62
Hydrothermally altered clasts		2.02	1.70		2.01		1.91

Dense rock equivalent (DRE)= 2.4 g/cm^3

seams also run through the larger clasts. These clasts have a density of around 2.4 g/cm^3, similar to the andesitic lava fragments (Table 5.3). Independent pyrite crystals up to 2 mm in diameter were cannibalised from previous eruption-generated deposits.

The mud coating represents a large proportion of the fine fraction of the deposit, and is composed of crystalline pyrite, hypersthene, augite, plagioclase, scoria fragments and minor smectite and kaolin clays.

5.6.3 2007L Morphology

Post-2007L channels are highly dynamic, complex braided systems which take months to develop a single channel, except in areas constrained by outcrops of lava bedrock that rapidly returned to the pre-March 18 2007L configuration. Within the first three months following emplacement, recent remobilisation was distinguishable from the cleanliness—absence of mud coating—of the cobbles. The surface of the fresh deposits is covered by predominantly small cobbles and pebbles which were still mobile in the bed load even following the 2007E snow slurry lahars. Larger grains (above 70 cm) have shorter transport histories and may be sourced from the eroded 1995E and 1995R terraces. Rounding of clasts increased towards the active channel.

The most distinctive morphological features of the new deposits are highly defined streamlined cluster bedforms distributed throughout the valley. The majority of these bedforms are openwork, jumbled accumulations of loose boulders about 60 cm wide and 5 m long (Fig.5.11). Most of these bedforms are loosely organised, but occasional organised bedforms of the same dimensions also occur. The bedforms display vertical normal grading and an upstream fining. Additionally, along the margins of less constrained segments of the channel, small openwork pebble levees up to 1.5 m in length appear on top of 2007L terraces.

Unlike the marginal terraces of the 1975 and 1995 lahars, the 2007L deposit has isolated elongate terraces occurring throughout the valley. These island terraces are frequently situated downstream of an obstruction, like an outcrop of bedrock, or large boulder (i.e. lee-side or eddy bars). The terraces above the channel are better-cemented, and require a rock hammer to pick apart.

Dewatering and compaction resulted in the mobilisation of fines (silt) within the deposit, pooling at layers of impermeability and escaping along eroded

surfaces (Fig 5.12). In some cases the fines are pushed to the surface by escaping pore water. Fines on the surface of the deposit were also subjected to remobilisation making small mud and slurry flows, some displaying levees and small entrained pebbles. As dewatering continued, the deposits were easily liquefied, as described in fresh 1995E and 1995R deposits by Cronin et al. (2000), and were occasionally subjected to minor surface collapses.

The mud coating that covers the deposits displays some variability. Some grains are coated all the way around; some clasts had only surficial coating on one side, having been deposited before coating occurred. The coating became far more resilient after drying and persisted through several rainstorms in March and April 2007.

The mud coating is distributed throughout the valley in three ways. The highest coating is preserved up to 3 m above the deposit surface, a lower clean phase (up to 1 m), and in places a second mud or pebble coating only slightly above the deposit surface (20 to 30 cm). High water and splash marks of sandy mud coat the walls of the valley and erosional scarps, and are frequently associated with stranded clasts.

As with previous deposits, low density debris highlights the high water mark as the buoyant material is rafted even on top of the deposit. Downstream of the fan, flow margins were marked by rafted anthropogenic debris and vegetation. These high water marks are undulatory and have a high frequency of splash marks.

Along the margins of the newly eroded channel, veneer deposits of 2007L between 2 to 50 cm coat historic terraces and bedrock walls. Overridden, but not eroded terraces developed rounded whaleback morphology and occur frequently along the edges of the active channel (Fig. 5.11).

5.6.4 2007L Incision

The morphology of the valley was highly dynamic within the first two months following deposition. Incrementally, interrupted by flood events, the initial braided stream system that had developed on top of the lahar deposit in the first days following emplacement, was replaced by a single consolidated channel. One month after the event (11.4.07) a semi-consolidated channel had developed.

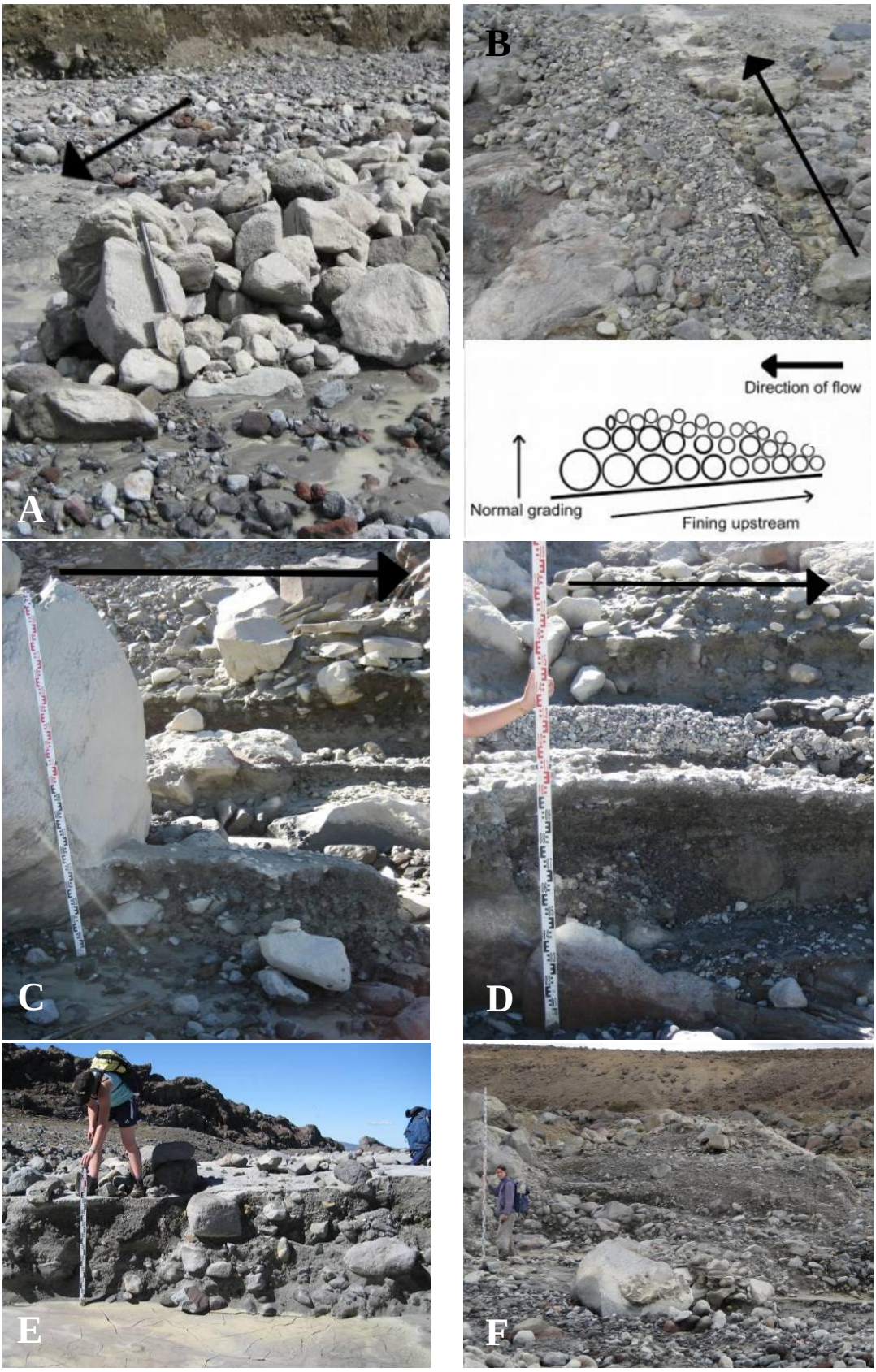

Fig. 5.11 Fresh 2007L deposit morphology and bedforms between 7 and 8 km from Crater Lake. **A**. Streamlined openwork, jumbled cluster bedform (120 cm by 400 cm at 6.5 km). **B**. Organised streamlined cluster bedform with normal grading and upstream fining (60 cm by 500 cm at 7.5 km). **C**. Preserved intermediate terrace behind boulder obstruction. Staff at 2 m. **D.** Openwork levee

(*continued from* Fig. 5.11 pg.101) (150 cm long at 7 km; staff at 2 m). **E.** Minor exposure within first week of emplacement. Poorly sorted with subrounded clasts. Significant ponding of silt along surfaces out of reach of active channel. **F.** 'Whaleback' remnant terraces of 1995R. Staff at 3 m (9 km from source). Black arrows indicate flow direction.

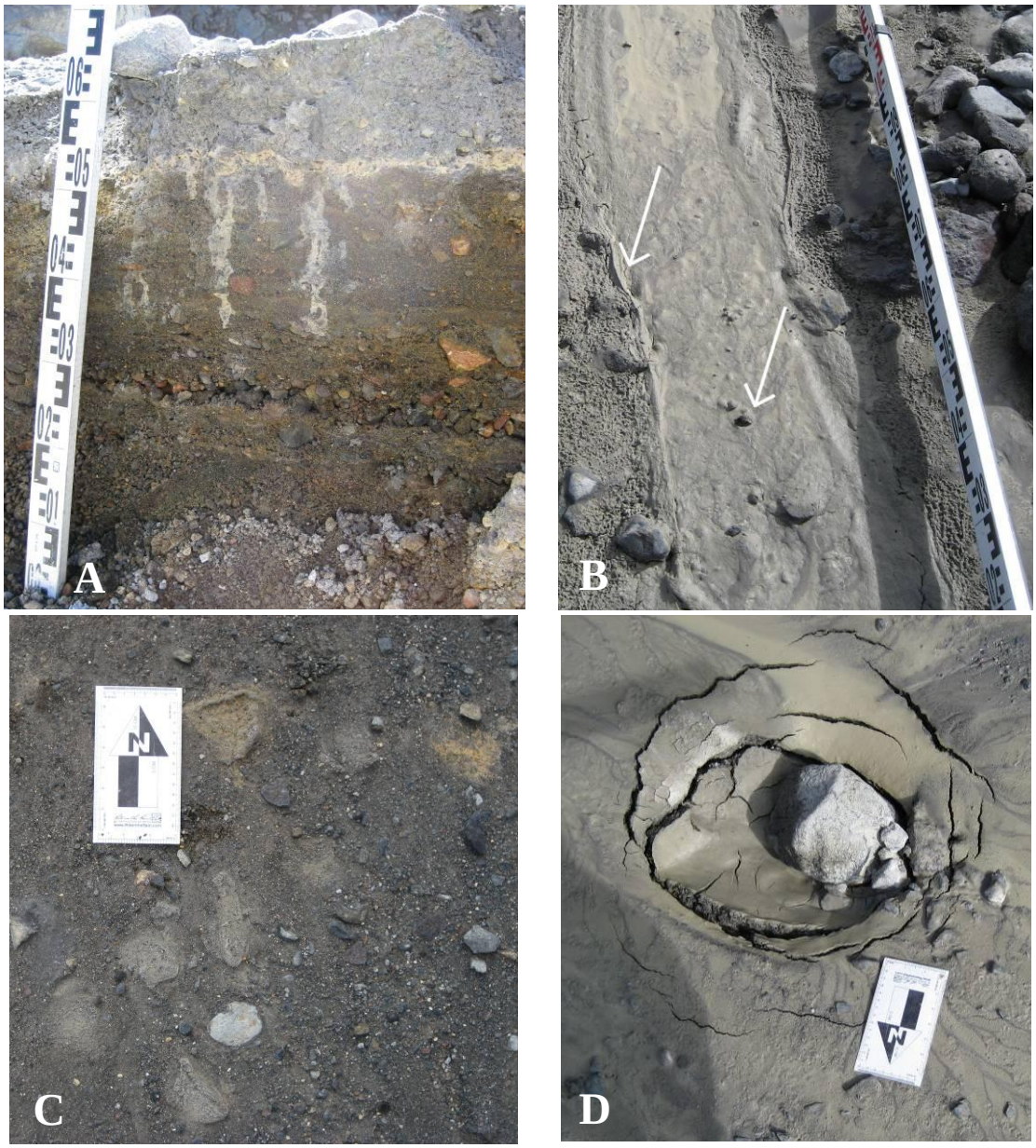

Fig. 5. 12 Dewatering and collapse structures of fresh 2007L lahar deposits taken within the first week after emplacement. **A**. Silt pooling at depositional contacts with existing diamictons. Staff at 64 cm. **B**. Flow of mud across the surface of fresh deposits. Arrows point out minor levees and dragged pebbles. Staff at 1 m. **C**. Silt pushed out of the surface with escaping pore water. **D.** Collapse structure of compacting deposits.

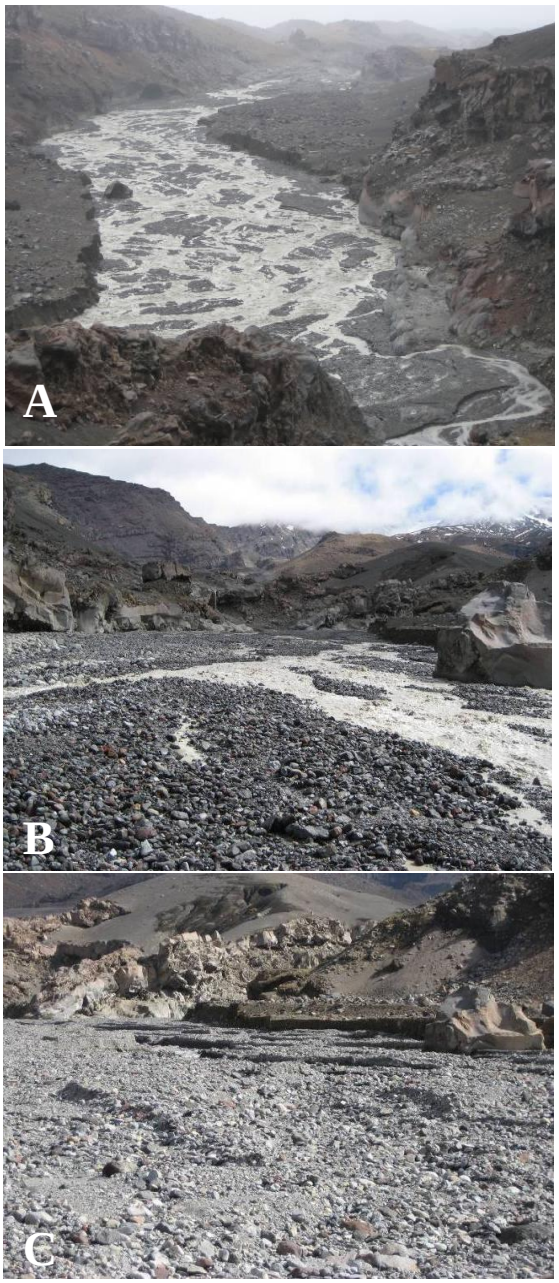

Fig. 5.13 Sedimentary response of the Whangaehu River to increased sediment load of the 2007L lahar deposits. Channel consolidation and incision progressed rapidly in the first two months after deposition. **A.** Complex braided morphology of the first month post-emplacement at the convergence 6 km from Crater Lake (30.3.07). **B.** Large outsized clast from 1975 terrace undercut by 2007L flow. Highly braided saturated deposit surface on March 23, 2007. Just east of convergence, 6.2 km from Crater Lake. **C.** Same location, consolidation of streams and increased incision by April 25, 2007.

While incision had begun along this main channel, no significant exposure was present even two months later (Fig. 5.13). The abandoned braids became host to pools of heavy sands.

The turbidity of river water significantly decreased by 11.4.07, but increased during storm events. The elevation of the stream bed was also noticeably less than 30.3.07 and 25.3.07 due to local erosion of the 2007L lahar deposits by fluvial action, exposing underlying units, including bedrock channel and Mangaio Formation. Settling had slowed significantly by late April (25.4.07), and many terraces that had been present in the fresh deposit had been redistributed.

5.6.5 Distinguishing 2007L from relict terraces

Because of the complex interaction between the 2007L lahar and the pre-existing deposits, distinguishing fresh deposits from relict terraces can be difficult because of 2007L mud coatings and saturation. However, fresh characteristics will change with time. Plants will re-grow or die, and the mud coating will significantly diminish.

Overrun plants are frequently visible on terrace surfaces and edges. The roots are exposed and the foliage is plastered with a mud coating and streamlined (Fig 5.10). By November 2007 the vegetation had not yet recovered and the 2007L deposits had developed a yellow hue instead of the light grey of fresh deposits.

While some pre-existing deposits were completely eroded by the new flow (1999 and most of 1995R), others are only partially eroded. The overtopping flow partially eroded mid-channel pre-2007L deposits creating whaleback type structures (resembling glacial drumlins). Deposits accumulated behind an obstruction can be either preserved either on the pre-existing terrace, or slack-water accumulations from the new flow.

Some temporary features of the fresh deposit are similar to observations made in 1945, 1953, and 1975 (Reed 1945; O'Shea 1954; Nairn et al. 1979). Green and yellow discolouration on deposit surfaces caused by sulphur leaching appeared within days of emplacement. A blue silt was observed as part of the general mud coating and resembles descriptions of Crater Lake mud that was exposed during dome growth in 1945 (Reed 1945) and observed on deposits in 1995 (Cronin et al. 1997c).

5.7 2007E

5.7.1 2007E Sedimentology

The deposits of the 2007E lahar are unique compared to the historic deposits already described in the Whangaehu Gorge. The deposits were described two days following deposition and then again 14 and 36 days after deposition once the snow component had completely melted. Initial deposits were composed of well sorted granular snow with 40-50% sediment concentrations.

Sedimentology of snow-rich deposit

The initial thickness of the deposits was up to 2 m but the snow melted rapidly, which in conjunction with compaction, decreased the terrace heights by 40 cm in one day. Three distinct units were identified in the gorge, the top unit only reached a maximum of 3 cm and was not always distinct. The two lower units displayed strong normal grading with a matrix of well sorted approximately 2 mm granular snow and silt (Fig. 5.14.a).

The lower unit is between 90 and 130 cm thick and contains subrounded clasts of andesitic lava and scoria up to 30 cm in diameter with snow and ice up to 25 cm. The contact between the two lower units was distinct, as it was erosive and typically marked by a concentration of clasts in the upper unit and a mild colour change from grey to grey-brown. The upper unit is between 20 and 60 cm thick.

The lower contact between 2007E and 2007L was sporadically exposed prior to melting and does not reflect substantial erosion. The bulk density of the lahar 7 km from source (RTMT) was >0.6 g/cm^3.

Sedimentology post-melting

The melting process was slowed by spring storms and snow accumulation over the deposits. However, by 36 days following emplacement the overall deposit thickness had decreased by half with only 30 cm of snow overlain by 15-20 cm of sediment. The melted deposit had a very porous texture where cavities had been left behind after the melting of snow and elutriation of fines (Fig. 5.14.b).

Along the southern bank isolated pockets of the deposit were completely melted. Accumulations were preserved when the deposit was significantly above the active channel. The melted deposit was up to 20 cm of pebbly silt positioned directly on top of 2007L with a reasonably distinct contact highlighted by accumulations of silt up to 5 cm thick in locations. Collapse of the 2007E exposed more of the 2007L deposits, although the contact became more difficult to distinguish as the 2007E deposit progressively changed colour with exposure.

Although the clasts were predominantly subangular to subrounded silt to 6 cm pebbles, frequent flaky or elongate particles occurred in all grain sizes. The

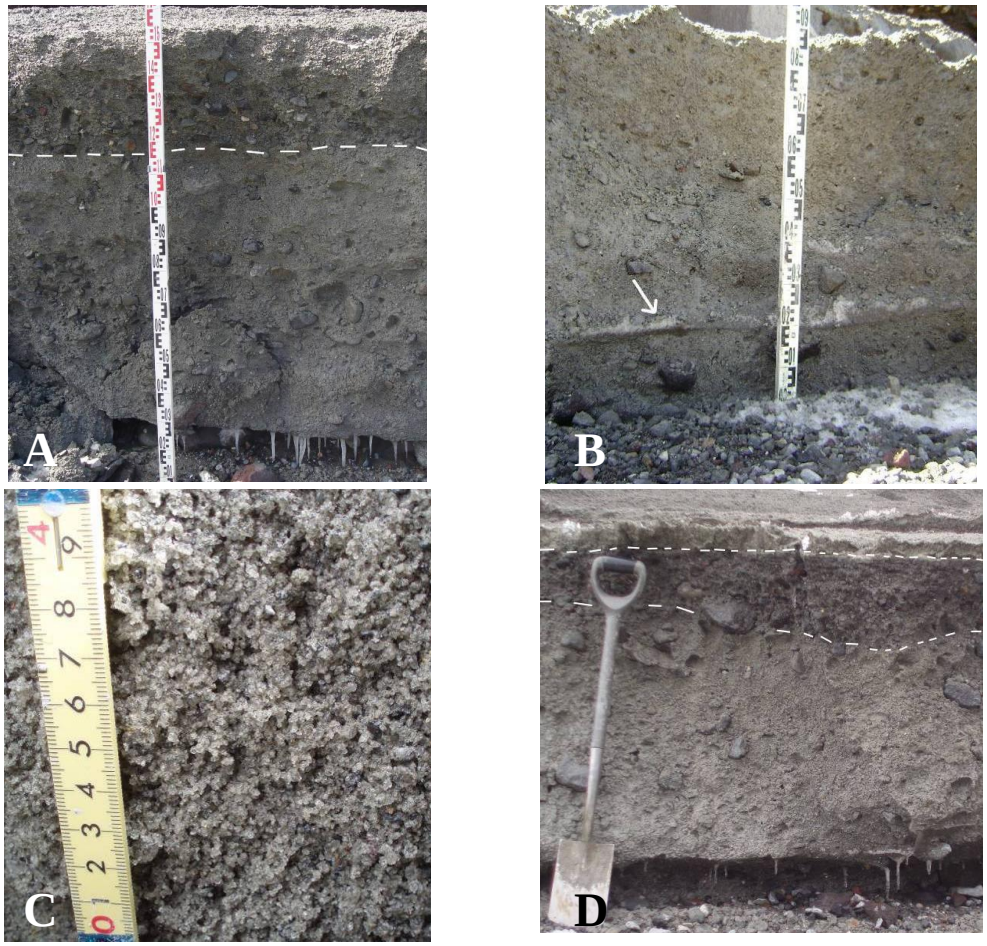

Fig. 5.14.a 2007E internal structure before melting. **A.** Two units of silty snow with normal grading of outsized clasts. The contact is highlighted by a concentration of pebble sized clasts. The thickness of the upper unit fluctuates. Total thickness 150 cm at 7 km from Crater Lake. **B.** Compressed snow layer between first two units. Average thickness of 3 cm. **C.** Silty granular snow typical of 2007E deposits. Two days post-event. Photo: Kyoko Kataoka. **D.** Three pulses at RTMT, 7 km from Crater Lake. Erosion visible along contact between the first and second pulses. The third pulse has a maximum thickness of 3 cm occurring only along the active channel. Spade is 90 cm.

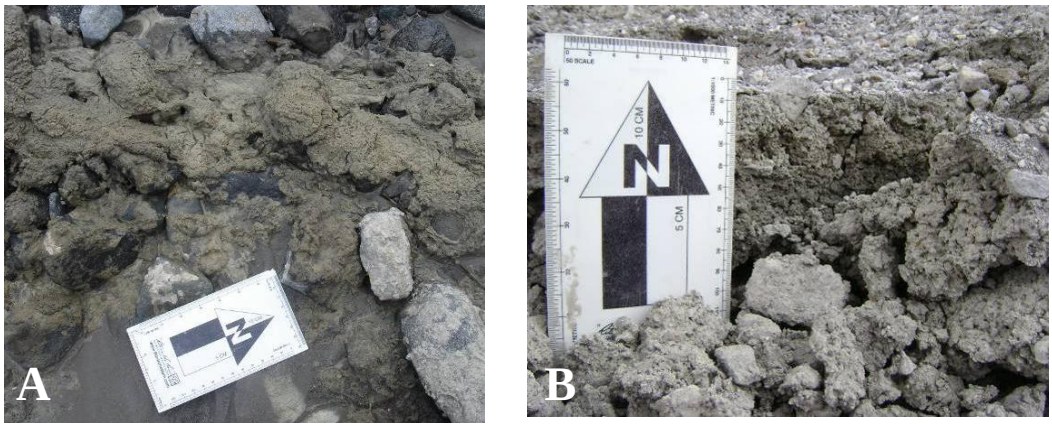

Fig. 5.14.b 2007E deposits after melting. **A.** Snow collapse structures at the Wahianoa Aqueduct 23.5 km from Crater Lake (1 day post deposition). **B** Hollow texture with pebble veneer (7 km from Crater Lake; 1 month post deposition).

melted deposit had a sorting of approximately 2.45, which is average for historic Whangaehu Gorge lahar deposits.

5.7.2 2007E Componentry

The 2007E deposits contain clasts of clear ice, granular snow and blocks of perennial snow. The sediment within the deposits is similar to previous deposits, being dominated by clasts of scoria and lava. The fresh 2007E deposits contained aggregates of Crater Lake sediment that remould when disturbed. A veneer of sulphur and blue, iron-bearing, silt appeared on erosional surfaces of the 2007E deposit for the first three days following emplacement (Fig. 5.15).

Fig. 5.15 Components unique to the 2007E flow. **A.** Perennial snow blocks, up to 25 cm, occur in the second of the major concentrated pulses near the surface of the deposit. The snow had coarser crystal sizes than the matrix of seasonal snow. **B.** Flaky clasts up to 6 cm in diameter of lake mud that remould rapidly when disturbed. The arrow indicates remoulded clast. Arrow 10 cm. **C.** Clast of clear ice occur in first pulse, lower unit, of 2007E. Approximately 6 cm across. Photo: Michael Tayler. **D.** Accumulation of gypsum on hydrothermally altered clast. Divisions on scale are 10 cm.

Three types of snow were observed in the 2007E deposits. The bulk of the deposit was granular snow with crystals averaging 2 mm in diameter. In addition to sediment clasts dispersed through the deposit were blocks of perennial snow displaying coarser crystals of snow and clear ice. The snow blocks occur just below the surface of the upper unit and were measured up to 25 cm in diameter. Clear ice occurred in both units and the largest clast was 8 cm in diameter.

The componentry was difficult to distinguish in the deposits prior to melting. Within one month the surface of the deposit was concentrated with pebble sized clasts of a variety of compositions. There was an abundance of Crater Lake derived materials including lake sediment, pyrite, native sulphur, and hydrothermally altered andesite and sinter. Initial deposit displayed significant coating of sulphur and the blue coating observed in March of 2007. Individual clasts also had coatings of sulphur up to 3 cm. Gypsum occurred as minor crystalline flakes and thick (2 cm) coatings on hydrothermally altered clasts. Overall components of the deposit were very low in density (71 vol. % low density clasts) being dominated by hydrothermally altered material with clasts up to 30 cm in diameter and equal proportions of scoria and andesite. Lake sediment was common, but only up to 8 cm in diameter.

5.7.3 2007E Morphology

Initial morphology

Two distinct terrace surfaces occurred on the fresh 2007E deposits, a rough, ropey surface of the lower two flow units, and a smooth surface that occurred along the active channel. The ropey surface occurs in conjunction with steep lobate flow margins. In some locations the flow was deposited at steep angles on channel walls as a coating up to 10 cm thick. In other locations the deposit did not fully cover the valley floor, leaving steep margins around windows of 2007L sediment. The morphology of the 2007E surface is highly fractured displaying steps perpendicular to flow direction and longitudinal shear deformation structures at intervals (Fig. 5.16.a). The perpendicular deformation fractures concentrated around obstructions in the flow path and at flow margins and these concentrations were truncated by longitudinal shear features.

The third unit displayed a distinctly smooth surface that overlapped and muted the underlying fractured surface of lower units. These flows also had distinct flow edges that lapped up on the thicker deposits along the active channel.

The active channel cut through the entire thickness of the deposit leaving a wide straight walled channel on the surface of the 2007L deposit.

Within days of deposition the deposit began displaying collapse structures with circular scarps and step like slumps (Fig. 5.16a).

Morphology post-melting

After one month the bulk of the deposit had decreased in thickness by half. Small portions of the deposit had completely melted, leaving behind c. 20 cm accumulations of pebbly sand and silt. In some locations the melting was accelerated around large exposed boulders, creating depressions. Boulders buried by the 2007E projected from the top of the deflated deposit, with a veneer up to 3 cm thick. The deposits were easily compacted by walking on them and the sharp erosional faces of the initial deposit were replaced with gently sloping hummocky faces.

Throughout the melting process, elutriation of fine sand and silt occurred along erosional faces and deposit contacts. Small islands of sediment were created by the collapse of ice tunnels throughout the deposit. In addition to snow loss, within the first two months following deposition the sediment of the 2007E was significantly reduced in volume.

The ropey texture that was so prominent the first week following emplacement became obscured as the surface of the deposit became increasingly sediment rich. After two months, the extent of the smooth surfaced late phase pulse was only distinguishable based on the smaller size of outsized clasts (Fig.5.16.b).

5.8 Chronostratigraphic markers

5.8.1 Bridge Debris

Just over 7 kilometres downstream from Crater Lake, the DOC Round the Mountain Track crosses the Whangaehu River. Lahar events in 1975, 1995, 1999

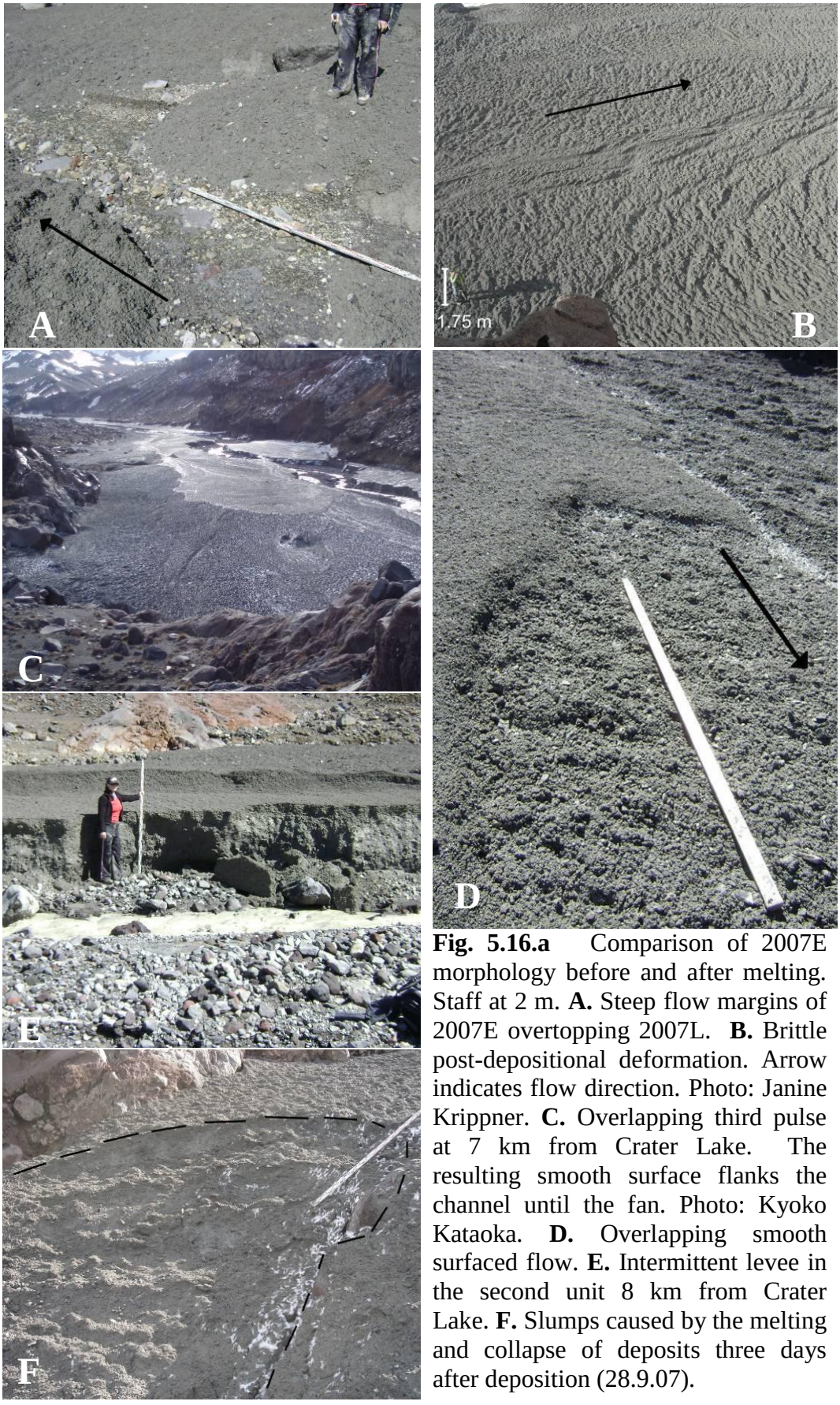

Fig. 5.16.a Comparison of 2007E morphology before and after melting. Staff at 2 m. **A.** Steep flow margins of 2007E overtopping 2007L. **B.** Brittle post-depositional deformation. Arrow indicates flow direction. Photo: Janine Krippner. **C.** Overlapping third pulse at 7 km from Crater Lake. The resulting smooth surface flanks the channel until the fan. Photo: Kyoko Kataoka. **D.** Overlapping smooth surfaced flow. **E.** Intermittent levee in the second unit 8 km from Crater Lake. **F.** Slumps caused by the melting and collapse of deposits three days after deposition (28.9.07).

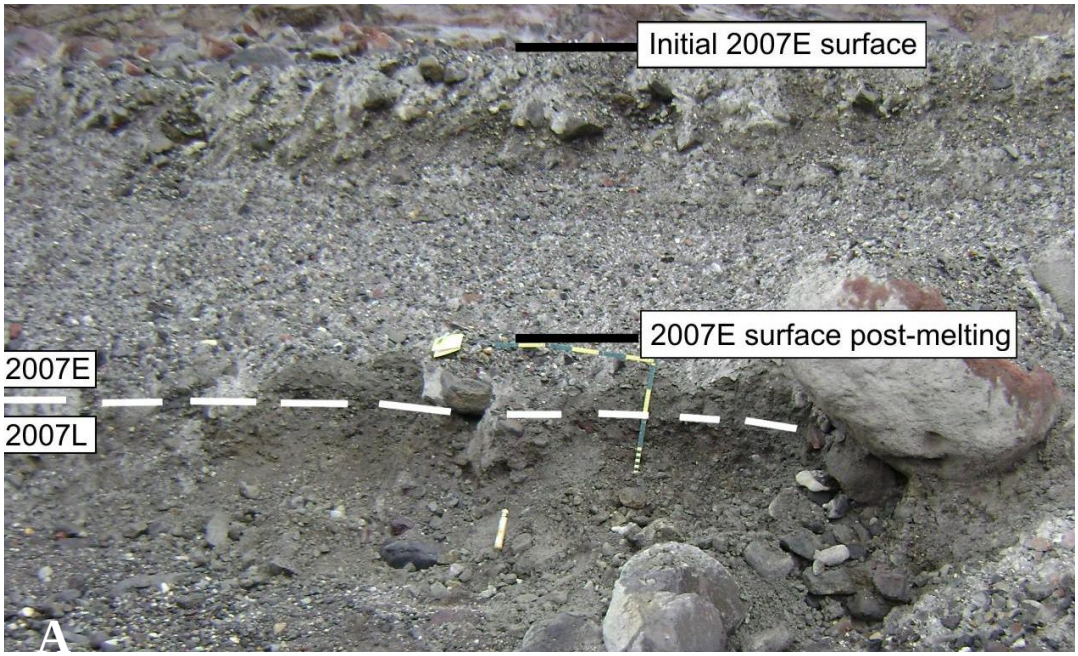

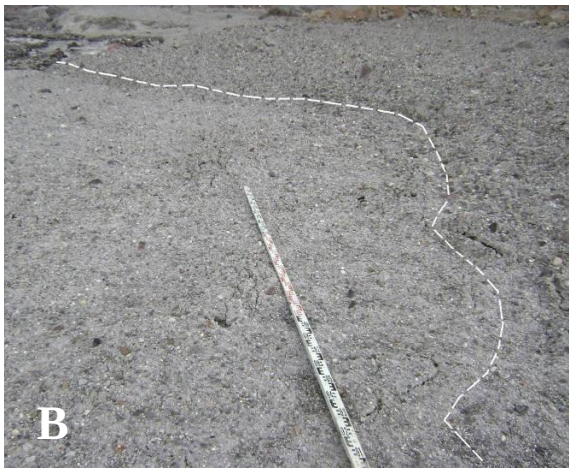

Fig. 5.16.b Geomorphology of the 2007E deposits after melting. **A.** Relative terrace surfaces in 2007E deposit following melting of the snow component. (7.5 km from Crater Lake). Initial deposit thickness ranged from 90-120 cm in the gorge and were reduced to 20 cm by December 2007. **B.** Terrace surface post-melting, November, ropey and smooth surface textures are barely discernible.

and 2007L caused significant damage to this bridge. The first three bridges were completely destroyed and scattered debris throughout the channel east of the RTMT. Initial construction was plank and rail spanning a narrow gorge in the andesite bedrock. The most recent designs (2000) have been cable suspension bridges spanning a wider section of the gorge about 13 m above the active channel. This new location prevented the complete destruction of the footbridge in March 2007, but still resulted in sufficient damage to require bridge replacement in June 2007 (Fig. 5.17).

The debris from the three previous bridges are distinctive and provided convenient chronostratigraphic markers within the deposit terraces for up to 3 km from the bridge site (Fig. 5.18). The low density of the pine planks and beams means the debris was distributed on the tops of the terraces after rafting along the top of the active flow. The most distinguishing characteristics of the debris are

the nail type, presence or absence of brackets, plank/beam style, and the degree of weathering of the wood surface (Table 5.4).

Table 5.4 Debris from RTMT bridges destroyed by historic lahars.

Event	Wood Style	Distinctive hardware	Degree of weathering
1975	Plank	Capped nails	Highly altered, grey
1995	Plank	Plain nail heads	Slightly altered
1999	Beam & Plank	Plain nails & brackets	Fresh

The bridges constructed on the RTMT, however, are not the only source of debris. The Tukino ski field is located about 3.5 km upstream of the bridge. Various construction projects at the ski field and skier traffic has resulted in some debris being dumped in the Whangaehu Valley. As a consequence, only large near complete bridge pieces were utilised in terrace identification.

5.8.2 Debris Descriptions

April 24, 1975

The 1975 bridge was constructed of narrow pine planks with very distinctive capped nails. The nails have rusted significantly, but remain in the wood (Fig. 5.17). The planks are highly weathered, taking on a greyish hue and softened edges. All of the planks are broken, but fairly large (minimum of 60 by 10 cm) planks are still present. Smaller wood fragments are scattered on the surface, but are difficult to identify, and as such, were not included in terrace identifications or debris counts. Several planks are located above the top of the terrace along the valley walls. These planks are stranded up to two metres on surrounding hill slopes and represent what is left of the high water marks.

September 25, 1995

A slightly more complex bridge built in the same location was washed away by the September 1995 lahar. The planks are significantly larger (110 x 20 cm) than the 1975 debris and have plain nail heads (Fig. 5 17). The wood surface displays some alteration due to exposure, but not as severe as the 1975 planks. Even though the 1995E terrace was not completely inundated, the low density bridge debris is easily remobilised, for example removal by the 2007L lahar.

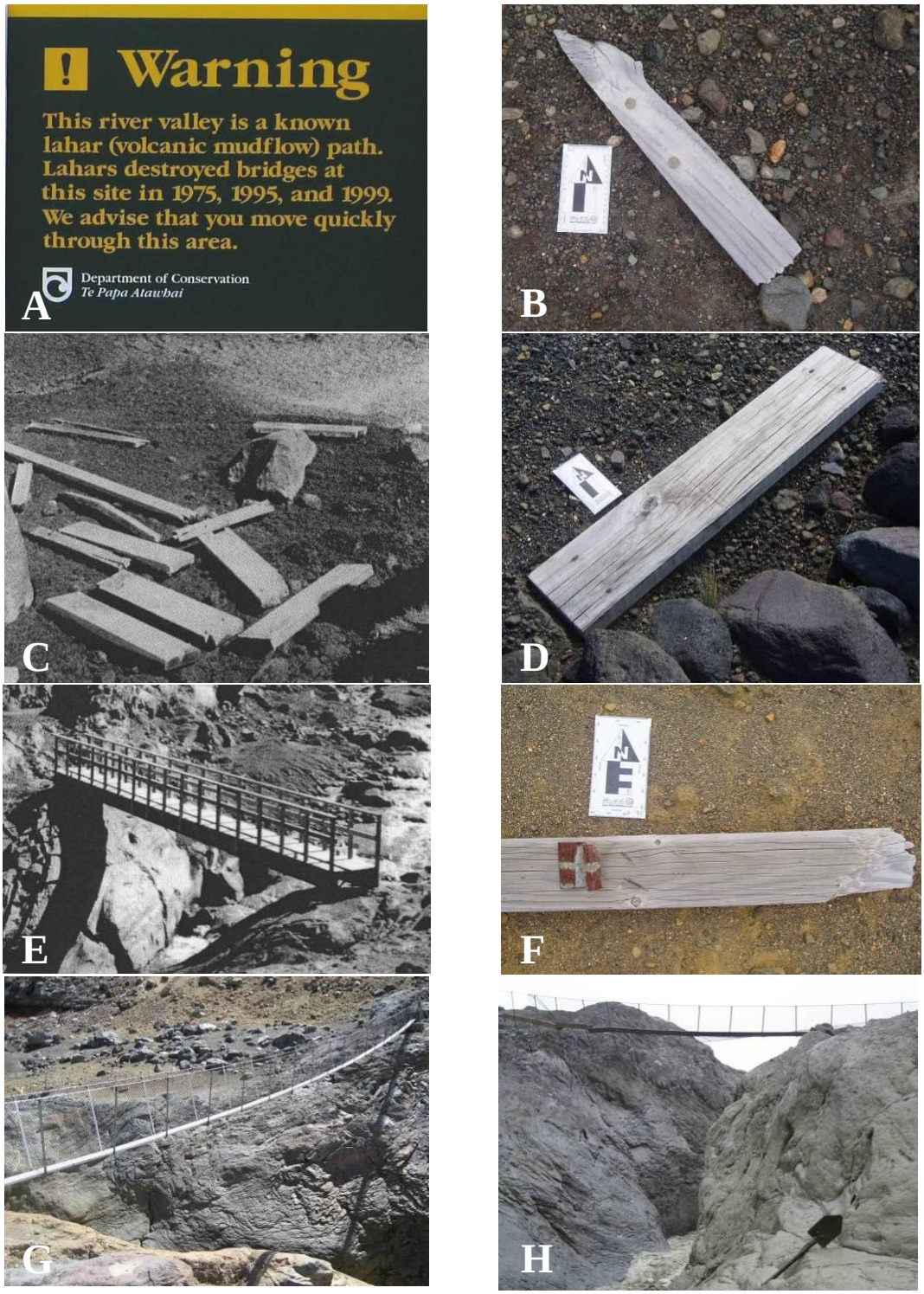

Fig. 5. 17 Chronostratigraphic debris from the Round the Mountain Track bridges destroyed by historic lahars. **A**. DOC warning sign at the RTMT. **B**. 1975 debris with characteristic capped nail heads. Arrow is 10 cm. **C**. 1995E bridge debris (DOC 1996). **D**. 1995E bridge debris in 2007, slightly weathered broad planks. **E**. Replacement of the bridge destroyed during 1995/96 eruption sequence (DOC 1996). **F**. Debris from 1999 lahar, with distinctive brackets on fairly fresh wood. **G**. 2000 replacement swing bridge, relocated downstream to a position 13 m above the active channel. **H**. The improved design was damaged by the 2007L lahar, and replaced in June 2007. Spade points at bolts from the 1995 bridge, reflecting the relative position of the bridges.

1999

After the cessation of the 1995/96 eruptive sequence DOC once again constructed a plank and beam bridge on the RTMT (Fig. 5.17). A rain-generated lahar destroyed the bridge in the fall of 1999. There were two accumulations of 1999 bridge beams on the southern bank of the river within 1 km of the bridge site, and by the bund (removed shortly after emplacement by DOC). The beams were up to 132 cm long with distinctive brackets affixed at each end. The location of the 1999 bridge debris along the active channel resulted in its complete removal by the 2007L lahar.

5.8.3 Tephra

Additional chronostratigraphic constraints are provided by several tephra layers occurring on the top of the gorge diamictons. The most common tephra is from the 1995/96 sequence, occurring on the 1975 and 1995E terraces. However, additional fall material was added to the older terrace surfaces by the 1945 eruption. Any juvenile eruptive material that falls within the valley contributes to the sediment budget of future lahars.

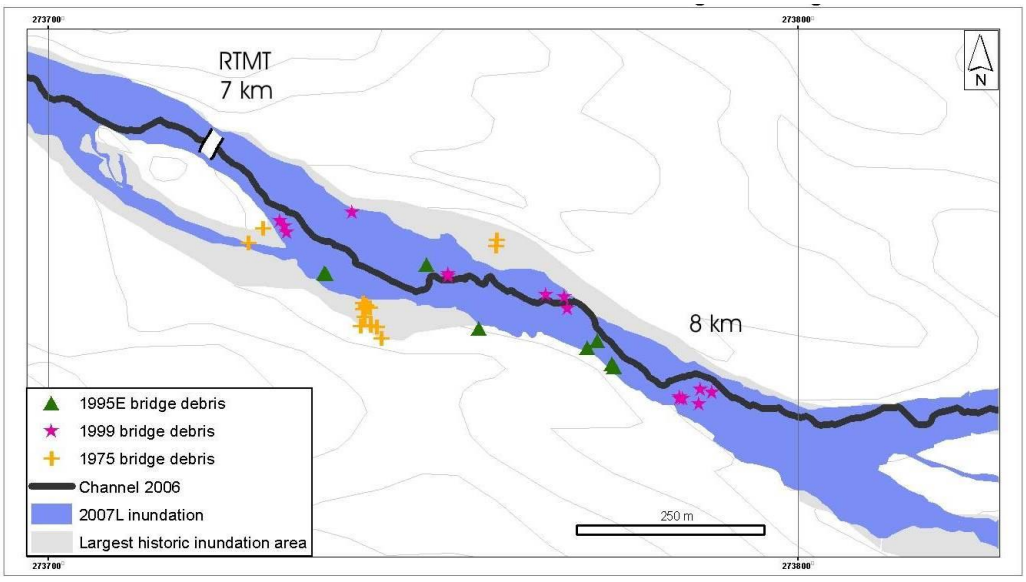

Fig. 5.18 Location of chronostratigraphic debris at the RTMT from bridges destroyed in 1975, 1995 and 1999.

Within the 'spillway' a thin accumulation of remobilised 1945 tephra was revealed by erosion by the 2007L lahar. Undisturbed 1945 material is exposed immediately below 1975 boulders 7 km from source and reflects a

phreatomagmatic origin. The 1995 tephras are fine light grey phreatomagmatic accumulations grading into coarser magmatic material (Fig. 5.19).

As the prevailing winds around Ruapehu are from the south and west ,tephra accumulation, even from small events, is common. Eruptions that have likely contributed to lahars within the Whangaehu include: 1889, 1895, 1903, 1925 (Hodgson 1993), 1945, 1966, 1969, 1971, 1975 and 1977. However, the volume erupted by each event is on the order of <0.1 km^3 (Nakagawa et al. 1999) and the amount accumulated within the catchment of the Whangaehu River is less.

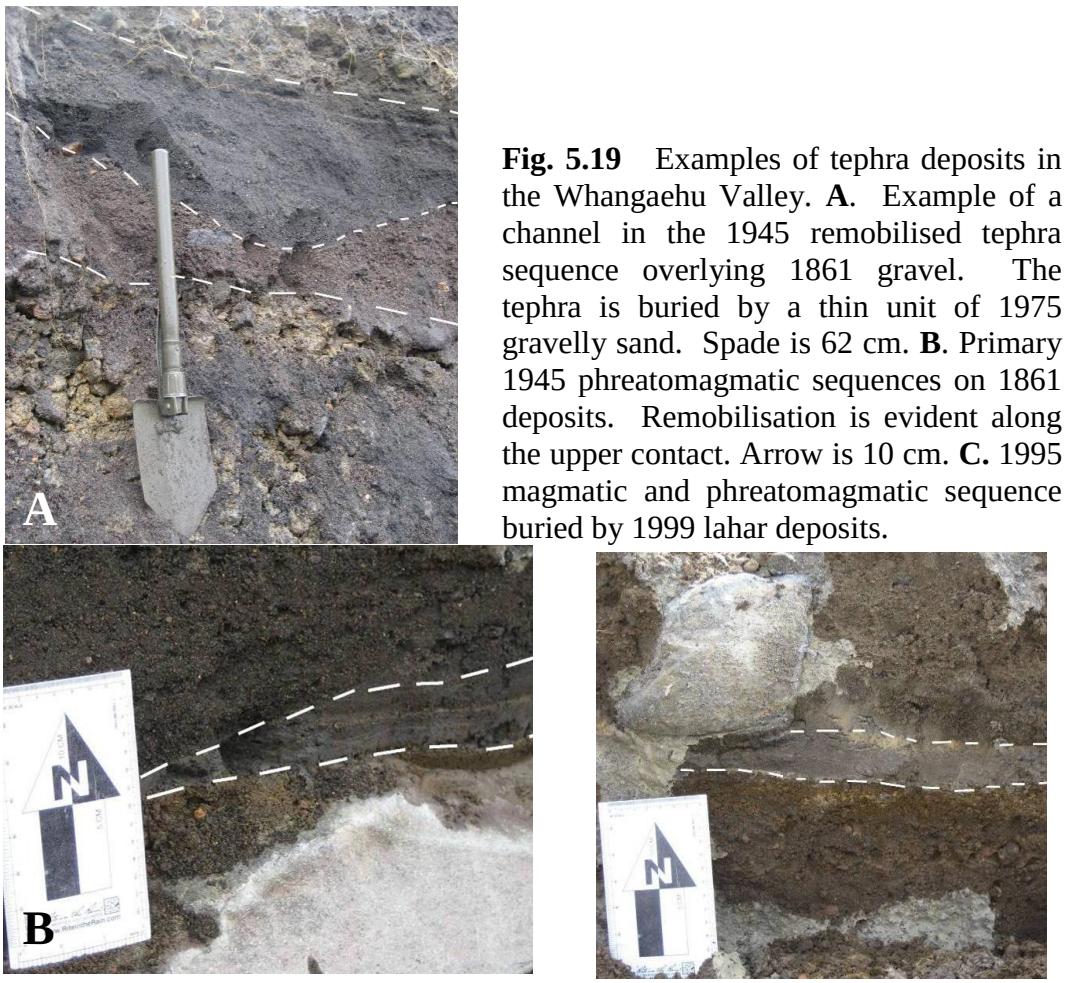

Fig. 5.19 Examples of tephra deposits in the Whangaehu Valley. **A**. Example of a channel in the 1945 remobilised tephra sequence overlying 1861 gravel. The tephra is buried by a thin unit of 1975 gravelly sand. Spade is 62 cm. **B**. Primary 1945 phreatomagmatic sequences on 1861 deposits. Remobilisation is evident along the upper contact. Arrow is 10 cm. **C.** 1995 magmatic and phreatomagmatic sequence buried by 1999 lahar deposits.

Chapter 6 Velocity and discharge estimates for historic lahars in the Whangaehu Gorge

Peak discharge is considered the most convenient measure for the comparison of debris flow magnitude (Pierson 1997, 1998; Leung et al. 2003). However, it does not reflect flow density, which is potentially significant for estimating the energy of the flow and distinguishing between debris flow rheology lahars (i.e. 2007L) and snow-slurry lahars (i.e. 2007E). Peak discharge (Q_p) and velocity are also used to calculate debris flow arrival times and estimate inundation areas. Peak discharge is calculated from the velocity (V) through a cross-sectional area (A), which can be simplified as the product of flow depth (d) and width of the deposit (w):

$$Q_p = V \times A \quad \text{or} \quad Q_p = V \times d \times w$$

The complexity of the internal flow structure and unsteady nature of flow rheology limits the creation of realistic flow models. Flow velocity can be calculated through superelevation marks (common in sinuous, steep-walled, valley-confined flow paths like the Whangaehu Gorge), extrapolation from video footage (including PIV analysis), direct measurement (2007 lahars) and numerical modelling (Table 6.1). Simple calculations such as Manning's equation can be used to estimate instantaneous velocity for lahars with reasonable accuracy, although empirical evidence suggests that values of n appropriate for Newtonian

Table 6.1 Methods of calculating instantaneous velocities and peak discharge for historic lahars of the Whangaehu Gorge.

Event	Velocity in gorge (m/s)	Discharge (m^3/s)	Method	Source
1953	7.9-9.1	2000	Lahar transit times	Manville 2004
1975	10	5000	Instantaneous velocities from super-elevation	Nairn et al. 1979
1995E	9.1	1800	Instantaneous velocities from super-elevation	Cronin et al. 2000
2007L	6-8	1700-2500	Arrival time, super-elevation, and volume calculations	Manville 2007 pers. comm.
2007E	5-12	1000	Arrival time	Manville 2007 pers. comm.

flows need to be increased by a factor of 2 or 3 for sediment-laden lahars of similar volumetric discharge. The result is dependent on the input parameters, which must be obtained from detailed knowledge of the field area, and trial and error calibration (Pierson 1995; Costa 1997).

Although historic Whangaehu Valley lahars are well documented at Karioi gauging station (56.5 km from Crater Lake), direct measurements in the gorge (1-11 km) have only been possible in 2007. Initial flow evolution is critical for understanding how lahars mobilise, bulk and attenuate; however, observation and quantification of near source behaviour is limited. Historic lahar instantaneous velocity and peak discharge have been calculated for the 1975, 1995E and 2007L lahars in the Whangaehu Gorge using superelevation measurements based on high-water marks. Field evidence can similarly be used to derive instantaneous velocity using Manning's equation. A comparison between superelevation derived velocities and Manning's velocities enable calibration of Manning's n, the coefficient of roughness for the Whangaehu Gorge. Because of the continual remobilisation and eruptive activity in October 1995 there are no discharge estimates for the 1995R lahars within the gorge, similarly, there were no observations of the 1999 lahar. Estimations based on terrace heights and detailed channel geometry allows velocity calculations for historic mobilisation events.

Manning's equation [2] for instantaneous mean flow velocity is based on the channel geometry, slope and hydraulic radius (Fig. 6.1):

$$V = \frac{1}{n} \times S^{1/2} \times R^{2/3}$$

where n is Manning's coefficient of channel roughness (Chow 1959). The channel geometry is also defined by its slope (*S*) and hydraulic radius (*R*). Hydraulic radius is defined by the relationship between wetted perimeter (*P*) and cross-sectional area (*A*) of the channel:

$$R = A / P$$

[2] $V = \frac{1}{n} \times S^{1/2} \times R^{2/3}$ is used for metric calculations. Alternatively, for imperial units Manning's equation is $V = \frac{1.49}{n} R^{2/3} S^{1/2}$ (Chow 1959). The value of n is not affected by this conversion.

A straight regular section of the Whangaehu Gorge with large historic lahar terraces was selected to represent the least complicated section of the upper flow path between the convergence (6 km from Crater Lake) and the RTMT bridge (7 km). Without major bends, waterfalls, or obstructions the channel cross-section was approximated as a trapezoid (Fig. 6.1):

$$A = \frac{(x + w)}{2} \times d$$

x represents the width of the active channel, *w* represents the width of the deposit surface and *d* is the stage height, or flow depth.

The instantaneous velocity obtained from Manning's equation can then be used to estimate the Q_p for that location based on the cross-sectional area of the flow.

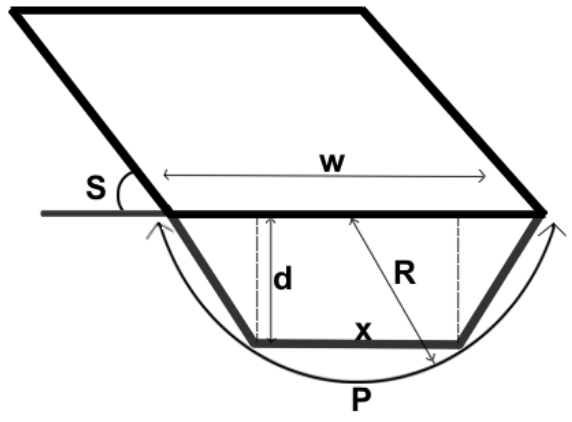

$$A = \frac{(x + w)}{2} \times d$$

$$R = A / P$$

$$V = \frac{1}{n} \times S^{1/2} \times R^{2/3}$$

$$Q_p = V \times d \times w$$

$$Q_p = V \times A$$

S = slope
w = width of deposit surface
x = width of active channel
d = flow depth/stage height
P = wetted perimeter
A = cross-sectional area
V = mean flow velocity
n = Manning's roughness coefficient

Fig. 6.1 Cross-sectional geometry of an idealised channel. The shape of the channel is represented by a trapezoid. Measurements of channel width and slope are derived from the 2006 and 2007 LiDAR based DEM. LiDAR courtesy of GNS and Massey University.

Discharge of the 1975 lahar was estimated by Nairn et al. (1979) at the convergence, 6 km from Crater Lake, where high water marks were well documented by oblique photos. The RTMT is the current location of lahar monitoring equipment installed and operated by GNS and Massey University, including a radar stage gauge, AFMs and a broadband seismometer, enabling calibration of estimated velocities and discharge with measured events from 2007. The gorge between 6 and 7 km from Crater Lake is broad (150 m) with a slope of approximately 0.046 and fairly simple geometry, making it an ideal location for calibration of the Manning's equation.

6.1 Determination of Manning's roughness

The roughness of a channel can be described in terms of Manning's n, a dimensionless iteratively derived coefficient of roughness (Chow 1959). Although initially designed for uniform steady, sub-critical Newtonian flow, Manning's equation has been found to fit lahar models for flows with established flow path geometries and flow histories (Costa 1997; Manville 2004).

The roughness of a flow path is derived from grain size, vegetation, channel irregularity, channel alignment, obstructions and relative size of the channel. As flow depth increases, the effects of channel roughness decrease (Chow 1959; Manville et al. 2002), although the relationship between channel roughness and high sediment concentrations in high magnitude flows is not yet understood. Flow through the RTMT section of the gorge is channel confined and fairly deep, making grain size and geomorphology the most significant contribution to channel roughness. Vegetation in the Whangaehu Valley is negligible.

Natural boulder dominated channels typically have estimated n values between 0.034 and 0.04 (Chow 1959). The complexities of the first 11 km of the gorge have been described by n = 0.15 to include the macro-roughness generated by major bifurcations and numerous waterfalls that occur throughout the gorge and the hydraulic jumps generated at transitions between sub- and super-critical flow at these features (Manville 2004). Based on lahar modelling in the Cascades ,Costa (1997) determined that for a hydraulic radius <10 m a value of 0.10 > n >0.05 is generally appropriate.

The highest flow velocities will occur where frictional resistance is lowest, in the least complicated flow path. Oblique aerial photos and terrace thicknesses indicate that some of the highest flow depths occur in the RTMT section between 6 and 7 km from Crater Lake. Consequently, when using precise cross-sectional measurements, peak discharge estimates from a small uncomplicated section of the gorge will be representative of the greatest velocity and the highest discharge for Whangaehu Valley lahars. The estimates for this section of the gorge can easily be compared with measurements of 2007 lahar events from a GNS gauging site located 100 m from RTMT.

6.2 Calibration

The accuracy of the Manning's equation is dependent on the accuracy of the parameters used. As the values of n can be subjective, knowledge of the flow path is critical, and the use of previously measured and modelled flows reflects the suitability of such assumptions.

Using LiDAR based measurements of the channel geometry and flow depth of the 1975, 1995E, 2007E eruption-generated and 2007L Crater Lake outburst lahars, Manning's equation-derived discharge and instantaneous velocities were compared with estimates presented by Nairn et al. (1979), Cronin et al. (2000) and GNS arrival time data (Manville pers. comm. 2007) (Table 6.2).

The superelevation derived estimates produced by Cronin et al. (1997c) for the 1995E lahar match well with Manning's estimates using n = 0.11, with a Q_p = 1800 m^3/s. Arrival time gauged velocities and discharge from March 2007 were similarly reproduced with LiDAR derived geometries and n = 0.11 and Q_p = 2500 m^3/s (Manville pers. comm. 2007). There are, however, some discrepancies

Table 6.2 Calibration of Manning's equation for the RTMT section (6 to 7 km from Crater Lake) of the Whangaehu Gorge.

Event	Source	Stage height (m)	Manning's n	Q_p peak discharge (m^3/s)
1975	Nairn et al. 1979	6	0.03	5000
1975	this study	12	0.03	12000
1975	this study	12	0.11	7500
1995E	Cronin et al. 2000	5	0.11	1800
2007L	Manville pers. comm. 2007	12	0.11	(maximum) 2500
2007E	Manville pers. comm. 2007	2	0.04	1000

between superelevation, arrival time and volume based estimates of 2007L mean velocity and peak discharge suggesting a range of Q_p from 1700 m^3/s to 2500 m^3/s.

Field observations and the 2006 LiDAR revealed that the 1975 deposits were significantly larger than initial estimates made by Nairn et al. (1979). Nairn et al. (1979) estimated the peak discharge in the gorge from super-elevation derived velocity of 10 m/s and an estimated flow depth of 6 m. This would produce a peak discharge of c. 5000 m^3/s. However, the 6 m flow depth is a 50% underestimation of the actual flow depth, as reflected in terrace height and historic aerial photos. Erosion caused by the 1995E and 1995R/1999 revealed that the 1975 deposits reached thicknesses of 9-12 m throughout the gorge. In the RTMT region, the terraces average 10 m thick. Oblique aerial photos from 1975 reveal high water marks between 2 and 3 m above the surface of the deposit. Hence, the flow depth of the 1975 lahar near the RTMT (6 to 7 km from Crater Lake) may have been as high as 12 m.

An application of estimations provided by Nairn et al. (1979) to the Manning's equation would require n = 0.03 to produce a peak discharge on the order of 5000 m^3/s. If the same input parameters are used, using the revised maximum flow depth of 12 m, the cross-sectional flow area is doubled, and therefore the discharge is also doubled. This results in a velocity of 14-15 m/s and a discharge through the gorge as high as 10,000 m^3/s producing estimates significantly above that of the more accepted superelevation calculation.

In order to produce an instantaneous velocity for the 1975 lahar through the revised flow path geometries that is comparable to super elevation derived velocity estimates (c. 10 m/s) a Manning's n = 0.11 is reasonable. Resulting in Q_p = 7500 m^3/s. This agrees well with the Manning's n used to reproduce super elevation derived velocities and discharges for the 1995E and gauged 2007L lahars.

6.3 Applying Manning's n

After calibration of Manning's n for the RTMT section of the Whangaehu Gorge, velocity and discharge estimates for the 1861, 1995R and 1999 are possible. Flow depth in the RTMT section for the 1995R and 1999 lahars was not measured directly, but terrace height can be used as an estimate. Using n = 0.11

for terrace confined flow, discharge was estimated around 420 m^3/s for 1995R and 250 m^3/s for 1999 (Table 6.3). These results are well-matched (Fig. 6.2) to the relative magnitude of historic lahars based on terrace height and downstream observations (Cronin et al. 2000).

Although the 1861 lahar deposits are incomplete, the thickness and distribution of the diamicton (on both sides of topographic divides like the spillway) allow estimates of flow thickness and hydraulic radius. Flow depth estimates are minimum values as the upper contact of the deposits is erosional.

Table 6.3 Velocity and peak discharge estimates based on calibrated slope area calculations for the 1861, 1995R, 1999 and 2007E lahars in the Whangaehu Valley.

Event	Stage height (m)	Manning's n	Velocity (m/s)	Q_p peak discharge (m^3/s)
1861	17	0.15	12	11000
1861	10	0.11	10	7500
1995R	3.5	0.11	4	420
1999	2.5	0.11	3	250
2007E	2	0.11	3	300
2007E	2	0.035	10	1000

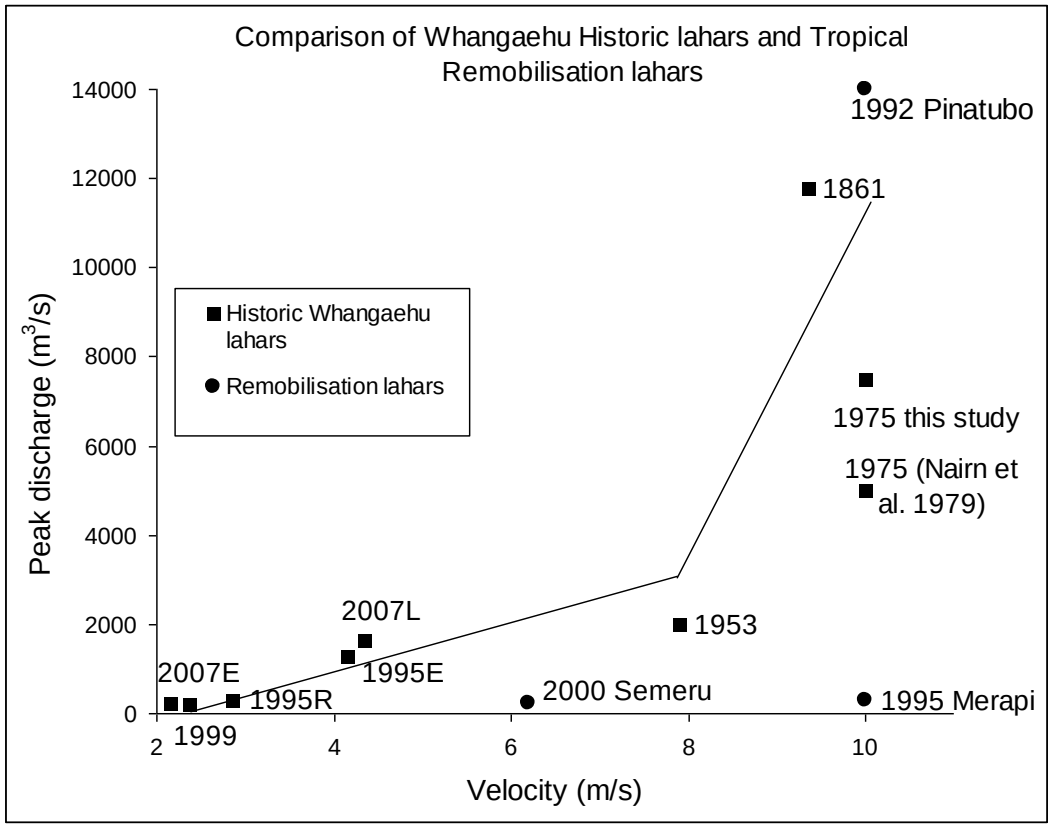

Fig. 6.2 Lahar velocity and peak discharge for historic lahars in the Whangaehu Gorge and similar scale remobilisation lahars from Indonesia and the Philippines.

The height of the 1861 deposit surface above the active channel reaches 10 m under a 1975 gravel bar east of the RTMT bridge, while within the spillway the deposit is 17 m above the active channel. Near the RTMT gauging site stranded boulders have been speculatively associated with the 1861 deposits and are approximately 15 m above the channel. Using the calibrated n = 0.11 a flow depth of 10 m returns a velocity on the order of 10 m/s and Q_p = 7500 m^3/s in the gorge. Flow depth estimates up to 17 m produce flow velocities around 12 m/s and Q_p = 16000 m^3/s. However, the distribution of the 1861 deposits reflects significant interaction of the flow with topographic divides which contribute to flow resistance and may require greater values of n. Using a manning's n on the order of n = 0.15 and flow depth up to 17 m produces a more reasonable estimate on the order of 9 m/s and Q_p = 11000 m^3/s.

The 2007E lahar presents additional challenges to Manning's calibrations as the flow was more than 40 wt. % snow. The surface morphology of the deposits, including pressure ridges, a ropey texture, and longitudinal shear suggests that the flow was visco-plastic. Granular snow slurries may interact differently with channel roughness than more dilute Newtonian and denser sediment-laden flows. Velocity estimates for the largest pulse of the 2007E lahar based on arrival times reflect high average velocities on the order of 12 m/s. However, slope-area calculations using n = 0.11 would produce much lower instantaneous velocities, c. 3 m/s and Q_p = 300 m^3/s. In order to replicate velocity estimates obtained from transit times a much lower resistance coefficient (n = 0.035) is required, close to the value predicted for Newtonian flows bouldery channels similar to the RTMT section of the gorge.

The range of lahar behaviours and magnitudes that have occurred historically in the Whangaehu Valley provide the opportunity to investigate the lahar potential of Crater Lake and glacier clad volcanoes. While channel confined flows non-cohesive debris flows with volumes between 10^5 and 10^6 m^3 can be modelled using an iteratively calculated coefficient of roughness and slope area calculations, exceptional examples, such as high magnitude flows and snow slurry lahars reflect how much more is to be learned about lahar evolution.

Chapter 7 Magnitude of lahars in the Whangaehu Valley

7.1 Lahar magnitude

Lahar magnitude comparison is dependent on the parameters used to describe an event's scale. New Zealand and international lahar literature utilise a myriad of parameters to indicate the size of a flow and its impact; but used most commonly are volume, peak discharge, competence and deposit thickness. If the parameters are applied to the historic lahar deposits of the Whangaehu Gorge 1861 has the largest volume, 1953 had the greatest human impact, 1995E had the highest content of high density clasts and 1975 had the greatest peak discharge and competence.

Jakob (2005) proposed a scale for debris flows based on volume, peak discharge and inundation area. The historic Ruapehu lahars fall in class 5 and 6 (with volumes ranging from 10^4 to 10^6 m^3), similar to other small to medium volcanic debris flows (Mt Spurr; Waythomas 2001; Semeru; Lavigne and Suwa 2004). The ancient lahars of the Onetapu Formation, with estimated volume over 10^7 m^3 would have been similar to the lahar produced in the South Fork Toutle River in 1980 on Mt. St. Helens. The peak discharges associated with events of this scale are on the order of $3x10^4$ to 10^6 m^3/s (Jakob 2005). As the Crater Lake plays a major role in the volcanic activity and the formation of lahars, comparison of historic lahar magnitude can only be extended to the lifetime of the lake.

The scale of historic lahar deposits in the Whangaehu River suggest a correlation between trigger mechanism and flow size (Mastin and Witter 2000). Lake outburst and large eruption-triggered events produce flows with volumes up to 10^6 m^3 and peak discharges greater than 1500 m^3/s. However, this pattern is a direct result of the relationship between trigger mechanism and sediment/water budgets. The size of an eruption, or rain storm does not directly correlate to the size of accompanying lahars. Although debris flow magnitude increases with increased sediment budget and longer return time (Jakob 2005) phreatomagmatic eruptions in 1975 and 1995 were responsible for some of the largest events within the Whangaehu Valley, occurring without widespread tephra accumulation (Donoghue and Neall 2001). Remobilisation lahars up to $9.5x10^5m^3$ (1995R) are larger than many eruption-generated flows (September 18, 1995 $1x10^5m^3$; Cronin

et al. 1997c; 2007E $1x10^2m^3$). Additionally, larger eruptions would not necessarily increase the volume of water that would reach the catchments and contribute to lahar formation, due to losses to the eruption column and the rate of debris mobilisation relative to accumulation.

However, trigger mechanism does control water budget as the volume of water released and contributed to lahar formation: snow melt/collapse and precipitation are dependant on the nature of the trigger. The trigger mechanism only contributes to the sediment budget during juvenile producing eruptions. The volume of sediment available for lahar formation is a result of weathering, debris stability and time; thus, return rate, or frequency of lahar occurrence, contributes to flow size (Jakob 2005).

In the case of Crater Lake release lahars, a discrete volume of water is released, and trigger mechanism directly controls the magnitude of the resulting lahar. For eruption-generated lahars the scale of an eruption is only one of many factors that determine the size of lahars produced. Deposit saturation and deposit consolidation control the volume of water required for sediment mobilisation, but only contribute to the overall flow volume in the case of remobilisation events. The volume of water available for lahar formation is also controlled by seasonal variations, the volume of snow within the crater basin and on the Whangaehu Glacier.

Of all the size parameters utilised in lahar quantification, peak discharge and volume estimates are the most consistent for historic Whangaehu Valley lahars, obtained predominantly for Tangiwai (39 km from Crater Lake) and Karioi (56.5 km).

The southern branches of the Whangaehu Valley are for the most part separated from the main northern channel by an elevated bedrock divide. These divides are overtopped by particularly high volume flows and eruption-generated flows travelling down the Whangaehu Glacier that jump the northern gorge and directly enter the southern channel. Three main divisions occur: at 1.5 km (above the Alpine Hut), 2.5 km near the Tukino Ski field and at 8.4 km (the chute divide). The distribution of lahar deposits on either side of the first division correlates to eruption-generated and lake release lahars (Fig. 7.1). Eruption-generated flows travel down the Whangaehu Glacier and bypass the divide, and are routed directly into the southern channel. Water expelled from the normal Crater Lake outlet

remains in normal stream channel on the north side of the divide and only reaches southern branches when flow volume is high (i.e. 2007L). Remobilisation lahars occur wherever significant volumes of debris have accumulated, but are generally confined to the active channel region.

Lahar deposit distribution on either side of the RTMT spillway and Chute divide are controlled by lahar size. Flows over a certain volume, defined by the height of the active channel relative to the spill-over points in the channel wall leading to the normally isolated southern channels. The volume required to overtop these divides is dependent on recent sedimentation and erosion within the channel.

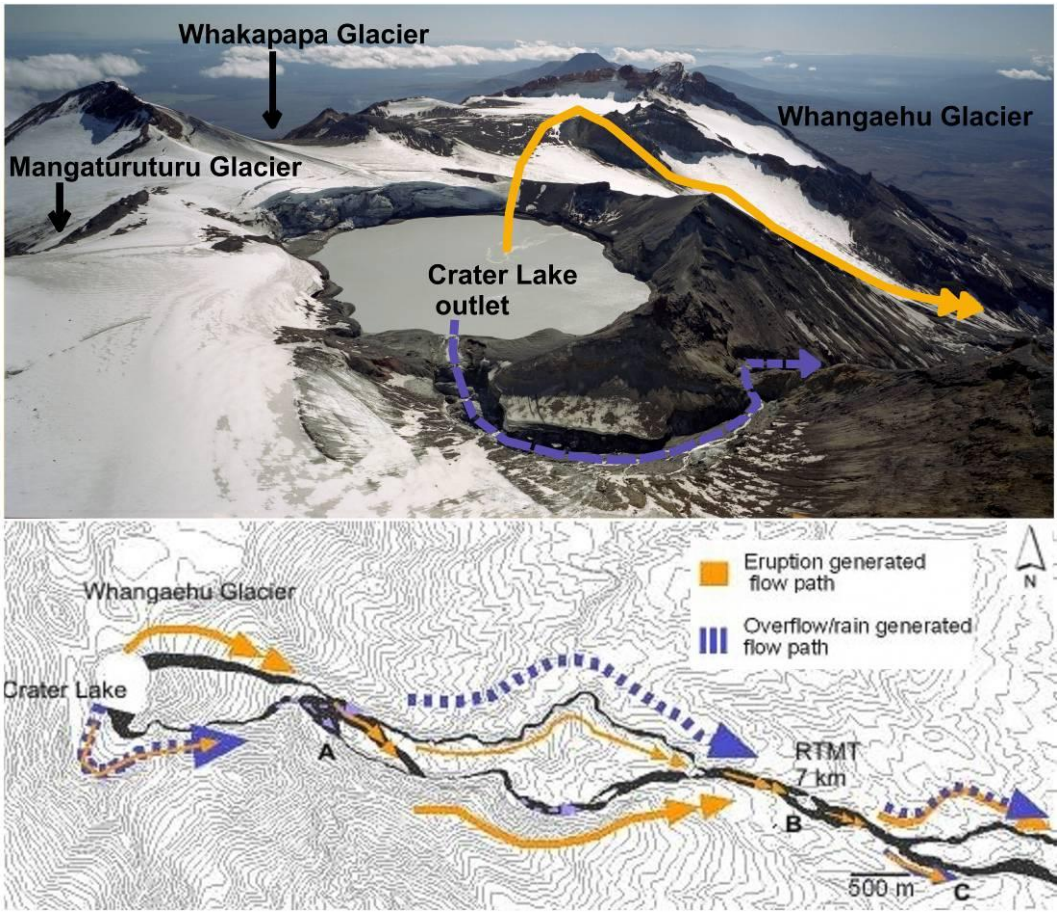

Fig. 7.1 Flow path bifurcations in the Whangaehu Gorge. **A.** 1.5 km from Crater Lake where water routed over the Whangaehu Glacier is diverted into the southern channel. Flows with volumes greater than the overflow point on the channel reach the isolated southern channels. **B.** The spillway 600 m long, located 7 km from Crater Lake at the Round the Mountain Track (RTMT). **C.** The Chute (8.4 km from Crater lake), a straight highly erosional gully that rejoins the northern branch on the Whangaehu Fan 17.5 km from Crater Lake.

Palmer et al. (1993) observed an absence of abrupt changes in distal Whangaehu fan lithofacies of the kind that are observed in typical alluvial fans. This is the result of Whangaehu Fan dissection, variable sizes of lahars across the fan and the greater sediment transport distance of lahars compared to typical fluvial systems. The fan morphology itself is atypical of alluvial fan growth, as an ideal fan is incised only at the head of the fan where the stream flow loses most of its energy, depositing sediment and remaining unchannelised downstream (Palmer et al. 1993). The Whangaehu lahars, however, have incised numerous channels into the fan surface, fan aggradation occurs only when deposits overtop these channels.

7.2 Lahar potential

Historic Whangaehu Valley lahar volumes, as measured or estimated 39 km from source, have reached up to $6x10^6$ m^3 and remained valley constrained, threatening development immediately surrounding the river channel, predominantly road and rail bridges. However, pre-historic events represented by the Onetapu Formation have been estimated at $>1.5x10^7 m^3$ (Hodgson et al. 2007). As historic lahars are fairly frequent, but small in volume, the sediment budget within the Whangaehu Valley does not have time to accumulate significant volumes of debris. The size and frequency of lahars produced along a flow path is dictated by the available sediment budget (Bovis and Jakob 1999). Juvenile material not mobilised by eruption-generated lahars are progressively removed by remobilisation and lake release events. The snow pack on the summit contributes directly to the volume of resulting lahars, but eruptions have historically occurred in spring and summer when the snow pack has already begun melting. Thus, it can be expected that the only means of achieving the volumes of water and sediment to produce an event on the order of 10^7 m^3 would be a sector collapse or large eruption in winter. The pre-historic lahars of the Onetapu Formation are predominantly cohesive, having significantly more clay than historic Whangaehu Valley lahars. High clay content and the large volume of the deposits suggest that large scale events are the result of sector collapse incorporating material from the hydrothermally altered volcanic flanks (Hodgson 1993; Vallance and Scott 1997; Capra et al. 2004; Hodgson et al. 2007).

The lahar activity of the last 2000 years reflects a much smaller scale than international examples. Eruption-generated lahars at Nevado del Ruiz in 1985 reached magnitudes of up to 10^7 m^3 and 10^8 m^3 at Mt. St. Helen's in the North Fork Toutle River in 1980. Sector collapses at Mt. Rainier (5.7 k.a.) reached volumes of 10^9 m^3 (Vallance and Scot 1997).

The depositional record of the Whangaehu suggests that lahar volumes can reach up to 10^6 m^3 as a result of eruption-generated melting, ejection of lake water and Crater Lake release. Smaller events are produced by small scale eruptions, lava dome growth within Crater Lake, volcanic tremors caused by changes in lake floor bathymetry and injections of fluid from the sub-lake, vent-hosted hydrothermal system and precipitation related remobilisation. Lahar mitigation can focus on revising warning systems to include smaller scale unpredicted events, and preparation for larger eruption-generated lahars and predictable Crater Lake release events. However, significantly larger events can be produced by the collapse of the volcanic flank, which has already happened nine times in the last 2000 years (Hodgson et al. 2007).

Chapter 8 Discussion

The reconstruction of lahars in the Whangaehu Gorge is based on a combination of the sedimentology, petrology and geomorphology of the deposit, which provide information about their triggering mechanism, flow behaviour, bulking history and deposition. Trigger mechanisms have been established for the majority of historic events, enabling the correlation of sedimentary and geomorphologic characteristics with triggering mechanism and the potential for interpreting prehistoric deposits.

8.1 Lahar evolution

8.1.1 Trigger mechanism

Historic lahars have been generated in the Whangaehu Valley by three major trigger mechanisms. Despite some outward similarity of the deposits, the events present different challenges for hazard mitigation. The rate of lahar generation controls the time it takes for a lahar to reach peak discharge (Fairchild 1987), which is reflected the shape of the flow hydrograph (Table 8.1). Inundation area and peak discharge are the most important factors in quantifying lahars for the purposes of mitigating lahar related hazards, followed by velocity (Pierson 1997; Leung et al. 2003).

Table 8.1 Peak discharge for historic lahars exiting the Whangaehu Gorge (11 km from Crater Lake).

Event	Peak discharge	Source
1953	1500-2000 m^3/s	Manville 2004
1975	5000- 7500 m^3/s	Nairn et al. 1979/ this study
1995E	1400-1800 m^3/s	Cronin et al. 2000
1995R	420 m^3/s	this study
1999	220 m^3/s	this study
2007L	1700-2500 m^3/s	Manville 2007 pers. comm.
2007E	1000 m^3/s	this study

8.1.2 Eruption

In the event of an eruption any volcano with a semi-permanent water source, or a very wet climate, can be expected to experience sediment-laden mass flows during the eruption or shortly thereafter (e.g. Mt. St. Helen's 1980, Nevado

del Ruiz 1985, Redoubt 1990, Pinatubo 1991). Eruptions through a crater lake can trigger lahars through the melting of snow and ice, ejection of lake water, volumetric displacement of lake water and collapse of snow and ice by ballistic impacts (Pierson 1997; Mastin and Witter 2000). Historic eruption-generated lahars in the Whangaehu Valley have been produced by two main mechanisms requiring two distinct mitigation approaches. During phreatic and magmatic eruptions water is ejected from the Crater Lake onto the summit area, incorporating snow and ice from the Whangaehu Glacier before being routed into the Whangaehu Gorge. Disturbance of the lake by gas release, rising magma, lava dome growth and explosion-generated waves displace lake water over the outlet on the southern edge of Crater Lake. Discrete lahars derived from the ejection of Crater Lake water during volcanic eruptions have occurred in 1895/99, 1969, 1975, 1995 and 2007 (Table 8.2). In 1945 the growth of a lava dome progressively emptied the crater lake by evaporation and volumetric displacement

Table 8.2 Lahar triggering mechanisms with historic examples from the Whangaehu Valley, Mt. Ruapehu.

Trigger Mechanism	Whangaehu Gorge Example
Eruption Generated	
Discrete (melting, eruption of lake water)	1889/95, 1969, 1975, September 1995 and September 2007
Seismic activity associated with an eruption	1968
Progressive release during growth of a lava dome (melting and displacement of lake water)	1945
Remobilisation	
Destabilisation of tephra deposits	September 1995 to April 1996
Precipitation event	October 1995 and 1999
Lake release	
Crater lake dam failure	(1861), 1953 and March 2007
Temporary damming	(1925)

The use of () indicates unconfirmed trigger mechansim confirmed.

of water through the lake outlet. In 1968 prolonged seismic tremors associated with rising magma caused a series of displacement lahar pulses to travel through the outlet down the Whangaehu Valley.

Primary-eruption generation

Lahars produced by the ejection of Crater Lake water and the melting of snow and ice at the crater range in size from small snow slurries, e.g. September-October 1995 and September 2007 (Cronin et al. 1996b; Manville et al. 2000a) to valley wide debris flows, e.g. 1975 (Nairn et al. 1979; Pierson 1995; Cronin et al. 1997b). Explosion-derived melting and lake water ejection result in near-instantaneous lahar inception. This results in the rapid formation of a steep hydrograph as the flow rapidly reaches peak discharge (Manville 2004). As historic eruptions on Ruapehu have been predominantly small scale phreatic, phreatomagmatic and strombolian events, the lahars have been proportionally small.

Water is ejected from Crater Lake as a result of an explosion at various depths below the lake (Table 2.1). Shock wave generation promotes an upwelling of lake water and spray dome at the surface of the lake. Vertical jets of steam and gas entrain hot juvenile and crater wall components, warm lake mud and low temperature lake water (a directional component can be imparted by vent orientation). Water is lost to steam, adding to eruption energy. The collapse of the spray jet creates a base surge, frequently compared to underwater nuclear testing at Bikini Atoll (Nairn et al. 1979). Surge clouds have been described at Ruapehu in 1968, 1971 (Healy et al. 1978), 1975 (Nairn et al. 1979), 1995 and September 2007.

The bulk of water ejected from the lands within the crater basin and returns to the lake, entraining significant volumes of snow and ice from the Crater Basin Glacier and thus complicating estimates of ejected water volume from net lake level fall. However, water ejected outside the crater lake basin is dispersed over the summit so the volume of water is divided among all of the catchments draining Ruapehu. As eruption energy increases, the volume of water incorporated into the eruption column also increases, and is removed from the lahar-producing water budget. The water budget for explosion-generated lahars

includes basal surge, vertical jets, rain out of eruption column, melting and collapse of glacial snow and ice by hot ejecta and base surge.

The interaction of ejected water and debris with perennial snow and glacial ice increases the lahar forming water budget (Dinehart 1997; Pierson 1997) and can create unique snow-dominated flows (Pierson and Janda 1994; Waitt et al. 1994). The lithic components of phreatic eruptions are cold and do not induce as much melting as juvenile producing eruptions.

The volume of water contributed by the melting of snow is unpredictable and controlled by snow accumulations and extent of ballistic ejection. Models of snow contributions to lahar volume was attempted by Otway et al. (1995) but requires further study. On Ruapehu snow slurries have been created by phreatomagmatic (1969 and 1995) phreatic eruptions (2007E). Snow-dominated debris flows have also been described at Mt St. Helens (1982- 1984), Redoubt (1989) and Nevado del Ruiz (1989) (Pierson and Janda 1994; Waitt et al. 1994).

The 1975 debris flow in the Whangaehu Gorge was the largest of the historic eruption-generated lahars. However, in April 1975 the snow pack was quite small, having been decreased by summer melting (Patterson 1976), if the eruption had occurred in the winter the lahars may have been far more voluminous. There were no observed snow slurries associated with the 1975 eruption.

Progressive displacement of Crater Lake water

In 1945 lake water was lost to steam through contact with the hot lava dome, however, the volume displaced into the valley was still significant for a short period. The heightened discharge was observed at the outlet (Oliver 1945; Reed 1945), but there is no documentation on the downstream affects of the lake emptying. Discharge of lake water reached 1.42 m^3/s in July 1945 (Oliver 1945), significantly less than discharge during outburst floods i.e. 1953 (~500 m^3/s; Manville 2004), but more than background outflows of 0.05 to 0.25 m^3/s (Oliver 1945; Christenson and Wood 1993). Instead of a discrete lahar, the result was most likely a sustained high flow within the valley from March to July 1945. Aerial photographs indicate that aggradation and terrace redistribution occurred within the gorge over an area of $3x10^5$ m^2 (Table 4.1).

In 1968 water displacement occurred as a result of rising magma beneath Crater Lake. The eruption and lahars were not large in volume, but they are

significant for the delayed inception of a discrete lahar event. The 1968 eruption was one of two phreatic events that resulted in the displacement of lake water during a period of activity from 1964 to 1969 (Vignaux and Weir 1990). However, water was released from the lake as the result of the prolonged seismic activity and uplift of the crater floor and not a discrete explosion. The result was a series of seven debris flow pulses that produced a multi-peaked hydrograph.

Although discrete deposits do not appear in the geologic record, the mobilisation and aggradation caused by a non-explosive lake empting would result in a reorganisation of lahar deposits and decrease the preservation of sedimentary structures and morphology. For mitigation purposes it is most appropriate to discuss dome growth-related events as eruption-generated, although, the flow behaviour of progressive release events would be expected to differ from instantaneous release events.

Displacement of lake water also contributes to lahar volume during more explosive eruptions. During the early (September) phases of the 1995/96 eruption sequence lahar explosion-generated lahar volumes were augmented significantly by displacement of lake water through the outlet.

8.1.3 Remobilisation

The mobilisation of debris by precipitation, snow melt and destabilisation can be concurrent or independent of volcanic activity. The destabilisation and failure of debris creates instantaneous remobilisation, producing small volume lahars that peak rapidly. The remobilisation of tephra and volcanic ejecta on snow clad volcanoes is outlined by Manville et al. (2000a). The failure of a sediment mass can be described in terms of Coulomb friction (Iverson 1997) where failure occurs when driving forces (gravity) exceeds the resisting forces (internal strength and friction). Volcanoes are typically covered in a large supply of unconsolidated material at steep angles. Failure occurs as a result of saturation, destabilisation by earthquake and collapse of debris laden snow. Saturation of unconsolidated tephra can cause failure by increasing the pore pressure reducing friction between particles and decreasing normal stress (buoyant lift). Saturation also increases the gross weight of the deposit, increasing basal shear. The resulting shear surface can be along a change in permeability, grain size, or lithological contacts.

Remobilisation lahars are typically smaller in volume than eruption-triggered lahars, as a function of their frequency, lack of erosion and self-contained water budget. The volume of water in the sediment mass at the initiation of motion represents the bulk of the water budget for the entire flow: saturated debris, snow collapse etc. Motion begins as a saturated sediment mass, not a dilute bulking flow. The resulting flow is already at, or near, sediment capacity, resulting in limited erosion. Without significant dilution the flow cannot bulk. This is reflected in the dominance of scoria and low density hydrothermally altered clasts in remobilisation lahar deposits. Unlike the highly erosive concentrated eruption-generated and outburst flood lahars that entrain all sediment within the gorge, remobilisation lahars mobilise primary tephra from the upper slopes of the volcano and only entrain low density clasts from the flow path. Low density material is more readily mobilised compared to similar sized higher density clasts, a detailed investigation of the hydrodynamic properties of vesiculated clasts was conducted by Manville et al. (2002). The lack of erosion and bulking associated with remobilisation lahars is distinctive (Cronin et al. 1997c). Without bulking and high sediment concentrations flow attenuation and debulking will occur more rapidly (Fig. 5.17) as evidenced by their small volume and short run out distances.

The 1995R lahar represents syn-eruption remobilisation, and the 1999 lahar represents inter-eruption remobilisation. The volume, discharge and sediment concentrations of these two events are less than the historic eruption-generated lahars (Table 2.3).

Based on observations following the 1995/96 eruption sequence, approximately 15% of the total tephra volume deposited on the flanks of Ruapehu was removed in the first six months after the eruption ceased (Manville et al. 2000a). The 1999 rain-generated lahar continued this process, but also reworked the 1995R deposits already within the valley. The frequency of remobilisation events is limited by distributions of tephra. Historic eruptions with prolonged magmatic activity such as those in 1895, 1945 and 1995 deposited sufficient tephra (specifically on snow) to cause remobilisation (Healy et al. 1978 and Nairn et al. 1979), however, this record is limited by the poor documentation of secondary lahars prior to 1995.

Despite the small volumes of material mobilised, rain-generated lahars can still be destructive, in the Whangaehu Valley the RTMT bridge was destroyed in both 1995 and 1999. The damage from remobilisation lahars from October 1995 to April 1996 was greater than the eruption-generated lahars (Manville et al. 2000a). Tephra transported by the 28 October 1995 rain-triggered lahar in the Mangatoetoenui Stream (Hodgson and Manville 1999) seriously impacted the Rangipo hydro-electric power station. The vulnerability of catchments like the Mangatoetoenui Stream to rain-triggered lahars had not been previously considered.

8.1.4 Crater Lake outburst

Temporary damming and rapid release of stored water occurs at volcanoes around the world, even those without such a long standing crater lake as Ruapehu (Mt. St. Helen's, Pierson 1997; Mt. Spurr, Waythomas 2001; El Chichón, Macías et al. 2004). Temporary blockages created by a landslide, pyroclastic flow, glacial moraine or lahar deposits can result in the impoundment of significant volumes of water on steep slopes. Failure of the dam can occur as the result of piping, liquefaction through earthquake, overtopping and incision. Piping occurs as a result of high hydraulic pressures forcing water through a permeable dam, eroding sediment from the front of the dam backward, creating pipes, or seeps. Liquefaction and mass collapse are dependent on the composition of the dam and can occur in conjunction with piping. If the dam is overtopped before collapse occurs, progressive downward erosion can remove the impounding material at an accelerating rate producing a catastrophic break-out.

Dam breach has been successfully modelled using comparisons with failures of artificial impoundments (Walder and O'Connor 1997; Manville et al. 1999; Scott et al. 2001; Manville 2004). Depending on the rate of dam failure, the release of water can be instantaneous or prolonged, controlling lahar development (White et al. 1997; Manville et al. 1999; Manville 2004). Collapse of the tephra barrier emplaced across the outlet to Crater Lake by the 1995/96 eruptions in March 2007 was the result of long term piping and headword erosion of seeps which first appeared in early January: small sloughing failures at one of the seeps scarps resulted in a small breach in the eastern side of the dam at 10:07 a.m.. Outflow through this channel undermined the western side of the dam which

collapsed at 11:21 a.m. The remaining thin septum of dam material was pushed out by the weight of the lake resulting in formation of a major breach 20 m wide by 11:22 a.m. that rapidly grew to its maximum size by downcutting and lateral erosion by 11:35 a.m. Approximately 1.4 million m^3 of water was released from Crater Lake as it drew down by 6.3 m within 2 hours of breach initiation. Peak breach discharge is estimated at c. 540 m^3/s (Manville 2007 pers. comm.).

The Whangaehu Valley has had two confirmed historic Crater Lake release lahars (1953 and 2007L). Additionally, events in 1861 and 1925 are not associated with eruptive activity which could suggest outburst origin. The componentry of the 1861 provides further evidence for an outburst origin, as it lacks the abundant lake sediment fragments which are typically found in eruption-triggered lahars (see section 7.3.3). Because of the position of the Crater Lake outlet, lake release events can only occur in the Whangaehu Valley. The estimated volume of the 1861 lahar would make it the largest historic event in the Whangaehu Valley. The 2007L lahar is the second largest measured in the Whangaehu Valley (Table 5.1). With careful observation, Crater Lake outburst hazards from Ruapehu are the easiest to mitigate.

The sediment budget of intra-eruption lahars is controlled by the availability of loose tephra, volume of lahar deposits within the flow path and the accumulation of talus and landslide debris from channel walls (Bovis and Jakob 1999). All the sediment for the 12 m of aggradation caused by the 2007L lahar was derived from the 1975, 1995 and 1999 lahar deposits, landslides and the tephra dam. In the present cycle, Crater Lake outburst floods occur 10 years following a (larger volume) juvenile producing event (1945 to 1953 and 1995 to 2007).

8.2 Active flow

8.2.1 Bulking

The high sediment concentrations of lahars observed on Ruapehu is the result of sediment bulking that occurs predominantly along the debris covered, high gradient Whangaehu Gorge.

Rheological flow transitions occur with the increase or decrease in sediment concentration. Sediment concentration is controlled by the availability

of sediment, relative to the fluid, and the ability of the flow to transport particles (Palmer et al. 1993; Manville 2004). Bulking is discussed as a comparison of the initial water volumes released by a triggering mechanism and the final flow volumes (Patterson 1975) or bulking factor. For dry sediment in steep valleys a flow can usually bulk by a factor of three. However, if materials are saturated or in the presence of snow (Pierson 2002), remobilisation only requires an additional 10% water content (Capra et al. 2004) and can result in bulking factors up to 5.

Historic Whangaehu debris flows bulk by factors of between 3 and 5.7 (Manville 2004) in the gorge. The method of bulking, entrainment, is critical to understanding flow evolution

8.2.2 Method of entrainment

The mechanics of particle entrainment by debris flows is not well understood. Erosion by concentrated sediment flow is widely recognised (Stock and Dietrich 2003; 2006) and bulking is acknowledged as a critical part of lahar flow evolution (Pierson 1995), but the process of incorporating volumes of sediment into an active flow is still a matter of debate. Particles can be incorporated into a moving flow independently through selective entrainment, failure along banks or mass mobilisation of an unconsolidated bedload. The configuration of volumes of unconsolidated sediment on an impermeable steep slope is highly conducive to erosion (Fig. 1.3; Paerschi et al. 2002; Glade 2006). The depositional record of the Whangaehu Gorge reflects extensive erosion associated with high magnitude lahar events (10^6 m^3) which effectively reset the sediment budget over the first 11 km of the flow path. Bedrock was exposed over parts of the flow path in 1995, 1999 and again in 2007. Smaller scale lahar events are confined by terraces of unconsolidated sediment. The grain size distribution and componentry of the deposits resulting from these smaller magnitude events suggest that the scale of the event affects the method of entrainment.

Particles overridden by a unidirectional flow are subject to fluid drag, lift, gravity, the weight of the overriding flow and friction. The entrainment of particles is retarded by grain roughness, particle organisation and density. As lahar deposits are highly heterogeneous in grain shape, size and orientation the process of entrainment is highly complex. Additionally, debris flows themselves

are highly variable events, subjecting the channel to fluctuating velocities, sediment concentrations and stress.

Discussion of particle entrainment typically focuses on turbulent flow, following the assumption that laminar flow does not entrain new material. If turbulence is required for entrainment, debris flows that maintain a high concentration over long distances must continue to exhibit turbulence (Komar and Li 1987; Li and Komar 1986; Iverson 1997; Hunt 1999). In Newtonian fluids particles are entrained through grain by grain selective entrainment, which has been modelled repeatedly (Li and Komar 1986; Komar and Li 1986; Hunt 1999). The dense fluid of passing debris flow exerts a shear stress to the bed and banks (Pierson 1995), this stress produces a fluid drag and creates lift. Individual particle motion is initiated when the particle's weight is overcome by the drag force of the flowing fluid (Li and Komar 1986). The direction of net movement is a result of the relative rate of motion between the particle and fluid and resisting forces (Iverson 1997), where a positive upward motion results in entrainment. However, the rapid and complete erosion of debris in the Whangaehu Gorge suggests that a more effective method of particle entrainment is occurring.

Particles of different grain sizes respond differently to overriding fluid forces. The entrainment of gravel sized particles is controlled by grain shape as entrainment becomes more difficult with increased obliquity and angularity (Li and Komar 1986). Fine grains are typically entrained first, as the small mass requires less force to erode and transport (Allen 1984; Komar and Li 1986; (Bridge and Bennett 1992). However the relative exposure of a grain and the increased surface roughness of smaller particles (due to larger surface area to mass ratio) complicates this relationship (Komar and Li 1986; Pierson and Costa 1987). The sediments eroded by lahars in the Whangaehu Gorge are very poorly sorted and have complicated surface morphologies with concentrations of large grains in gravel bars and bedforms. Whangaehu Valley lahars entrain high density clasts, and very low density materials (Manville et al. 2002) including snow and ice (Otway et al. 1995).

Sediment entrainment is retarded by the organisation of existing bedload (Allen 1984). Not only does an unsteady flow exert inconsistent shear on the bed, the resisting forces are inconsistent as a result of the heterogeneity of the deposit being eroded. Nevertheless, entrainment of large volumes of sediment occurs.

Either the heterogeneity of driving forces is balanced by the heterogeneity of resisting forces or complete erosion suggests a more expansive method of entrainment. Particle entrainment is limited by the existing concentration of a flow, as the flow continues to bulk the forces exerted on unincorporated materials changes, affecting the ability of the flow to continue bulking.

Bedforms and bar forms create local variations in velocity and fluid drag, creating local increases and decreases in erosion. Significant aggradation in sections of the gorge, and limited incision, decreases the appearance of erosion resulting from the 2007L lahar. However, the post-event LiDAR indicates up to $2.6x10^6m^3$ of material was entrained from the valley. Following the 2007L lahar sporadic remnant terraces, drumlin or whaleback types structures (Fig. 5.11) were identified 8 km from Crater Lake, however, exposure of bedrock along this stretch was also common. The initial volume of $1.4x\ 10^6m^3$ of released lake water bulked by a factor of 2.85 (Manville 2007, pers. comm.), which is too significant to occur by selective particle entrainment alone.

Following the 2007L lahar erosional scarps in the 1975 and 1995E lahar terraces reflected the contribution of bank collapse to flow volume. Previous lahar terraces were cut back by repeated collapse from undercutting and over-steepening of banks, gouging and scour by suspended particles and saturation overweighing. The most intense scour occurs along channel bends, cutbanks (Allen 1984). Similarly landslips from the valley walls, including a landslide 500 m below the outlet of the crater contributed 900,000 m^3 of sediment to the flow. Syn-event landslides were also documented in 1975 in oblique aerial photographs (Fig. 4.5). Erosion of competent rock has been discussed in detail by Stock and Dietrich (2003; 2006).

In conjunction with downward incision, scour and bank collapse may represent the major mass erosional force in the gorge, especially for smaller volume flows that remain confined by larger terraces. However, in the case of valley wide flows that significantly overrun previous deposits another method of entrainment should be considered.

An increase in pore pressure in saturated unconsolidated material, without compaction, can result in liquidisation (Allen 1984). As the valley is filled with unconsolidated poorly sorted material on an impermeable surface, compaction of the underlying flow would be minimal, causing pore pressures to increase and a

net upward movement and erosion of particles. This is similar to the process of flow fluidisation by the maintenance of high pore fluid pressures through compaction during flow motion (Iverson 1997).

Remobilisation lahars and snow slurry lahars are associated with less erosion (Cronin et al. 1997c) and limited bulking. The sediment and water budget of remobilisation lahars predominantly originates from the source location. The high concentration of October 1995 scoria in small volume 1995R and 1999 reflects less recycling of previous lahar deposits with lower energy events.

The contact underlying the 2007E deposits mantles the surface of 2007L deposits and does not reflect significant erosion. The low density and low concentration of sediment clasts in snow slurry lahars contributes to their limited erosive power. Snow slurries from 1995 and 2007 contained predominantly fresh and perennial snow (Cronin et al. 1996b). Mixed avalanches at Redoubt have been described with clasts of glacial ice up to 1.5 m in diameter (Pierson and Janda 1994), suggesting some erosion of the glacial surface. Of the sedimentary components in the 2007E deposit the dominance of low density clasts reflects a selective entrainment of low density materials, dominantly derived from the Crater Lake.

The low erosion associated with snow slurries suggests two things about erosion by typical non-cohesive debris flows. The ability of a debris flow to erode the subsurface is controlled by the density (sediment concentration) and flow thickness. A debris flow exerts a normal stress on the underlying channel, controlling the pore pressure of the underlying sediments. Thick high density fluids produce high pore pressures and thus fluidisation and erosion of underlying sediments. While the snow slurries are lesser in volume, density and lithic content, the flow lacks a significant erosive mechanism. The high density of concentrated debris flows may therefore contribute greatly to flow bulking. At the same time other methods of erosion, like tool scour, require high sediment concentrations.

Channel bed liquification cannot be directly observed, as yet, and will require further investigation. As the data from the 2007L lahar has not been completely processed, further evidence downstream may further elucidate the nature of flow/channel interactions and bulking.

8.2.3 Transport

Internal flow strength is the resistance of a flow to deformation and enables a fluid to transport sediment. Energy is transferred through grain and fluid interactions, grain on grain interactions and fluid-channel interactions. All of these forces act simultaneously and it is the interaction of the forces and not the sum that drives flow behaviour (Iverson and Balance 2001).

The transfer of energy within a flow can be described as granular temperature, or the vibrational energy of clasts within a moving debris flow. Granular temperature increases with decreased rigidity (increased deformation) and increased energy dissipation (Iverson 1997). The interactions of particles in this scheme can be dissipative or constructive.

Flow rheology is typically discussed under simplified umbrella terms; however, the behaviour of a given debris flow fluctuates with time, space and concentration. The complexity of these processes and the heterogeneity of natural debris and flow paths makes it necessary to discuss each force independently, but with an understanding of the constraints produced by the interactions of the processes.

Non-cohesive debris flows are unsteady and non-uniform (changing laterally and with distance), with rapid transitions between erosional and depositional regimes. Without the yield strength that develops with cohesion, flow regime can fluctuate directly as a product of sediment concentration and flow velocity (Iverson 1997).

Low-energy grain support mechanisms include buoyancy and matrix support while the higher energy mechanisms include turbulence, dispersive stress, and fluidisation (Pierson and Scott 1985; Pierson and Costa 1987). Cohesive flows have the highest capacity (Lavigne and Thouret 2002), where fluid yield strength develops at clay mineral concentrations of only 10% solids by volume, while silt-rich materials require concentrations of 30-35 volume % to behave cohesively (Pierson and Scott 1985). In the absence of significant clay, a high proportion of silt enables a non-cohesive flow to transport larger clasts by trapping water in pore spaces, hindering the gravitational settling of particles (Pierson 1997; Capra et al. 2004) and frictional grain collisions (Smith and Lowe 1991). The historic lahars of the Whangaehu Gorge are silty, and in the case of

1995E up to 12 wt. % silt. Historic lahar deposits in the Whangaehu Gorge are all very poorly sorted silty gravels to gravelly silts.

Pore fluid pressure in the moving fluid is a result of ambient pressures of fluid weight. Compaction of the flow occurs as a result of frictional resistance, but the poor sorting and inconsistencies in flow path causes pore pressures to be discontinuous throughout the flow and fluctuate with time. Higher pore fluid pressures increases flow capacity and generally occur with decreased rigidity and decreased energy dissipation (retarded granular temperature)(Iverson 1997).

The capacity of a flow is controlled by available sediment, the nature of the flow path, gradient and morphology and flow velocity (Manville and White 2003). Large grains are more effectively transported by higher flow velocities. Due to frictional resistance along flow margins the centre of the flow maintains the highest velocities throughout flow (Iverson 1997). As a result the largest clasts are moved centrally away from the flow margins (Pierson and Scott 1985). Large scale bars and streamlined bedforms occur centrally in the valley with smooth surfaces occurring along margins (e.g. 1975 deposits). Flows that travel in overflow channels have less volume and lower velocities and as a result the deposits display smaller grain sizes. While the chute acts as an overflow channel the confined and un-convoluted nature of the southern branch from 8 km to 11 km allows lahars to maintain a high velocity and larger boulders (1.5 m in diameter) are transported up to 3 km reflecting a higher capacity than typical overflow channels.

High sediment concentrations are maintained by an exchange between deposition and bulking. Large clasts are deposited as smaller grain sizes are entrained, carrying the same effective concentration, but of the appropriate grain size for the flow energy (Cronin et al. 1997c). The unsteady nature of non-cohesive debris flows means that deposition and bulking occur at the same time, maintaining flow energy.

Bulking decreases the sorting of a deposit by incorporating unorganised sediment into a flow. Gravitational sorting in an active concentrated flow is hindered by the incorporation of unsorted sediment (Vallance and Scott 1997). As long as the flow remains poorly sorted high pore fluid pressures will maintain high sediment concentrations and flow energy.

8.2.4 Dilution/debulking

Dilution is not a major factor in the formation of lahars within the Whangaehu Valley due to the small catchment area of the upper gorge. Water in the gorge is derived from the summit region of Ruapehu: snow melt and lake water. While precipitation can contribute to the saturation of a deposit prior to remobilisation or entrainment, the impact of precipitation on the volume of a lahar within the 11 km of the gorge is dependant on the overall volume of the flow. In events like 1975 when 8 cm of rain fell during the hours preceding the event, the rain did not significantly impact the overall volume of the flow. Although the river was swollen during lahar evolution, the volume of water released from the crater lake far outweighs the volume contributed by rain within the gorge. Downstream, however, the impact of precipitation increases with the contributing catchment area. The first substantial tributary input to the Whangaehu River is the Wahianoa River approximately 35 km from Crater Lake. High sediment concentrations are thus maintained in the gorge, with debulking on the fan occurring by deposition of particles rather than the addition of water. Without dilution to promote turbulent mixing grading and stratification of deposits cannot occur and sorting will remain poor (Capra et al. 2004).

The overall process of downstream flow evolution is accompanied by continuous energy loss and debulking of the flow through sedimentation and percolation losses. On volcanic ring plains the greatest reduction in lahar discharge and volume is attributed to deposition and infiltration losses on the low-angle, highly permeable fan surfaces (Palmer et al. 1993; Manville 2004). The formation of levees can also significantly reduce the mass of the flow (30-50%) (Ferrucci et al. 2005). Due to the impermeable nature of the gorge, infiltration losses are most significant on the Whangaehu Fan.

Observations of active flow and resulting deposits indicate that most of the historic lahars of the Whangaehu Valley left the 11 km long gorge as non-cohesive debris flows to hyperconcentrated flows and decreased in concentration dramatically on the low-angle fan. The 1975 lahar is the only historic lahar known to travel as far as Tangiwai (39 km) with sediment concentrations high enough to be classed as a debris flow. The others transformed to turbulent hyperconcentrated flows after significant sediment loss on the Whangaehu Fan (Cronin et al. 1997c; Table 7.3). The 1975 lahar maintained these high

concentrations despite significant decreases in flow volume relative to the lahars of 1953 and 1995 (Patterson 1976; Nairn et al. 1979).

Flow dilution by stream water is minimal when turbulent mixing is hindered by high sediment concentrations (debris flow >80wt.% sediment). On Ruapehu (1995 and 2007L) fresh stream water was pushed ahead of the flow up to 39 km from Crater Lake (similar to Mt. St. Helens; Pierson 1995). The arrival of Crater Lake water was reflected by a drop in pH to <3 (Cronin et al. 1996b; Cronin et al. 1999; Manville et al. 2000b).

8.2.5 Deposits

The deposits of the Whangaehu Gorge reflect the unsteady nature of the flow in both sedimentology and geomorphology. The spatial and temporal fluctuations in fluid flow are reflected both in the grain size diversity and morphology of diamicton terraces (Bridge and Bennett 1992; Iverson 1997).

Deposition results as a loss of energy, when the flow can no longer carry particles of a specific size. This can occur throughout the entire flow at the same time (dramatic change in slope like on the Whangaehu Fan) or localised (cluster bedforms, bar forms, behind obstructions). Preservation of these bed features only occurs if the transport rate continues to vary with time and space (i.e. deposition cannot occur uniformly throughout the flow or a uniform surface would be produced) (Allen 1984). The thickness of the deposit does not reflect the flow during transport, but it reflects the rate and duration of deposition during flow (Pierson and Scott 1985; Iverson 1997; Pierson 1997; Manville and White 2003). Flow thickness is usually greater than final deposit thickness (Pierson 1990; Pierson 1997). High water marks observed in 1975, 1995 and 2007 indicate that flow depth within the Whangaehu Gorge can be up to 5 metres greater than deposit thickness.

The patterns of aggradation from the 2007L and older historic lahar terrace heights signify repeated transitions from erosive to depositional behaviour throughout the 11 km Whangaehu Gorge (Fig. 4.1) and typically correlate with geometry of the flow path. Deposition within the gorge occurs as a result of increasing channel width, overtopping of topographic divides, decreases in channel gradient and localised velocity decreases resulting from flow obstructions (Allen 1984; Capra et al. 2004). Ungraded debris flow deposits are the result of

overcapacity deposition, where the energy of the flow can no longer transport the concentrated sediment load. Localised fluctuations in velocity and increased friction from the channel bed result in the formation of bars and bedforms of pebbles to boulders.

The deposits in the Whangaehu Gorge are poorly sorted ungraded gravels that display significant non-systematic variation in grain size distribution and morphology. Following aggradation by the 2007L and 2007E deposits the best example of stratigraphic variation is exposed in the erosional scarps of 1975 lahar deposits. Morphological variations are best observed in the 2007L lahar deposits even though they have been subdued by the 2007E lahar.

A typical debris flow deposit has a poor sorting, and thick ungraded beds with both clast and matrix support. The development of normal grading is attributed to turbulence and particle-on-fluid interactions. Inverse and non-graded deposits are associated with grain-on-grain interaction in combination with dispersive grain pressure and buoyancy. The Whangaehu Valley lahar deposits, except 1999 and 2007E, are typical of grain-dominated concentrated non-cohesive debris flows (Table 8.3). Both the 1975 and 1995E deposits display pulse

Table 8.3 Flow transformation between the Whangaehu Gorge and Whangaehu Fan.

Event	Gorge 0-11 km [1]	Field evidence	11-17.4 km [1] (fan)	Tangiwai 42 km [1]	84 km [1]
1861	DF	Clast size, ungraded		DF [6]	
1953				Hcf [4]	Hcf [3]
1975	DF (unstable, periods of Hcf)	Ungraded, matrix support	DF [2]	DF [4]	Hcf [4]
1995E	DF	Ungraded, matrix supported	DF [5]	Hcf [4]	Hcf [4]
1995R	DF	Ungraded, variable clast support	DF [5]	Hcf [4]	Hcf [4]
1999	DF to Hcf	Subtle normal grading	No observations		
2007L	DF	Ungraded, variable clast support	Hcf [7]	Hcf [7]	Hcf [7]
2007E	Snow slurry	Normal grading	Snow slurry	-	-

DF= debris flow
Hcf= hyperconcentrated-flow
[1] Distance from Crater Lake
[2] Paterson 1976
[3] Hodgson 1993
[4] Cronin et al. 1997b
[5] Cronin et al. 1997c
[6] Taylor 1861
[7] 2007 Observations

structures and lenses of isolated grain sizes, or slight improvements of sorting. The relative proportions of matrix and outsized clasts, and thus clast/matrix support fluctuates and is accentuated by laterally discontinuous pulse contacts and non-systematic increased concentrations of grain sizes. These inconsistencies reflect the instability of the debris flows, which is the result of non-uniform pore pressures (Iverson and Vallance 2001) caused by poor sorting and are consistent with descriptions of multiple peaked lahars (Nairn et al. 1979; Pierson et al. 1990; Cronin et al. 2000). The occasional appearance of graded beds within the 1975 lahar deposits reflect a transition to more turbulent behaviour probably from a temporary decrease in sediment concentration.

The maximum grain size of deposits increases with terrace thickness (flow magnitude) and increased scale of barforms and bedforms. Maximum grain sizes in historic Whangaehu Gorge lahars reached 546 cm in large eruption-generated and Crater Lake outburst events and 108 cm in remobilisation lahars (Table 5.1). The diamictons all display between 15 -50% or less matrix dominated by silt with variable concentrations of sand. The greatest fluctuations in sand abundance occur in the 1995E, 1999 and 2007L deposits. These fluctuations correlate to variations in flow path, including significant bends and obstructions. The greatest difference is an over all decrease in grain size with decreasing event volume.

The repeated transition between erosional and depositional behaviours was well reflected in the fresh 2007L deposits. Multiple terrace levels occur throughout the flow path, reflecting a continued erosion and re-deposition of debris. Early phase terraces are preserved occasionally behind large boulder obstructions (Fig 5.11) but decrease in size with time. Additionally, a complex series of mud coatings and apparent high water marks were temporarily preserved on the valley walls 4 to 8 km from Crater Lake. These coatings included a high water mark up to 5 m, a mud-free wash up to 1 m and remnant gravel 30 cm above the main deposit (Fig. 5.10). These traces reflect a sequence of pulses representing the peak stage of flow (highest water mark), a dilute low concentration flow phase (mud-free wash) and a recessional depositional flow phase (recessional terraces). Mud coatings on clasts on the deposit surface suggest that some of the gravels accumulated during a muddy phases of the flow and were not disturbed by subsequent phase of the flow. Some large boulders (4 m) have all three mud coatings preserved, suggesting that they were in situ from

the earliest phases of the lahar. The fluctuating concentration and stage height reflected in the high water marks illustrate the unstable nature of debris flows within the gorge with transitions occurring rapidly over short distances.

The geomorphology of the terrace surfaces for the 1975, 1995E and 2007L all displayed large scale bar and cluster bedforms, sporadic levees and pools of fines. The diversity of surface features on these terraces reflects multiple depositional mechanisms as a result of multiple transport and support mechanisms. Traction bedforms are the result of local fluctuations in velocity caused by the roughness of the channel bed and minor obstructions (Brayshaw et al. 1983; Manville et al. 2002; Wittenberg and Newson 2005). Bar and bedforms develop during later stages of flow as energy and sediment concentration decreases. Roughly to highly streamlined cluster bedforms are a dominant feature on the surface of large volume deposits. The matrix-free boulder bedforms are predominantly jumbled and loosely organised, narrowing and fining upstream. There are however, a few examples of tightly arranged, well organised bedforms of similar dimensions with vertical normal grading on the 2007L deposits. The organisation of the bedforms reflects the rate of flow recession, as well as the angularity and sorting of the transported sediment (Allen 1984; Wittenberg and Newson 2005) (Fig.5.11). Slower accumulation, involving fine grain fractions, would require kinetic sieving to remove the fine material (Giordano et al. 2002), and would produce a more organised structure. The cluster bedforms develop through sheltering of grains by an obstacle clast, with smaller grains accumulating upstream. The presence of organised and unorganised bedforms within the same deposit reflects the variability in flow within the gorge. Large gravel bars in the 1975 deposit occur centrally in the valley as a result of the high concentration of large (1-4 m) boulders. The scale of these features reflects the magnitude of an event that eroded and transported and concentrated very large clasts.

The height difference between the high water marks and the final deposit is partially a result of recessional erosion and deposit compaction; however, it most likely represents vertical stratification in the parent flow (Cronin et al. 1999; Manville et al. 2000b; Cronin et al. 2000). Historic areal photographs of the 1975 lahar in the near the RTMT also have significant high water marks 2-3 m above the deposit surfaces. Overbank erosion and sandy deposits of the 1975 and 2007L deposits support the argument for a dilute flow top. Splash marks associated with

these peak stage mud coatings reflect increased turbulence at the top of the flow (Pierson et al. 1990; 1975; 2007L) and indicate a vertically segregated flow. The amplification of a flow by confinement would affect both segments of a stratified flow, exaggerating the thickness of a dilute flow top. This difference may be accentuated by the flow resistance encountered at the front of the flow by accumulated debris, boulder dams, or rapid confinement of the flow path (Pierson 2002).

A second type of flow observed in the Whangaehu Valley is snow-dominated granular slurries. The deposits of such flow comprise c. 2 mm diameter granular snow crystals with an overall bulk density of 0.6 g/cm^3 (2007E). In a typical concentrated flow the fluid, including silt in suspension, has a lower density than the material being transported (Iverson and Vallance 2001). However, in the case of the 2007E lahar, the bulk of the material within the flow, granular snow, has a density less than water. Granular flow occurs when particle concentrations are high enough that the pore water pressures are no longer in excess of hydrostatic pressures, so the full weight of the mass is borne by grain to grain contact or collisions. In typical pseudo-plastic materials viscosity decreases with shear, in snow-dominated fluids frictional melting also decreases the viscosity of the flow (Pierson and Costa 1987; Pierson and Janda 1994; Cronin et al. 1996b). The high levels of shear in granular slurries are similar to those modelled in Bingham plastics (Allen 1984; Manville et al. 1999; Felix and Thomas 2004). In the 2007E deposits the surface morphology displayed pressure ridges and longitudinal shear, reflecting a plug like motion. The presence of melt water is dependent on the ambient temperature as well as internal temperature of the flow. The contact between 2007E pulse units is highlighted by lenses of clear ice, indicating frictional or pressure melting occurred at some point during motion or deposition. The high permeability of the deposit prevented the accumulation and freezing of pore fluids, as evidenced by the continued friability of the deposit.

High internal strength in snow slurries is reflected by the presence of levees, steep lobate flow fronts and margins and high angled ramping of deposits on channel walls (Fig. 5.15) (Pierson and Costa 1987; Iverson 1997; Mangeney et al. 2007). Shear reflects a plastic-like behaviour as a result of decreasing velocity with depth (Iverson 1997). Velocities calculated from arrival times and super-elevation marks reveal rapid pulsing flow (Manville 2007 pers. comm.). The

preservation of fragile gypsum crusts and unconsolidated lake sediment are indicative of a laminar visco-plastic flow.

The un-melted deposit displayed normal grading which is typically associated with an increase in turbulence (Smith and Lowe 1991). Because of the low inter-granular friction and contrast between the density of the granular snow, <1 g/cm^3, and the lithic clasts transported by the flow c. 2.4 g/cm^3, gravitational settling of particles can occur without turbulent mixing.

The surface of the deposit reflected a highly concentrated shear dominated motion, although the morphology was predominantly post-depositional. The surface was dominated by a complex series of surface fractures. Deformation marks perpendicular to flow are from brittle failure of creeping motion in the last stages of flow or just after deposition. The greatest frequency of deformation marks occur along flow margins and near obstructions, at the locations of greatest frictional resistance (lateral static zones; Pierson and Costa 1987) (Fig. Z.4). These deformation marks reflect the transition from mobile slurry flow to brittle frozen deposit. However, these features were obscured within a few weeks of deposition and indistinguishable by two months following deposition.

8.2.6 Flow path controls on deposition

The complexity of the first 11 km of the channel in the Whangaehu Valley exerts significant controls on lahar evolution. Each variation in flow path geometry elicits a response in the developing flow, contributing to the overall flow rheology (Cronin et al. 2000).

The normal path of the Whangaehu River is confined to the northern branches of the bifurcations that occur throughout the 11 km gorge. During normal conditions the southern channels contain snow melt and rainwater. Substantial flow only reaches the southern branches when lahars have high flow volume, dilute flow tops and eruption triggered routing. Consequently, the occurrence of deposits within the southern splits of the Whangaehu Valley reflects triggering mechanism, flow volume and flow rheology.

The complex nature of the flow path also results in temporary blockage or division of a flow. The divided or slowed segments then rejoin the main flow delaying portions of the sediment load. These pulses coalesce with distance and become less noticeable downstream (Pierson et al. 1990). Observations of active

flow at Tangiwai (39 km from Crater Lake) in 1968, 1975 and 1995 (Nairn et al. 1979; Cronin et al. 1997c) suggest this coalescence cannot occur until 40 km downstream (Vignaux and Wier 1990).

Multiple flow surges and confined flow path amplify lahar discharge, and attenuation does not occur until the flow becomes unconfined (Pierson 2002). Typically only small volumes of material overtop topographic divides, resulting in overbank floodplain type deposits. The chute is overtopped by small volume rain-generated flows (1995R) capturing a significant volume of material. The straight confined gorge maintains high flow velocity and encourages erosion, resulting in limited deposits along the 1.5 km Chute.

8.3 Interpreting the geologic record

Although the endurance of the depositional record within the Whangaehu Gorge is limited, the characterisation of these deposits will help with the identification of smaller scale events within the ancient record downstream. The historic record reflects substantial underrepresentation of remobilisation and snow slurry-type lahars in the ancient record. Events in both March and September 2007 provided evidence of the transience of many of the most distinct sedimentological and geomorpholocial signatures of individual events and trigger mechanisms.

The small scale, and thus small deposit volume of remobilisation and snow slurry lahars (0.20 m to 2 m deep) deposits makes them highly vulnerable to further reworking by normal stream flow and subsequent larger eruption-trigger or dam-failure lahars. Within the last 150 years the distribution of lahar deposits within the gorge has changed dramatically. Even large volume deposits, like the 1861 diamicton, are subject to erosion by high discharge lahar events. The 2007L removed deposits of the 1995R and 1999 lahars. Minor remnant terraces that were still identifiable in March 2007 were completely buried by the 2007E lahar deposits. After melting the 2007E deposits rapidly became less distinguishable from the 2007L. Of the 46 historic events recorded only 9 events were described in detail, based on 6 depositional units and aerial photographs. The pulse-like nature and repeated periods of erosion during a single non-cohesive debris flow event makes flow contacts difficult to distinguish.

Soft components, like lake sediment and scoria, are altered more strongly by abrasion during transport than resistant clasts such as andesitic lava. The degree of clast rounding reflects how long, or how many times, a given clast has been in the transport system. Highly rounded clasts reflect remobilisation and/or erosion from existing deposits. The 2007L lahar displayed the highest degree of rounding, being dominated by sub-rounded cobbles. This increased rounding and decreased grain size relative to previous deposits of a magnitude $>10^5$ m^3 (1975 and 1995E) suggest that the clasts were sourced from previous deposits and clast rounding increased with reworking.

The greatest variability between individual events and trigger mechanisms is the componentry. While the signature of an individual eruption, or lake outburst is reduced by the recycling of lahar deposits in the valley, direct comparison of deposit componentry would allow for differentiation.

8.3.1 Componentry

Historic lahars of the Whangaehu Valley have a limited sediment supply. The sediment budget includes material from the crater and hydrothermal system, andesitic lavas of the channel walls, juvenile material, previous lahar deposits and glacial snow and ice. As a result the deposits are composed of five major materials: andesite lava, scoria, sand to silt sized diagenetic minerals, hydrothermally altered clasts and snow/ice (Table 8.4). The proportion of these

Table 8.4 Distinctive componentry

Component	Trigger mechanism		
	Eruption	Remobilisation	Outburst
Fresh scoria	minor to significant	dominant	present
Angular andesite	present to significant	minor	present
Crater lake sediments	significant	minor	minor to none
Hydrothermal material	present[1]	significant[2]	present
Snow and glacial ice	none to dominant	none to present	none to minor
Diagenetic material[3] (pyrite, sulphur, gypsum)	significant	none	significant

[1] dominant in snow slurry
[2] low density
[3] indicative of Crater Lake water involvement

components reflects a combination of the triggering and bulking history of the event. However, the temporary nature of some components like gypsum, sulphur and snow make correlations between deposit and triggering mechanism in the geologic record more difficult.

Increasing travel distance, continued bulking and erosion downstream decrease the signature of any given sediment source. For the first 11 km from Crater Lake the sediment budget of the Whangaehu River is a closed system. The range of sediment types increases on the Whangaehu Fan that is exposed to eolian transport from the Rangipo Desert. The first major tributary, the Wahianoa River does not reach the Whangaehu River until 35 km from Crater Lake (Fig. 2.2).

8.3.2 Juveniles: lava, scoria and tephra

Andesitic lava

Lava on Ruapehu is dominantly two pyroxene plagioclase andesite that range in colour from black to light pink-grey. Clasts of andesite lithics have the greatest density and occur in the Whangaehu Gorge sediments in all grain sizes. Andesite lithics can be juvenile eruptives, accidental lithics from the vent walls, talus from the channel walls, or material cannibalised from previous lahar deposits. In the last 150 years there has been only one major lava producing eruption, in 1945, which was confined to dome growth inside the crater basin (Reed 1945; Oliver 1945). The majority of andesite lithic clasts are therefore all reprocessed and cannot be attributed a specific sediment source or trigger mechanism. However, the inclusion of lithic clasts reflects the erosive power of a flow as their high density makes lithic clasts the most difficult clast to mobilise (Fig. 7.1). The frequency and size of andesite lava clasts in all of the historic deposits decreases with increasing distance from Crater Lake.

Scoria

Historic eruptions on Ruapehu have produced mainly andesitic scoria and tephra (Healy et al. 1978; Nairn et al. 1979; Nakagawa et al. 1999). The eruptive style of Ruapehu has remained constrained in the last 150 years, producing small phreatic and mineralogically similar strombolian eruptions. The quantity of juvenile material produced in the last 2000 years is under 0.1 km^3 (Nakagawa et

al. 1999). The volume of fresh scoria that reaches the Whangaehu Valley is limited by the volume of material ejected and the dominating wind direction. During the most voluminous tephra producing eruption in 1995 up to 80 cm of ash accumulated on the summit glaciers, but only 10 cm of ash was deposited on the Tukino ski field and the upper Whangaehu Gorge (1-7 km) (Scott and Sherburn 1998). As wind directions are predominantly to the north east the greatest accumulations of ash are divided between the Mangatoetoenui catchment and the upper Whangaehu Glacier (Fig. 2.3).

Scoria is by far the most common component in the historic lahar deposits ranging from ash to 35 cm diameter bombs. Scoria is predominantly red or brown to black and displays greater rounding than lithic clasts. Each eruption has a unique geochemical signature with variable vesicularity (10-48%). The low density of scoriaceous material (average <2 g/cm^3) means that it is preferentially eroded and transported by lahars (Table 5.3). The scoria breaks down rapidly through grain collisions and weathering, contributing to the sand and silt fractions.

Because of the ease of remobilisation, the signature of an individual eruption, based on scoria, is rapidly obscured within the sedimentary record as progressive lahars erode and incorporate older scoria fragments. Caution must be exercised with using tephras to correlate a deposit with generation as lahar events can occur at any time during and after eruption. A high incidence of scoria, or the presence of tephra in a lahar deposit, indicates a generation during or shortly after a volcanic eruption. However, a low occurrence of scoria and tephra does not necessarily signify non-eruptive lahar generation, and conversely high concentrations of scoria do not necessarily indicate direct eruption-generation. The texture and fractionation of tephra, can be used to reconstruct the role of Crater Lake water in the eruption.

The historic remobilisation lahar deposits (1995R and 1999) are dominated by scoria, but do not occur as a direct product of an eruption. Tephra deposited in the gorge that is not incorporated into a lahar is frequently reworked by precipitation and can be difficult to distinguish from surrounding diamictons. Because of its low density scoria is transported for longer distances within the flow than dense andesite clasts.

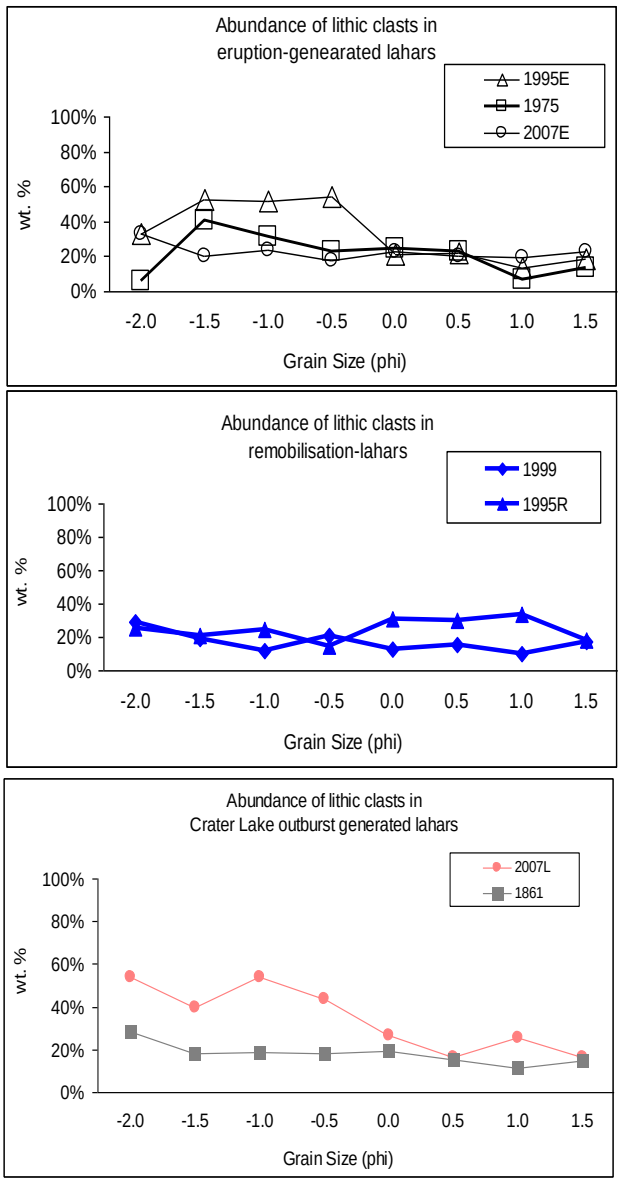

Fig. 8.1 The abundance of andesitic lithic clasts within historic lahar deposits. Eruption-generated lahars, and the 2007 Crater Lake release lahar have the highest concentrations of lithics.

8.3.3 Signature of Crater Lake

Diagenetic Minerals

The fine grained fractions of historic deposits contain andesitic glass and a number of minerals from tephra, broken down juvenile material and Crater Lake water precipitate. The most abundant minerals are plagioclase, pyroxene (hypersthene and augite) followed by lesser quantities of sulphur, pyrite, and gypsum. Feldspar and pyroxene first occur in the coarse sand fraction (1 mm) and are derived from tephra and the chemical and mechanical weathering of scoria and andesitic lava. Native sulphur can occur as coatings on large clasts up to 5 mm thick and as discrete grains up to 2 mm in diameter are ejected from the lake from

a pool of liquid sulphur residing at the bottom of the lake and sulphur rich lake water (Christenson and Wood 1993; Scott and Shepburn 1998). Cubic pyrite grains occur independently (2 mm) and on the surface of lithic and scoria clasts (0.1 mm). Pyrite is a product of the hydrothermal system, as was observed in large quantities on ejecta and on lake mud in 1975 (Nairn et al. 1979) precipitating rapidly from the enriched Crater Lake water (Christenson and Wood 1993). Gypsum appears as discrete crystals up to 4 mm in diameter and as crusts up to 3 cm thick on altered clasts. Gypsum and anhydrite is precipitated in and around the lake and on ejecta following eruption. Gypsum precipitating in the vesicles of scoria was observed around the crater lake by Nairn et al. (1979). The relationship between anhydrite and gypsum can be used to calculate the depth the clasts were erupted from because of the temperature required to produce the dehydrated calcium sulphate.

The components derived from the hydrothermal system are temporary, with low preservation, even in historic deposits. Within the first few days of deposition coatings of sulphur and a blue-grey pyrite silt degrade. Within a few months the deposits change from a light grey to a yellowish hue. The soft structure of gypsum and sulphur are no longer distinguishable in any great quantities in deposits over ten years old (e.g. 1995E and 1995R).

Hydrothermally altered clasts

In addition to minerals that precipitate directly from hydrothermal condensate, the materials that make up the crater have been subject to long term hydrothermal alteration. Clasts include lake sediment and cristobalite veined andesite and light coloured low density sinter. The clasts are all light in colour and density and frequently very brittle.

Clasts of Crater Lake sediments are pale grey and white clay-rich silt and sandstones with a high occurrence of anhydrite. The sediment is poorly sorted with minor clasts of altered andesite in a clay- rich matrix that contains anhydrite, pyrite and sulphur (Nairn et al. 1979). Some clasts of lake sediment have been contact metamorphosed into sanidine-bearing metaquartzites prior to ejection, but clastic texture is still distinguishable (Nairn et al. 1979).

Unconsolidated lake mud is composed of gypsum, kaolin and smectite clay minerals, feldspar, sulphur, cristobalite, natroalunite and minor quartz. Lake

sediment is periodically exposed during periods of decreased lake level, but typically lake mud is only observed on ejecta coated by light grey lake sediment (1975, Nairn et al. 1979; 2007E). The deposits contain minor abundance of clay minerals (<3%). Clay can be derived from three sources: extensive hydrothermal alteration near the crater, the weathering of andesitic glass, and Crater Lake sediments (Cronin et al. 1997c; Vallance and Scott 1997; Pierson 2002).

Crater Lake sediment is incorporated into the lahar sediment budget after ejection from the lake floor, as exemplified by the 2007E lahar. However, the low density of lake sediment and cannibalistic nature of bulking lahars does not conclusively link the presence of Crater Lake sediment with eruption-generation (e.g. 2007L). However, the absence of Crater Lake sediment (as in 1861) suggests a lahar generation that does not involve disruption of the lake bottom, including uplift of the lake floor or Crater Lake outburst.

Traces of elemental sulphur and pyrite also indicate the involvement of Crater Lake water, either from an eruption (Patterson 1976; Cronin et al. 1997c) or Crater Lake outburst (Taylor 1861; O'Shea 1954; 2007 observations). Similarly the low pH of the crater lake dramatically reduces the pH of the Whangaehu River, with recorded values during the 1975 lahar of 1.9 (Paterson 1976). Enrichment by crater lake water is also reflected in increased abundances of Cl^- and Mg^+ (Healy et al. 1978).

8.3.4 Snow and ice

As Ruapehu is home to six glaciers and a significant seasonal snow pack lahars can incorporate not only snow melt, but competent blocks of snow and glacial ice. In the case of the early phase 1995 and September 25, 2007 eruption snow slurry lahars were composed of 50-70% granular snow. Snow and ice can travel significant distances within the flow, i.e. up to 42 km from source in 1995 (Cronin et al. 1996b) and 23 km in 2007. Clear glacial ice and perennial snow (crystals larger than that of the surrounding matrix) reflect erosion by even small volume eruption-generated lahars.

Snow slurries can form when large volumes of snow are mobilised by a low temperature eruption. Spring and winter eruptions have ample loose snow to incorporate into a flow, and may create lahars in events that would not have had

the volume of sediment or water necessary to travel far under other circumstances (5-20% sediment; Cronin et al. 1996b).

The occurrence of snow slurries decreases with time during an eruption sequence as snow is removed from the summit (Cronin et al. 1996b; Manville et al. 2000a). Snow mobilisation can occur with the ejection of lake water on to snow pack, the impact of ballistics on an unstable snow surface, melting around the crater or erosion of perennial ice and snow by Crater Lake water or an overriding flow (Pierson and Janda 1994; Waitt et al. 1994; Otway et al. 1995). However, the mechanics of snow incorporation requires further investigation (Otway et al. 1995).

The low sediment content of snow slurry lahars suggests that they are underrepresented in the ancient record. Although textures formed as the result of melting snow are fragile and are not likely to be discernable in the record, the abundance of hydrothermally altered material may be distinctive when compared with surrounding deposits. Cronin et al. (1997c) estimated that 50% of the sediment within the initial eruption-driven (snow slurry) lahars in 1995 was directly derived from the lahar-producing eruptions themselves. In 2007E similarly, the abundance of Crater Lake mud on clasts and increased occurrence of sulphur, gypsum and pyrite suggest that a large proportion of the material was derived directly from the lake.

8.3.5 Signature of component recycling

The sequence of lahars occurring between September 1995 and 2007 reflect a progressive increase in low density scoriaceous material and a decrease in andesite lithic content with increasing time following tephra producing events (Fig. 8.1). The September 1995 eruption-generated lahar (1995E) occurred early in the eruption sequence, when tephra accumulations were small in volume and predominantly located in the Mangatoetoenui Valley north of the Whangaehu Valley. The 1995E deposits have characteristically high andesitic lithic content (over 30 % bulk weight) (Table 8.5). By October 28, 1995, after the largest tephra producing event on October 11 and 12, enough loose material had accumulated in the valley to produce a large rain generated lahar with concentration of >30%wt. andesite lithics. The 1995R lahar deposits were derived from remobilised scoria deposited near Crater Lake, and did not entrain

Table 8.5 Sediment lithology of 1995 lahars from September 18, prior to the 1995E lahar (Cronin et al. 1997c).

Snow Slurry	Distance from Crater Lake	Hydrothermally altered clasts and lake sediment	Sulphur spheroids	Fresh scoria	Unaltered andesite	Number of grains counted
LH1	9.5	42.5	6.5	1.0	50.0	762
LH1	16	31.0	3.0	11.5	54.0	1008
LH3	9.5	31.5	1.0	5.0	62.5	967
LH3	23.5	33.5	2.5	10.0	54.0	785

significant andesitic lava during transport. The 1999 remobilisation lahar occurred 4 years after the cessation of eruptive activity, remobilising the 1995R deposits. The 1999 deposits have the lowest lithic content, and highest fine-grained glass content of all historic lahar deposits. The small scale of the remobilisation events limited their ability to entrain dense lithic clasts, and instead concentrated scoria. The proportion of glass fragments increase as the scoria is repeatedly abraded and broken down. The 2007L lahar was more erosive, and closer in size to the 1995E lahar in volume, which increased the andesitic lava and other high density clast content. The scoria, lithics, pyrite and hydrothermally altered material were all recycled from previous lahar deposits. The small snow slurry lahar, 2007E, was not erosive and contained predominantly hydrothermally altered materials from the bottom of Crater Lake ejected in the eruption of September 25, 2007.

8.3.6 Distinguishing deposits

On Ruapehu lahar sediment/water concentration has not been correlated to triggering mechanism. The greatest variation among the historic deposits is in lithology (e.g. Cronin et al. 1997c). The simplest means of distinguishing eruption triggered deposits is utilising the stratigraphic associations of lahar deposits and eruption sequences (Park and Schmincke 1997). Tephra layers and quenching textures in juvenile clasts provide the only evidence of eruption related processes (Cronin et al. 1996a). Lithologic evidence of triggering mechanism is limited by the incorporation of significant volumes of material from pre-existing deposits.

Although the recycling of lahar deposits makes the occurrence of a specific component inconclusive, increased abundance, or absence of a

component can be correlated to trigger mechanism. The absence of Crater Lake sediment indicates the lake bottom was not disturbed in association with lahar-generation. Elemental sulphur and pyrite are temporary components that indicate eruption-generation. An abundance of dense materials reflects high event magnitude and erosive power; while a concentration of low density material suggests small volume lahars, such as remobilisation or snow slurry lahars. Concentrations of hydrothermally altered materials in thin deposits (with or without preserved snow collapse textures) may reflect snow slurry-generation.

Chapter 9 Conclusions

The preserved historic lahar deposits of the Whangaehu Catchment are an incomplete record of lahar events of the last 150 years; however, they capture the range of volcaniclastic flow types and magnitudes while poorly representing event frequency. An understanding of lahar potential, behaviour, size and frequency is critical to hazard mitigation. Within the last 12 years alone, a significant range of trigger mechanisms have produced lahars in the Whangaehu Gorge. Historic lahar events have occurred in several cycles of eruption, remobilisation and Crater Lake outburst floods. In 1945 and 1995/96, lake emptying eruptions and blockage of the natural outlet of the Crater Lake at the headwaters of the Whangaehu River resulted in lake break-out lahars 8 and 11 years later respectively. Following the most recent magmatic eruption phase, significant remobilisation of unconsolidated tephra continued for at least 4 years (1995-1999). As a result of the blockage of the outlet, when Crater Lake refilled, the water level was temporarily raised above the stable crater rim. In both cases destabilisation of the dam by seeping and hydraulic pressure led to formation of a breach and high magnitude (10^6 m^3) outburst flood. Between these two significant magmatic sequences, small eruption-triggered lahars with volumes between 10^3 to 10^6 m^3 were produced by phreatic and phreatomagmatic eruptions which indirectly resulted in remobilisation-generated lahars reaching up to 10^5 m^3.

The depositional history of the Whangaehu Gorge, as reconstructed in this study from historical accounts, aerial photos and stratigraphy, is not inclusive and focused only on events with a photographic record. Lahars triggered by eruptions are the most frequently recorded events in the Whangaehu Valley as a result of their dramatic origin and volume. Remobilisation lahars have shorter travel distances than large volume eruption-triggered lahars, and frequently do not leave seismic records (Cronin et al. 1997 c). As a result, eruption-generated events may be overrepresented in the record. Historically remobilisation events have gone unnoticed or were poorly documented (e.g. 1999 lahar). Combined with the typically small volume of remobilisation events and lack of associated erosion the signature of remobilisation events underestimates event frequency. Small volume deposits are subject to rapid reprocessing by fluvial action, or removal by

subsequent lahars. The differentiation of these less distinct events is critical to developing accurate estimates of lahar frequency in the Whangaehu Valley.

The 1995/96 sequence is the most well documented sequence of historic eruption-generated and remobilisation lahars, but observations tend to be incomplete owing to the *ad hoc* nature of observations. In contrast, the ensuing potential break-out lahar was forecast a decade in advance, enabling a comprehensive science plan to be developed to maximise the data collection from a single, discrete lahar event, with a measured starting hydrograph (Manville 2007 pers. comm.) and detailed pre-and post-event sedimentology and geomorphology. Consequently, the March 2007 lahar is the most well documented lahar event in the world.

While lahar trigger mechanisms on Ruapehu are diverse, the deposits of the resulting lahars are texturally similar. Historic lahar deposits in the Whangaehu Gorge are typically ungraded, heterogeneous, very poorly sorted, gravelly silts. These deposits are the result of non-cohesive debris flows that range from 10^3 to 10^6 m^3 and remain channelised through the Whangaehu Gorge and Fan. Snow slurry lahars (i.e. 2007E), consisting of 50-70 wt. % granular snow, produced by the ejection of lake water onto snow covered glaciers, left thin deposits up to 70 cm with snow collapse structures that fade with time. The distribution and grain size of these deposits reflect the relative size of the events, enabling a magnitude-frequency relationship to be developed for Ruapehu lahars.

9.1 Under-representation within the historic record

Because the Whangaehu Valley is the main outlet of Crater Lake, it is the most lahar-prone catchment on Ruapehu. Evidence from the ancient lahar record of the Onetapu Formation in the Whangaehu Fan, on the eastern side of the mountain, suggests that the Crater Lake has been established close to its current position draining in the Whangaehu Valley for the last 2000 years. The lahar deposits within the Whangaehu Fan are the preserved ancient record of lahar activity; however, the construction and removal of historic lahar terraces in the Whangaehu Gorge indicate that the record of the fan is incomplete. Over the last 150 years Ruapehu has had 46 recorded lahars, but reconstruction is only possible for 9 of these events, 2 of which occurred during the course of this study. Small scale eruption-generated lahars, like in September 2007, and remobilisation lahars

may not have been observed or documented due to their small size and the inaccessibility of the upper reaches of the volcano in the early part of the 20th century. The preservation of lahar deposits within the gorge and fan is dependent on their grain size, volume and distribution. As the historic lahar events have all been channel confined they are not likely to leave a significant deposit. While not necessarily subject to complete remobilisation, the reworking caused by subsequent lahar events and fluvial processing will sufficiently alter the deposits as to leave them indistinguishable. The events of 2007 exemplify the rapid modification of lahar deposits within the upper Whangaehu Valley. Even the deposits within the southern bifurcations of the gorge, which are disturbed only by the largest lahar volumes are not preserved in the long term.

Although the scale and hazards associated with Ruapehu lahars are quite small they bear great significance on our ability to interpret the geologic record. Erosion and deposition caused by frequent lahars in the Whangaehu Valley limit the formation of soils that would aid in the identification of flow boundaries. The accumulation of tephra beds can help distinguish those events that occur in conjunction with eruptions, but undisturbed tephra within the flow path is rare. Tephra preservation is more likely on the fan where overbank deposits are not as erosive, or in spillways and eddies. It can be difficult to distinguish a single lahar event from a series (Giordano et al. 2002). However, the distinction between discrete $>10^6$ volume events and long term accumulations of small lahar deposits is possible through the identification of large scale clasts, and in the case of the Onetapu Formation lahars, clay content (Hodgson 1993).

The transient nature of the most distinct components is only another reminder of the low preservation of volcaniclastic debris on steep slopes. Triggering mechanism can be correlated to a deposit based on the appearance of clasts from different sources. Materials within the Whangaehu Gorge are derived from primary eruption products, the Crater Lake, landslides and erosion of the crater wall and unconsolidated terraces of lahar deposits.

Although Whangaehu lahar sediment budgets contain largely recycled material the historic lahar deposits of the Whangaehu Gorge reflect a subtle trend correlating trigger mechanism and proportions of clast types. Remobilisation lahars are associated with the mobilisation of primary tephra with limited bulking and are consequently dominated by low density material and have few

components derived from the crater lake. Eruption-generated snow slurries consist predominantly of material incorporated at the same elevation where the snow was entrained, in the case of 2007E this was hydrothermally altered debris recently ejected from the lake. Initial snow dominated deposits contain snow melt and collapse structures. A high degree of clast rounding reflects significant recycling of clasts from previous lahar deposits, which may suggest Crater Lake release. A high abundance of accidental lithics suggest higher magnitude events, and recent eruptive activity. The proportion of components in the deposit controlled by the abundance of materials in the eroded deposits and can be used to derive lahar generation in a comparative sense and not independently.

9.2 Mitigation

An understanding of the variety of lahar types produced within the Whangaehu Gorge is essential for hazard analysis and the development/maintenance of a mitigation strategy. Mitigation is dependent on simplified modelling, but as research, like the collaborative project on the March 2007 lahar, continues models now incorporate a greater number of flow aspects and increase realism.

Eruption-generated lahars are only as predictable as the eruption that causes them. However, predictions of precise volume, peak discharge and run out distance are limited by the number of variables that can be feasibly incorporated into a model. The 1995/96 eruption sequence exemplifies the wide range of lahars that can be produced over a few months under changing conditions. The eruption on September 25, 2007 also reflected the challenge of un-expected lahar forming events. The confined nature of the Whangaehu Valley makes hazards easily mitigatable, compared to the ski fields on the western side of the mountain where lahars can be triggered by the ejection of Crater Lake water and debris down the Whakapapanui and Whakapapiti Glaciers (e.g. 1969, 1975, and September 2007; Otway et al. 1995).

Remobilisation lahars are not predictable except in their inevitability. Volumes of unconsolidated sediment on steep slopes are unstable and can be remobilised by a variety of processes (Manville et al. 2000a), but the period between October 1995 and 1999 displays the prolonged nature of this remobilisation. The frequency of remobilisation lahars is very high at tropical

volcanoes (Merapi; Mt. Semeru; Lavigne and Thouret 2002; Lavigne and Suwa 2004), but is still a significant issue in more temperate environments like Ruapehu (Pinatubo; Arboleda and Martinez 1996; La Fossa; Ferruci et al. 2005). Remobilisation requires an available volume of debris in a sediment budget (i.e. fresh pyroclastic material) and will remain a hazard until that budget is decreased.

The impoundment of water by temporary dams can result in outburst floods and debris flow formation. The investigation and preparation that led up to the March 2007 lahar response is an excellent example of how lake outburst events can be anticipated and managed (Hancox et al. 2001; Manville et al. 2007). With sufficient observation, dam outburst floods are the most mitigatable lahar hazard on volcanoes with crater lakes. Because of the persistence of the crater lake, refilling occurs over a period of years enabling preparation for lake release events. Temporary impoundment of water on volcanoes, however, does not always occur on a practical time frame for observation and prediction (Nevado del Ruiz, Mt. St. Helens). Temporary lakes can form from pyroclastic flows, landslides, glacial ice and self-damming lahars. To predict and model outburst floods several parameters are required: lake volume, dam dimensions, dam stability (components, seepage, structure), rate of filling and geometry of flow path.

Although less constrained than outburst floods, a potential range of lahar types can still be estimated for eruption-generated and remobilisation lahars based on sediment budget, water budget and flow path. Numerical models can then be calibrated based on historic activity.

The hazards associated with lahars in the Whangaehu Valley affect development immediately along the river including road and railway bridges as well as cause ecological disruption and contamination. In response to historic lahars the structures that are vulnerable to Whangaehu Valley lahars have already been identified. The success of the 2007L Crater Lake outburst lahar preparation and response is encouraging. The methods and results of the decade-long project can be adapted to other lahar prone areas. In order to understand recent and future lahar events the flow path, and sediment and water budgets must be understood. This is of course climate dependant as tropical and snow clad volcanoes present different range of hazards that can lead to sediment mass flow formation.

Through the identification and detailing of the range of lahar trigger mechanisms, volumes and flow behaviours mitigation strategies can be improved. The success of the events in March 2007 is encouraging to researchers, hazard mitigators and planners alike. But at the same time the events of September 2007 remind volcano watchers that there is still much we cannot predict.

The value of the unique timing of events in 2007 cannot be overstated. The opportunity to observe stable conditions prior to and following a Crater Lake release lahar and the geomorphic change resulting it captured by pre- and post-event airborne LiDAR surveys, vertical orthophotography and oblique ground and aerial imagery is exceptional. The occurrence of a small snow slurry lahar within the time frame of the project is fortuitous. The benefits of the data and observations from these events have not yet been fully exploited, and will have international applicability.

References

Allen JRL 1984. Sedimentary Structures their Character and Physical Basis. Developments in Sedimentology 30, Elsevier: p.1256.

Arboleda RA, Martinez ML 1996. 1992 Lahars in the Pasig-Potrero River System *in* Newhall CG, Punongbayan RS ed. Fire and Mud: Lahars of Mt. Pinatubo. Philippine Institute of Volcanology and Seismology and University of Washington Press p. 1126.

Bathurst J, Burton A, Ward T 1997. Debris flow run-out and landslide sediment delivery model tests. Journal of Hydraulic Engineering 123: 410-419.
Beetham RD 1982. Ruapehu Crater Lake rim stability EG 82/023 NZGS Earth Deformation Survey.

Bovis MJ, Jakob M 1999. The role of debris supply conditions in predicting debris flow activity. Earth Surface Processes and Landforms 24: 1039-1054.

Brayshaw AC, Frostick LE, Ried I 1983. The hydrodynamics of particle clusters and sediment entrainment in coarse alluvial channels. Sedimentology 30: 137-143.

Bret L, Fevre Y, Join J, Robineau B, Bachelery P 2003. Deposits related to degradation processes on Piton des Neiges Volcano (Reunion Island): overview and geological hazard. Journal of Volcanology and Geothermal Research 123: 25-41.

Bridge JS, Bennett SJ 1992. A model for the entrainment and transport of sediment grains of mixed sizes, shapes and densities. Water Resources Research 28: 337-363.

Capra L, Macías J, Scott KM, Abrams M, Garduño-Monroy VH 2002. Debris avalanches and debris flows transformed from collapses in the Trans-Mexican Volcanic Belt, Mexico- behaviour, and implications for hazard assessment. Journal of Volcanology and Geothermal Research 113: 81-110.

Capra L, Poblete MA, Alvarado R 2004. The 1997 and 2001 lahars of Popocatépetl volcano (Central Mexico): textural and sedimentological constraints on their origin and hazards. Journal of Volcanology and Geothermal Research 131: 351-369.

Christenson BW, Wood CP 1993. Evolution of a vent-hosted hydrothermal system beneath Ruapehu Crater Lake, New Zealand. Bulletin Volcanology 55: 547-565.

Chow VT 1959. Open-channel Hydraulics. McGraw-Hill book company, New York USA p. 680.

Costa J 1997. Hydraulic modelling for hazards at Cascades Volcanoes. Environmental and Engineering Geoscience 3: 21-30.

Cronin SJ, Neall VE, Palmer AS 1996a. Geological history of the north-eastern ring plain of Ruapehu Volcano, New Zealand. Quaternary International 35-36: 21-28.

Cronin S, Neall V, Lecointre J, Palmer A 1996b. Unusual "snow slurry" lahars from Ruapehu volcano, New Zealand, September 1995. Geology 24: 1107-1110.

Cronin SJ, Neall VE, Palmer AS 1997a. Lahar history and hazard of the Tongariro River, north-eastern Tongariro Volcanic Centre, New Zealand. New Zealand Journal of Geology and Geophysics, 40: 383-393.

Cronin S, Hodgson KA, Neall VE, Palmer AS, Lecointre JA 1997b. 1995 Ruapehu lahars in relation to the late Holocene lahars of Whangaehu River, New Zealand. New Zealand Journal of Geology and Geophysics 40: 507-520.

Cronin SJ, Neall VE, Lecointre JA, Palmer AS 1997c. Changes in Whangaehu river lahar characteristics during the 1995 eruption sequence, Ruapehu volcano, New Zealand. Journal of Volcanology and Geothermal Research 76: 47-61.

Cronin SJ, Neall VE, Lecointre JA, Palmer AS 1999. Dynamic interactions between lahars and stream flow: A case study from Ruapehu volcano, New Zealand. Geological Society of America Bulletin 111: 28-38.

Cronin S, Neall V, Lecointre J, Palmer A 2000. Transformation, internal stratification, and depositional processes within a channelised, multi-peak lahar flow. New Zealand Journal of Geology and Geophysics 43: 117-128.

Crosta G, Chen H, Frattini P, 2006. Forecasting hazard scenarios and implications for the evaluation of countermeasure efficiency for large debris avalanches. Engineering Geology 83: 236-253.

Dinehart RL 1997. Sediment transport in the hyperconcentrated phase of the March 19, 1982 lahar *in* Pierson and Waitt ed. Hydrological Consequences of Hot-Rock Snowpack interactions at Mt. St. Helen's volcano. USGS Open File Report 96-179: 37-52.

Donoghue SL, Neall VE, Palmer AS, Stewart RB 1997. The volcanic history of Ruapehu during the past 2 millennia based on the record of Tufa Trig tephras. Bulletin of Volcanology 59: 136-146.

Donoghue SL, Neall VE 2001. Late Quaternary constructional history of the South Eastern Ruapehu ring plain, New Zealand. New Zealand Journal of Geology and Geophysics 44: 439-466.

Fagents S, Baloga S 2005. Calculation of lahar transit times using digital elevation data. Journal of Volcanology and Geothermal Research 139: 135-146.

Fairchild LH 1987. The importance of lahar initiation processes. Geological Society of America Review in Engineering Geology Volume VII: 51-61.

Ferrucci M, Pertusati S, Sulpizio R, Zanchetta G, Pareschi M, Santacorce R 2005. Volcaniclastic debris flows at La Fossa Volcano (Volcano Island, southern Italy): Insights for the erosion behavior of loose pyroclastic material on steep slopes. Journal of Volcanology and Geothermal Research 145: 173-191.

Fisher RV 1971. Features of coarse grained, high-concentration fluids and their deposits. Journal of Sedimentary Petrology 41: 916-927.

Glade T 2006. Linking debris flow hazard with geomorphology. Geomorphology 66: 189-213.

Gledhill K, Scott BJ 2001. Monitoring strategies that could be developed to deal with a Crater Lake dam-failure scenario at Ruapehu Volcano. IGNS Science Report 2001/6: p. 22.

Giordano G, De Rita D, Fabbri M, Rodani S 2002. Facies associations of rain-generated versus crater lake-withdrawal lahar deposits from Quaternary volcanoes, central Italy. Journal of Volcanology and Geothermal Research 118: 145-159.

Gregg DR 1960. Volcanoes of Tongariro National Park. New Zealand Department of Scientific and Industrial Research Information Series 28: p. 82.

Hackett WR, Houghton BF 1989. A facies model for a Quaternary andesitic composite volcano: Ruapehu, New Zealand. Bulletin of Volcanology 51: 51-68.

Hancox GT, Keys H, Webby MG 2001. Assessment and mitigation of dam-break lahar hazards from Mt Ruapehu Crater Lake following the 1995-96 eruptions. *in* ed. McManus KJ 2001 *Engineering and Development in Hazardous Terrains, New Zealand Geotechnical Society* NZ Institute of Professional Engineers, Christchurch, New Zealand: 385-409.

Healy J, Lloyd EF, Rishworth DEH, Wood CP, Glover RB, Dibble RR 1978. The eruption of Ruapehu, New Zealand, on 22 June 1969. New Zealand Department of Scientific and Industrial Research Bulletin 224: p. 80.

Hodgson KA 1993. Late Quaternary lahars from Mount Ruapehu in the Whangaehu River Valley, North Island, New Zealand. Unpublished PhD Thesis, Massey University.

Hodgson KA, Manville VR 1999. Sedimentology and flow behaviour of a rain-triggered lahar, Mangatoetoenui Stream, Ruapehu volcano, New Zealand. GSA Bulletin 111: 743-754.

Hodgson KA, Lecointre JA, Neall VE 2007. Onetapu Formation: The last 2000 yr of laharic activity at Ruapehu volcano. New Zealand. New Zealand Journal of Geology and Geophysics 50: 81-99.

Hunt A G 1999. A probabilistic treatment of fluvial entrainment of cohesionless particles. Journal of Geophysical Research 104: 15409-15413.

Iverson RM 1997. The physics of debris flows. Reviews of Geophysics 35: 245-296.

Iverson RM, Vallance JW 2001. New views of granular mass flows. Geology 29: 115-118.

Jakob M 2005. A size classification for debris flows. Engineering Geology 79: 151-161.

Johnston DM 1997. A chronology of the 1945 eruption of Ruapehu volcano, New Zealand. IGNS Science Report 97/2: p. 50.

Komar PD, Li Z 1986. Pivoting analyses of the selective entrainment of sediments by shape and size with application to the gravel threshold. Sedimentology 33: 425-436.

Lavigne F, Thouret J, Voight B, Suwa H, Sumaryono A 2000. Lahars at Merapi. Central Java: An Overview. Journal of Volcanology and Geothermal Research 100: 423- 456.

Lavigne F, Thouret J 2002. Sediment transportation and deposition by rain-triggered lahars at Merapi Volcano, Central Java, Indonesia. Geomorphology 49: 45-69.

Lavigne F, Suwa H 2004. Contrasts between debris flows, hyperconcentrated flows and stream flows at a channel of Mount Semeru, East Java, Indonesia. Geomorphology 61: 41-58.

Lecointre JA., Neall VE, Palmer AS 1998. Quaternary lahar stratigraphy of the western Ruapehu ring plain, New Zealand. New Zealand Journal of Geology and Geophysics 41: 225-245.

Lecointre J, Hodgson K, Neall V, and Cronin S 2004. Lahar-triggering mechanisms and hazard at Ruapehu Volcano, New Zealand. Natural Hazards 31: 85-109.

Lirer L, Vinci A, Alberico I, Gifuni T, Bellucci F, Petrosino P, Tinterri R 2001. Occurrence of inter-eruption debris flow and hyperconcentrated flood-flow deposits on Vesuvio volcano, Italy. Sedimentary Geology 139: 151-167.

Li Z, Komar PD 1986. Laboratory measurements of pivoting angles for applications to selective entrainment of gravels in a current. Sedimentology 33: 413-423.

Lowe DR, Williams SN, Leigh, H, Connor DB, Bemmell JB, Stoiber RE 1986. Lahars initiated by the 13 November 1985 eruption of Nevado del Ruiz, Colombia. Nature 324: 51- 53.

Macías JL, Capra L, Scott KM, Espínadola JM, García-Palomo A, Costa JE 2004. The 26 May 1982 breakout flows derived from failure of a volcanic dam at El Chichón, Chiapas, Mexico. Geological Society of America Bulletin 116: 233-246.

Manville V, White JDL, Houghton BF, Wilson CJN 1999. Paleohydrology and sedimentology of a post-1.8 ka breakout flood from intracaldera Lake Taupo, North Island, New Zealand. GSA Bulletin 111: 1435-1447.

Manville V, Hodgson KA, Houghton BF, Keys JR, White JDL 2000. Tephra, snow and water: complex sedimentary responses at an active snow-capped stratovolcano, Ruapehu, New Zealand. Bulletin of Volcanology 62: 278-293.

Manville V, White JDL, Hodgson KA 2000. Dynamic interactions between lahars and stream flow: A case study from Ruapehu volcano, New Zealand: Discussion and Reply. Geological Society of America Bulletin 112: 1149-1152.

Manville V, Segschneider B, White D, 2002. Hydrodynamic behaviour of Taupo 1800a pumice: implications for the sedimentology of remobilized pyroclasts. Sedimentology 49: 955-976.

Manville V, White JDL 2003. Incipient granular mass flows at the base of sediment laden floods and the roles of flow competence and flow capacity in the deposition of stratified bouldery sands. Sedimentary Geology 155: 157-173.

Manville V 2004. Paleohycaulic analysis of the 1953 Tangiwai lahar: New Zealand's worse volcanic disaster. Acta Vulcanologica 16: 1-15.

Manville V, Wilson C 2004. The 26.5 ka Oruanui eruption, New Zealand: a review of the roles of volcanism and climate in the post-eruptive sedimentary response. New Zealand Journal of Geology and Geophysics 47: 535-547.

Manville V, Newton E, White J, 2005. Fluvial responses to volcanism: resedimentation of the 1800a Taupo ignimbrite eruption in the Rangitaiki River catchment, North Island, New Zealand. Geomorphology 65: 49-70.

Manville V, Hodgson KA, Nairn IA 2007. A review of breakout floods from volcanogenic lakes in New Zealand. New Zealand Journal of Geology and Geophysics 50: 131-150.

Mastin LG, Witter JB 2000. The hazards of eruptions through lakes and seawater. Journal of Volcanology and Geothermal Research 97: 195-214.

Nakagawa M, Wada K, Thordarson T, Wood CP, Gamble JA 1999. Petrologic investigations of the 1995 and 1996 eruptions of Ruapehu volcano, New Zealand: formation of discrete and small magma pockets and their intermittent discharge. Bulletin of Volcanology 61: 15-31.

Nairn IA, Wood CP, Hewson CAY 1979. Phreatic eruptions of Ruapehu: April 1975. New Zealand Journal of Geology and Geophysics 22: 155-173.

New Zealand Geological Survey, DSIR 1989. Volcano and geothermal observations 1988. New Zealand Volcanological Record no.17: 51.

O'Shea BE 1954. Ruapehu and the Tangiwai Disaster. New Zealand Journal of Science and Technology B 26: 174-189.

Oliver RL 1945. Further activity of Mount Ruapehu, May-July, 1945. The New Zealand Journal of Science and Technology July 1945: 24-32.

Otway PM, Hodgson KA, Nairn IA 1995. Whakapapa ski fields lahar study. Institute of Geological and Nuclear Sciences Science Report 95/93: p. 90.

Palmer BA, Neall VE 1989. The Murimotu Formation—9500 year old deposits of a debris avalanche and associated lahars, Mount Ruapehu, North Island, New Zealand. New Zealand Journal of Geology and Geophysics 32: 477-486.

Palmer, BA 1991. Holocene lahar deposits in the Whakapapa Catchment, northwestern ring plain, Ruapehu volcano (North Island, New Zealand). New Zealand Journal of Geology and Geophysics 34: 177-190.

Palmer BA, Alloway BV, Neall VE 1991. Volcanic-debris-avalanche deposits in New Zealand—Lithofacies organization in unconfined, wet-avalanche flows *in* Fischer RV, and Smith GA Sedimentation in Volcanic Settings SEPM Special Publication No. 45: 89-98.

Palmer BA, Purves AM, Donoghue S. L. 1993. Controls on accumulation of a volcaniclastic fan, Ruapehu composite volcano, New Zealand. Bulletin of Volcanology 55: 176-189.

Pareschi M, Santacroce R, Sulpizio R, Zanchetta G 2002. Volcaniclastic debris flows in the Clanio Valley (Campania, Italy): insights for the assessment of hazard potential. Geomorphology 43: 219-231

Paterson BR 1976. The effects of lahars from the 1975 April Mt. Ruapehu eruption and the threat of future eruptions on Tongariro Power Development. New Zealand Geological Survey Report, Lower Hutt, Wellington DSIR: p. 19.

Pierson TC, Scott KM 1985. Downstream dilution of a lahar: transition from debris flow to hyperconcentrated streamflow. Water Resources Research 21: 1511-1524.

Pierson TC, Costa JE 1987. A rheologic classification of sub-aerial sediment-water flows. Geological Society of America Reviews in Engineering Geology Volume VII: 1-12.

Pierson TC, Janda RJ, Thouret JC, Borrero CA 1990. Perturbation and melting of snow and ice by the 13 November 1985 eruption of Nevado del Ruiz, Colombia, and consequent mobilization, flow and deposition of lahars. In: S.N. Williams (Editor), Nevado del Ruiz Volcano, Colombia, Journal of Volcanology and Geothermal Research 41: 17-66.

Pierson TC, Janda RJ 1994. Volcanic mixed avalanches: A distinct eruption-triggered mass-flow process at snow-clad volcanoes. Geological Society of America Bulletin 106:1351-1358.

Pierson TC 1995. Flow characteristics of large eruption-triggered debris flows at snow-clad volcanoes: constraints for debris-flow models. Journal of Volcanology and Geothermal Research 66: 283-294.

Pierson TC 1997. Transformation of water flood to debris flow following the eruption triggered transient-lake breakout from the crater on March 19, 1982 *in* Pierson TC, Waitt ed. Hydrological Consequences of Hot-Rock Snowpack interactions at Mt. St. Helen's volcano. USGS Open File Report 96-179: 19-36.

Pierson TC 1998. An empirical method for estimating travel times for wet volcanic mass flows. Bulletin of Volcanology 60: 98-109.

Pierson TC 2002. Evaluation of lahar mitigation proposals at Mt. Ruapehu. DOC Science Internal Series 63: p. 18.

Reed JJ 1945. Activity at Ruapehu, March- April, 1945. The New Zealand Journal of Science and Technology July 1945: 17-23.

Ruapehu Bulletin 27 March 2007. vol. 23 no. 1175: 5.

Scott BJ, Sherburn S 1998. Volcano and geothermal observations 1995. New Zealand Volcanological record 24. IGNS Report 98/3: p. 115.

Scott KM, Marcia JL, Naranjo JA, Rodriguez S, McGeehin JP 2001. Catastrophic Debris Flows transformed from landslides in volcanic terrains. USGS Professional Paper 1630: p. 59.

Segschneider B, Landis CA, Manville V, White JD, Wilson CJ, 2002a. Environmental response to a large, explosive rhyolite eruption: sedimentology of the post-1.8 ka pumice-rich Taupo volcaniclastics in the Hawke's Bay region, New Zealand. Sedimentary Geology: 257-299.

Segschneider B, Landis CA, White JD, Wilson CJ, Manville V 2002b. Resedimentation of the 1.8 ka Taupo ignimbrite in the Mohaka and Ngaruroro River catchments, Hawke's Bay, New Zealand. New Zealand Journal of Geology and Geophysics 45: 85-101.

Smith GA, Fritz WG 1989. Volcanic influences on terrestrial sedimentation. Geology 17: 375-376.

Smith G, Lowe D 1991. Lahars: Volcano-hydrological events and deposition in the debris flow- hyperconcentrated flow continuum *in* Fischer, RV, Smith GA Sedimentation in Volcanic Settings, SEPM Special Publication No. 45: 59-70.

Stock JD, Dietrich WE 2003. Valley incision by debris flows: Evidence of a topographic signature. Water Resources Research 39: doi:10.1029/2001WR001057.

Stock JD, Dietrich WE 2006. Erosion of steepland valleys by debris flows. Geological Society of America Bulletin 118: 1125- 1148.

Sousa J, Voight B 1991. Continuum simulation of flow failures. Geotechnique 41: 515-538.

Taylor R 1861. Journal of Rev. Richard Taylor: 1833-1873. Typescript in Alexander Turnbull Library, Wellington.

Vallance JW, Scott KM 1997. The Osceola Mudflow from Mount Rainier: Sedimentology and hazard implications of a huge clay-rich debris flow. GSA Bulletin 109: 143-163.

Vignaux M, Weir GJ 1990. A general model for Mt. Ruapehu lahars. Bulletin of Volcanology 52: 381-390.

Villamor P, Berryman KR 2006. Late Quaternary geometry and kinematics of faults at the southern termination of the Taupo Volcanic Zone, New Zealand. New Zealand Journal of Geology and Geophysics 49: 1-21.

Waitt RB, Gardner CA, Pierson TC, Major JJ, Neal CA 1994. Unusual ice diamicts emplaced during the December 15, 1989 eruption of Redoubt Volcano, Alaska. Journal of Volcanology and Geothermal Research 62: 409-428.

Walder JS, O'Connor JE 1997. Methods for predicting peak discharge of floods caused by failure of natural and constructed earthen dams. Water Resources Research 33: 2337-2348.

Waythomas CF, Walder JS, McGimsey RG, Neal CA 1996. A catastrophic flood caused by drainage of a caldera lake at Aniakchak Volcano, Alaska, and implications for volcanic hazard assessment. GSA Bulletin 108: 861-871.

Waythomas CF 2001. Formation and failure of volcanic debris dams in the Chakachatna River Valley associated with eruptions of the Spurr volcanic complex, Alaska. Geomorphology 39: 111-129.

Webby MG 1999. Mt. Ruapehu Crater Lake lahar hazard. Conversation advisory science notes 231: p.19.

Wittenberg L, Newson MD 2005. Particle clusters in gravel-bed rivers: an experimental morphological approach to bed material transport and stability concepts. Earth Surface Processes and Landforms 30: 1315-1368.

White JDL, Houghton BF, Hodgson KA, Wilson CJN 1997. Delayed sedimentary response to the A.D. 1886 eruption of Tarawera, New Zealand. Geology 25: 459-462.

Reference Addendum

Dibble RR 1972: Seismic and related phenomena at active volcanoes in New Zealand, Hawaii and Italy. Unpublished Ph.D. thesis, Victoria University of Wellington: p 557., 2 vols.

Leung M, Santos J, Haimes Y 2003. Risk modelling, assessment, and management of lahar flow threat. Risk Analysis 23: 1323-1335.

Appendix

Table A.1.1 Grid references for matrix (>16 mm) samples and field sieving locations. New Zealand Map Grid 1949.

Way Point	Unit	Sample Name	Northings	Eastings
12	1975	N75-1 sample	2737464	6209466
13	1975	N75-2 sample	2737462	6209465
16	1975	N75-3 sample	2737645	6209424
17	1995E	N95i-1 sample	2737456	6209410
18	1995E	N95i-2 sample	2737464	6209411
19	1995R	N95r-1 sample	2737465	6209392
20	1995E	N95e-1 sample	2737465	6209418
35	1995R	S95r-1 sample	2737465	6209418
35	1995E	S95e-2 sample	2737615	6209355
61	1975	S75-1 sample	2737410	6209347
64	1995E	S95e-2 sample	2737366	6209395
69	1999	N99-1 sample	2737094	6209607
70	1999	N95r-2 sample	2737082	6209613
71	1995E	N95e-3 sample	2737127	6209640
78	1975	S75-2 sample	2737019	6209593
81	1975	S95E-3 sample	2736571	6209737
83	1999	S95R-2- sample	2736546	6209767
92	1975	N75-4 sample	2739559	6209191
93	1995E	N95E-4 sample	2739533	6209184
94	1995R	N95R-3 sample	2739513	6209154
95	1975	N75-5 sample	2738497	6209223
97	1995E	S95R-3 sample	2738962	6209284
100	1975	S95E-4 sample	2738725	6209275
108	1999	S95R-4 sample	2739539	6209110
109	1995E	S95E-5 sample	2739518	6209098
110	1975	S75-3 sample	2739523	6209092
112	1995E	C95E-1 sample	2738882	6208990
113	1995E	C95E-2 sample	2738197	6209121
114	1995E	C95E-3 sample	2738051	6209116
118	1995E	S95R-5 sample	2736851	6209715
122	1995R	N95R-4 sample	2737645	6209384
123	99	N95R-5 sample	2737652	6209369
133	2007	N07-1 sample	2736246	6209839
134	1975	N95E-5 sample	2736366	6209806
135	2007	S07-1 sample	2736435	6209753
136	2007	N07-2 sample	2736871	6209700
137	2007	S07-2 sample	2736971	6209667
138	2007	N07-3 sample	2739838	6208997
139	2007	S07-3 sample	2739767	6209021
140	Mangaio Fmtn	N95R-6 sample	2739669	6209060
141	2007	S07-4 sample	2739099	6209238
143	2007	N07-4 sample	2738932	6209340
144	2007	S07-5 sample	2738704	6209291
146	2007	N07-4 sample	2737326	6209525
147	1975	N75-1a,b, hc samples	2737368	6209517
149	2007	N07-5 sample	2737577	6209404
150	2007	N07-6 sample	2737603	6209392
152	1975?	S95R-6 sample	2736241	6209778

153	1975		S95E-6 sample	2736713	6209742
	1975		S95E-7 sample	2736713	6209742
154	Mangaio Fmtn		WP-2 sample	2737185	6209608
155	1861		ML-1 sample	2737147	6209472
156	1861		ML-3 sample/ 45J-1	2737109	6209507
157			45J-2 sample	2737219	6209455

Field sieving locations

WH016-01		1995	WH016-01	2736982	6209661
WH017-01		2007	WH017-01	2736982	6209661
WH018-01		1861	WH018-01	2736323	6209806
WH019-01		2007	WH019-01	2736007	6209937
WH020-01		2007	WH020-01	2735571	6210197
WH021-01		2007	WH021-01	2735723	6210096
WH022-01	active landslide		WH022-01	2731766	6210150
WH023-01		2007	WH023-01	2735207	6210437
WH023-02		2007	WH023-02	2735207	6210437
WH024-01		2007	WH024-01	2738961	6209313
WH033-01		1995	WH033-01	2737440	6209428
WH034-01		2007	WH034-01	2740064	6208698
WH035-01		1975	WH035-01	2737145	6209479
WH035-02	alluvial gravel		WH035-02	2737145	6209479
WH036-01		2007	WH036-01	2737479	6209394

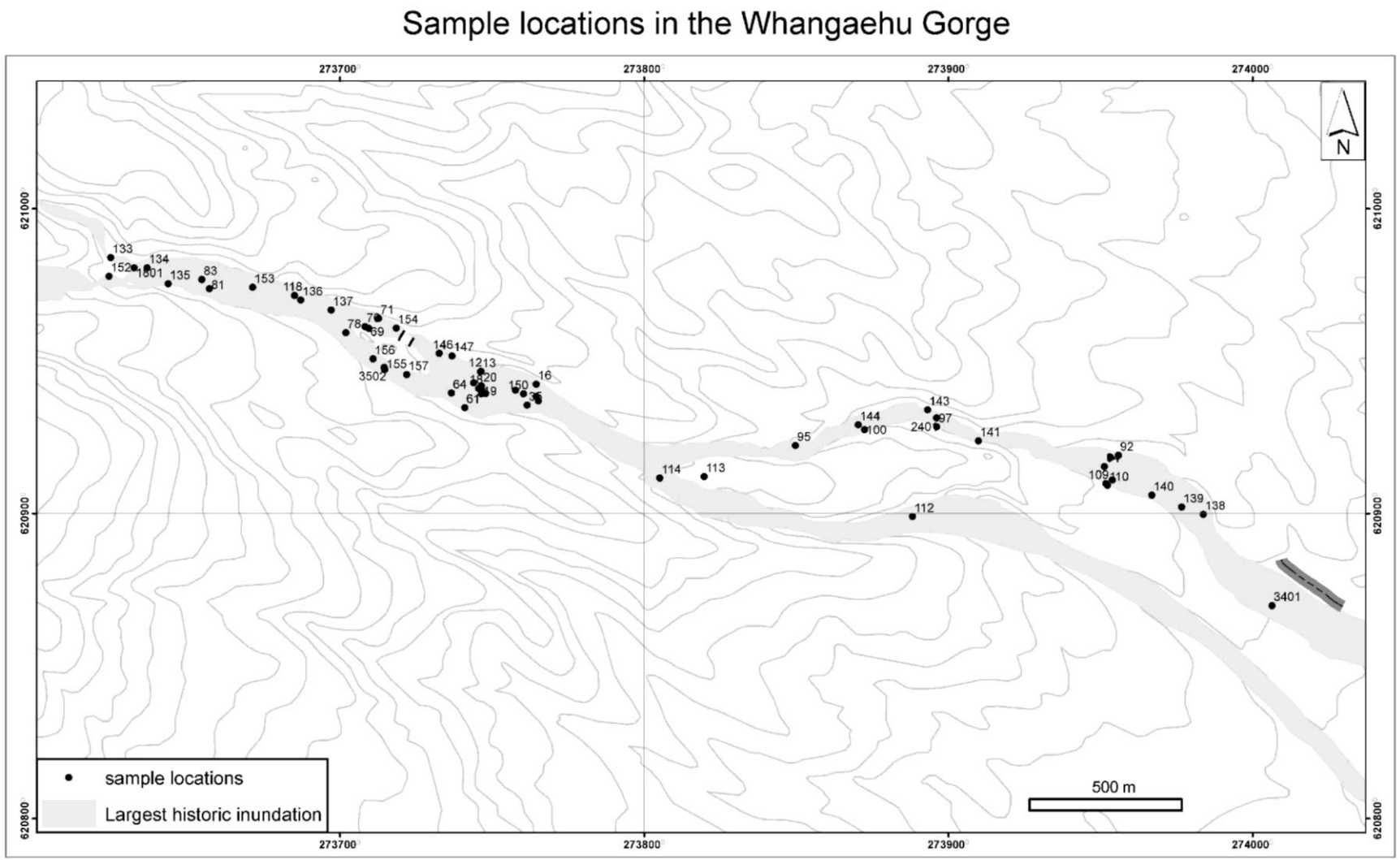

Fig. A.1.1 Sample locations in the Whangaehu Gorge, including matrix and field sieving locations.

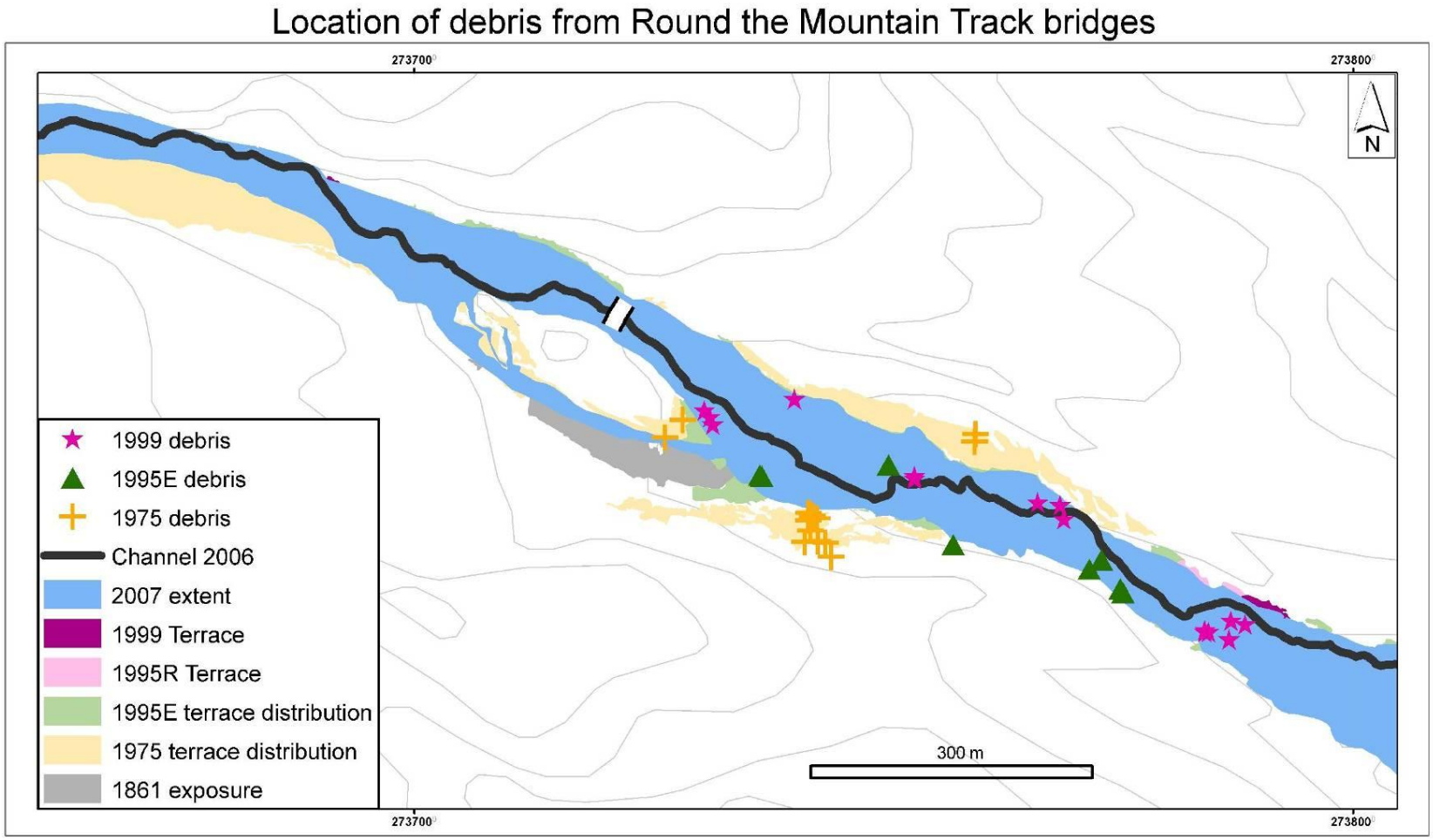

Fig. A.1.2 Locations of chronostratigraphic bridge debris in the Whangaehu Gorge. Location of debris from the Round the Mountain Track bridges destroyed by lahars in 1975, September 1995 and 1999. Debris located within the 2007L inundation area was removed from the gorge during the March 18, 2007 lahar.

Table A1.2.1 Grid references for wood debris from the 1975 lahar. New Zealand Map Grid 1949.

Way Point	Northing	Easting
14	2737597	6209437
15	2737598	6209445
26	2737420	6209353
27	2737422	6209342
28	2737416	6209330
29	2737430	6209331
30	2737438	6209329
31	2737444	6209314
57	2737424	6209356
58	2737424	6209358
59	2737429	6209355
60	2737420	6209361
76	2737267	6209441
77	2737286	6209460

Table A.1.2.2 Grid references for wood debris from the 1995E lahar. New Zealand Map Grid 1949.

Way Point	Northing	Easting
39	2737505	6209412
45	2737719	6209301
46	2737755	6209276
47	2737752	6209280
48	2737810	6209240
52	2737868	6209226
55	2737574	6209327
62	2737368	6209401
63	2737370	6209400
106	2737732	6209311

Table A.1.2.3 Grid references for wood debris from the 1999 lahar. New Zealand Map Grid 1949.

Way Point	Northing	Easting
10	2737405	6209482
33	2737692	6209354
36	2737318	6209455
37	2737315	6209463
38	2737309	6209470
40	2737533	6209400
41	2737533	6209397
43	2737664	6209372
44	2737688	6209369
49	2737842	6209234
52	2737842	6209236
51	2737846	6209234
52	2737868	6209226
53	2737885	6209242
54	2737870	6209246

Fig. A.2.1

Sample Number: **ML-1** **1861**

Total sample weight: 452.7

Sieve Phi	Sieve mm	weight retained (g)	>2 mm (g)	Wt. %	Cu. Wt. %
-4.0	16.000	61.400		13.563	1.006
-3.5	11.314	58.900		13.011	0.870
-3.0	8.000	44.790		9.894	0.740
-2.5	5.657	27.530		6.081	0.641
-2.0	4.000	28.500		6.296	0.580
-1.5	2.828	24.600		5.434	0.517
-1.0	2.000	21.500		4.749	0.463
-0.5	1.414	19.600		4.330	0.415
0.0	1.000	17.400		3.844	0.372
0.5	0.707	17.000		3.755	0.334
1.0	0.500	18.400		4.065	0.296
1.5	0.354	15.500		3.424	0.255
2.0	0.250	14.400	15.618	3.450	0.221
2.5	0.177	13.000	15.861	3.504	0.187
3.0	0.125	10.600	15.232	3.365	0.152
3.5	0.088	60.895	6.492	1.434	0.118
4.0	0.063		5.936	1.311	0.104
4.5	0.044		5.386	1.190	0.091
5.0	0.031		4.744	1.048	0.079
5.5	0.022		18.931	4.182	0.068
6.0	0.016		11.487	2.537	0.026
6.5	0.011		0.428	0.095	0.001
			% mud	10.268	

Percentiles	phi	mm
95%	-3.795	13.881
84%	-3.385	10.446
75%	-3.039	8.219
50%	-1.342	2.535
25%	1.579	0.335
16%	2.880	0.136
5%	5.717	0.019

Folks' Graphic Stats	phi	mm
Mean (Mz)	-0.616	1.532
Sorting (SI)	3.007	
Mode	-4.000	
Skewness(Sk)	-0.416	

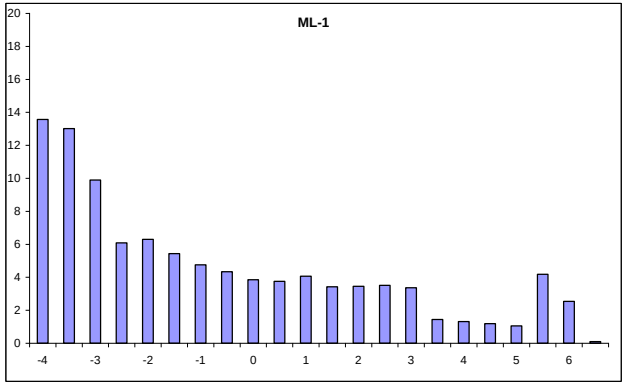

Sample Number: **ML-3** **1861**

Total sample weight: 461.180

Sieve Phi	Sieve mm	weight retained (g)	>2 mm (g)	Wt. %	Cu. Wt. %
-4.0	16.000	103.800		22.507	1.028
-3.5	11.314	59.780		12.962	0.803
-3.0	8.000	59.190		12.834	0.674
-2.5	5.657	37.850		8.207	0.545
-2.0	4.000	31.150		6.754	0.463
-1.5	2.828	17.960		3.894	0.396
-1.0	2.000	14.410		3.125	0.357
-0.5	1.414	12.630		2.739	0.325
0.0	1.000	11.510		2.496	0.298
0.5	0.707	12.150		2.635	0.273
1.0	0.500	15.500		3.361	0.247
1.5	0.354	15.360		3.331	0.213
2.0	0.250	15.190	15.354	3.329	0.180
2.5	0.177	13.530	14.763	3.201	0.147
3.0	0.125	10.300	13.263	2.876	0.115
3.5	0.088	43.733	4.154	0.901	0.086
4.0	0.063		3.971	0.861	0.077
4.5	0.044		3.828	0.830	0.068
5.0	0.031		3.618	0.784	0.060
5.5	0.022		15.672	3.398	0.052
6.0	0.016		8.157	1.769	0.018
6.5	0.011		0.173	0.038	0.000
			% mud	7.643	

Percentiles	phi	mm
95%	-3.826	14.182
84%	-3.582	11.972
75%	-3.295	9.812
50%	-2.224	4.672
25%	0.939	0.522
16%	2.298	0.203
5%	5.530	0.022

Folks' Graphic Stats	phi	mm
Mean (Mz)	-1.169	2.249
Sorting (SI)	2.888	
Mode	-4.000	
Skewness(Sk)	-0.598	

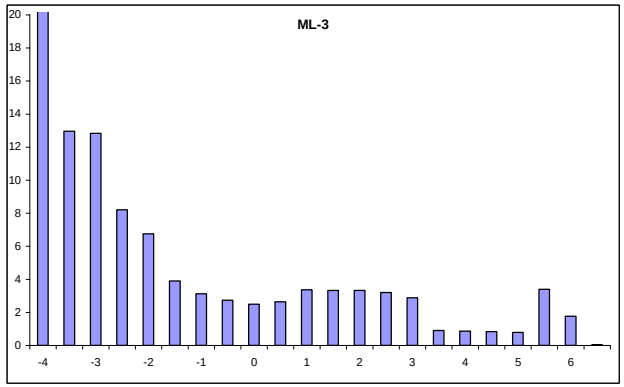

Fig. A.2.1 Matrix (<16 mm) grain size distribution data.

Fig. A.2.1 cont.
1975

Sample Number: **N75-1** **1975**

Total sample weight: 791.3g

Sieve Phi	Sieve mm	weight retained (g)	>2 mm (g)	Wt. %	Cu. Wt. %
-4.0	16.000	3.200		0.404	106.96%
-3.5	11.314	46.660		5.897	106.56%
-3.0	8.000	52.520		6.637	100.66%
-2.5	5.657	58.490		7.392	94.02%
-2.0	4.000	63.890		8.074	86.63%
-1.5	2.828	75.470		9.537	78.56%
-1.0	2.000	88.590		11.196	69.02%
-0.5	1.414	76.250		9.636	57.82%
0.0	1.000	71.900		9.086	48.19%
0.5	0.707	60.380		7.630	39.10%
1.0	0.500	49.270		6.226	31.47%
1.5	0.354	32.710		4.134	25.24%
2.0	0.250	23.660		2.990	21.11%
2.5	0.177	16.650	16.958	2.143	18.12%
3.0	0.125	12.670	14.668	1.854	15.98%
3.5	0.088	61.511	3.335	0.421	14.12%
4.0	0.063		3.719	0.470	13.70%
4.5	0.044		4.524	0.572	13.23%
5.0	0.031		5.190	0.656	12.66%
5.5	0.022		25.229	3.188	12.00%
6.0	0.016		16.969	2.144	8.82%
6.5	0.011		0.439	0.055	6.67%
			% mud	6.616	

Percentiles

	phi	mm
95%	-2.574	5.953
84%	-1.837	3.573
75%	-1.314	2.486
50%	-0.094	1.067
25%	1.529	0.346
16%	2.995	0.125
5%	4.872	0.034

Folks' Graphic Stats

	phi	mm
Mean (Mz)	0.354	0.782
Sorting (SI)	2.336	
Mode	-1.250	
Skewness(Sk)	-0.306	

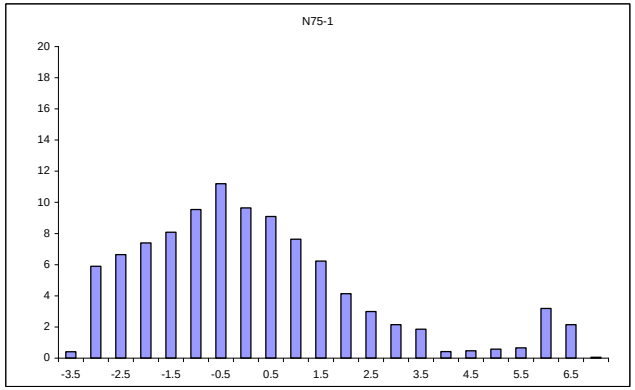

Sample Number: **N75-2** **1975**

Total sample weight: 698.800

Sieve Phi	Sieve mm	weight retained (g)	>2 mm (g)	Wt. %	Cu. Wt. %
-4.0	16.000	18.000		2.576	100.00%
-3.5	11.314	53.200		7.613	97.42%
-3.0	8.000	70.200		10.046	89.81%
-2.5	5.657	66.110		9.461	79.77%
-2.0	4.000	52.740		7.547	70.30%
-1.5	2.828	49.510		7.085	62.76%
-1.0	2.000	50.030		7.159	55.67%
-0.5	1.414	43.600		6.239	48.51%
0.0	1.000	44.450		6.361	42.27%
0.5	0.707	48.640		6.961	35.91%
1.0	0.500	49.690		7.111	28.95%
1.5	0.354	39.130		5.600	21.84%
2.0	0.250	29.140	29.140	4.170	16.24%
2.5	0.177	20.230	20.354	2.913	12.07%
3.0	0.125	14.830	15.129	2.165	9.16%
3.5	0.088	49.300	0.652	0.093	6.99%
4.0	0.063		1.366	0.195	6.90%
4.5	0.044		2.761	0.395	6.71%
5.0	0.031		4.091	0.585	6.31%
5.5	0.022		21.598	3.091	5.73%
6.0	0.016		17.599	2.518	2.63%
6.5	0.011		0.810	0.116	0.12%
			% mud	6.706	

Percentiles

	phi	mm
95%	-3.341	10.132
84%	-2.711	6.547
75%	-2.248	4.751
50%	-0.604	1.520
25%	1.278	0.412
16%	2.029	0.245
5%	5.617	0.020

Folks' Graphic Stats

	phi	mm
Mean (Mz)	-0.429	1.346
Sorting (SI)	2.542	
Mode	-3.250	
Skewness(Sk)	-0.250	

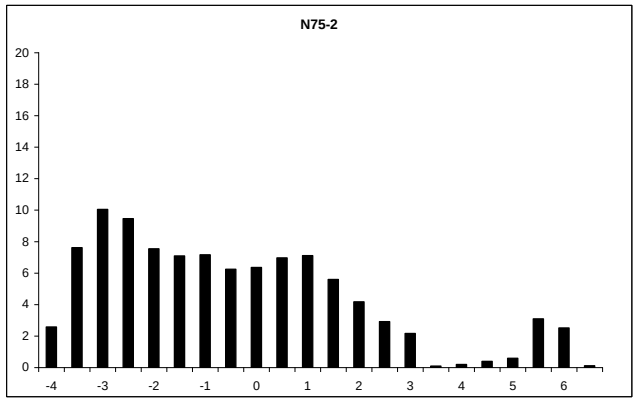

Fig. A.2.1 cont.

Sample Number: N75-3 1975

Total sample weight: 436.525

Sieve Phi	Sieve mm	weight retained (g)	>2 mm (g)	Wt. %	Cu. Wt. %
-4.0	16.000	5.660		1.297	99.99%
-3.5	11.314	19.530		4.474	98.69%
-3.0	8.000	13.500		3.093	94.22%
-2.5	5.657	18.120		4.151	91.13%
-2.0	4.000	15.090		3.457	86.97%
-1.5	2.828	18.440		4.224	83.52%
-1.0	2.000	18.460		4.229	79.29%
-0.5	1.414	20.900		4.788	75.06%
0.0	1.000	20.580		4.715	70.28%
0.5	0.707	23.340		5.347	65.56%
1.0	0.500	26.650		6.105	60.21%
1.5	0.354	26.190		6.000	54.11%
2.0	0.250	29.590	30.164	6.910	48.11%
2.5	0.177	33.900	39.378	9.021	41.20%
3.0	0.125	37.150	49.539	11.348	32.18%
3.5	0.088	109.173	16.448	3.768	20.83%
4.0	0.063		14.276	3.270	17.06%
4.5	0.044		10.925	2.503	13.79%
5.0	0.031		7.300	1.672	11.29%
5.5	0.022		25.949	5.944	9.62%
6.0	0.016		15.588	3.571	3.67%
6.5	0.011		0.445	0.102	0.10%
			% mud	13.793	

Percentiles

	phi	mm
95%	-3.087	8.500
84%	-1.570	2.969
75%	-0.493	1.408
50%	1.843	0.279
25%	3.316	0.100
16%	4.163	0.056
5%	5.888	0.017

Folks' Graphic Stats

	phi	mm
Mean (Mz)	1.478	0.359
Sorting (SI)	2.793	
Mode	3.000	
Skewness(Sk)	0.145	

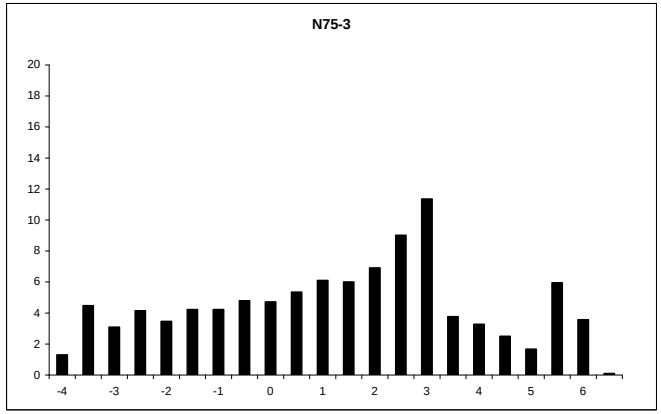

Sample Number: N75-4 1975

Total sample weight: 499.510

Sieve Phi	Sieve mm	weight retained (g)	>2 mm (g)	Wt. %	Cu. Wt. %
-4.0	16.000	5.550		1.111	95.17%
-3.5	11.314	10.000		2.002	94.06%
-3.0	8.000	23.760		4.757	92.06%
-2.5	5.657	21.620		4.328	87.30%
-2.0	4.000	24.320		4.869	82.97%
-1.5	2.828	27.410		5.487	78.11%
-1.0	2.000	27.740		5.553	72.62%
-0.5	1.414	28.520		5.710	67.07%
0.0	1.000	30.170		6.040	61.36%
0.5	0.707	30.140		6.034	55.32%
1.0	0.500	36.880		7.383	49.28%
1.5	0.354	36.430		7.293	41.90%
2.0	0.250	39.700	39.958	7.999	34.61%
2.5	0.177	40.270	42.314	8.471	26.61%
3.0	0.125	37.350	41.894	8.387	18.13%
3.5	0.088	55.337	6.180	1.237	9.75%
4.0	0.063		5.838	1.169	8.51%
4.5	0.044		5.355	1.072	7.34%
5.0	0.031		4.524	0.906	6.27%
5.5	0.022		16.505	3.304	5.36%
6.0	0.016		9.858	1.974	2.06%
6.5	0.011		0.431	0.086	0.09%
			% mud	7.342	

Percentiles

	phi	mm
95%	-3.922	15.161
84%	-2.118	4.342
75%	-1.217	2.325
50%	0.940	0.521
25%	2.595	0.166
16%	3.127	0.114
5%	5.555	0.021

Folks' Graphic Stats

	phi	mm
Mean (Mz)	0.650	0.637
Sorting (SI)	2.747	
mode	2.250	
Skewness(Sk)	0.096	

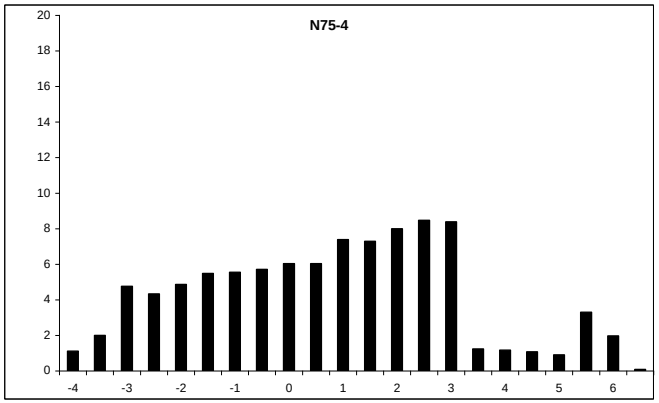

Fig. A.2.1 cont.

Sample Number: N75-5 1975

Total sample weight: 1123.900

Sieve Phi	Sieve mm	weight retained (g)	>2 mm (g)	Wt. %	Cu. Wt. %
-4.0	16.000	12.570		1.118	95.83%
-3.5	11.314	105.340		9.373	94.71%
-3.0	8.000	75.900		6.753	85.33%
-2.5	5.657	68.810		6.122	78.58%
-2.0	4.000	57.530		5.119	72.46%
-1.5	2.828	52.950		4.711	67.34%
-1.0	2.000	58.650		5.218	62.63%
-0.5	1.414	60.980		5.426	57.41%
0.0	1.000	65.580		5.835	51.98%
0.5	0.707	80.250		7.140	46.15%
1.0	0.500	65.880		5.862	39.01%
1.5	0.354	63.360		5.638	33.15%
2.0	0.250	57.000	57.281	5.097	27.51%
2.5	0.177	50.210	54.242	4.826	22.41%
3.0	0.125	55.160	65.857	5.860	17.59%
3.5	0.088	146.608	15.381	1.369	11.73%
4.0	0.063		14.211	1.264	10.36%
4.5	0.044		12.603	1.121	9.09%
5.0	0.031		11.218	0.998	7.97%
5.5	0.022		50.264	4.472	6.97%
6.0	0.016		27.376	2.436	2.50%
6.5	0.011		0.745	0.066	0.07%
			% mud	9.094	

Percentiles

	phi	mm
95%	-3.631	12.390
84%	-2.901	7.471
75%	-2.208	4.619
50%	0.170	0.889
25%	2.246	0.211
16%	3.135	0.114
5%	5.721	0.019

Folks' Graphic Stats

	phi	mm
Mean (Mz)	0.135	0.911
Sorting (SI)	2.926	
Mode	-3.500	
Skewness(Sk)	-0.085	

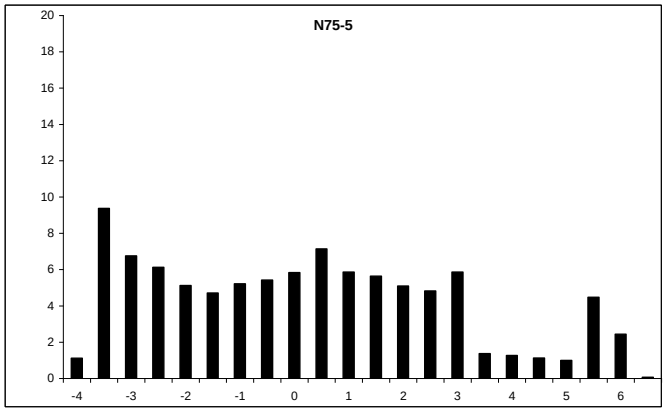

Sample Number: S75-1 1975

Total sample weight: 699.000

Sieve Phi	Sieve mm	weight retained (g)	>2 mm (g)	Wt. %	Cu. Wt. %
-4.0	16.000	88.900		12.718	100.00%
-3.5	11.314	0.000		0.000	87.28%
-3.0	8.000	53.970		7.721	87.28%
-2.5	5.657	23.410		3.349	79.56%
-2.0	4.000	20.570		2.943	76.21%
-1.5	2.828	21.770		3.114	73.27%
-1.0	2.000	23.710		3.392	70.15%
-0.5	1.414	27.180		3.888	66.76%
0.0	1.000	30.500		4.363	62.87%
0.5	0.707	34.800		4.979	58.51%
1.0	0.500	46.130		6.599	53.53%
1.5	0.354	62.150		8.891	46.93%
2.0	0.250	87.310	87.368	12.499	38.04%
2.5	0.177	97.240	97.576	13.959	25.54%
3.0	0.125	78.000	78.650	11.252	11.58%
3.5	0.088	3.360	0.733	0.105	0.33%
4.0	0.063	695.640	0.505	0.072	0.23%
4.5	0.044		0.263	0.038	0.15%
5.0	0.031		0.104	0.015	0.12%
5.5	0.022		0.442	0.063	0.10%
6.0	0.016		0.261	0.037	0.04%
6.5	0.011		0.008	0.001	0.00%
			% mud	0.154	

Percentiles

	phi	mm
95%	-3.803	13.962
84%	-2.787	6.904
75%	-1.794	3.468
50%	1.268	0.415
25%	2.519	0.174
16%	2.842	0.139
5%	3.293	0.102

Folks' Graphic Stats

	phi	mm
Mean (Mz)	0.441	0.737
Sorting (SI)	2.482	
Mode	2.250	
Skewness(Sk)	0.435	

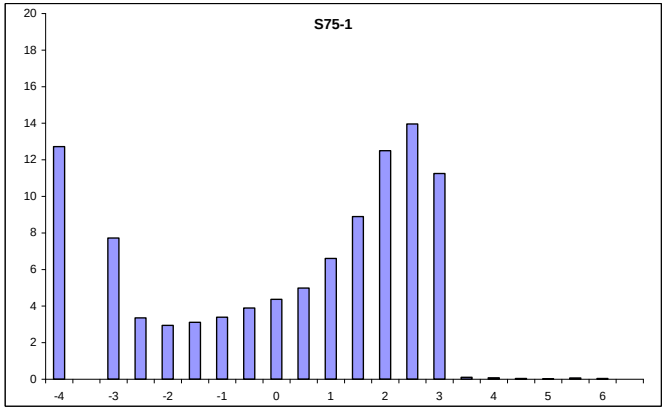

Fig. A.2.1 cont.

Total sample weight: 540.100

Sieve Phi	Sieve mm	weight retained (g)	>2 mm (g)	Wt. %	Cu. Wt. %
-4.0	16.000	0.000			99.92%
-3.5	11.314	3.810		0.705	99.92%
-3.0	8.000	31.890		5.904	99.21%
-2.5	5.657	17.970		3.327	93.31%
-2.0	4.000	33.000		6.110	89.98%
-1.5	2.828	39.760		7.362	83.87%
-1.0	2.000	50.970		9.437	76.51%
-0.5	1.414	56.380		10.439	67.07%
0.0	1.000	57.940		10.728	56.63%
0.5	0.707	54.980		10.180	45.91%
1.0	0.500	52.010		9.630	35.73%
1.5	0.354	36.590		6.775	26.10%
2.0	0.250	26.320	26.414	4.891	19.32%
2.5	0.177	17.560	18.583	3.441	14.43%
3.0	0.125	11.280	13.665	2.530	10.99%
3.5	0.088	49.640	3.438	0.637	8.46%
4.0	0.063		3.566	0.660	7.82%
4.5	0.044		3.823	0.708	7.16%
5.0	0.031		3.901	0.722	6.46%
5.5	0.022		18.587	3.441	5.73%
6.0	0.016		12.385	2.293	2.29%
6.5	0.011		0.439	0.081	0.08%
		% mud		7.246	

Percentiles

	phi	mm
95%	-2.643	6.247
84%	-1.511	2.849
75%	-0.920	1.892
50%	0.309	0.807
25%	1.581	0.334
16%	2.340	0.198
5%	6.219	0.013

Folks' Graphic Stats

	phi	mm
Mean (Mz)	0.379	0.769
Sorting (SI)	2.305	
Mode	-0.250	
Skewness(Sk)	-0.194	

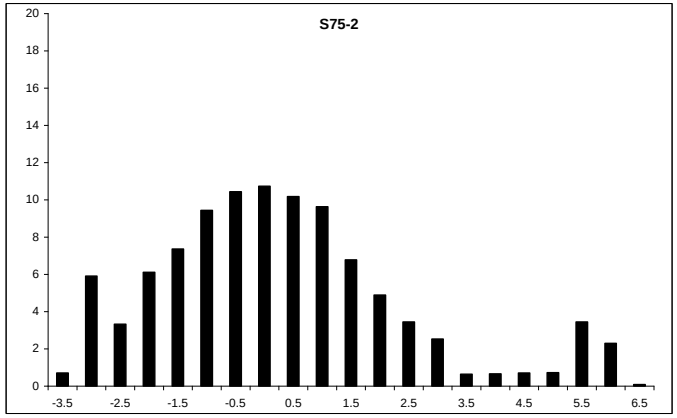

Sample Number: **S75-3** **1975**

Total sample weight: 510.580

Sieve Phi	Sieve mm	weight retained (g)	>2 mm (g)	Wt. %	Cu. Wt. %
-4.0	16.000	25.200		4.936	100.00%
-3.5	11.314	13.700		2.683	95.06%
-3.0	8.000	14.600		2.859	92.38%
-2.5	5.657	12.000		2.350	89.52%
-2.0	4.000	9.770		1.914	87.17%
-1.5	2.828	13.010		2.548	85.26%
-1.0	2.000	24.560		4.810	82.71%
-0.5	1.414	50.340		9.859	77.90%
0.0	1.000	50.610		9.912	68.04%
0.5	0.707	56.470		11.060	58.13%
1.0	0.500	51.670		10.120	47.07%
1.5	0.354	37.800		7.403	36.95%
2.0	0.250	30.600	30.838	6.040	29.54%
2.5	0.177	25.040	26.690	5.227	23.51%
3.0	0.125	21.280	25.234	4.942	18.28%
3.5	0.088	73.930	5.536	1.084	13.34%
4.0	0.063		5.247	1.028	12.25%
4.5	0.044		5.073	0.994	11.22%
5.0	0.031		5.078	0.995	10.23%
5.5	0.022		28.676	5.616	9.24%
6.0	0.016		18.099	3.545	3.62%
6.5	0.011		0.379	0.074	0.07%
		% mud		11.223	

Percentiles

	phi	mm
95%	-3.488	11.220
84%	-1.253	2.384
75%	-0.353	1.277
50%	0.867	0.548
25%	2.376	0.193
16%	3.230	0.107
5%	7.344	0.006

Folks' Graphic Stats

	phi	mm
Mean (Mz)	0.948	0.518
Sorting (SI)	2.762	
Mode	0.250	
Skewness(Sk)	-0.125	

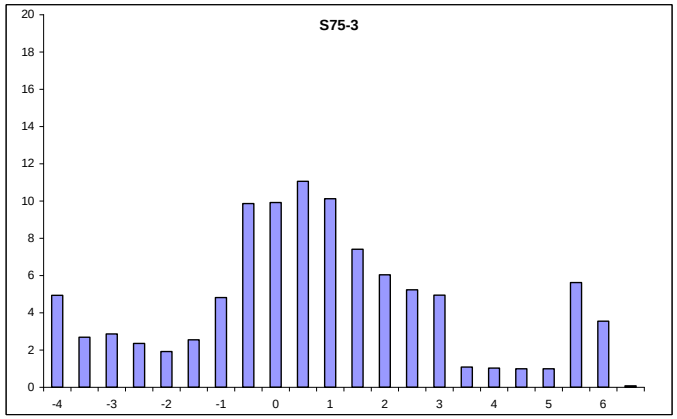

Fig. A.2.1 cont.

Sample Number: N75-1a 1975

Total sample weight: 1034.960

Sieve Phi	Sieve mm	weight retained (g)	>2 mm (g)	Wt. %	Cu. Wt. %
-4.0	16.000	168.220		16.254	100.00%
-3.5	11.314	100.620		9.722	83.75%
-3.0	8.000	107.080		10.346	74.03%
-2.5	5.657	88.200		8.522	63.68%
-2.0	4.000	94.080		9.090	55.16%
-1.5	2.828	75.910		7.335	46.07%
-1.0	2.000	71.240		6.883	38.73%
-0.5	1.414	57.390		5.545	31.85%
0.0	1.000	48.870		4.722	26.30%
0.5	0.707	47.920		4.630	21.58%
1.0	0.500	42.250		4.082	16.95%
1.5	0.354	30.160		2.914	12.87%
2.0	0.250	23.280	23.440	2.265	9.96%
2.5	0.177	16.180	16.830	1.626	7.69%
3.0	0.125	11.220	12.576	1.215	6.07%
3.5	0.088	52.166	2.127	0.206	4.85%
4.0	0.063		2.829	0.273	4.64%
4.5	0.044		4.136	0.400	4.37%
5.0	0.031		5.125	0.495	3.97%
5.5	0.022		22.136	2.139	3.48%
6.0	0.016		13.366	1.291	1.34%
6.5	0.011		0.483	0.047	0.05%
		% mud		4.372	

Percentiles

	phi	mm
95%	-3.846	14.381
84%	-3.508	11.374
75%	-3.050	8.282
50%	-1.716	3.286
25%	0.138	0.909
16%	1.117	0.461
5%	3.438	0.092

Folks' Graphic Stats

	phi	mm
Mean (Mz)	-1.369	2.583
Sorting (SI)	2.260	
Mode	-3.250	
Skewness(Sk)	-0.320	

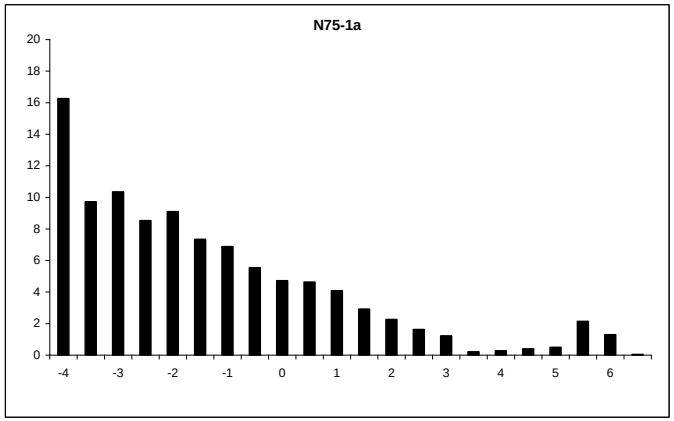

Sample Number: N75-1b 1975

Total sample weight: 465.060

Sieve Phi	Sieve mm	weight retained (g)	>2 mm (g)	Wt. %	Cu. Wt. %
-4.0	16.000	56.480		12.145	100.55%
-3.5	11.314	50.970		10.960	88.41%
-3.0	8.000	51.700		11.117	77.45%
-2.5	5.657	41.400		8.902	66.33%
-2.0	4.000	35.990		7.739	57.43%
-1.5	2.828	29.800		6.408	49.69%
-1.0	2.000	27.400		5.892	43.28%
-0.5	1.414	24.510		5.270	37.39%
0.0	1.000	24.280		5.221	32.12%
0.5	0.707	19.610		4.217	26.90%
1.0	0.500	21.820		4.692	22.68%
1.5	0.354	15.200		3.268	17.99%
2.0	0.250	12.000	12.032	2.587	14.72%
2.5	0.177	8.800	9.214	1.981	12.13%
3.0	0.125	6.800	8.085	1.738	10.15%
3.5	0.088	40.661	2.332	0.501	8.41%
4.0	0.063		3.013	0.648	7.91%
4.5	0.044		3.893	0.837	7.26%
5.0	0.031		4.290	0.922	6.43%
5.5	0.022		16.433	3.534	5.51%
6.0	0.016		8.919	1.918	1.97%
6.5	0.011		0.251	0.054	0.05%
		% mud		7.265	

Percentiles

	phi	mm
95%	-3.771	13.656
84%	-3.299	9.842
75%	-2.890	7.413
50%	-1.520	2.868
25%	0.725	0.605
16%	1.804	0.286
5%	5.572	0.021

Folks' Graphic Stats

	phi	mm
Mean (Mz)	-1.005	2.007
Sorting (SI)	2.691	
Mode	-4.000	
Skewness(Sk)	-0.410	

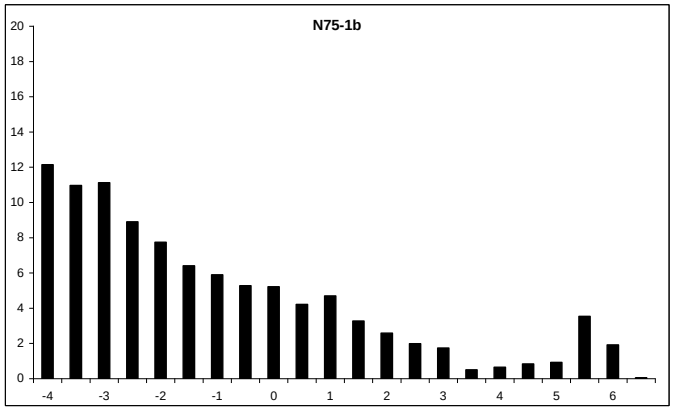

Fig. A.2.1 cont.

Sample Number: **N75-1hc** **1975**

Total sample weight: 465.600

Sieve Phi	Sieve mm	weight retained (g)	>2 mm (g)	Wt. %	Cu. Wt. %
-4.0	16.000	0.000		0.000	
-3.5	11.314	0.000		0.000	
-3.0	8.000	13.960		2.998	100.99%
-2.5	5.657	11.280		2.423	97.99%
-2.0	4.000	25.950		5.573	95.57%
-1.5	2.828	37.560		8.067	90.00%
-1.0	2.000	40.220		8.638	81.93%
-0.5	1.414	46.860		10.064	73.29%
0.0	1.000	48.600		10.438	63.23%
0.5	0.707	53.450		11.480	52.79%
1.0	0.500	60.270		12.945	41.31%
1.5	0.354	42.130		9.049	28.37%
2.0	0.250	31.400		6.744	19.32%
2.5	0.177	17.960	18.197	3.908	12.57%
3.0	0.125	9.340	10.303	2.213	8.67%
3.5	0.088	31.042	1.063	0.228	6.45%
4.0	0.063		0.896	0.192	6.22%
4.5	0.044		1.199	0.257	6.03%
5.0	0.031		1.857	0.399	5.77%
5.5	0.022		13.782	2.960	5.38%
6.0	0.016		10.926	2.347	2.42%
6.5	0.011		0.320	0.069	0.07%
			% mud	6.032	

Percentiles

	phi	mm
95%	-1.949	3.860
84%	-1.128	2.186
75%	-0.599	1.514
50%	0.622	0.650
25%	1.686	0.311
16%	2.246	0.211
5%	5.563	0.021

Folks' Graphic Stats

	phi	mm
Mean (Mz)	0.580	0.669
Sorting (SI)	1.982	
Mode	0.750	
Skewness(Sk)	-0.139	

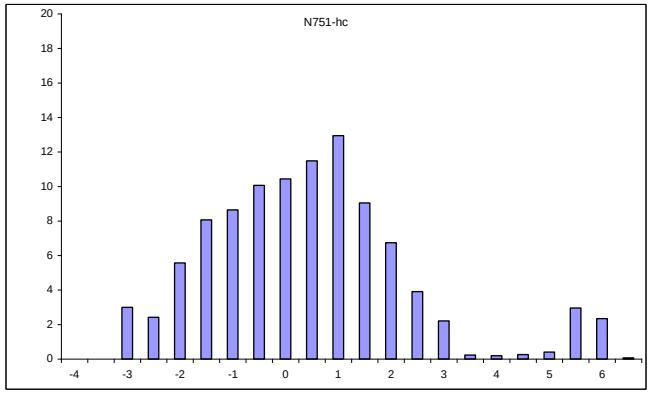

Sample Number: **N95E-5** **1975**

Total sample weight: 606.1

Sieve Phi	Sieve mm	weight retained (g)	>2 mm (g)	Wt. %	Cu. Wt. %
-4.0	16.000	18.050		2.978	1.000
-3.5	11.314	87.570		14.448	0.970
-3.0	8.000	41.400		6.831	0.826
-2.5	5.657	41.190		6.796	0.757
-2.0	4.000	23.920		3.947	0.689
-1.5	2.828	21.100		3.481	0.650
-1.0	2.000	27.390		4.519	0.615
-0.5	1.414	31.440		5.187	0.570
0.0	1.000	33.090		5.459	0.518
0.5	0.707	39.300		6.484	0.464
1.0	0.500	50.700		8.365	0.399
1.5	0.354	51.200		8.447	0.315
2.0	0.250	53.790	54.013	8.912	0.231
2.5	0.177	35.810	36.887	6.086	0.141
3.0	0.125	19.420	21.796	3.596	0.081
3.5	0.088	30.730	3.394	0.560	0.045
4.0	0.063		3.477	0.574	0.039
4.5	0.044		3.550	0.586	0.033
5.0	0.031		3.207	0.529	0.027
5.5	0.022		9.015	1.487	0.022
6.0	0.016		4.210	0.695	0.007
6.5	0.011		0.200	0.033	0.000
			% mud	3.330	

Percentiles

	phi	mm
95%	-3.430	10.778
84%	-3.049	8.278
75%	-2.445	5.446
50%	0.166	0.891
25%	1.885	0.271
16%	2.396	0.190
5%	3.425	0.093

Folks' Graphic Stats

	phi	mm
Mean (Mz)	-0.162	1.119
Sorting (SI)	2.400	
Mode	-3.750	
Skewness(Sk)	0.115	

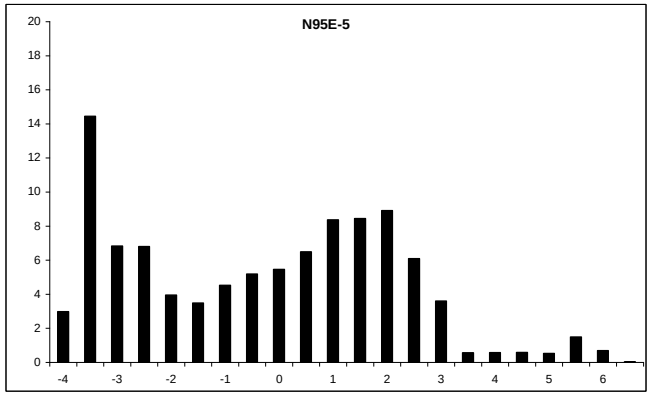

Fig. A.2.1 cont.
Sample Number: S95E-6 1975

Total sample weight: 658.160

Sieve Phi	Sieve mm	weight retained (g)	>2 mm (g)	Wt. %	Cu. Wt. %
-4.0	16.000	12.500		1.899	0.972
-3.5	11.314	37.830		5.748	0.953
-3.0	8.000	27.730		4.213	0.895
-2.5	5.657	42.010		6.383	0.853
-2.0	4.000	45.200		6.868	0.790
-1.5	2.828	47.950		7.285	0.721
-1.0	2.000	48.260		7.333	0.648
-0.5	1.414	38.240		5.810	0.575
0.0	1.000	30.270		4.599	0.517
0.5	0.707	30.920		4.698	0.471
1.0	0.500	36.800		5.591	0.424
1.5	0.354	36.000		5.470	0.368
2.0	0.250	39.800	40.206	6.109	0.313
2.5	0.177	39.600	44.754	6.800	0.252
3.0	0.125	32.920	45.352	6.891	0.184
3.5	0.088	93.465	17.265	2.623	0.115
4.0	0.063		15.371	2.335	0.089
4.5	0.044		11.425	1.736	0.065
5.0	0.031		6.470	0.983	0.048
5.5	0.022		15.938	2.422	0.038
6.0	0.016		8.959	1.361	0.014
6.5	0.011		0.246	0.037	0.000
			% mud	6.539	

Percentiles	phi	mm
95%	-3.474	11.114
84%	-2.395	5.262
75%	-1.712	3.277
50%	0.180	0.883
25%	2.514	0.175
16%	3.173	0.111
5%	4.943	0.033

Folks' Graphic Stats	phi	mm
Mean (Mz)	0.319	0.801
Sorting (SI)	2.668	
Mode	-1.250	
Skewness(Sk)	-0.103	

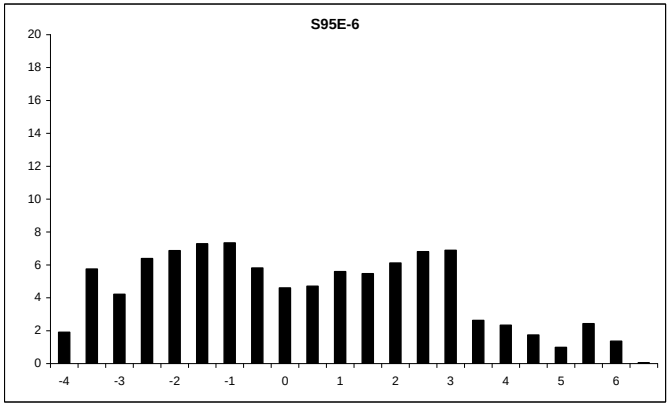

Fig. A.2.1 cont.
Sample Number: S95E-3 1975

Total sample weight: 890.2

Sieve Phi	Sieve mm	weight retained (g)	>2 mm (g)	Wt. %	Cu. Wt. %
-4.0	16.000	27.300		3.067	0.990
-3.5	11.314	53.160		5.972	0.959
-3.0	8.000	89.610		10.066	0.900
-2.5	5.657	82.650		9.284	0.799
-2.0	4.000	72.290		8.121	0.706
-1.5	2.828	72.100		8.099	0.625
-1.0	2.000	69.700		7.830	0.544
-0.5	1.414	62.710		7.044	0.466
0.0	1.000	51.800		5.819	0.395
0.5	0.707	48.790		5.481	0.337
1.0	0.500	42.100		4.729	0.282
1.5	0.354	30.780		3.458	0.235
2.0	0.250	25.630	26.180	2.941	0.200
2.5	0.177	23.450	29.880	3.357	0.171
3.0	0.125	22.200	36.804	4.134	0.137
3.5	0.088	106.807	19.340	2.172	0.096
4.0	0.063		16.540	1.858	0.074
4.5	0.044		12.016	1.350	0.056
5.0	0.031		7.050	0.792	0.042
5.5	0.022		19.130	2.149	0.034
6.0	0.016		10.834	1.217	0.013
6.5	0.011		0.515	0.058	0.001
			% mud	5.565	

Percentiles	phi	mm
95%	-3.422	10.719
84%	-2.704	6.516
75%	-2.236	4.713
50%	-0.720	1.647
25%	1.340	0.395
16%	2.662	0.158
5%	4.709	0.038

Folks' Graphic Stats	phi	mm
Mean (Mz)	-0.254	1.192
Sorting (SI)	2.574	
Mode	-3.250	
Skewness(Sk)	-0.298	

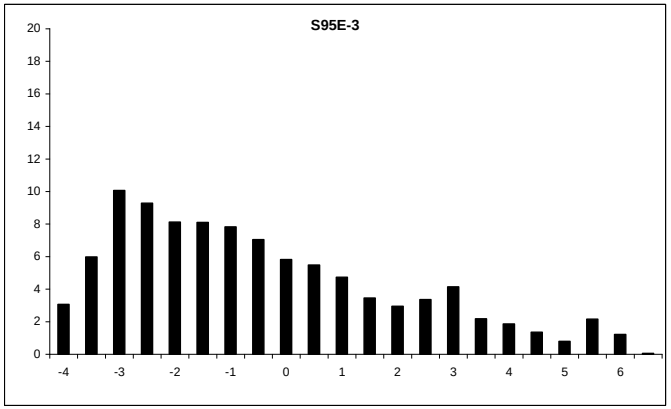

Fig. A.2.1 cont.

Sample Number: S95E-4 1975

Total sample weight: 694.925

Sieve Phi	Sieve mm	weight retained (g)	>2 mm (g)	Wt. %	Cu. Wt. %
-4.0	16.000	17.600		2.533	0.997
-3.5	11.314	58.370		8.399	0.972
-3.0	8.000	82.200		11.829	0.888
-2.5	5.657	77.480		11.149	0.770
-2.0	4.000	74.160		10.672	0.658
-1.5	2.828	63.000		9.066	0.551
-1.0	2.000	51.310		7.384	0.461
-0.5	1.414	41.220		5.932	0.387
0.0	1.000	31.030		4.465	0.328
0.5	0.707	31.910		4.592	0.283
1.0	0.500	27.860		4.009	0.237
1.5	0.354	24.000		3.454	0.197
2.0	0.250	22.050	22.156	3.188	0.162
2.5	0.177	20.040	21.337	3.070	0.130
3.0	0.125	16.670	19.653	2.828	0.100
3.5	0.088	53.847	4.220	0.607	0.071
4.0	0.063		4.317	0.621	0.065
4.5	0.044		4.516	0.650	0.059
5.0	0.031		4.403	0.634	0.053
5.5	0.022		18.686	2.689	0.046
6.0	0.016		12.762	1.836	0.019
6.5	0.011		0.756	0.109	0.001
		% mud		5.918	

Percentiles

	phi	mm
95%	-3.370	10.339
84%	-2.798	6.954
75%	-2.412	5.323
50%	-1.217	2.324
25%	0.858	0.552
16%	2.037	0.244
5%	5.211	0.027

Folks' Graphic Stats

	phi	mm
Mean (Mz)	-0.659	1.579
Sorting (SI)	2.509	
Mode	-3.250	
Skewness(Sk)	-0.422	

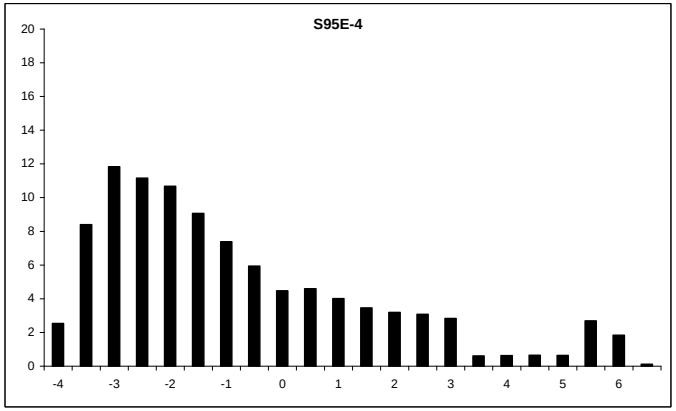

Sample Number: C95E-1 1975

Total sample weight: 553.930

Sieve Phi	Sieve mm	weight retained (g)	>2 mm (g)	Wt. %	Cu. Wt. %
-4.0	16.000	0.000		0.000	1.017
-3.5	11.314	7.710		1.392	1.017
-3.0	8.000	6.770		1.222	1.003
-2.5	5.657	19.900		3.593	0.990
-2.0	4.000	26.570		4.797	0.954
-1.5	2.828	36.000		6.499	0.906
-1.0	2.000	42.090		7.598	0.841
-0.5	1.414	43.490		7.851	0.766
0.0	1.000	41.460		7.485	0.687
0.5	0.707	47.300		8.539	0.612
1.0	0.500	53.400		9.640	0.527
1.5	0.354	50.000		9.026	0.430
2.0	0.250	44.000	44.484	8.031	0.340
2.5	0.177	41.100	45.888	8.284	0.260
3.0	0.125	28.700	39.356	7.105	0.177
3.5		74.383	13.803	2.492	0.106
4.0			11.595	2.093	0.081
4.5			8.338	1.505	0.060
5.0			4.873	0.880	0.045
5.5			13.170	2.378	0.036
6.0			6.709	1.211	0.012
6.5			0.167	0.030	0.000
		% mud		8.067	

Percentiles

	phi	mm
0.95	-1.954	3.874
0.84	-0.990	1.987
0.75	-0.401	1.321
0.5	1.139	0.454
0.25	2.559	0.170
0.16	3.119	0.115
0.05	4.833	0.035

Folks' Graphic Stats

	phi	mm
Mean (Mz)	1.089	0.470
Sorting (SI)	2.056	
Mode	1.000	
Skewness(Sk)	-0.026	

0.000

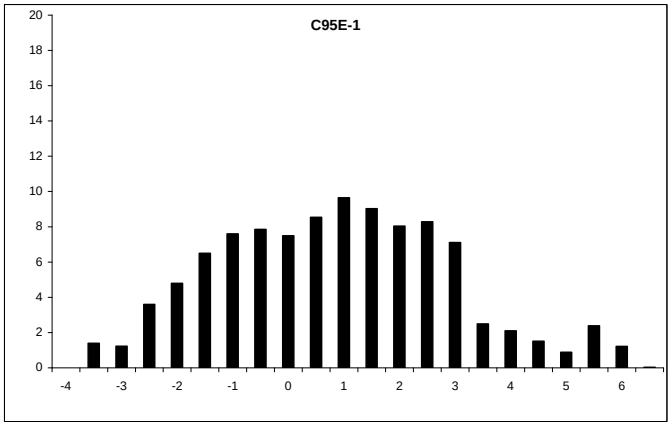

Fig. A.2.1 cont.
1995E

Sample Number: **N95E-1** **1995E**

Total sample weight: 586.1

Sieve Phi	Sieve mm	weight retained (g)	>2 mm (g)	Wt. %	Cu. Wt. %
-4.0	16.000	28.530		4.868	0.976
-3.5	11.314	41.930		7.154	0.927
-3.0	8.000	35.960		6.135	0.855
-2.5	5.657	50.150		8.557	0.794
-2.0	4.000	39.890		6.806	0.709
-1.5	2.828	37.320		6.368	0.640
-1.0	2.000	31.400		5.357	0.577
-0.5	1.414	28.980		4.945	0.523
0.0	1.000	26.690		4.554	0.474
0.5	0.707	26.740		4.562	0.428
1.0	0.500	28.970		4.943	0.383
1.5	0.354	26.450		4.513	0.333
2.0	0.250	23.820	23.936	4.084	0.288
2.5	0.177	23.500	24.996	4.265	0.247
3.0	0.125	21.400	25.395	4.333	0.205
3.5	0.088	99.900	6.097	1.040	0.161
4.0	0.063		6.559	1.119	0.151
4.5	0.044		7.232	1.234	0.140
5.0	0.031		7.578	1.293	0.127
5.5	0.022		38.225	6.522	0.114
6.0	0.016		27.662	4.720	0.049
6.5	0.011		1.138	0.194	0.002
			% mud	13.963	

Percentiles

	phi	mm
95%	-3.737	13.329
84%	-2.874	7.332
75%	-2.242	4.732
50%	-0.265	1.202
25%	2.466	0.181
16%	3.559	0.085
5%	5.993	0.016

Folks' Graphic Stats

	phi	mm
Mean (Mz)	0.140	0.908
Sorting (SI)	3.082	
Mode	-2.750	
Skewness(Sk)	-0.238	

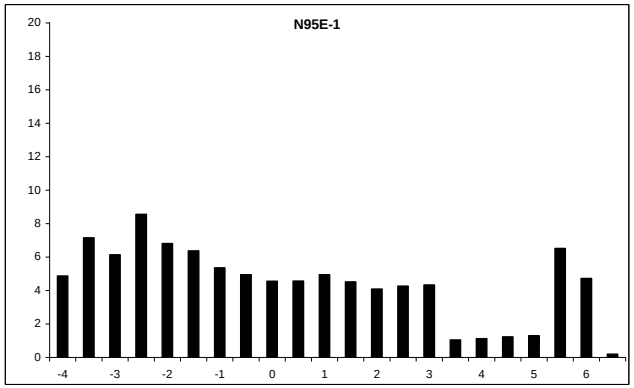

Sample Number: **N95E-3** **1995E**

Total sample weight: 485.65

Sieve Phi	Sieve mm	weight retained (g)	>2 mm (g)	Wt. %	Cu. Wt. %
-4.0	16.000	0.000		0.000	1.032
-3.5	11.314	13.900		2.862	1.032
-3.0	8.000	40.100		8.257	1.003
-2.5	5.657	40.700		8.381	0.921
-2.0	4.000	50.500		10.398	0.837
-1.5	2.828	50.600		10.419	0.733
-1.0	2.000	43.900		9.039	0.629
-0.5	1.414	38.000		7.825	0.538
0.0	1.000	30.000		6.177	0.460
0.5	0.707	27.200		5.601	0.398
1.0	0.500	27.700		5.704	0.342
1.5	0.354	21.400		4.406	0.285
2.0	0.250	17.100	17.431	3.589	0.241
2.5	0.177	15.000	17.682	3.641	0.205
3.0	0.125	11.800	17.881	3.682	0.169
3.5	0.088	72.947	8.366	1.723	0.132
4.0	0.063		7.961	1.639	0.115
4.5	0.044		7.282	1.499	0.098
5.0	0.031		6.014	1.238	0.083
5.5	0.022		21.386	4.404	0.071
6.0	0.016		12.539	2.582	0.027
6.5	0.011		0.506	0.104	0.001
			% mud	9.827	

Percentiles

	phi	mm
95%	-2.679	6.402
84%	-2.020	4.055
75%	-1.583	2.996
50%	-0.256	1.194
25%	1.898	0.268
16%	3.118	0.115
5%	5.737	0.019

Folks' Graphic Stats

	phi	mm
Mean (Mz)	0.281	0.823
Sorting (SI)	2.560	
Mode	-1.750	
Skewness(Sk)	-0.369	

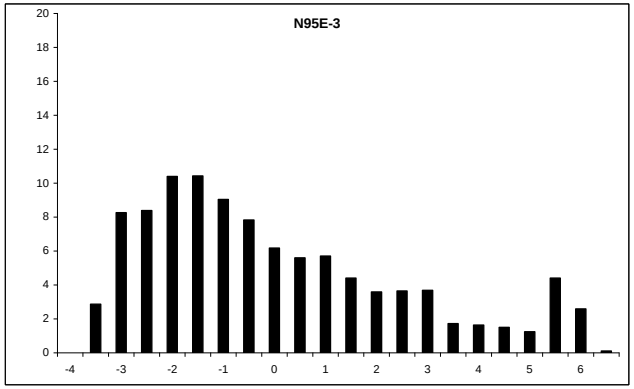

Fig. A.2.1 cont.

Sample Number: **N95E-4** **1995E**

Total sample weight: 846.8

Sieve Phi	Sieve mm	weight retained (g)	>2 mm (g)	Wt. %	Cu. Wt. %
-4.0	16.000	29.700		3.507	0.997
-3.5	11.314	33.000		3.897	0.961
-3.0	8.000	26.800		3.165	0.922
-2.5	5.657	36.200		4.275	0.891
-2.0	4.000	34.800		4.110	0.848
-1.5	2.828	31.400		3.708	0.807
-1.0	2.000	30.000		3.543	0.770
-0.5	1.414	33.100		3.909	0.734
0.0	1.000	37.000		4.369	0.695
0.5	0.707	46.300		5.468	0.652
1.0	0.500	60.600		7.156	0.597
1.5	0.354	74.020		8.741	0.525
2.0	0.250	66.100	66.451	7.847	0.438
2.5	0.177	85.290	90.346	10.669	0.360
3.0	0.125	71.500	84.458	9.974	0.253
3.5	0.088	147.829	19.002	2.244	0.153
4.0	0.063		18.547	2.190	0.131
4.5	0.044		16.586	1.959	0.109
5.0	0.031		12.780	1.509	0.089
5.5	0.022		39.348	4.647	0.074
6.0	0.016		22.179	2.619	0.028
6.5	0.011		1.221	0.144	0.001
			% mud	10.878	

Percentiles

	phi	mm
95%	-3.353	10.220
84%	-1.902	3.737
75%	-0.719	1.646
50%	1.645	0.320
25%	3.014	0.124
16%	3.466	0.091
5%	5.759	0.018

Folks' Graphic Stats

	phi	mm
Mean (Mz)	1.070	0.476
Sorting (SI)	2.723	
Mode	2.250	
Skewness(Sk)	0.209	

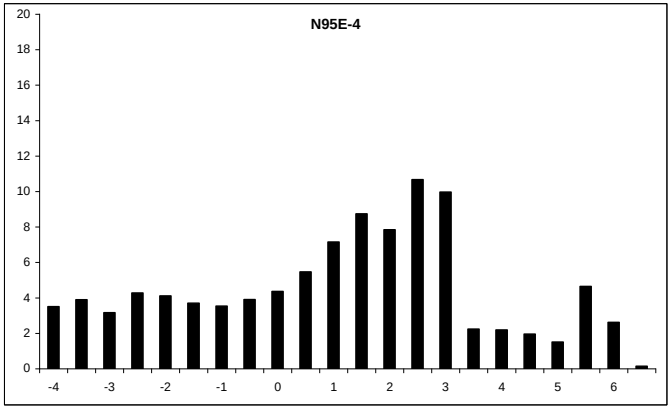

Sample Number: **N95i-1** **1995E**

Total sample weight: 784.25

Sieve Phi	Sieve mm	weight retained (g)	>2 mm (g)	Wt. %	Cu. Wt. %
-4.0	16.000	44.710		5.701	1.002
-3.5	11.314	102.100		13.019	0.945
-3.0	8.000	115.460		14.722	0.815
-2.5	5.657	77.850		9.927	0.668
-2.0	4.000	62.270		7.940	0.568
-1.5	2.828	60.190		7.675	0.489
-1.0	2.000	47.980		6.118	0.412
-0.5	1.414	36.810		4.694	0.351
0.0	1.000	27.630		3.523	0.304
0.5	0.707	25.340		3.231	0.269
1.0	0.500	25.580		3.262	0.237
1.5	0.354	20.820		2.655	0.204
2.0	0.250	20.060	20.233	2.580	0.177
2.5	0.177	18.020	20.230	2.580	0.152
3.0	0.125	15.720	21.290	2.715	0.126
3.5	0.088	85.078	8.282	1.056	0.099
4.0	0.063		8.444	1.077	0.088
4.5	0.044		8.248	1.052	0.077
5.0	0.031		7.222	0.921	0.067
5.5	0.022		27.263	3.476	0.058
6.0	0.016		16.971	2.164	0.023
6.5	0.011		0.895	0.114	0.001
			% mud	7.727	

Percentiles

	phi	mm
95%	-3.544	11.664
84%	-3.097	8.555
75%	-2.780	6.868
50%	-1.570	2.969
25%	0.791	0.578
16%	2.336	0.198
5%	5.609	0.020

Folks' Graphic Stats

	phi	mm
Mean (Mz)	-0.777	1.713
Sorting (SI)	2.745	
Mode	-3.250	
Skewness(Sk)	-0.503	

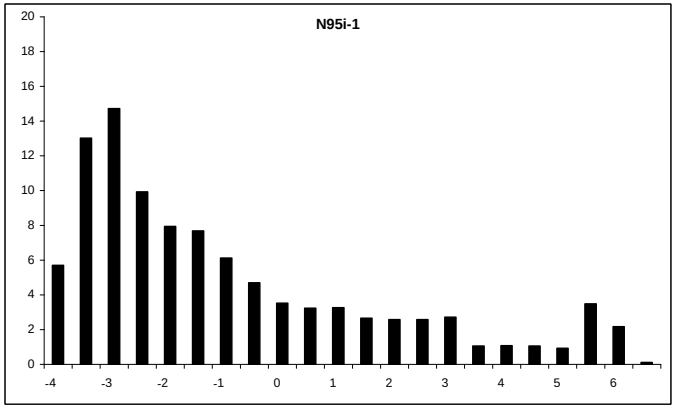

Fig. A.2.1 cont.

Sample Number: **N95i-2** **1995E**

Total sample weight: 454.7

Sieve Phi	Sieve mm	weight retained (g)	>2 mm (g)	Wt. %	Cu. Wt. %
-4.0	16.000	30.890		6.793	1.015
-3.5	11.314	35.060		7.711	0.947
-3.0	8.000	21.490		4.726	0.869
-2.5	5.657	25.470		5.601	0.822
-2.0	4.000	29.400		6.466	0.766
-1.5	2.828	22.100		4.860	0.702
-1.0	2.000	20.570		4.524	0.653
-0.5	1.414	17.930		3.943	0.608
0.0	1.000	16.400		3.607	0.568
0.5	0.707	17.200		3.783	0.532
1.0	0.500	20.500		4.508	0.494
1.5	0.354	21.230		4.669	0.449
2.0	0.250	22.570	23.036	5.066	0.403
2.5	0.177	23.600	27.175	5.977	0.352
3.0	0.125	22.920	31.106	6.841	0.292
3.5	0.088	113.781	11.467	2.522	0.224
4.0	0.063		11.189	2.461	0.199
4.5	0.044		10.577	2.326	0.174
5.0	0.031		9.073	1.995	0.151
5.5	0.022		34.893	7.674	0.131
6.0	0.016		23.463	5.160	0.054
6.5	0.011		1.091	0.240	0.002
			% mud	17.396	

Percentiles

	phi	mm
95%	-3.525	11.511
84%	-2.688	6.444
75%	-1.875	3.667
50%	0.926	0.526
25%	3.308	0.101
16%	4.800	0.036
5%	6.039	0.015

Folks' Graphic Stats

	phi	mm
Mean (Mz)	1.013	0.496
Sorting (SI)	3.321	
Mode	-3.750	
Skewness(Sk)	-0.052	

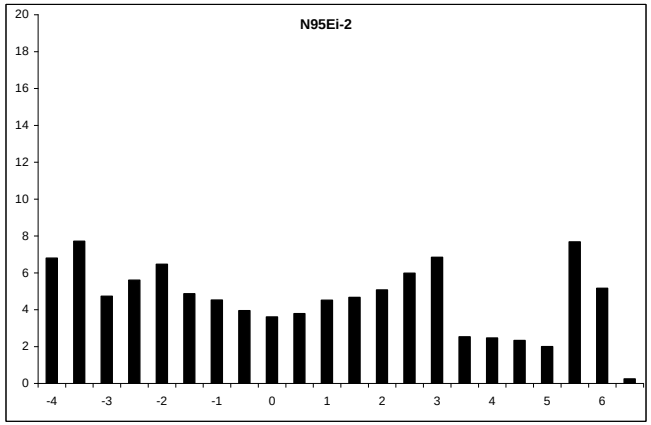

Sample Number: **S95E-1** **1995E**

Total sample weight: 585.78

Sieve Phi	Sieve mm	weight retained (g)	>2 mm (g)	Wt. %	Cu. Wt. %
-4.0	16.000	58.400		9.970	1.036
-3.5	11.314	26.900		4.592	0.936
-3.0	8.000	69.100		11.796	0.890
-2.5	5.657	69.500		11.865	0.772
-2.0	4.000	58.320		9.956	0.654
-1.5	2.828	49.900		8.519	0.554
-1.0	2.000	46.630		7.960	0.469
-0.5	1.414	38.800		6.624	0.389
0.0	1.000	31.500		5.377	0.323
0.5	0.707	26.900		4.592	0.269
1.0	0.500	24.300		4.148	0.223
1.5	0.354	17.500		2.987	0.182
2.0	0.250	12.900	13.035	2.225	0.152
2.5	0.177	9.500	11.161	1.905	0.130
3.0	0.125	6.800	11.052	1.887	0.111
3.5	0.088	59.684	6.597	1.126	0.092
4.0	0.063		7.027	1.200	0.081
4.5	0.044		6.960	1.188	0.069
5.0	0.031		5.790	0.988	0.057
5.5	0.022		18.118	3.093	0.047
6.0	0.016		9.077	1.550	0.016
6.5	0.011		0.267	0.046	0.000
			% mud	6.865	

Percentiles

	phi	mm
95%	-3.569	11.868
84%	-2.787	6.900
75%	-2.406	5.299
50%	-1.182	2.269
25%	0.711	0.611
16%	1.867	0.274
5%	5.342	0.025

Folks' Graphic Stats

	phi	mm
Mean (Mz)	-0.700	1.625
Sorting (SI)	2.514	
Mode	-2.750	
Skewness(Sk)	-0.387	

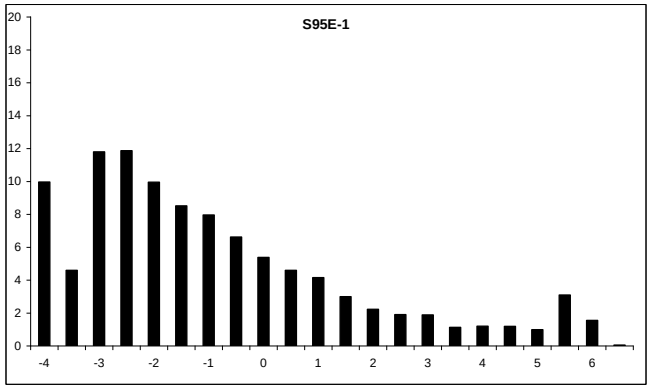

Fig. A.2.1 cont.

Sample Number: **S95E-2** **1995E**

Total sample weight: 920.42

Sieve Phi	Sieve mm	weight retained (g)	>2 mm (g)	Wt. %	Cu. Wt. %
-4.0	16.000	12.970		1.409	1.005
-3.5	11.314	47.400		5.150	0.991
-3.0	8.000	76.400		8.301	0.939
-2.5	5.657	98.460		10.697	0.856
-2.0	4.000	92.540		10.054	0.749
-1.5	2.828	91.300		9.919	0.649
-1.0	2.000	75.250		8.176	0.550
-0.5	1.414	59.880		6.506	0.468
0.0	1.000	46.100		5.009	0.403
0.5	0.707	40.400		4.389	0.353
1.0	0.500	39.500		4.292	0.309
1.5	0.354	32.900		3.574	0.266
2.0	0.250	29.900	30.570	3.321	0.230
2.5	0.177	26.100	31.230	3.393	0.197
3.0	0.125	24.600	36.139	3.926	0.163
3.5	0.088	130.986	15.952	1.733	0.124
4.0	0.063		15.273	1.659	0.106
4.5	0.044		13.938	1.514	0.090
5.0	0.031		11.282	1.226	0.075
5.5	0.022		36.190	3.932	0.062
6.0	0.016		20.286	2.204	0.023
6.5	0.011		0.926	0.101	0.001
			% mud	8.977	

Percentiles	phi	mm
95%	-3.104	8.599
84%	-2.424	5.367
75%	-2.003	4.009
50%	-0.697	1.621
25%	1.722	0.303
16%	3.038	0.122
5%	5.657	0.020

Folks' Graphic Stats	phi	mm
Mean (Mz)	-0.028	1.019
Sorting (SI)	2.693	
Mode	-2.750	
Skewness(Sk)	-0.409	

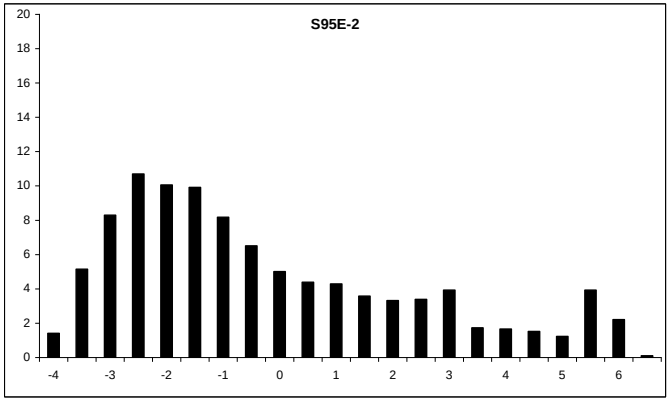

Sample Number: **C95E-2** **1995E**

Total sample weight: 698

Sieve Phi	Sieve mm	weight retained (g)	>2 mm (g)	Wt. %	Cu. Wt. %
-4.0	16.000	42.490		6.087	0.964
-3.5	11.314	48.510		6.950	0.903
-3.0	8.000	100.040		14.332	0.833
-2.5	5.657	88.000		12.607	0.690
-2.0	4.000	72.930		10.448	0.564
-1.5	2.828	58.900		8.438	0.459
-1.0	2.000	53.420		7.653	0.375
-0.5	1.414	42.260		6.054	0.299
0.0	1.000	28.900		4.140	0.238
0.5	0.707	22.600		3.238	0.197
1.0	0.500	17.920		2.567	0.164
1.5	0.354	14.150		2.027	0.139
2.0	0.250	12.420	12.495	1.790	0.118
2.5	0.177	12.710	13.824	1.981	0.100
3.0	0.125	10.960	14.038	2.011	0.081
3.5	0.088	46.446	4.983	0.714	0.060
4.0	0.063		5.489	0.786	0.053
4.5	0.044		5.552	0.795	0.045
5.0	0.031		4.569	0.655	0.037
5.5	0.022		13.348	1.912	0.031
6.0	0.016		7.987	1.144	0.012
6.5	0.011		0.250	0.036	0.000
			% mud	4.542	

Percentiles	phi	mm
95%	-3.888	14.800
84%	-3.048	8.271
75%	-2.709	6.540
50%	-1.694	3.236
25%	-0.099	1.071
16%	1.082	0.472
5%	4.209	0.054

Folks' Graphic Stats	phi	mm
Mean (Mz)	-1.220	2.330
Sorting (SI)	2.259	
Mode	-3.000	
Skewness(Sk)	-0.401	

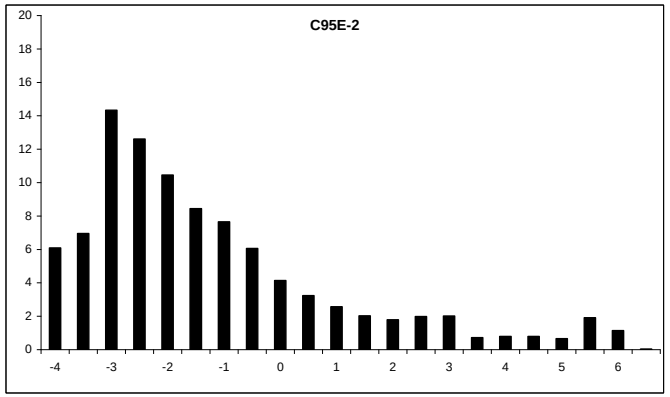

Fig. A.2.1 cont.

Sample Number: **C95E-3** **1995E**

Total sample weight: 706.98

Sieve Phi	Sieve mm	weight retained (g)	>2 mm (g)	Wt. %	Cu. Wt. %
-4.0	16.000	0.000		0.000	
-3.5	11.314	15.500		2.192	1.000
-3.0	8.000	35.200		4.979	0.978
-2.5	5.657	74.500		10.538	0.928
-2.0	4.000	99.000		14.003	0.823
-1.5	2.828	85.600		12.108	0.683
-1.0	2.000	64.400		9.109	0.562
-0.5	1.414	46.600		6.591	0.471
0.0	1.000	34.000		4.809	0.405
0.5	0.707	29.700		4.201	0.357
1.0	0.500	28.300		4.003	0.315
1.5	0.354	24.300		3.437	0.275
2.0	0.250	22.900	23.038	3.259	0.240
2.5	0.177	22.200	24.366	3.446	0.208
3.0	0.125	19.900	25.461	3.601	0.173
3.5	0.088	104.880	8.357	1.182	0.137
4.0	0.063		9.089	1.286	0.125
4.5	0.044		10.281	1.454	0.113
5.0	0.031		10.540	1.491	0.098
5.5	0.022		38.568	5.455	0.083
6.0	0.016		19.479	2.755	0.029
6.5	0.011		0.701	0.099	0.001
			% mud	11.255	

Percentiles	phi	mm
95%	-2.718	6.580
84%	-2.081	4.231
75%	-1.740	3.340
50%	-0.661	1.581
25%	1.859	0.276
16%	3.184	0.110
5%	5.803	0.018

Folks' Graphic Stats	phi	mm
Mean (Mz)	0.147	0.903
Sorting (SI)	2.607	
Mode	-2.000	
Skewness(Sk)	-0.489	

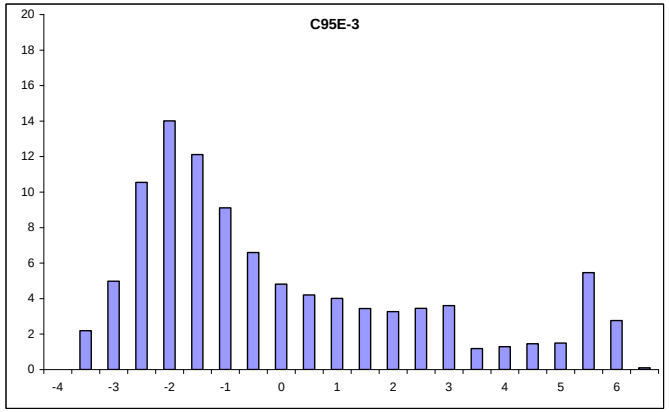

13.362

Sample Number: **S95R-3** **1995E**

Total sample weight: 739.82

Sieve Phi	Sieve mm	weight retained (g)	>2 mm (g)	Wt. %	Cu. Wt. %
-4.0	16.000	23.900		3.231	1.011
-3.5	11.314	28.570		3.862	0.978
-3.0	8.000	33.290		4.500	0.940
-2.5	5.657	44.600		6.028	0.895
-2.0	4.000	57.580		7.783	0.835
-1.5	2.828	58.460		7.902	0.757
-1.0	2.000	54.820		7.410	0.678
-0.5	1.414	50.780		6.864	0.604
0.0	1.000	48.350		6.535	0.535
0.5	0.707	47.980		6.485	0.470
1.0	0.500	45.140		6.101	0.405
1.5	0.354	37.140		5.020	0.344
2.0	0.250	32.750	32.942	4.453	0.294
2.5	0.177	28.680	30.965	4.185	0.249
3.0	0.125	28.450	34.273	4.633	0.207
3.5	0.088	127.123	9.308	1.258	0.161
4.0	0.063		10.856	1.467	0.148
4.5	0.044		12.769	1.726	0.134
5.0	0.031		13.080	1.768	0.116
5.5	0.022		46.789	6.324	0.099
6.0	0.016		24.830	3.356	0.035
6.5	0.011		1.391	0.188	0.002
			% mud	13.362	

Percentiles	phi	mm
95%	-3.131	8.761
84%	-2.045	4.126
75%	-1.457	2.746
50%	0.268	0.831
25%	2.489	0.178
16%	3.535	0.086
5%	5.885	0.017

Folks' Graphic Stats	phi	mm
Mean (Mz)	0.586	0.666
Sorting (SI)	2.761	
Mode	-1.500	
Skewness(Sk)	-0.209	

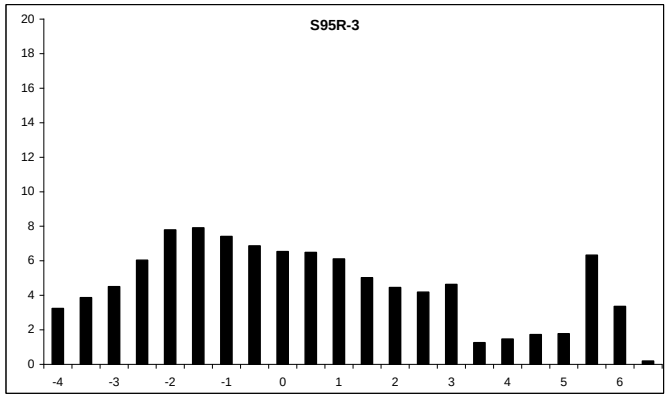

Fig. A.2.1 cont.

Sample Number: **S95R-5** **1995E**

Total sample weight: 565.63

Sieve Phi	Sieve mm	weight retained (g)	>2 mm (g)	Wt. %	Cu. Wt. %
-4.0	16.000	14.000		2.475	1.015
-3.5	11.314	16.530		2.922	0.990
-3.0	8.000	15.850		2.802	0.961
-2.5	5.657	23.830		4.213	0.933
-2.0	4.000	22.170		3.920	0.891
-1.5	2.828	19.530		3.453	0.852
-1.0	2.000	18.510		3.272	0.817
-0.5	1.414	19.200		3.394	0.784
0.0	1.000	19.570		3.460	0.750
0.5	0.707	22.500		3.978	0.716
1.0	0.500	27.200		4.809	0.676
1.5	0.354	28.900		5.109	0.628
2.0	0.250	35.600	40.038	7.079	0.577
2.5	0.177	42.900	53.590	9.474	0.506
3.0	0.125	43.300	60.286	10.658	0.411
3.5	0.088	205.174	19.682	3.480	0.305
4.0	0.063		22.567	3.990	0.270
4.5	0.044		21.937	3.878	0.230
5.0	0.031		68.809	12.165	0.191
5.5	0.022		37.144	6.567	0.070
6.0	0.016		2.270	0.401	0.004
6.5	0.011		0.000	0.000	0.004
			% mud	23.012	

Percentiles	phi	mm
95%	-2.803	6.980
84%	-1.331	2.516
75%	0.007	0.995
50%	2.532	0.173
25%	4.251	0.053
16%	5.129	0.029
5%	5.650	0.020

Folks' Graphic Stats	phi	mm
Mean (Mz)	2.110	0.232
Sorting (SI)	2.896	
Mode	5.000	
Skewness(Sk)	0.229	

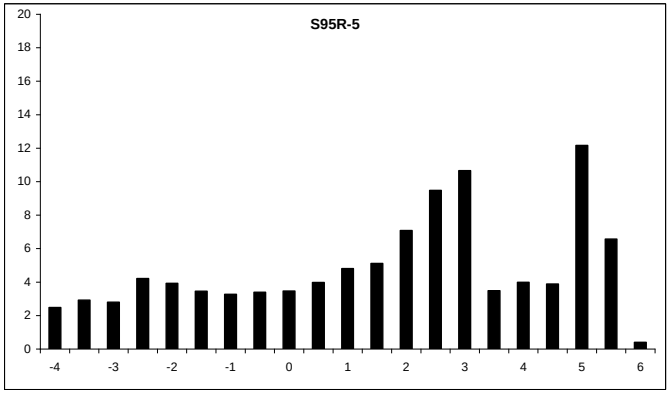

Sample Number: **N95R-1** **1995R**

Total sample weight: 784

Sieve Phi	Sieve mm	weight retained (g)	>2 mm (g)	Wt. %	Cu. Wt. %
-4.0	16.000	33.800		4.311	1.000
-3.5	11.314	72.800		9.286	0.957
-3.0	8.000	103.840		13.245	0.864
-2.5	5.657	72.640		9.265	0.732
-2.0	4.000	53.780		6.860	0.639
-1.5	2.828	40.070		5.111	0.570
-1.0	2.000	33.700		4.298	0.519
-0.5	1.414	27.050		3.450	0.476
0.0	1.000	29.200		3.724	0.442
0.5	0.707	42.370		5.404	0.404
1.0	0.500	35.320		4.505	0.350
1.5	0.354	31.460		4.013	0.305
2.0	0.250	31.850	31.927	4.072	0.265
2.5	0.177	29.450	30.647	3.909	0.225
3.0	0.125	38.950	42.676	5.443	0.185
3.5	0.088	107.720	6.638	0.847	0.131
4.0	0.063		8.340	1.064	0.123
4.5	0.044		10.324	1.317	0.112
5.0	0.031		11.022	1.406	0.099
5.5	0.022		42.424	5.411	0.085
6.0	0.016		22.648	2.889	0.031
6.5	0.011		1.326	0.169	0.002
			% mud	11.192	

Percentiles	phi	mm
95%	-3.463	11.027
84%	-2.909	7.512
75%	-2.570	5.936
50%	-0.776	1.713
25%	2.187	0.220
16%	3.234	0.106
5%	5.821	0.018

Folks' Graphic Stats	phi	mm
Mean (Mz)	-0.151	1.110
Sorting (SI)	2.942	
mode	-3.000	
Skewness(Sk)	-0.363	

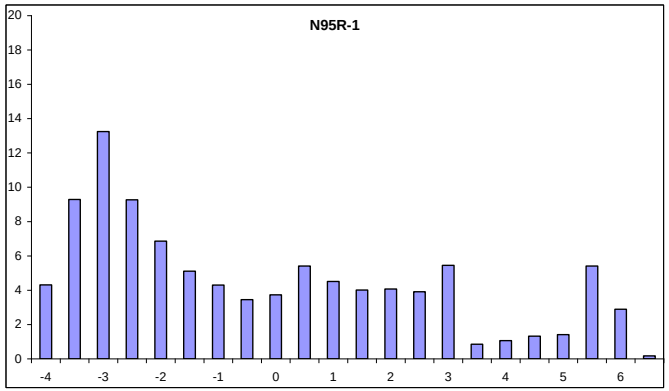

Fig. A.2.1 cont.

Sample Number: **N95R-3** **1995R**

Total sample weight: 769

Sieve Phi	Sieve mm	weight retained (g)	>2 mm (g)	Wt. %	Cu. Wt. %
-4.0	16.000	0.000		0.000	0.957
-3.5	11.314	26.290		3.419	0.957
-3.0	8.000	64.040		8.328	0.922
-2.5	5.657	56.800		7.386	0.839
-2.0	4.000	61.820		8.039	0.765
-1.5	2.828	68.390		8.893	0.685
-1.0	2.000	55.830		7.260	0.596
-0.5	1.414	48.870		6.355	0.523
0.0	1.000	42.690		5.551	0.460
0.5	0.707	43.620		5.672	0.404
1.0	0.500	48.010		6.243	0.348
1.5	0.354	42.360		5.508	0.285
2.0	0.250	55.620	55.884	7.267	0.230
2.5	0.177	35.800	38.299	4.980	0.157
3.0	0.125	27.030	33.015	4.293	0.108
3.5	0.088	58.291	8.517	1.108	0.065
4.0	0.063		8.078	1.050	0.054
4.5	0.044		6.863	0.892	0.043
5.0	0.031		4.843	0.630	0.034
5.5	0.022		13.444	1.748	0.028
6.0	0.016		7.667	0.997	0.010
6.5	0.011		0.332	0.043	0.000
			% mud	4.311	

Percentiles

	phi	mm
95%	-3.403	10.577
84%	-2.505	5.676
75%	-1.905	3.744
50%	-0.316	1.245
25%	1.819	0.283
16%	2.482	0.179
5%	4.172	0.055

Folks' Graphic Stats

	phi	mm
Mean (Mz)	-0.113	1.081
Sorting (SI)	2.394	
Mode	-1.500	
Skewness(Sk)	-0.154	

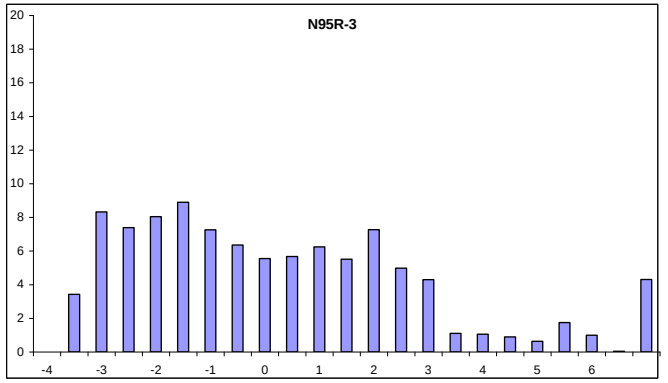

Sample Number: **N95R-4** **1995R**

Total sample weight: 677.49

Sieve Phi	Sieve mm	weight retained (g)	>2 mm (g)	Wt. %	Cu. Wt. %
-4.0	16.000	0.000		0.000	
-3.5	11.314	23.080		3.407	1.000
-3.0	8.000	29.400		4.340	0.966
-2.5	5.657	40.160		5.928	0.923
-2.0	4.000	44.140		6.515	0.863
-1.5	2.828	38.510		5.684	0.798
-1.0	2.000	40.350		5.956	0.741
-0.5	1.414	50.340		7.430	0.682
0.0	1.000	50.610		7.470	0.607
0.5	0.707	56.470		8.335	0.533
1.0	0.500	51.670		7.627	0.449
1.5	0.354	37.800		5.579	0.373
2.0	0.250	30.600	30.985	4.574	0.317
2.5	0.177	25.040	29.864	4.408	0.272
3.0	0.125	21.280	32.873	4.852	0.227
3.5	0.088	138.040	16.559	2.444	0.179
4.0	0.063		16.204	2.392	0.155
4.5	0.044		15.026	2.218	0.131
5.0	0.031		12.295	1.815	0.108
5.5	0.022		39.004	5.757	0.090
6.0	0.016		21.026	3.104	0.033
6.5	0.011		1.125	0.166	0.002
			% mud	13.059	

Percentiles

	phi	mm
95%	-2.816	7.044
84%	-1.821	3.534
75%	-1.077	2.109
50%	0.696	0.617
25%	2.744	0.149
16%	3.888	0.068
5%	5.850	0.017

Folks' Graphic Stats

	phi	mm
Mean (Mz)	0.921	0.528
Sorting (SI)	2.740	
Mode	0.500	
Skewness(Sk)	-0.154	

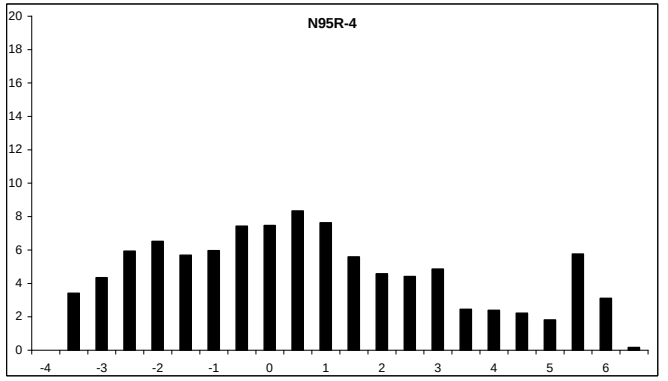

Fig. A.2.1 cont.

Sample Number: **S95R-1** **1995R**

Total sample weight: 670.5

Sieve Phi	Sieve mm	weight retained (g)	>2 mm (g)	Wt. %	Cu. Wt. %
-4.0	16.000	8.540		1.274	1.000
-3.5	11.314	0.000		0.000	0.987
-3.0	8.000	3.170		0.473	0.987
-2.5	5.657	3.500		0.522	0.983
-2.0	4.000	3.990		0.595	0.977
-1.5	2.828	12.590		1.878	0.971
-1.0	2.000	21.440		3.198	0.953
-0.5	1.414	40.400		6.025	0.921
0.0	1.000	65.620		9.787	0.860
0.5	0.707	90.700		13.527	0.762
1.0	0.500	107.300		16.003	0.627
1.5	0.354	95.800		14.288	0.467
2.0	0.250	75.900		11.320	0.324
2.5	0.177	50.200	52.320	7.803	0.211
3.0	0.125	30.000	35.540	5.300	0.133
3.5	0.088	61.350	6.939	1.035	0.080
4.0	0.063		6.133	0.915	0.070
4.5	0.044		5.657	0.844	0.061
5.0	0.031		5.077	0.757	0.052
5.5	0.022		18.096	2.699	0.045
6.0	0.016		11.116	1.658	0.018
6.5	0.011		0.672	0.100	0.001
			% mud	6.058	

Percentiles

	phi	mm
95%	-0.960	1.945
84%	0.104	0.930
75%	0.546	0.685
50%	1.397	0.380
25%	2.328	0.199
16%	2.828	0.141
5%	5.142	0.028

Folks' Graphic Stats

	phi	mm
Mean (Mz)	1.443	0.368
Sorting (SI)	1.605	
Mode	1.000	
Skewness(Sk)	-0.139	

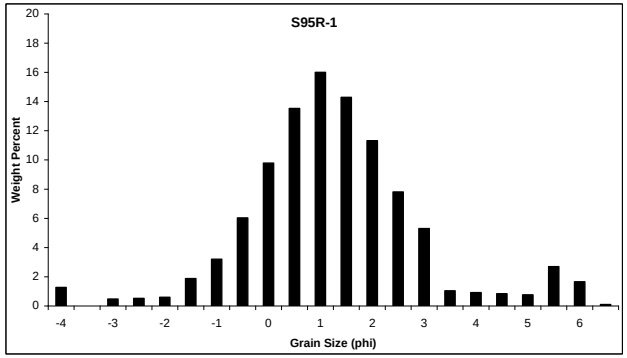

1999

Sample Number: **N99-1** **1999**

Total sample weight: 1312.995

Sieve Phi	Sieve mm	weight retained (g)	>2 mm (g)	Wt. %	Cu. Wt. %
-4.0	16.000	0.000		0.000	
-3.5	11.314	0.000		0.000	0.965
-3.0	8.000	11.000		0.838	0.965
-2.5	5.657	6.600		0.503	0.956
-2.0	4.000	11.200		0.853	0.951
-1.5	2.828	21.400		1.630	0.943
-1.0	2.000	27.900		2.125	0.927
-0.5	1.414	187.490		14.280	0.905
0.0	1.000	147.700	151.528	11.541	0.763
0.5	0.707	173.550	176.058	13.409	0.647
1.0	0.500	69.000	70.690	5.384	0.513
1.5	0.354	135.700	136.398	10.388	0.459
2.0	0.250	112.840	112.884	8.597	0.355
2.5	0.177	50.130	50.279	3.829	0.269
3.0	0.125	46.900	48.200	3.671	0.231
3.5	0.088	24.300	27.792	2.117	0.194
4.0	0.063	123.140	128.900	9.817	0.173
4.5	0.044	145.474	8.479	0.646	0.075
5.0	0.031		9.749	0.742	0.069
5.5	0.022		38.842	2.958	0.061
6.0	0.016		24.403	1.859	0.032
6.5	0.011		1.585	0.121	0.013
7.0	0.008		15.401	1.173	0.012
			% mud	6.853	

Percentiles

	phi	mm
95%	-1.861	3.633
84%	1.037	0.487
75%	0.044	0.970
50%	1.049	0.483
25%	2.612	0.164
16%	4.311	0.050
5%	6.248	0.013

Folks' Graphic Stats

	phi	mm
Mean (Mz)	2.132	0.228
Sorting (SI)	2.047	
Mode	-0.750	
Skewness(Sk)	-0.638	

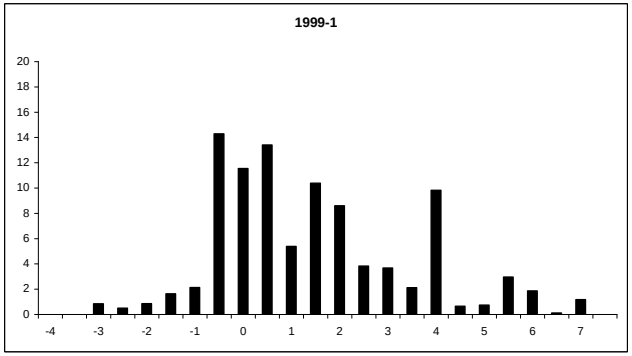

Fig. A.2.1 cont.

Sample Number: **N95R-2** **1999**

Total sample weight: 588.4

Sieve Phi	Sieve mm	weight retained (g)	>2 mm (g)	Wt. %	Cu. Wt. %
-4.0	16.000	14.040		2.386	1.000
-3.5	11.314	82.290		13.985	0.976
-3.0	8.000	56.280		9.565	0.836
-2.5	5.657	46.770		7.949	0.741
-2.0	4.000	38.970		6.623	0.661
-1.5	2.828	26.900		4.572	0.595
-1.0	2.000	24.600		4.181	0.549
-0.5	1.414	18.620		3.165	0.507
0.0	1.000	23.080		3.923	0.476
0.5	0.707	20.150		3.425	0.437
1.0	0.500	19.000		3.229	0.402
1.5	0.354	21.800		3.705	0.370
2.0	0.250	22.900	23.249	3.951	0.333
2.5	0.177	24.170	28.539	4.850	0.293
3.0	0.125	23.800	34.300	5.829	0.245
3.5	0.088	125.030	14.998	2.549	0.187
4.0	0.063		14.677	2.494	0.161
4.5	0.044		13.610	2.313	0.136
5.0	0.031		11.136	1.893	0.113
5.5	0.022		35.328	6.004	0.094
6.0	0.016		19.045	3.237	0.034
6.5	0.011		1.019	0.173	0.002
			% mud	13.619	

Percentiles

	phi	mm
95%	-3.407	10.604
84%	-3.013	8.074
75%	-2.549	5.852
50%	-0.383	1.304
25%	2.948	0.130
16%	4.023	0.062
5%	5.868	0.017

Folks' Graphic Stats

	phi	mm
Mean (Mz)	0.209	0.865
Sorting (SI)	3.164	
Mode	-3.500	
Skewness(Sk)	-0.300	

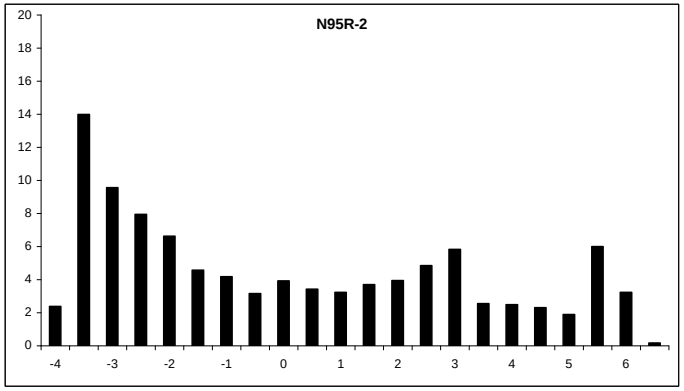

Sample Number: **N95R-5** **1999**

Total sample weight: 752.4

Sieve Phi	Sieve mm	weight retained (g)	>2 mm (g)	Wt. %	Cu. Wt. %
-4.0	16.000	131.600		17.491	0.808
-3.5	11.314	48.100		6.393	0.633
-3.0	8.000	55.200		7.337	0.569
-2.5	5.657	29.700		3.947	0.495
-2.0	4.000	28.700		3.814	0.456
-1.5	2.828	25.300		3.363	0.418
-1.0	2.000	24.100		3.203	0.384
-0.5	1.414	21.100		2.804	0.352
0.0	1.000	20.800		2.764	0.324
0.5	0.707	25.700		3.416	0.296
1.0	0.500	32.100		4.266	0.262
1.5	0.354	31.800		4.226	0.220
2.0	0.250	30.800		4.094	0.177
2.5	0.177	28.700		3.814	0.136
3.0	0.125	18.400		2.446	0.098
3.5	0.088	55.500		7.376	0.074
4.0	0.063				
4.5	0.044				
5.0	0.031				
5.5	0.022				
6.0	0.016				
6.5	0.011				

Percentiles

	phi	mm
95%	-4.370	20.679
84%	-4.084	16.963
75%	-3.835	14.276
50%	-2.532	5.783
25%	1.143	0.453
16%	2.211	0.216
5%	3.661	0.079

Folks' Graphic Stats

	phi	mm
Mean (Mz)	-1.468	2.767
Sorting (SI)	2.791	
Mode	-4.000	
Skewness(Sk)	-0.524	

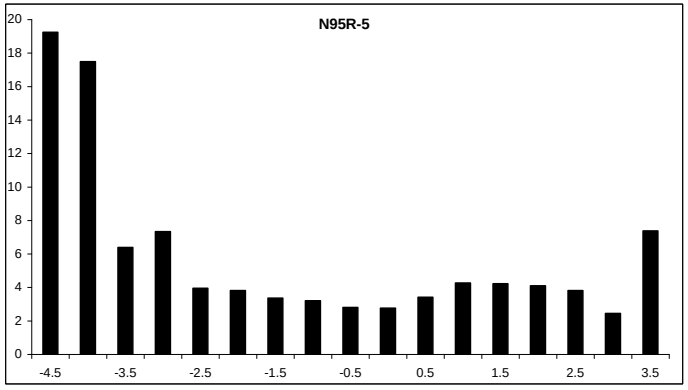

Fig. A.2.1 cont.

Sample Number: S95R-2 1999

Total sample weight: 823.97

Sieve Phi	Sieve mm	weight retained (g)	>2 mm (g)	Wt. %	Cu. Wt. %
-4	16.000	50.000		6.068	1.065
-3.5	11.314	81.850		9.934	1.004
-3	8.000	99.510		**12.077**	0.905
-2.5	5.657	60.110		7.295	0.784
-2	4.000	59.210		7.186	0.711
-1.5	2.828	43.320		5.257	0.640
-1	2.000	37.810		4.589	0.587
-0.5	1.414	34.390		4.174	0.541
0	1.000	29.540		3.585	0.499
0.5	0.707	53.100		6.444	0.464
1	0.500	43.000		5.219	0.399
1.5	0.354	59.200		7.185	0.347
2	0.250	57.070	57.462	6.974	0.275
2.5	0.177	53.260	55.761	6.767	0.205
3	0.125	38.090	43.765	5.311	0.138
3.5	0.088	78.000	7.936	0.963	0.085
4	0.063		7.674	0.931	0.075
4.5	0.044		7.220	0.876	0.066
5	0.031		6.303	0.765	0.057
5.5	0.022		24.324	2.952	0.049
6	0.016		15.381	1.867	0.020
6.5	0.011		0.795	0.096	0.001
			% mud	6.556	

Percentiles

	phi	mm
95%	-3.226	9.355
84%	-2.730	6.636
75%	-2.264	4.805
50%	-0.008	1.005
25%	2.179	0.221
16%	2.835	0.140
5%	5.445	0.023

Folks' Graphic Stats

	phi	mm
Mean (Mz)	0.032	0.978
Sorting (SI)	2.705	
Mode	-3.000	
Skewness(Sk)	-0.140	

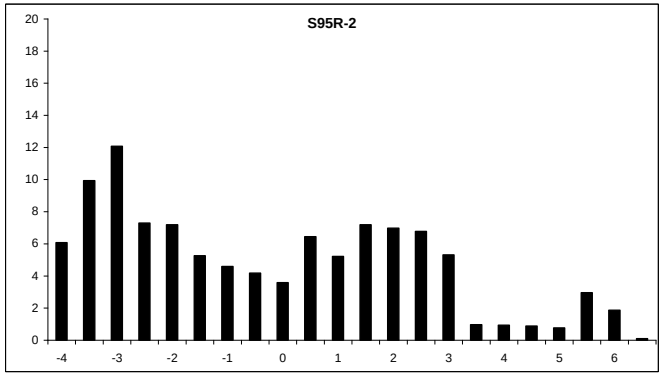

Sample Number: S95R-4 1999

Total sample weight: 559.1

Sieve Phi	Sieve mm	weight retained (g)	>2 mm (g)	Wt. %	Cu. Wt. %
-4.0	16.000	27.350		4.892	1.201
-3.5	11.314	56.180		10.048	1.152
-3.0	8.000	91.920		16.441	1.052
-2.5	5.657	73.720		13.185	0.888
-2.0	4.000	53.700		9.605	0.756
-1.5	2.828	36.520		6.532	0.660
-1.0	2.000	28.370		5.074	0.594
-0.5	1.414	23.000		4.114	0.544
0.0	1.000	23.380		4.182	0.502
0.5	0.707	22.400		4.006	0.461
1.0	0.500	26.000		4.650	0.421
1.5	0.354	23.100		4.132	0.374
2.0	0.250	23.110	23.260	4.160	0.333
2.5	0.177	21.320	22.647	4.051	0.291
3.0	0.125	21.100	24.521	4.386	0.251
3.5	0.088	120.314	6.149	1.100	0.207
4.0	0.063		8.749	1.565	0.196
4.5	0.044		12.708	2.273	0.180
5.0	0.031		14.837	2.654	0.157
5.5	0.022		49.486	8.851	0.131
6.0	0.016		22.621	4.046	0.042
6.5	0.011		1.062	0.190	0.002
			% mud	18.014	

Percentiles

	phi	mm
95%	-2.690	6.453
84%	-2.320	4.992
75%	-1.970	3.919
50%	0.029	0.980
25%	3.007	0.124
16%	4.943	0.033
5%	5.957	0.016

Folks' Graphic Stats

	phi	mm
Mean (Mz)	0.884	0.542
Sorting (SI)	3.126	
Mode	-3.000	
Skewness(Sk)	-0.362	

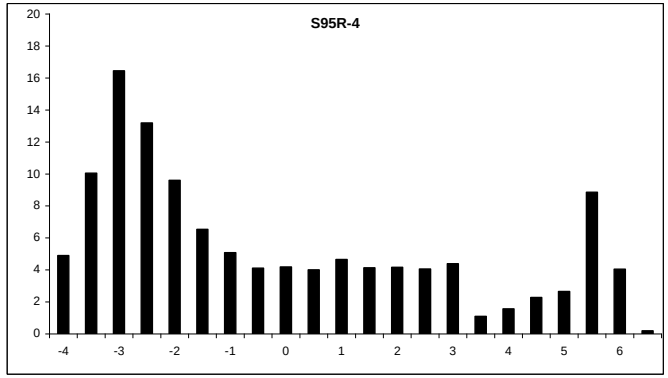

Fig. A.2.1 cont.
2007L

Sample Number: **N07-1** **2007L**

Total sample weight: 803.81

Sieve Phi	Sieve mm	weight retained (g)	>2 mm (g)	Wt. %	Cu. Wt. %
-4.0	16.000	151.890		18.896	0.979
-3.5	11.314	138.450		17.224	0.790
-3.0	8.000	128.840		16.029	0.618
-2.5	5.657	102.420		12.742	0.457
-2.0	4.000	51.160		6.365	0.330
-1.5	2.828	36.780		4.576	0.266
-1.0	2.000	28.940		3.600	0.221
-0.5	1.414	20.900		2.600	0.185
0.0	1.000	17.500		2.177	0.159
0.5	0.707	15.400		1.916	0.137
1.0	0.500	16.300		2.028	0.118
1.5	0.354	12.300		1.530	0.097
2.0	0.250	10.100	10.204	1.269	0.082
2.5	0.177	8.800	9.392	1.168	0.069
3.0	0.125	8.700	10.009	1.245	0.058
3.5	0.088	38.179	1.939	0.241	0.045
4.0	0.063		2.249	0.280	0.043
4.5	0.044		2.875	0.358	0.040
5.0	0.031		3.365	0.419	0.036
5.5	0.022		15.167	1.887	0.032
6.0	0.016		10.318	1.284	0.013
6.5	0.011		0.461	0.057	0.001
			% mud	4.004	

Percentiles

	phi	mm
95%	-3.923	15.174
84%	-3.632	12.401
75%	-3.384	10.440
50%	-2.633	6.202
25%	-1.321	2.499
16%	-0.027	1.019
5%	3.309	0.101

Folks' Graphic Stats

	phi	mm
Mean (Mz)	-2.097	4.279
Sorting (SI)	1.997	
Mode	-4.000	
Skewness(Sk)	-0.544	

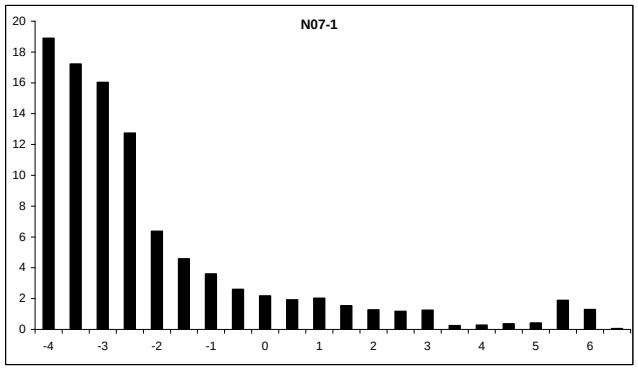

Sample Number: **N07-2** **2007L**

Total sample weight: 572.4

Sieve Phi	Sieve mm	weight retained (g)	>2 mm (g)	Wt. %	Cu. Wt. %
-4.0	16.000	67.600		11.810	0.951
-3.5	11.314	55.500		9.696	0.833
-3.0	8.000	58.100		10.150	0.736
-2.5	5.657	58.800		10.273	0.635
-2.0	4.000	20.500		3.581	0.532
-1.5	2.828	20.000		3.494	0.496
-1.0	2.000	12.500		2.184	0.461
-0.5	1.414	8.300		1.450	0.439
0.0	1.000	6.500		1.136	0.425
0.5	0.707	6.400		1.118	0.414
1.0	0.500	8.600		1.502	0.402
1.5	0.354	9.800		1.712	0.387
2.0	0.250	14.100	14.258	2.491	0.370
2.5	0.177	23.400	25.591	4.471	0.345
3.0	0.125	35.900	42.507	7.426	0.301
3.5	0.088	138.369	10.884	1.902	0.226
4.0	0.063		12.105	2.115	0.207
4.5	0.044		13.196	2.305	0.186
5.0	0.031		12.924	2.258	0.163
5.5	0.022		49.307	8.614	0.141
6.0	0.016		30.255	5.286	0.055
6.5	0.011		0.942	0.165	0.002
			% mud	18.628	

Percentiles

	phi	mm
95%	-3.994	15.935
84%	-3.528	11.539
75%	-3.071	8.401
50%	-1.552	2.932
25%	3.341	0.099
16%	5.071	0.030
5%	6.043	0.015

Folks' Graphic Stats

	phi	mm
Mean (Mz)	-0.003	1.002
Sorting (SI)	3.671	
Mode	-2.500	
Skewness(Sk)	-0.527	

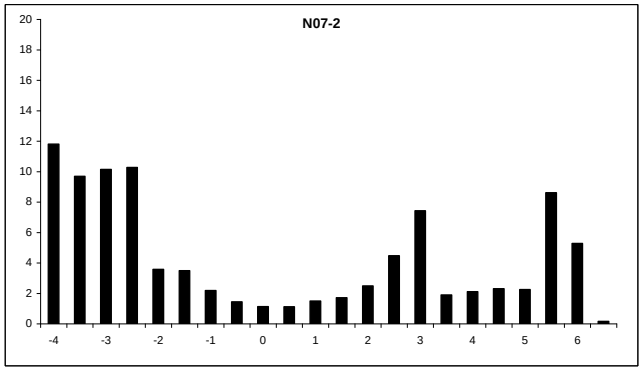

Fig. A.2.1 cont.

Sample Number: **N07-3** **2007L**

Total sample weight: 663.9

Sieve Phi	Sieve mm	weight retained (g)	>2 mm (g)	Wt. %	Cu. Wt. %
-4.0	16.000	50.050		7.539	1.000
-3.5	11.314	15.100		2.274	0.925
-3.0	8.000	35.580		5.359	0.902
-2.5	5.657	37.410		5.635	0.848
-2.0	4.000	43.700		6.582	0.792
-1.5	2.828	43.840		6.603	0.726
-1.0	2.000	41.990		6.325	0.660
-0.5	1.414	34.420		5.185	0.597
0.0	1.000	29.740		4.480	0.545
0.5	0.707	30.750		4.632	0.500
1.0	0.500	39.860		6.004	0.454
1.5	0.354	38.910		5.861	0.394
2.0	0.250	40.020	40.139	6.046	0.335
2.5	0.177	36.800	38.185	5.752	0.275
3.0	0.125	29.240	32.905	4.956	0.217
3.5	0.088	116.490	5.754	0.867	0.168
4.0	0.063		6.655	1.002	0.159
4.5	0.044		8.193	1.234	0.149
5.0	0.031		9.379	1.413	0.137
5.5	0.022		46.648	7.026	0.123
6.0	0.016		33.138	4.991	0.052
6.5	0.011		1.554	0.234	0.002
			% mud	14.899	

Percentiles	phi	mm
95%	-3.668	12.714
84%	-2.427	5.376
75%	-1.682	3.208
50%	0.502	0.706
25%	2.715	0.152
16%	3.943	0.065
5%	6.023	0.015

Folks' Graphic Stats	phi	mm
Mean (Mz)	0.673	0.627
Sorting (SI)	3.061	
Mode	-2.000	
Skewness(Sk)	-0.110	

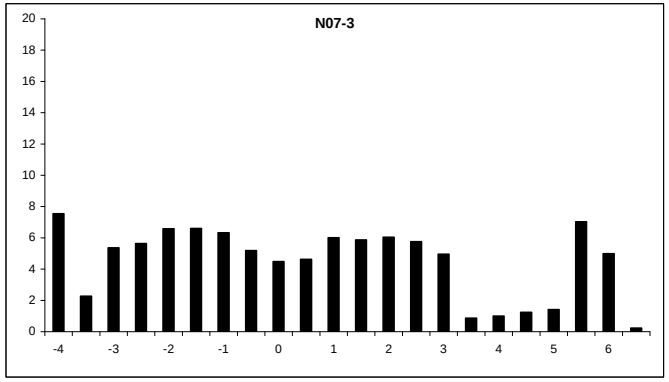

Sample Number: **N07-4a** **2007L**

Total sample weight: 426.3

Sieve Phi	Sieve mm	weight retained (g)	>2 mm (g)	Wt. %	Cu. Wt. %
-4.0	16.000	26.620		6.244	1.012
-3.5	11.314	22.470		5.271	0.950
-3.0	8.000	24.020		5.635	0.897
-2.5	5.657	21.820		5.118	0.841
-2.0	4.000	24.280		5.696	0.790
-1.5	2.828	21.900		5.137	0.733
-1.0	2.000	22.380		5.250	0.681
-0.5	1.414	22.210		5.210	0.629
0.0	1.000	21.930		5.144	0.577
0.5	0.707	24.000		5.630	0.525
1.0	0.500	25.300		5.935	0.469
1.5	0.354	23.100		5.419	0.410
2.0	0.250	18.400	18.423	4.322	0.356
2.5	0.177	15.420	15.750	3.695	0.312
3.0	0.125	12.900	14.088	3.305	0.275
3.5	0.088	104.665	2.699	0.633	0.242
4.0	0.063		4.510	1.058	0.236
4.5	0.044		7.397	1.735	0.225
5.0	0.031		9.772	2.292	0.208
5.5	0.022		49.547	11.623	0.185
6.0	0.016		28.796	6.755	0.069
6.5	0.011		0.602	0.141	0.001
			% mud	22.546	

Percentiles	phi	mm
95%	-3.500	11.312
84%	-2.491	5.620
75%	-1.651	3.140
50%	0.726	0.605
25%	3.385	0.096
16%	5.608	0.020
5%	6.140	0.014

Folks' Graphic Stats	phi	mm
Mean (Mz)	1.281	0.411
Sorting (SI)	3.485	
Mode	5.500	
Skewness(Sk)	-0.165	

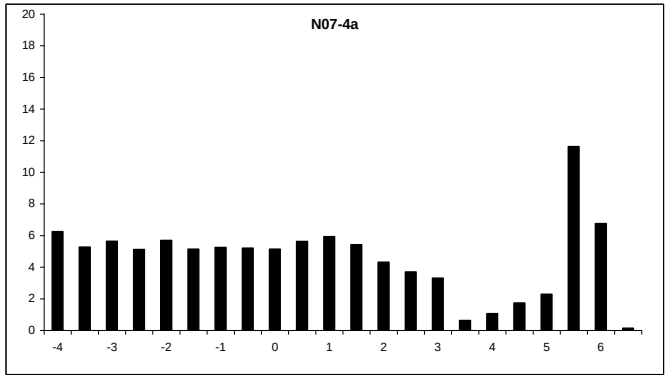

Fig. A.2.1 cont.

Sample Number: **N07-4b** **2007L**

Total sample weight: 770

Sieve Phi	Sieve mm	weight retained (g)	>2 mm (g)	Wt. %	Cu. Wt. %
-4.0	16.000	78.360		10.177	0.986
-3.5	11.314	25.120		3.262	0.884
-3.0	8.000	54.950		7.136	0.852
-2.5	5.657	37.660		4.891	0.781
-2.0	4.000	40.190		5.219	0.732
-1.5	2.828	35.020		4.548	0.679
-1.0	2.000	39.260		5.099	0.634
-0.5	1.414	43.880		5.699	0.583
0.0	1.000	51.500		6.688	0.526
0.5	0.707	52.960		6.878	0.459
1.0	0.500	53.880		6.997	0.390
1.5	0.354	46.580		6.049	0.320
2.0	0.250	41.190	41.443	5.382	0.260
2.5	0.177	33.820	36.044	4.681	0.206
3.0	0.125	25.090	30.690	3.986	0.159
3.5	0.088	99.762	8.117	1.054	0.119
4.0	0.063		7.952	1.033	0.109
4.5	0.044		7.762	1.008	0.098
5.0	0.031		7.370	0.957	0.088
5.5	0.022		34.300	4.455	0.079
6.0	0.016		25.540	3.317	0.034
6.5	0.011		0.844	0.110	0.001
			% mud	9.846	

Percentiles

	phi	mm
95%	-3.822	14.141
84%	-2.917	7.552
75%	-2.188	4.557
50%	0.194	0.874
25%	2.091	0.235
16%	2.991	0.126
5%	5.823	0.018

Folks' Graphic Stats

	phi	mm
Mean (Mz)	0.090	0.940
Sorting (SI)	2.938	
Mode	1.000	
Skewness(Sk)	-0.057	

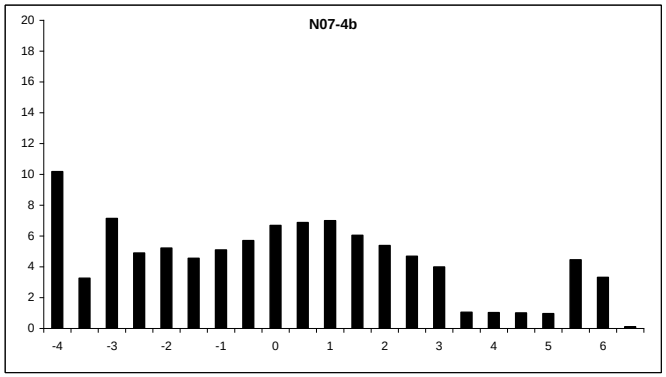

Sample Number: **N07-5** **2007L**

Total sample weight: 728.3

Sieve Phi	Sieve mm	weight retained (g)	>2 mm (g)	Wt. %	Cu. Wt. %
-4.0	16.000	15.400		2.115	1.001
-3.5	11.314	10.900		1.497	0.980
-3.0	8.000	23.100		3.172	0.965
-2.5	5.657	33.500		4.600	0.934
-2.0	4.000	49.000		6.728	0.888
-1.5	2.828	64.200		8.815	0.820
-1.0	2.000	73.400		10.078	0.732
-0.5	1.414	70.000		9.611	0.631
0.0	1.000	61.800		8.486	0.535
0.5	0.707	54.100		7.428	0.450
1.0	0.500	51.200		7.030	0.376
1.5	0.354	39.700		5.451	0.306
2.0	0.250	32.400	32.825	4.507	0.251
2.5	0.177	26.400	29.433	4.041	0.206
3.0	0.125	21.900	28.693	3.940	0.166
3.5	0.088	102.096	9.546	1.311	0.126
4.0	0.063		9.562	1.313	0.113
4.5	0.044		9.565	1.313	0.100
5.0	0.031		8.778	1.205	0.087
5.5	0.022		33.042	4.537	0.075
6.0	0.016		20.579	2.826	0.030
6.5	0.011		0.973	0.134	0.001
			% mud	10.015	

Percentiles

	phi	mm
95%	-2.760	6.772
84%	-1.647	3.131
75%	-1.101	2.146
50%	0.207	0.866
25%	2.014	0.248
16%	3.073	0.119
5%	5.775	0.018

Folks' Graphic Stats

	phi	mm
Mean (Mz)	0.545	0.686
Sorting (SI)	2.473	
Mode	-1.250	
Skewness(Sk)	-0.260	

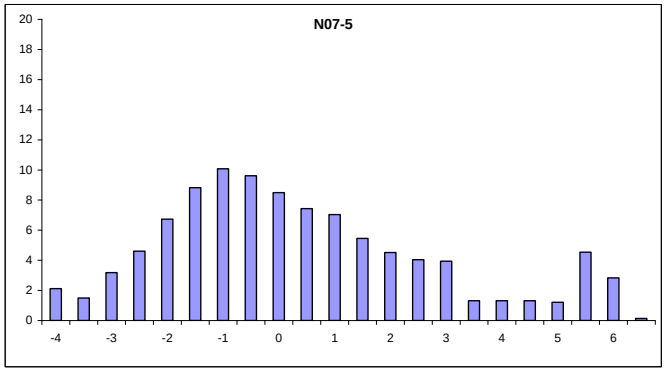

Fig. A.2.1 cont.

Sample Number: **N07-6** **2007L**

Total sample weight: 609.7955

Sieve Phi	Sieve mm	weight retained (g)	>2 mm (g)	Wt. %	Cu. Wt. %
-4.0	16.000	63.100		10.348	0.989
-3.5	11.314	61.680		10.115	0.885
-3.0	8.000	57.230		9.385	0.784
-2.5	5.657	37.260		6.110	0.690
-2.0	4.000	41.170		6.751	0.629
-1.5	2.828	44.750		7.339	0.562
-1.0	2.000	42.540		6.976	0.488
-0.5	1.414	39.480		6.474	0.419
0.0	1.000	34.260		5.618	0.354
0.5	0.707	32.460		5.323	0.298
1.0	0.500	36.290		5.951	0.244
1.5	0.354	29.700		4.870	0.185
2.0	0.250	24.100	24.294	3.984	0.136
2.5	0.177	17.200	18.445	3.025	0.096
3.0	0.125	11.340	13.956	2.289	0.066
3.5	0.088	30.263	3.419	0.561	0.043
4.0	0.063		3.101	0.509	0.038
4.5	0.044		2.738	0.449	0.033
5.0	0.031		2.289	0.375	0.028
5.5	0.022		8.619	1.413	0.024
6.0	0.016		5.950	0.976	0.010
6.5	0.011		0.290	0.048	0.000
			% mud	3.261	

Percentiles

	phi	mm
95%	-3.812	14.046
84%	-3.275	9.683
75%	-2.817	7.049
50%	-1.079	2.112
25%	0.948	0.518
16%	1.756	0.296
5%	3.354	0.098

Folks' Graphic Stats

	phi	mm
Mean (Mz)	-0.866	1.823
Sorting (SI)	2.344	
Mode	-1.750	
Skewness(Sk)	-0.182	

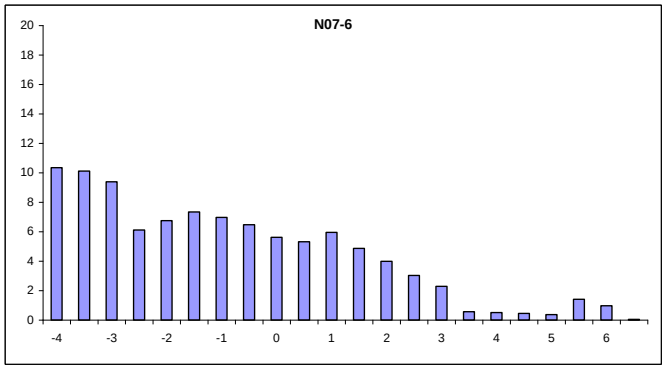

Sample Number: **S07-1** **2007L**

Total sample weight: 674.58

Sieve Phi	Sieve mm	weight retained (g)	>2 mm (g)	Wt. %	Cu. Wt. %
-4.0	16.000	82.700		12.259	1.013
-3.5	11.314	79.600		11.800	0.891
-3.0	8.000	112.100		16.618	0.773
-2.5	5.657	106.700		15.817	0.607
-2.0	4.000	72.800		10.792	0.448
-1.5	2.828	41.000		6.078	0.340
-1.0	2.000	22.700		3.365	0.280
-0.5	1.414	15.500		2.298	0.246
0.0	1.000	13.100		1.942	0.223
0.5	0.707	12.580		1.865	0.204
1.0	0.500	13.770		2.041	0.185
1.5	0.354	11.980		1.776	0.165
2.0	0.250	10.930	11.000	1.631	0.147
2.5	0.177	10.070	10.696	1.586	0.131
3.0	0.125	8.450	9.783	1.450	0.115
3.5	0.088	69.404	2.047	0.303	0.100
4.0	0.063		2.791	0.414	0.097
4.5	0.044		4.395	0.652	0.093
5.0	0.031		6.023	0.893	0.086
5.5	0.022		31.619	4.687	0.078
6.0	0.016		19.949	2.957	0.031
6.5	0.011		0.750	0.111	0.001
			% mud	9.300	

Percentiles

	phi	mm
95%	-3.742	13.377
84%	-3.285	9.747
75%	-2.932	7.629
50%	-2.163	4.479
25%	-0.559	1.473
16%	1.629	0.323
5%	5.794	0.018

Folks' Graphic Stats

	phi	mm
Mean (Mz)	-1.273	2.416
Sorting (SI)	2.673	
Mode	-3.000	
Skewness(Sk)	-0.606	

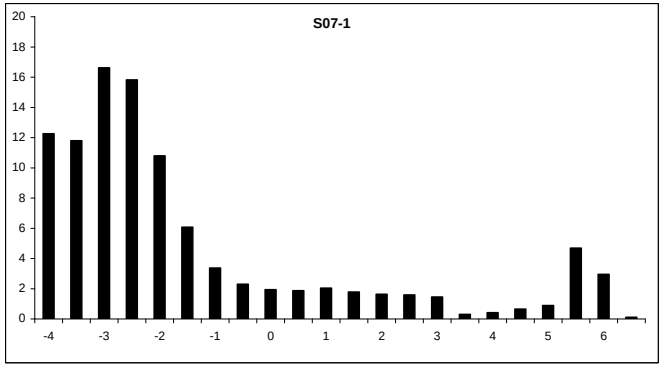

Fig. A.2.1 cont.

Sample Number: S07-2 2007L

Total sample weight: 799.9

Sieve Phi	Sieve mm	weight retained (g)	>2 mm (g)	Wt. %	Cu. Wt. %
-4.0	16.000	202.800		25.353	0.998
-3.5	11.314	80.800		10.101	0.745
-3.0	8.000	85.000		10.626	0.644
-2.5	5.657	52.900		6.613	0.537
-2.0	4.000	49.000		6.126	0.471
-1.5	2.828	35.900		4.488	0.410
-1.0	2.000	28.800		3.600	0.365
-0.5	1.414	24.200		3.025	0.329
0.0	1.000	23.200		2.900	0.299
0.5	0.707	24.200		3.025	0.270
1.0	0.500	27.300		3.413	0.240
1.5	0.354	23.500		2.938	0.205
2.0	0.250	23.200	23.445	2.931	0.176
2.5	0.177	23.600	24.931	3.117	0.147
3.0	0.125	20.300	23.204	2.901	0.116
3.5	0.088	73.492	4.089	0.511	0.087
4.0	0.063		4.237	0.530	0.081
4.5	0.044		4.668	0.584	0.076
5.0	0.031		5.013	0.627	0.070
5.5	0.022		27.556	3.445	0.064
6.0	0.016		22.914	2.865	0.030
6.5	0.011		0.735	0.092	0.001
		% mud		7.612	

Percentiles

	phi	mm
95%	-3.905	14.981
84%	-3.688	12.890
75%	-3.511	11.398
50%	-2.218	4.652
25%	0.827	0.564
16%	2.273	0.207
5%	5.703	0.019

Folks' Graphic Stats

	phi	mm
Mean (Mz)	-1.211	2.315
Sorting (SI)	2.946	
Mode	-4.000	
Skewness(Sk)	-0.578	

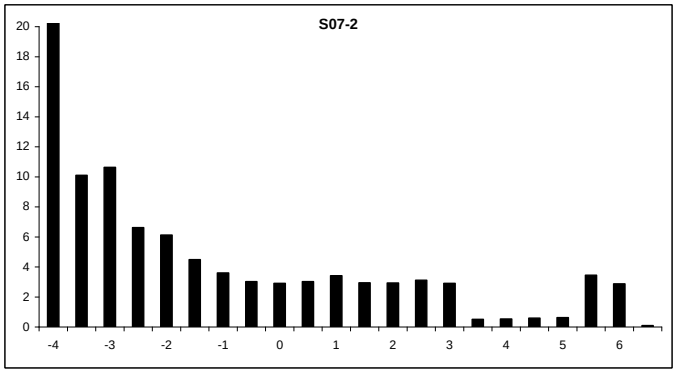

Sample Number: S07-3 2007L

Total sample weight: 684.6

Sieve Phi	Sieve mm	weight retained (g)	>2 mm (g)	Wt. %	Cu. Wt. %
-4.0	16.000	192.600		28.133	1.000
-3.5	11.314	116.100		16.959	0.719
-3.0	8.000	116.600		17.032	0.549
-2.5	5.657	44.300		6.471	0.379
-2.0	4.000	38.500		5.624	0.314
-1.5	2.828	36.600		5.346	0.258
-1.0	2.000	26.200		3.827	0.204
-0.5	1.414	18.200		2.658	0.166
0.0	1.000	13.400		1.957	0.139
0.5	0.707	11.100		1.621	0.120
1.0	0.500	11.900		1.738	0.104
1.5	0.354	10.700		1.563	0.086
2.0	0.250	9.900	9.980	1.458	0.071
2.5	0.177	7.900	8.900	1.300	0.056
3.0	0.125	6.000	8.498	1.241	0.043
3.5	0.088	24.600	3.787	0.553	0.031
4.0	0.063		3.917	0.572	0.025
4.5	0.044		3.643	0.532	0.019
5.0	0.031		2.639	0.385	0.014
5.5	0.022		4.948	0.723	0.010
6.0	0.016		2.023	0.295	0.003
6.5	0.011		0.065	0.010	0.000
		% mud		1.945	

Percentiles

	phi	mm
95%	-3.911	15.044
84%	-3.716	13.138
75%	-3.556	11.759
50%	-2.856	7.240
25%	-1.427	2.689
16%	-0.386	1.306
5%	2.735	0.150

Folks' Graphic Stats

	phi	mm
Mean (Mz)	-2.319	4.990
Sorting (SI)	1.840	
Mode	-4.000	
Skewness(Sk)	-0.583	

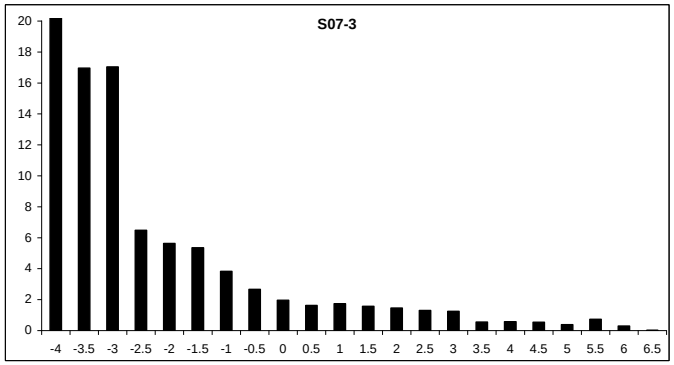

Fig. A.2.1 cont.

Sample Number: **S07-4** **2007L**

Total sample weight: 494.2

Sieve Phi	Sieve mm	weight retained (g)	>2 mm (g)	Wt. %	Cu. Wt. %
-4.0	16.000	51.800		10.482	0.998
-3.5	11.314	34.200		6.920	0.893
-3.0	8.000	53.400		10.805	0.824
-2.5	5.657	39.800		8.053	0.716
-2.0	4.000	36.800		7.446	0.635
-1.5	2.828	31.600		6.394	0.561
-1.0	2.000	26.800		5.423	0.497
-0.5	1.414	23.700		4.796	0.443
0.0	1.000	20.800		4.209	0.395
0.5	0.707	19.800		4.006	0.353
1.0	0.500	21.900		4.431	0.312
1.5	0.354	18.200		3.683	0.268
2.0	0.250	15.500	15.534	3.143	0.231
2.5	0.177	13.400	14.232	2.880	0.200
3.0	0.125	12.200	14.661	2.967	0.171
3.5	0.088	73.025	4.262	0.862	0.141
4.0	0.063		5.459	1.105	0.133
4.5	0.044		6.819	1.380	0.122
5.0	0.031		6.993	1.415	0.108
5.5	0.022		27.702	5.605	0.094
6.0	0.016		18.448	3.733	0.038
6.5	0.011		0.216	0.044	0.000
			% mud	12.177	

Percentiles	phi	mm
95%	-3.772	13.660
84%	-3.117	8.676
75%	-2.658	6.314
50%	-1.025	2.035
25%	1.747	0.298
16%	3.187	0.110
5%	5.891	0.017

Folks' Graphic Stats	phi	mm
Mean (Mz)	-0.318	1.247
Sorting (SI)	3.040	
Mode	-3.000	
Skewness(Sk)	-0.384	

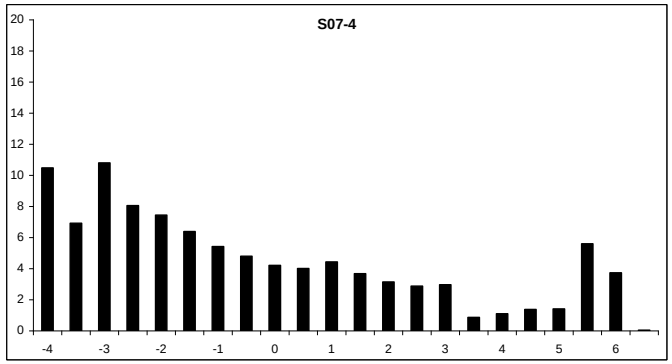

Sample Number: **S07-5** **2007L**

Total sample weight: 713.97

Sieve Phi	Sieve mm	weight retained (g)	>2 mm (g)	Wt. %	Cu. Wt. %
-4.0	16.000	180.200		25.239	1.000
-3.5	11.314	55.000		7.703	0.748
-3.0	8.000	97.700		13.684	0.671
-2.5	5.657	38.200		5.350	0.534
-2.0	4.000	30.500		4.272	0.481
-1.5	2.828	27.400		3.838	0.438
-1.0	2.000	25.500		3.572	0.399
-0.5	1.414	21.600		3.025	0.364
0.0	1.000	18.700		2.619	0.333
0.5	0.707	18.800		2.633	0.307
1.0	0.500	21.800		3.053	0.281
1.5	0.354	20.800		2.913	0.250
2.0	0.250	19.800	19.935	2.792	0.221
2.5	0.177	17.700	19.336	2.708	0.193
3.0	0.125	15.800	20.393	2.856	0.166
3.5	0.088	104.470	7.248	1.015	0.138
4.0	0.063		7.810	1.094	0.128
4.5	0.044		8.463	1.185	0.117
5.0	0.031		8.683	1.216	0.105
5.5	0.022		40.432	5.663	0.093
6.0	0.016		25.009	3.503	0.036
6.5	0.011		0.661	0.093	0.001
			% mud	11.660	

Percentiles	phi	mm
95%	-3.900	14.933
84%	-3.682	12.839
75%	-3.504	11.347
50%	-2.182	4.538
25%	1.507	0.352
16%	3.109	0.116
5%	5.876	0.017

Folks' Graphic Stats	phi	mm
Mean (Mz)	-0.918	1.890
Sorting (SI)	3.179	
Mode	-3.000	
Skewness(Sk)	-0.603	

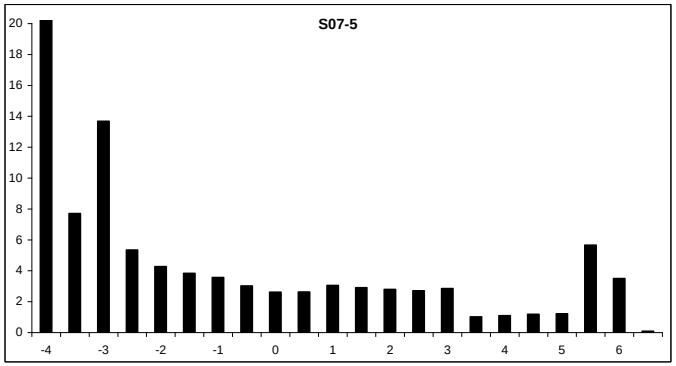

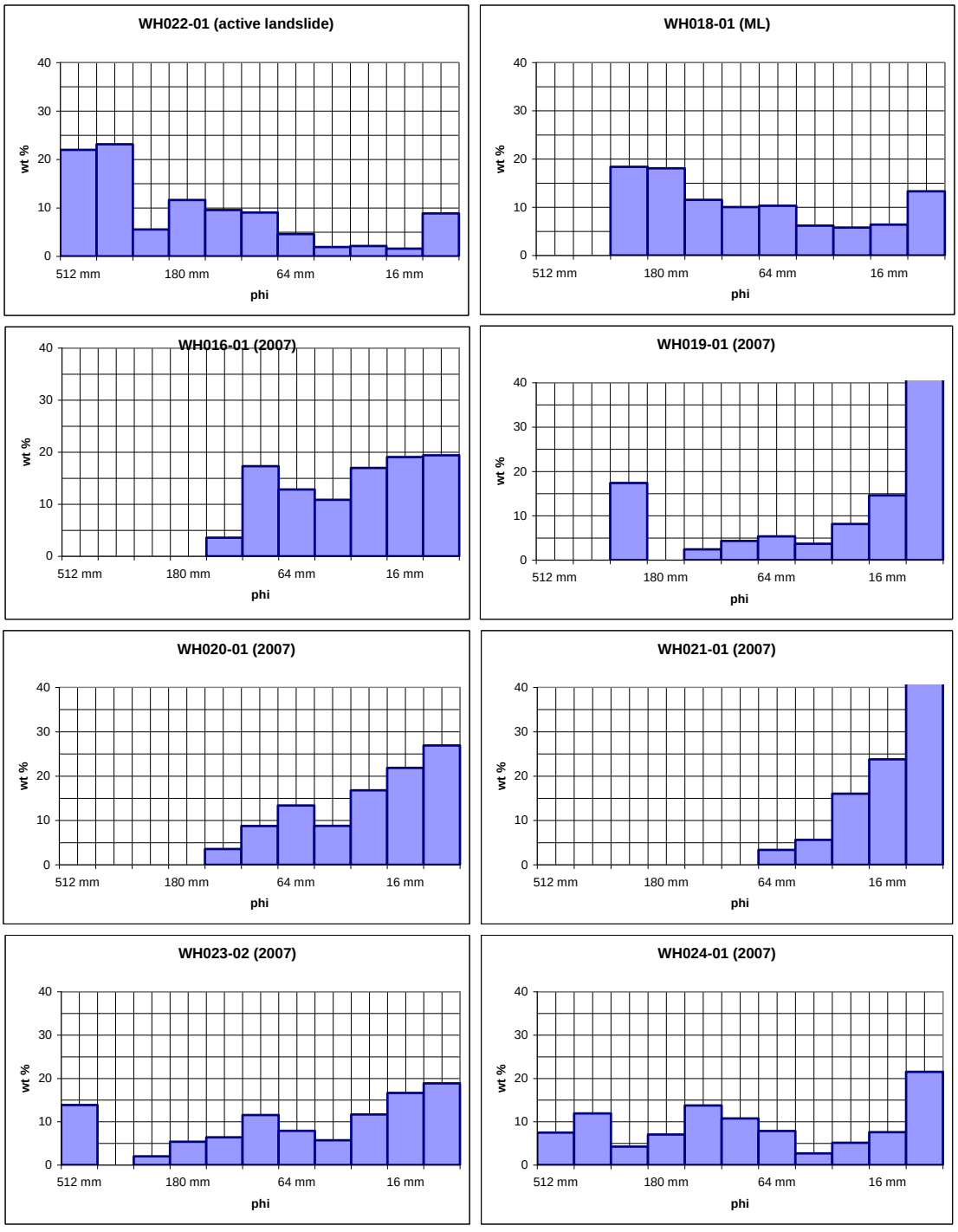

Fig. A.2.2 Field sieve results >16 mm. Fagents unpublished data, courtesy of the University of Hawaii.

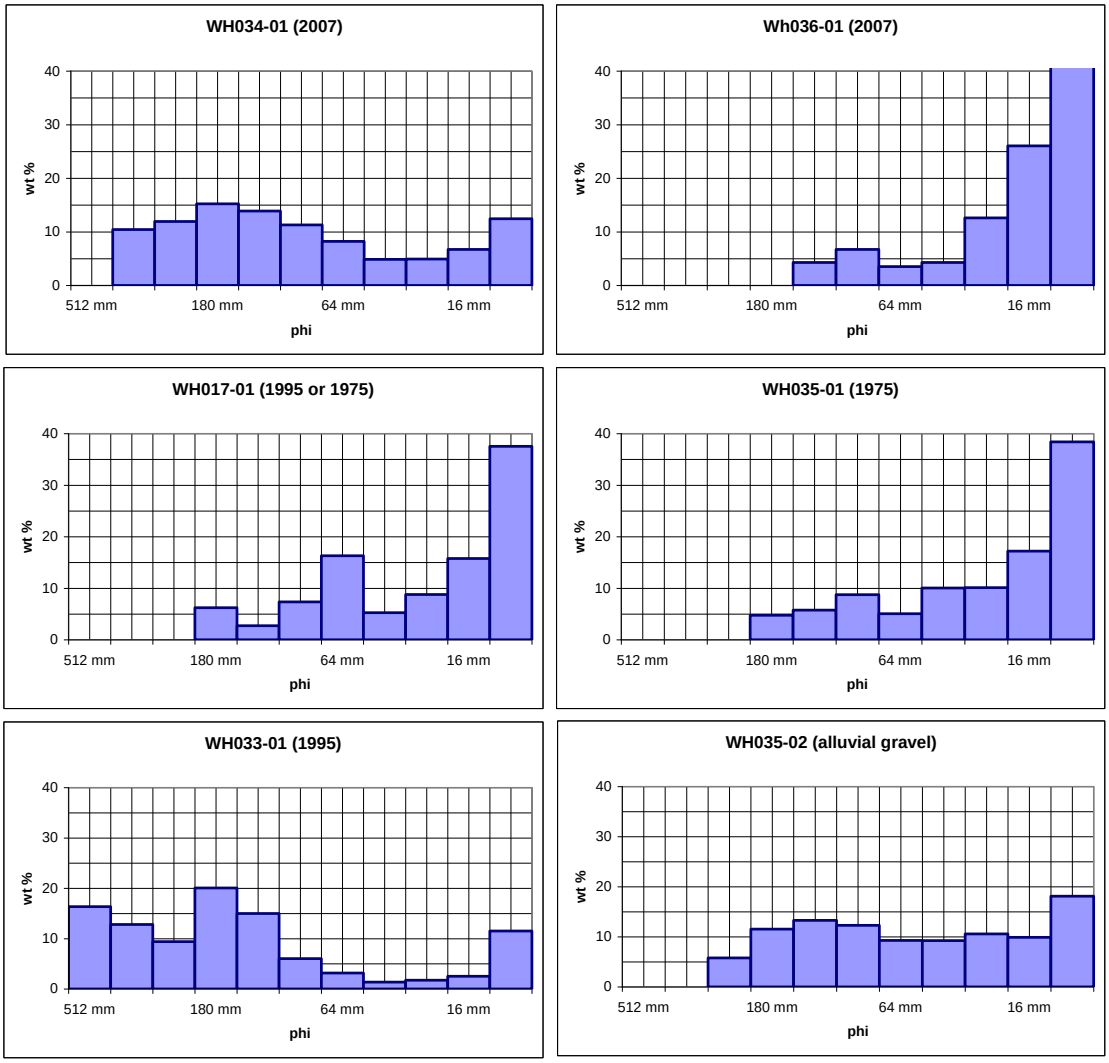

Fig. A.2.2 (cont.) Field sieve results >16 mm. Fagents unpublished data, courtesy of the University of Hawaii.

Table A.2.1 Statistics from the 25 m^3 grid grain counts including extra outsized clast measurements.

1975

Distance from crater lake (km)	mean	median	mode	max	SD
6	24.69	12	7	127	23.02
6.5				311	
6.5				127	
7	17.05	12	7	112	11.47
7	14.02	7	8	58	7.36
7				364	
9	15.12	8	6	91	14.05
9	25.88	12	8	362	32.83
9				11.7	
10	15.15	9	3	92	17.84
10	13.93	11	9	68	8.64

1995E

Distance from crater lake (km)	mean	median	mode	max	SD
6.5	17.23	12	8	187	15.61
6.5	24.17	12	7	239	33.08
7	18.9	12.5	5	311	13.2
7	19.93	11	10	176	22.31
7	48.42	38.5	24	311	12.25
7				311	
7				348	
7				228	
7	24.38	38.5	32	230	34.4
8.4	24.85	17	12	84	17.7
8.4	13.35	10	8	44	7.35
9	25.88	12	8	362	32.83
9	14.09	8	9	91	10.27
10	16.85	13	8	117	14.65
10	16.41	10	6	210	22.8
10				110	

1995R

Distance from crater lake (km)	mean	median	mode	max	SD
6.5	18.89	12	6	285	24.93
6	17.23	12	8	187	15.61
7	17.83	12	9	111	15.45
7				307	
7				481	
7				253	
7				230	
10	41.13	36	29	92	17.45

Table A.2.1 (cont.) Statistics from the 25 m^3 grid grain counts including extra outsized clast measurements.

2007 Distance from crater lake (km)	mean	median	mode	max	SD
6	21.07	17	15	107	13.76
6.5	21	18	11	101	12.96
7	17.75	15	14	77	8.86
9	19.76	18	12	61	8.86
10	25.15	22	19	134	13.71

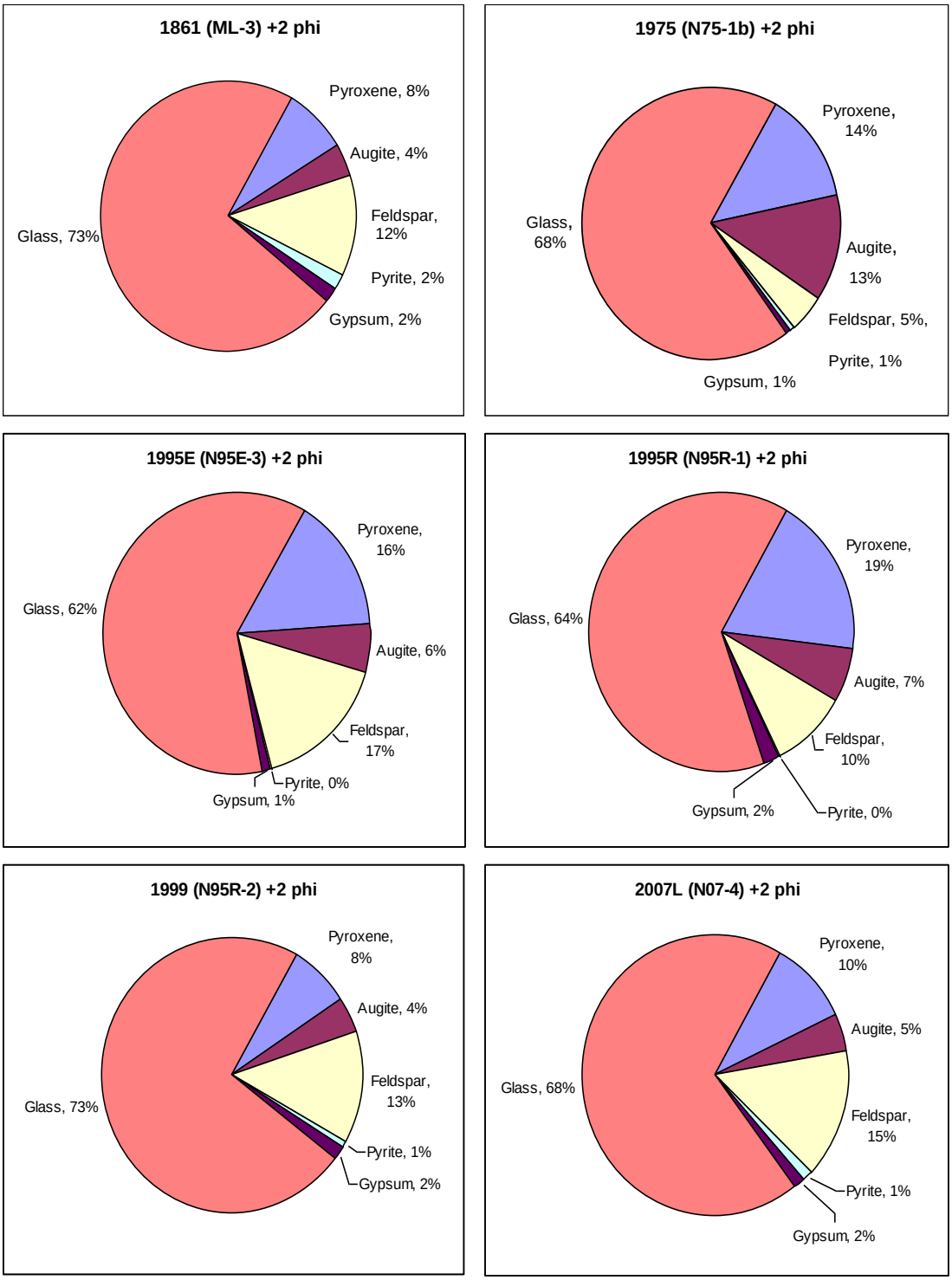

Fig. A.3.1 0.25 mm (+2 phi) grain size componentry. Identifications made under polarised light.

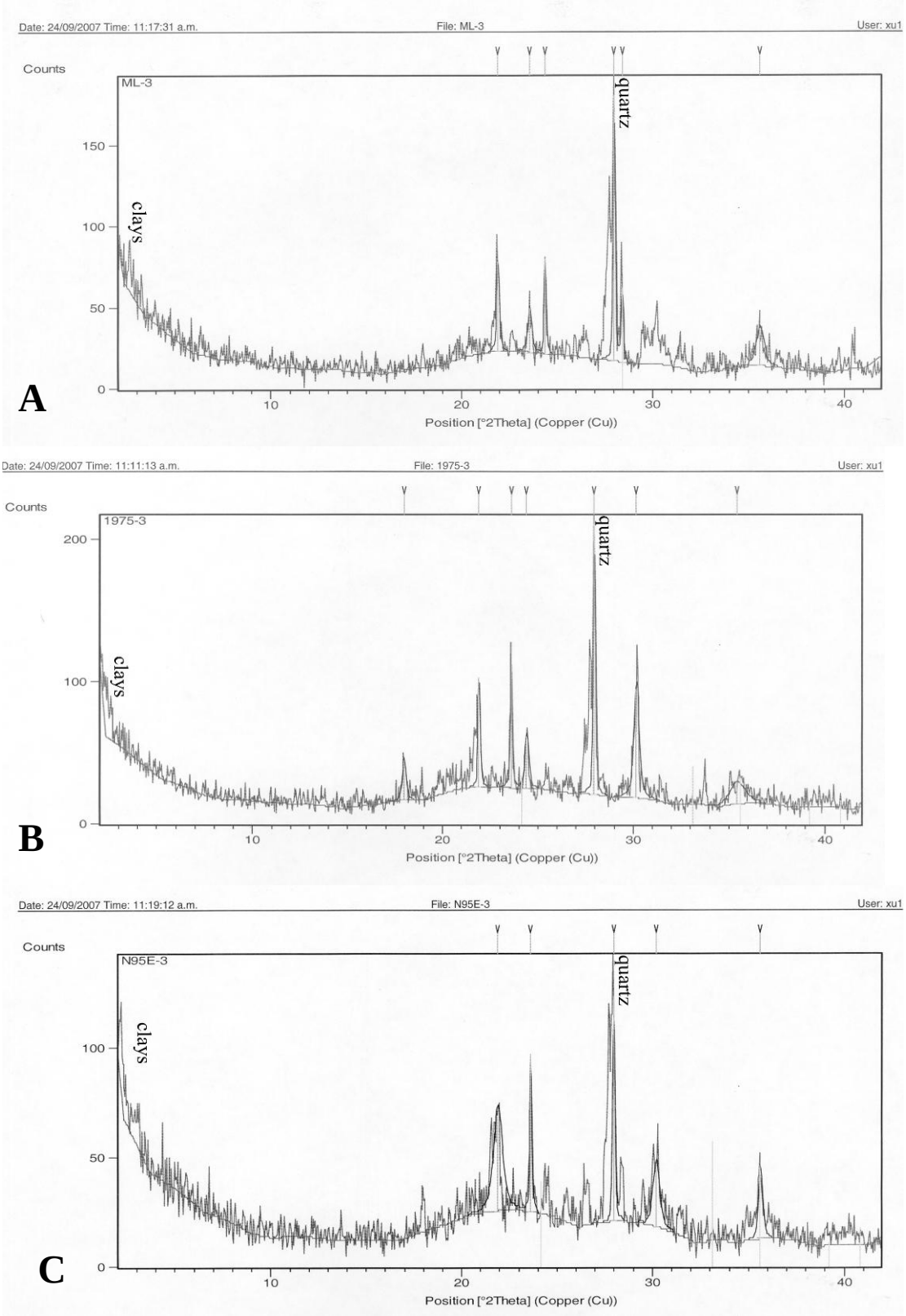

Fig. 4.1 XRD results for silt (<0.125 mm) fraction. Results indicate the presence of minor quartz and clay minerals. Petrographic studies reflect a dominance of andesitic glass in fine fractions. **A.** 1861 deposit **B.** 1975 deposits. **C.** 1995E deposit **D.** 1995R **E.** 1999 deposits **F.** 2007L deposits.

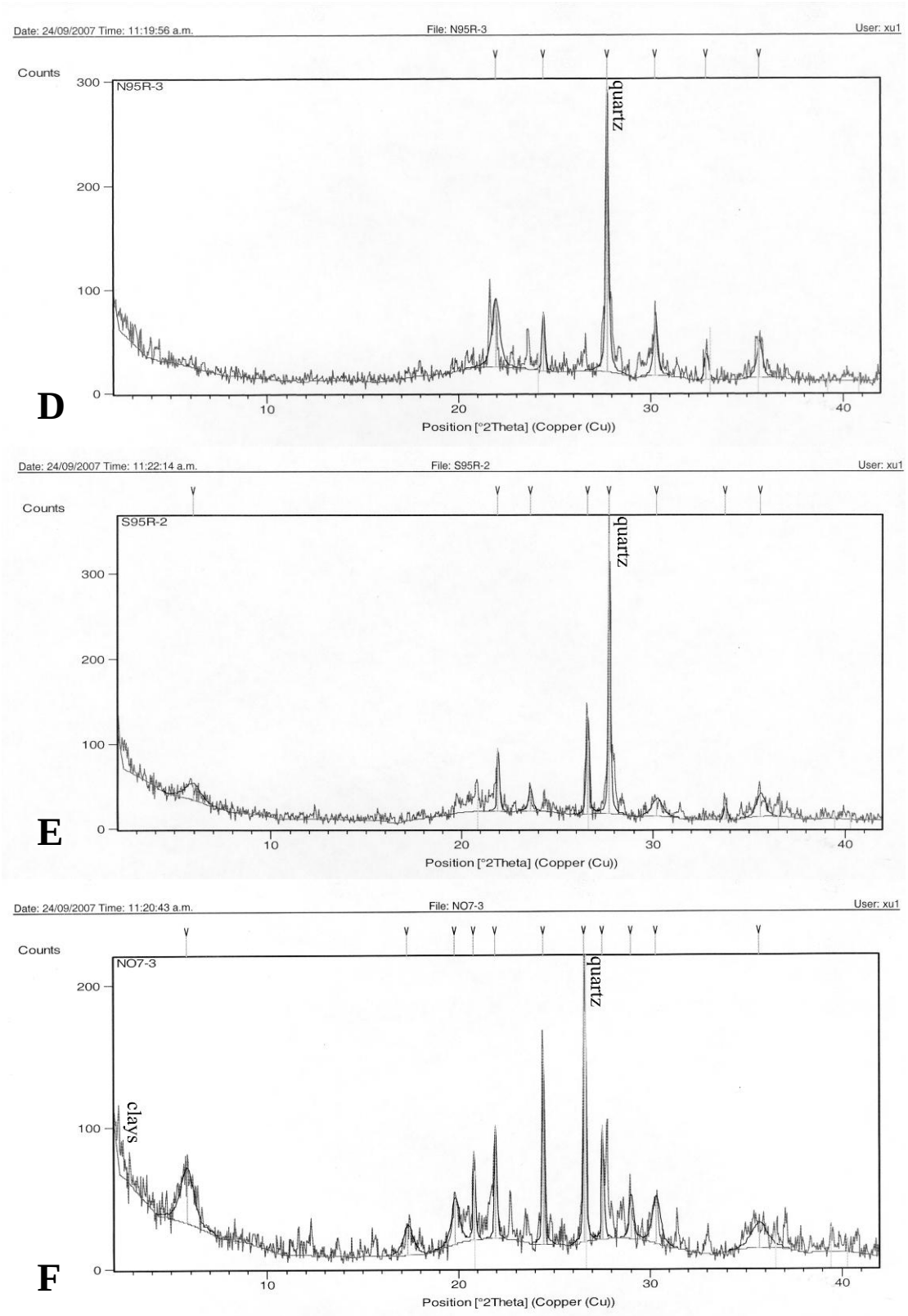

Fig. 4.1 cont. D. 1995R deposit **E.** 1999 deposit **F.** 2007L deposit.

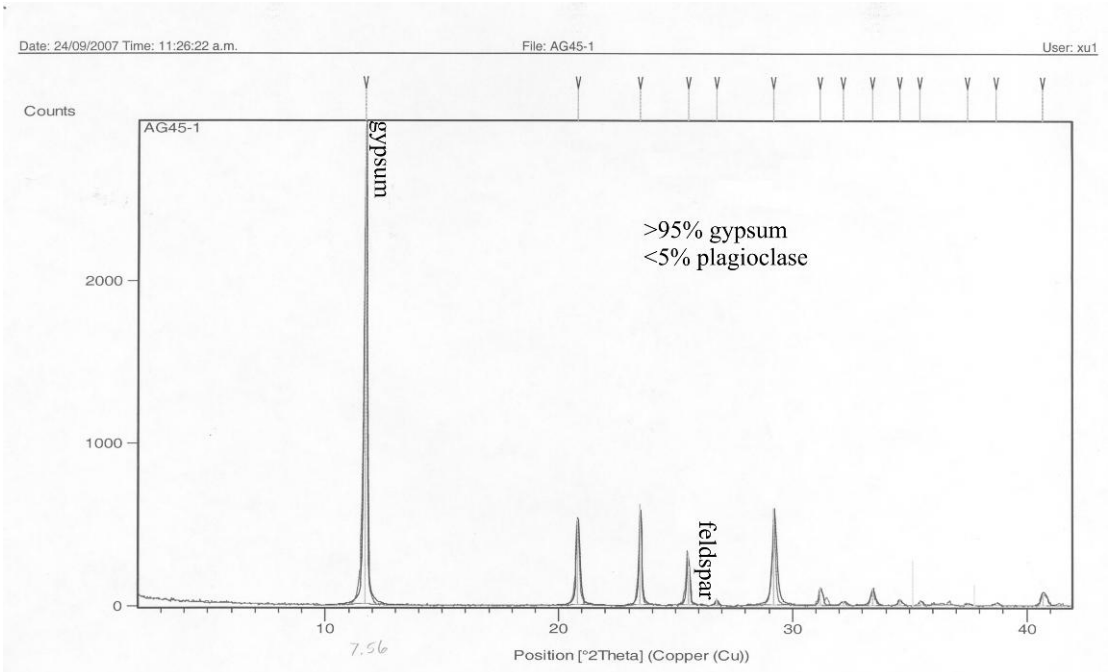

Fig. 4.2 XRD results for gypsum crystals dispersed in matrix samples.

Table A.5.1 Petrography of selected clasts from historic lahars of the Whangaehu Valley.

1995E andesitic lava	
Groundmass	Highly altered, hypocrystaline. Glassy with augite plagioclase and opaques
Plagioclase	Dominates subhedral, twinned, resorbed edges, minor inclusions
1861 red scoria	
Ground mass	Red glass, low vesicularity
Plagioclase	Dominant phenocrysts, subhedral large, anhedral when small Some inclusions
Hypersthene	Small, anhedral
Augite	Fractured, with alteration along fractures
1975 black scoria	
Ground mass	Black glass, brown around edges and vesicles
Plagioclase	Subhedral, alteration to sericite (decomposition)
Augite	Subhedral, cracked, distinct cleavage
Hypersthene (minor)	Euhedral
1995E black scoria	
Ground mass	Medium brown glass with small phenocrysts (50 µwide)
Plagioclase	Highly damaged, anhedral, strong twining, major and minor zoning (decomposition)
Hypersthene	Subhedral
Augite	Anhedral
1995E red scoria	
Ground mass	Pink to red brown. Hypocrystaline glassy matrix with barely discernable phenocrysts of plagioclase
Plagioclase	Highly fractured but still intact euhedral Twinning and zoning
Hypersthene	Altered rims, iron oxidation
Opaques	elongate

Table A.6.1 Effective width of the Whangaehu Valley from 6 to 10 km from Crater Lake.

Distance (km) from Crater Lake	1975	1995E	1995R	2007E
6.0-6.5	112.18	39.81		46
	92.43	34.32	25.02	47.04
6.5-7.0	102.19	45.97	29.09	50.87
	112.12	42.87	31	68.22
	141.52	66.68	56.64	59.72
	71.71			35.26
7.0-8.4	164.01	54.66	24.77	
	130.3	71.96	27.95	
	66.83	68.11	46.25	
	45.89			
	26.6	26.6		
	10.99	10.99		
	21.84			
	9.48	9.48		
8.4-9.0	33.55	33.55		
	30.39	30.39		
	25.28	15.98		
	66.51	30.61		
	52.34	27.6	16	
	55.87	27.7	12.7	
	62.91	29.94	13.84	
	74.56	23		
9.0-10.0	69.77	69.77		
	112.47	86.29		
	154.32	96.49	32.34	
	144.65	111.56	26.29	
	139.84	115.66	32.48	
		117.77	54.13	

Table A.6.2 Terrace heights through the Whangaehu Gorge

Distance from Crater Lake (km)	6.00	6.50	7.00	7.25	8.00	8.40	9.00	10.00	11.00
(m)									
1975	11.50	10.67	0.00	9.00	9.00	0.00	11.16	9.40	0.00
1995E	0.00	5.00	0.00	6.00	6.00	0.00	4.50	5.33	3.00
1995R	0.00	2.20	0.00	2.30	3.00	0.00	3.20	2.50	2.00
1999	3.38	1.79	0.00	1.25	2.00	2.00	1.50	1.06	1.00
2007L	8.17	6.33	0.00	6.13	6.00	2.00	8.00	3.08	1.27

Table A.7.1 Bulk density samples from September 27, 2007 Whangaehu Valley west of the RTMT.

Sample	Position (below surface)	Weight (g)	Bulk density (g/cm^3)
07b-1	Surface	1329.07	0.66
07b-1	Middle 25 cm	996.27	0.50
07b-1	Bottom 50 cm	1167.67	0.58
07b-2	Surface	775.79	0.39
07b-2	Middle 35-45 cm	1054.79	0.53
07b-3	Surface	1336.49	0.67
07b-3	Middle 35-45 cm	1053.46	0.53
07b-4	Surface	961.25	0.48
07b-4	Middle 35-45 cm	831.71	0.42
07b-5	Surface	1019.57	0.51
07b-5	Middle 80 cm	714.93	0.36
07b-5	Bottom 135 cm	779.85	0.39
07b-6	Surface	1145	0.57
07b-7	Surface	988.47	0.49
07b-7	Middle 40 cm	1207.82	0.60

Table A.7.2 Bulk density of snow slurry lahars in 1995 (Cronin et al. 1996).

September 18-23, 1995	g/cm^3
LH1	0.47
LH2	0.54
LH3	0.91
LH4	0.71

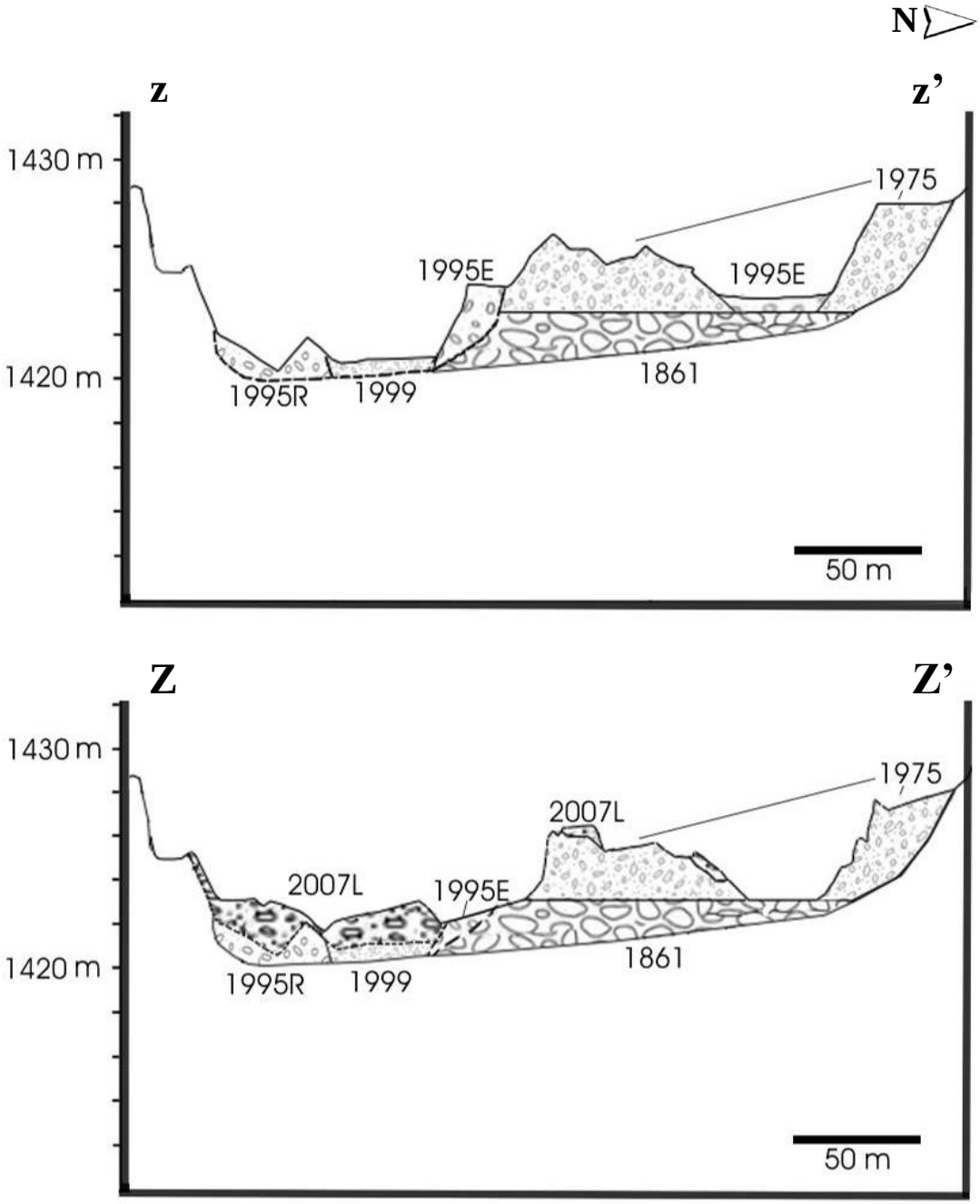

Fig. A.8.1 Cross-section revealing terrace modification by the 2007L lahar. 7.5 km from Crater Lake. Derived from LiDAR based DEMs: z-z' February 2006, Z-Z' April 2007. LiDAR courtesy of GNS and Massey University.

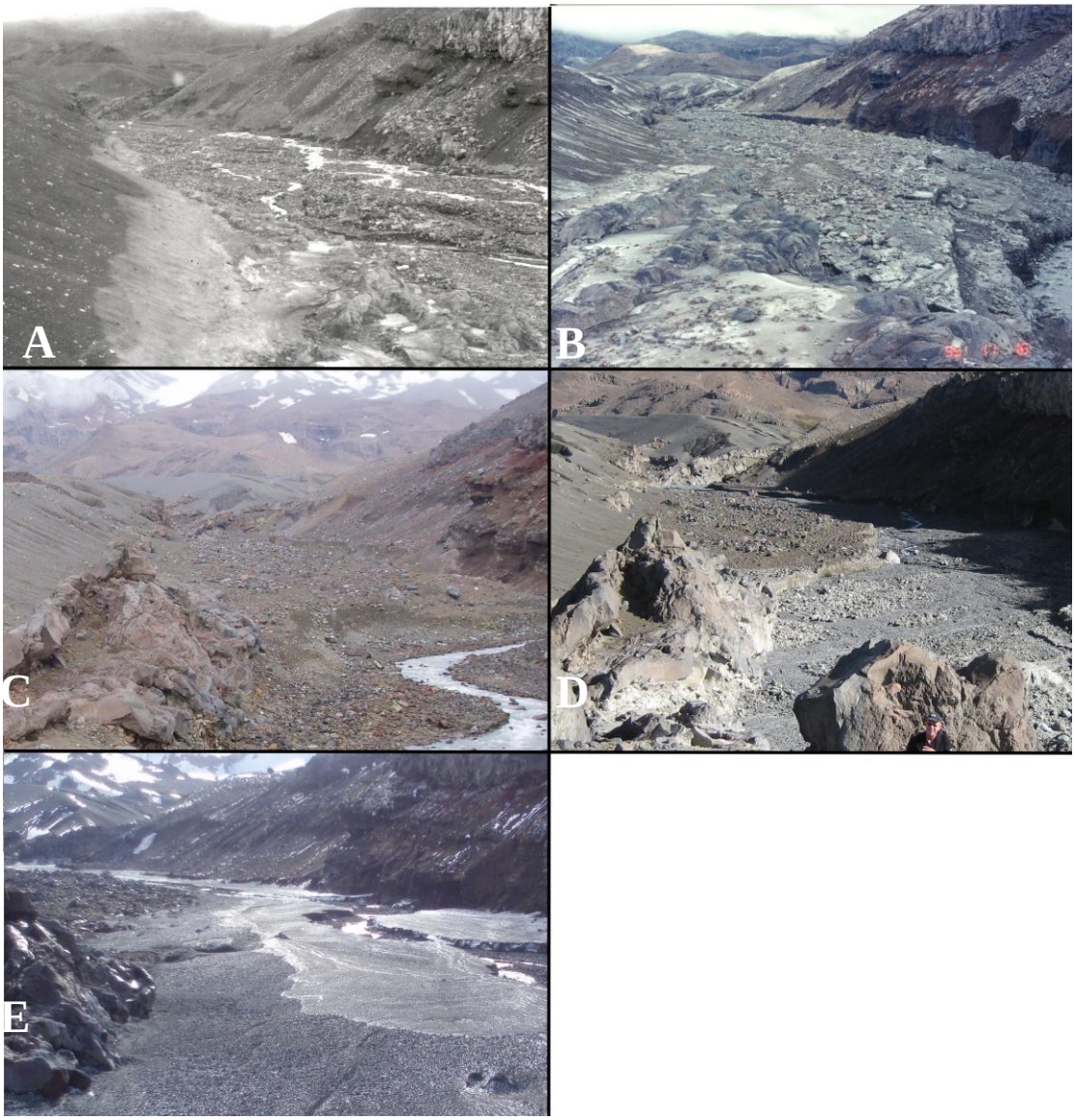

Fig. A.8.2 Historic photographs of the Whangaehu Gorge from 1975 to 2007 at the RTMT (7 km from Crater Lake). **A**. 1975 high water marks are 2 m above deposit surface. Photo: I. Nairn. **B**. November 1995 following the emplacement of the highest 1995R terrace. Photo: I. Nairn **C**. January 2007 including 1999 lahar deposits. **D**. March 2007, aggradation by 2007L resulted in a change in channel direction. **E**. September 2007 including the snow rich 2007E deposit. Photo: K.Kataoka

Fig. A.8.3 Historic photographs from the RTMT (7 km) reflecting terrace construction and erosion by historic lahar events. **A**. October 1995, between emplacement of 1995E and 1995R deposits. Photo: V. Manville. **B**. January, 2007 following emplacement of 1999 lahar. **C**. March 19, 2007 following emplacement of 2007L deposits. **D**. October 2007 following the 2007E snow slurry lahar. **E.** November, 2007 melting of the 2007E deposits. Geomorphic textures and thickness decrease. **F.** December, 2007 post-melting of the 2007E deposits. The thickness decreased to c. 70 cm and the distribution of sediment was significantly reduced in the three months following emplacement.